Open Research Online

The Open University's repository of research publications
and other research outputs

Gold Nanoparticles as a Delivery System of Oligonucleotides into the Brain

Thesis

How to cite:

Gromnicova, Radka (2017). Gold Nanoparticles as a Delivery System of Oligonucleotides into the Brain. PhD thesis The Open University.

For guidance on citations see FAQs.

© 2016 The Author

https://creativecommons.org/licenses/by-nc-nd/4.0/

Version: Version of Record

Link(s) to article on publisher's website:
http://dx.doi.org/doi:10.21954/ou.ro.0000bfbc

Copyright and Moral Rights for the articles on this site are retained by the individual authors and/or other copyright owners. For more information on Open Research Online's data policy on reuse of materials please consult the policies page.

oro.open.ac.uk

The Open University, Faculty of Science, Technology, Engineering and Mathematics; Department of Life, Health and Chemical Sciences; Walton Hall, Milton Keynes, United Kingdom

Gold nanoparticles as a delivery system of oligonucleotides into the brain

Radka Gromnicova, BSc

A thesis submission to The Open University for the degree of Doctor in Philosophy

October 2016

DECLARATION

I hereby declare that the work presented in this thesis is a result of my own academic and experimental enquiry; contributions made by other researchers are fully acknowledged in relevant parts of the text. Moreover, this work does not contain any material submitted for award of any other degree.

Radka Gromnicova

ABSTRACT

The treatment of brain disease is challenging due to the blood-brain barrier, a physiological structure that prevents the majority of potential therapeutic agents from entering the brain. One approach to overcome this problem is the use of nanoparticles as a delivery system. Several types of nanoparticle have shown promise as drug carriers, including gold nanoparticles. They exhibit relatively low cytotoxicity and can enter cells by both active and passive uptake mechanisms and can cross the blood-brain barrier *in vivo* and *in vitro*. The aim of this study was to investigate the potential of 5nm gold glyconanoparticles as a delivery system for oligonucleotides into the brain.

Three ligand formulations of gold glyconanoparticles were investigated, covalently coated with glucose, OEG-amine/galactose or OEG-amine/galactose/insulin. The two formulations with OEG-amine showed higher uptake efficiency into both human brain endothelial cells (hCMEC/D3) and primary astrocytes, as determined by electron microscopy. Nanoparticles located in subcellular compartments of endothelium were quantitated. Inhibition studies demonstrated that both active and passive transport mechanisms were involved in the uptake of these nanoparticles. However, knockdown of the insulin-receptor on the endothelium did not reduce transport of insulin-coated nanoparticles. It appeared that the OEG-amine coating alone induced much higher levels of vesicular transport, relative to cytosolic uptake.

The uptake efficiency of OEG-amine/galactose nanoparticles into different endothelial cells (kidney (ciGENC), bone marrow (BMEC) and lung primary (HMVEC-L)) was compared. Kidney endothelium had higher nanoparticle uptake than brain endothelium. Cellular properties that might influence this cell-selective uptake were investigated; the high level of nanoparticle uptake by kidney endothelium was correlated with a higher level of endocytosis and a different glycocalyx composition on these cells.

The transport characteristics of the three formulations of glyconanoparticles were investigated *in vivo*. The nanoparticles were injected intracarotid into rats and left to circulate for 10 min, in order to capture the first contact of glyconanoparticles with the brain, as detected by electron microscopy. The nanoparticles were observed in brain parenchyma of the cortex, striatum, hippocampus, median eminence and choroid plexus. However, a biodistribution study of the gold, by ICP-mass spectrometry showed that the great majority of the injected nanoparticles were present in the kidney.

Finally, a cargo molecule of DNA oligonucleotide was attached to the gold glyconanoparticles (galactose-coated) by the place-exchange reaction, forming ssDNA/galactose nanoparticles. Nanoparticles with different amounts of bound DNA were fractionated by FPLC and analysed by a novel electrophoretic mobility shift assay (EMSA). When comparing the uptake efficiency of dsDNA/galactose nanoparticles to galactose nanoparticles there was no reduction in uptake efficiency, despite addition of the highly negatively charged cargo.

To conclude, gold glyconanoparticles can cross the blood-brain barrier and enter cells of the brain in vivo and in vitro. Addition of a DNA oligonucleotide cargo does not alter their ability to cross endothelium and hence <5 nm gold glyconanoparticles may be a useful carrier of oligonucleotides into the brain.

ACKNOWLEDGEMENTS

I was very fortunate to have David Male as my supervisor who helped me to develop into a researcher. I could not have wished for better supervision and support, it was a pleasure to work with him. Also, my second supervisor Nacho Romero provided me with helpful comments and made me think about research from a different perspective. Moreover, I would like to thank to Basil Sharrack for providing this life-changing experience of PhD research for me.

I would like to thank all the collaborators that I met during my PhD journey, without them this work would not have been possible: Phil Williams and the rest of the team from Midatech Pharma UK, Ibon Perera and Julen Barrenetxea from Midatech Pharma Spain, Mehmet Kaya and his team from Istanbul University, Torben Lund from Middlesex University, Simon Satchell from Bristol University, and Heather Davies, the former manager of the EM Suite at the Open University. Also, as I provided research training to undergraduate students Ayse Gungor and Natasha Smith, they in turn did wonderful research relevant to this work.

The academics, administrators, lab support and peers from the Open University were very supportive during my journey and I am lucky to have made such good friends. I received help in reading parts of my thesis from wonderful academics: Cheryl Hawkes, Katja Rietdorf, Rachel Mcmullan and Martin Bootman.

I would like to thank my mum, my brother and my grandparents for their belief in me on starting my career as a scientist, despite being so far from home. Also, my PhD journey was made easy by enjoying the time with my horses, they are my islands of love and harmony.

Last but not least, Kim, for his endless support, encouragement and help throughout the journey that I have been on since I first walked into the Open University.

PREFACE

The choice of nanoparticles and the motivation of this thesis was based on previous finding that glycan-coated gold nanoparticles of diameter under <5 nm held a potential to be used as a delivery system across the blood-brain barrier and into the brain (Gromnicova et al. 2013). This work was done in a partnership with Midatech Pharma (former Midatech Ltd.). A patent was filed on use of these glycan-coated small gold nanoparticles for brain therapy, jointly held between David Male (the supervisor and lead investigator of the original study) and Thomas Rademacher (now former CEO of Midatech Ltd.).

PUBLICATION LIST

Publications prior to work shown in this thesis

Gromnicova, Radka, Heather A Davies, Peddagangannagari Sreekanthreddy, Ignacio A Romero, Torben Lund, Ivan M Roitt, James B Phillips, and David K Male. 2013. "Glucose-Coated Gold Nanoparticles Transfer across Human Brain Endothelium and Enter Astrocytes in Vitro." *PloS One* 8 (12): e81043. doi:10.1371/journal.pone.0081043.

Sreekanthreddy, Peddagangannagari, Radka Gromnicova, Heather Davies, James Phillips, Ignacio A Romero, and David Male. 2015. "A Three-Dimensional Model of the Human Blood-Brain Barrier to Analyse the Transport of Nanoparticles and Astrocyte/endothelial Interactions." F1000Research 4 (November). doi:10.12688/f1000research.7142.1.

Publications resulting from work shown in this thesis

Gromnicova, Radka, Mehmet Kaya, Ignacio A. Romero, Phil Williams, Simon Satchell, Basil Sharrack, and David Male. 2016. "Transport of Gold Nanoparticles by Vascular Endothelium from Different Human Tissues." *Plos One* 11 (8): e0161610. doi:10.1371/journal.pone.0161610.

Gromnicova, Radka, Canan Ugur Yilmaz, Nurcan Orhan, Mehmet Kaya, Heather Davies, Phil Williams, Ignacio A Romero, Basil Sharrack, and David Male. 2016. "Localisation and Mobility of Glucose-Coated Gold Nanoparticles within the Brain." *Nanomedicine (London, England)* 11 (6): 617–25.

Male, David K, Radka Gromnicova, and Conor McQuaid. 2016. "Gold Nanoparticles for Imaging and Drug Transport to the CNS." In *International Review of Neurobiology*. doi:10.1016/bs.irn.2016.05.003.

Table of Contents

LIST OF FIGURES

LIST OF TABLES

ABBREVIATIONS

ABC transporter	ATP-binding cassette transporter
ApoE	Apolipoprotein E
Aqp-4	Aquaporin 4
BCRP	Breast cancer resistance protein
BDNF	Brain-derived neurotrophic factor
BMEC	Bone marrow endothelial cells
BODIPY	boron-dipyrromethene
BSA	Bovine serum albumin
ciGENC	Conditionally immortalized glomerular endothelial cells
CTAB	cetyltrimethylammonium bromide
Da	Dalton
DLS	Diffraction light spectroscopy
DNA	Deoxyribonucleic acid
ds	Double-stranded
EBM-2	Endothelial basal medium 2
EBM-2 MV	Endothelial basal medium 2 - microvascular
EDS or EDX	energy-dispersive X-ray spectroscopy
EDTA	Ethylenediaminetetraacetic acid
EGF	Epidermal growth factor
EGFR	Epidermal growth factor receptor
EM	Electron microscopy
EMSA	Electrophoretic mobility shift assay
FACS	Flow cytometry
FBS	Foetal bovine serum
FDA	Food and Drug Administration
FITC	Fluorescein isothiocyanate
FPLC	Fast protein liquid chromatography
GFAP	Glial fibrillary acidic protein
GSH	Glutathione
hBMEC	Human brain microvascular endothelial cells
HBSS	Hank's balanced salt solution
hCMEC/D_3	Human cerebral microvascular endothelial cells D_3
HIV	human immunodeficiency virus
HMVEC-L	Human lung microvascular endothelial cells
HPLC	High-performance liquid chromatography
ICP-MS	Inductively-coupled plasma mass spectroscopy
IgG	Immunoglobulin G
IR	Insulin receptor
JAM	Junctional adhesion molecule
LDL	Low-density lipoprotein
LRP	Low density lipoprotein receptor-related protein
mAb	Monoclonal antibody
microCT	micro–computed tomography
MTT	3-(4,5-dimethylthiazol-2-yl)-2,5-diphenyltetrazolium bromide
NGF	Nerve growth factor
PAMAM	poly(amidoamine)

PB	Phosphate buffer
PBMEC	Porcine brain microvascular endothelial cells
PBS	Phosphate-buffered saline
PECAM-1	Platelet endothelial cell adhesion molecule
OEG	Poly(ethylene glycol)
PEI	polyethylenimine
PFA	paraformaldehyde
Pgp-1	p-glycoprotein
PLA	polylactides
PLGA	poly (D,L-lactide-co-glycolate)
PNA	Peanut agglutinin
RNA	Ribonucleic acid
ROS	Reactive oxygen species
SEM	Scanning electron microscopy OR standard error of the mean
SEC	Size exclusion chromatography
siRNA	small interfering RNA
SPR	Surface plasmon resonance
ss	Single-stranded
SV-BEC	bovine brain capillary endothelial cells
TAT	trans-activating transduction peptide
TBE	Tris/Borate/EDTA buffer
TEM	Transmission electron microscopy
TGFβ	Transforming growth factor beta
TNFα	Tumor necrosis factor
UEA	Ulex europaeus agglutinin
UV	Ultra-violet
VEGF	Vascular endothelial growth factor
WFL	Wisteria floribunda lectin
WGA	Wheat germ agglutinin

Chapter 1. General Introduction

In Europe, 50 % of disabilities are due to brain disorders (Olesen & Leonardi 2003) and in the U.S., 30 % of seniors die with one of the most prevalent brain disorders, Alzheimer's disease. Why are we not able to treat these disorders? Even though the progress of the pharmaceutical industry has been rapid, neuroscience has not been able to respond in the same way and be able to deliver the new drugs to the brain due to the major obstacle – the blood-brain barrier. The blood-brain barrier prevents 98% of small drugs from entering the brain (Pardridge 2005). As new therapeutic molecules emerge with the potential to treat brain disorders, the need is to have suitable methods to deliver therapies across the blood-brain barrier without affecting its properties. One of the potential ways to cross the blood-brain barrier is to use nanoparticles as carriers of therapeutic agents. This thesis is focused on gold nanoparticles as nano-carriers, and their usefulness as a candidate in nanomedicine, as well as their use as a delivery system into the brain.

1.1 The blood-brain barrier

The brain is a highly controlled and protected organ, since there are substances in the blood that may potentially harm it. This control is established at the level of blood vessels, thus regulating what is entering from the blood. This is crucial as there can be up to 400 miles of blood vessels in a single human brain (Zlokovic 2005). The components of the blood vessels in the brain form a barrier, called the blood-brain barrier. The blood-brain barrier was discovered in 1885 by Paul Ehrlich but it was not accepted by the scientific community until the 1960s (Ribatti et al. 2006). Brain endothelial cells, which form the actual barrier with the blood, need other cells of the "neurovascular unit", such as pericytes and astrocytes, in order to develop the phenotype responsible for the barrier function. At the capillary level, brain endothelial cells line the blood vessels and secrete a basal membrane that abuts astrocytic end feet and encloses pericytes (Figure 1.1) (Abbott et al. 2010).

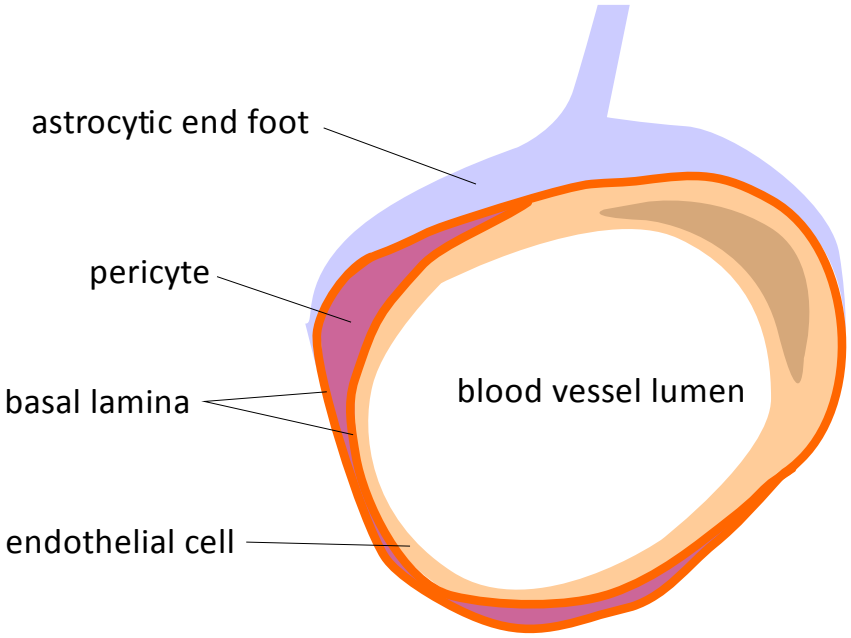

Figure 1.1. The structure of the blood-brain barrier. The blood-brain barrier is a functional structure at the level of brain microvessels, the scheme shows cells that compose the blood-brain barrier.

The blood-brain barrier has several key characteristics crucial for the function of the barrier. Firstly, tight junctions between the endothelial cells seal and restrict the paracellular movement of molecules. Next, specialized transporters, the efflux transporters, control substances that enter the brain. Lastly, enzymatic components protect the brain from toxins or neurotransmitters. These topics are detailed below.

1.1.1 Tight junction complex

Tight junctions are composed of several types of transmembrane proteins and also include adherens junctions (Figure 1.2). Tight junctions are important for maintaining the polarity of endothelial cells. Endothelial cells have transporters on the apical and basal sides to supply what is required by the brain. Thus tight junctions prevent unrestricted diffusion of the phospholipid bilayer that would impede this polarity. Also tight junctions are crucial for maintaining the barrier property of the brain endothelial cells, being a barrier to polar solutes such as glucose and amino acids that are necessary for the brain (Begley 2004b). Ions are restricted in crossing the brain endothelium, which gives the brain endothelium a high electrical resistance of about 1800 ohms/cm^2 (Butt et al. 1990).

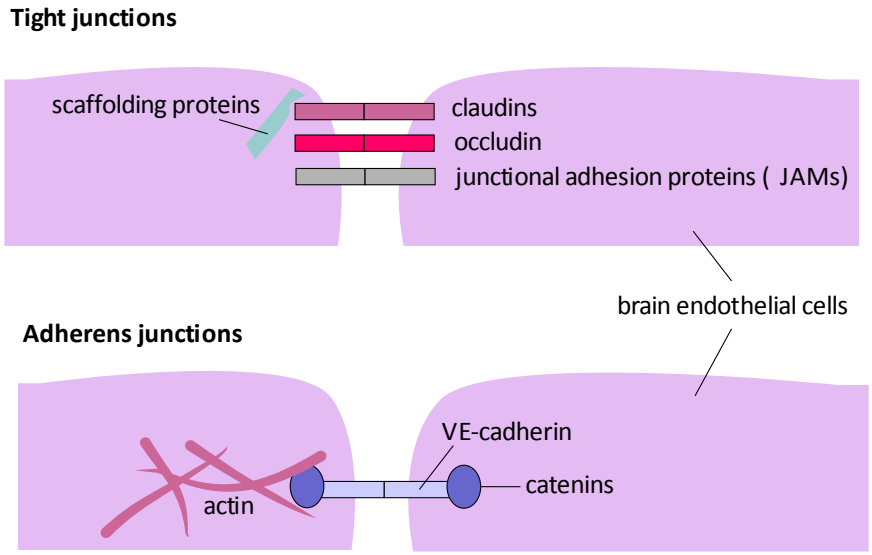

Figure 1.2The junctional complexes in brain endothelial cells, categorized as tight junctions or adherens junctions. Tight junctions include transmembrane proteins that span the plasma membrane, such as claudins, occludin and junctional adhesion proteins. These proteins are then bound to scaffolding proteins that attach them to the cytoskeleton. Adherens junctions include VE-cadherin (vascular-endothelial cadherin) that attaches via a group of proteins called catenins to actin filaments.

The proteins of the tight junctions are claudins, such as claudin 3, claudin 5 and claudin 12. Claudin 3 (Wolburg et al. 2003) and 5 (Nitta et al. 2003) were found to be crucial for maintenance of the blood-brain barrier. Other junctional transmembrane proteins are junctional adhesion molecules and occludins that are also needed for formation of tight junctions (Engelhardt 2007). These molecules are attached to the cellular cytoskeleton via scaffolding proteins (zonula occludens proteins).

Adherens junctions stabilize tight junctions and are present in all endothelial cells. Vascular endothelial cadherin spans the space between cells and intracellularly connects to catenins which then connect to actin filaments (Figure 2). In addition, another type of cadherin, cadherin-10 is present in junctions of non-leaky brain endothelial cells (Williams et al. 2005).

1.1.2 Transport systems on the brain endothelium

Brain endothelium employs many different transport systems in order to meet the needs of the brain for nutrients and to protect the brain from pathogens and molecules present in the blood that may harm the brain. The transport systems can be classified as passive diffusion, carrier-mediated (or solute) transport, and endocytosis/transcytosis (Figure 1.3) and are briefly detailed below.

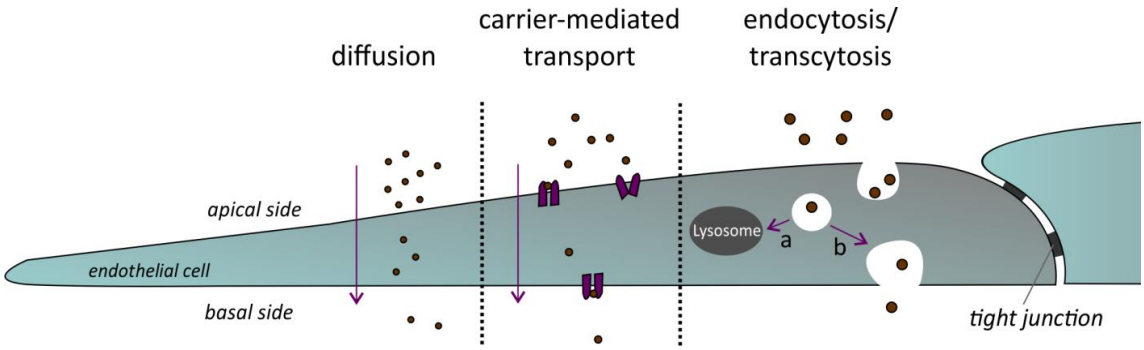

Figure 1.3. The transport systems at the brain endothelium. Three main transport pathways across the cell are diffusion, carrier-mediated transport and endocytosis/transcytosis. Diffusion allows small lipid or gas molecules to freely pass through the cell along their concentration gradient. Carrier-mediated transport involves transport of nutrients into the brain and may be active or passive. Macromolecules are endocytosed and then either (a) degraded in the lysosome or (b) transcytosed and released on the other side of the membrane.

1.1.2.1 Passive diffusion

Small molecules that are lipid-soluble with size under 400 Da enter the brain by passive diffusion (Pardridge 2010). Also non-polar molecules of this size and bases with a positive charge can use this route (Abbott et al. 2010). The exchange of gases such as oxygen and carbon dioxide happens via passive diffusion along the concentration gradient. As the cells of the brain lie no further than 25 μm from the capillaries (Schlageter et al. 1999), the oxygen supply is sufficient for all cells of the brain.

1.1.2.2 Carrier-mediated (solute) transport

As the brain is effectively sealed against the passage of many essential nutrients, there are several transporters that facilitate their transport. Therefore, carrier-mediated, i.e. solute transport is employed. It may work as a facilitated diffusion or may use sodium or proton gradients for the exchange (Abbott et al. 2010). The transported molecules can be glucose, amino acids, nucleosides and nucleotides, small peptides, organic cations and anions (Abbott et al. 2010).

Transport by specific transporters can not only involve influx but also efflux via specific efflux transporters of the ATP-binding cassette (ABC) transporters. The most notable ones are p-glycoprotein (pgp-1, ABCB1) and breast cancer resistance protein (BCRP). Both of these efflux transporters are located on the luminal side of the brain endothelial cells. The transporters remove lipophilic molecules, potentially harmful substances and drugs from the brain endothelium back into the blood (Begley 2004a). The principle of removal of these ligands involves a cascade of signalling. A sensing molecule (a transcription factor) in the cytosol binds a xenobiotic, is activated, moves into the nucleus to bind DNA and regulates transcription (Mahringer et al. 2011). These specific transcriptional factors have been found to detect xenobiotics. Therefore, they can exclude many potentially useful drugs, creating a major obstacle for the pharmaceutical industry in developing therapeutics for the brain.

1.1.2.3 Endocytosis and transcytosis

Macromolecules are transported into the brain via active endocytotic processes – they are taken up on the apical side and can then be exocytosed on the basal side, in the process of

transcytosis. In general, endocytotic vesicles merge with lysosomes as the final step in other cell types, but can be transcytosed particularly in endothelium (Abbott et al. 2010).

The endocytotic processes are traditionally categorized by the overall mechanism involved rather than what molecules pinched off or coated the final vesicle. Therefore, it is usual to classify brain endothelial endocytosis/transcytosis as receptor-mediated or adsorptive. Sometimes fluid-phase endocytosis is mentioned, however, this process is non-specific and non-adsorptive in comparison to receptor-mediated or adsorptive endocytosis. Receptor-mediated endocytosis involves a specific receptor, such as transferrin or insulin, which begins the endocytosis. In contrast, adsorptive endocytosis involves binding of charged macromolecules that cause endocytosis. The details of these transport systems are outlined in the Table 1.1. Many of these systems are exploited for drug delivery (section 1.3.6.3).

Table 1.1. Examples of macromolecule systems on the blood-brain barrier which deliver molecules from blood to brain (based on (Abbott et al. 2010)).

Transport system	Receptor (if known)	Ligand
Transferrin	Transferrin receptor TfR	Transferrin-iron
Lactoferrin	Lactoferrin receptor LfR	Lactoferrin
Apolipoprotein E	Apolipoprotein E receptor 2 ApoER2	Lipoproteins
LDL-receptor-related protein 1 and 2	LDL-receptor-related protein 1 and 2 receptor LRP1, LRP2	Lipoproteins, Amyloid-β, lactoferrin, α 2-macroglobulin, melanotransferrin, ApoE
Insulin	Insulin receptor IR	Insulin
Leptin	Not specified	Leptin
Tumour necrosis factor	Tumour necrosis factor receptor	TNFα
Epidermal growth factor	Not specified	EGF
Heparin-binding epidermal growth factor-like growth factor (diphtheria toxin receptor)	Heparin-binding epidermal growth factor-like growth factor HB-EGF (DTR)	Diphtheria toxin, protein CRM197

Macromolecule transport is often exploited and targeted as a way to overcome the blood-brain barrier (see section 1.2.2). The most commonly targeted is transferrin receptor or LRP-1 receptor. The expression of transferrin receptor is high in brain endothelium *in vivo*. The expression of LRP-1 receptor still remains controversial as studies suggest that it is expressed in both endothelial cells and pericytes (Helms et al. 2016).

1.1.3 Enzymatic blood-brain barrier

Brain endothelial cells also contain enzymes that are able to metabolize lipophilic toxic substances or neurotransmitters and thus protect the brain. The toxin and drug-metabolizing enzymes may be categorized by their role (Minn et al. 1991). Some enzymes functionalize lipophilic substrates, such as cytochromes P-450, other enzymes covert metabolites to polar molecules, by conjugating them with a small molecule which can be excreted (Minn et al. 1991). An example of the latter is glutathione-S-transferase that conjugates glutathione onto metabolites (Minn et al. 1991).

1.1.4 Modelling the blood-brain barrier for *in vitro* research

Models of the blood brain barrier have been used to test drug transport or transport of drug vehicles, such as nanoparticles, *in vitro*. The easiest way to model the blood-brain barrier is to use brain endothelial cells only, as these are the first line of cells which will be in contact with the blood and therefore with the tested substances. The brain endothelial cells can be either isolated from an organism or an established cell line can be used. Several animal species have been used to isolate brain endothelial cells, including pig, rat, cow, mouse or human (Helms et al. 2016).

Using an *in vitro* cell line of brain endothelium is another option to model the blood-brain barrier. A cell line needs to have characteristics such as relevant expression of molecules that provide phenotype of brain endothelial cells, tightness and lack of permeability and high electrical resistance. Established cell lines can be either animal or human. Typical animal cell lines include bovine (SV-BEC) (Durieu-Trautmann et al. 1991), porcine (PBMEC) (Teifel & Friedl 1996), rat (RBE4) (Roux et al. 1994) or mouse brain endothelial cells (bEnd5, bEnd3, cEND, cereBEND) (Reiss et al. 1998; Omidi et al. 2003; Förster et al. 2005; Silwedel & Förster 2006). From human tissue, several cell lines have been established, including hBMEC (Human brain microvascular endothelial cells) (Stins et al. 2001; Stins et al. 1997), hCMEC/D3 (human cerebral microvascular endothelial cells) (Weksler et al. 2005) or TY20 (spinal cord microvascular endothelial cells) (Maeda et al. 2013). Another way to create a model of brain endothelium is to use human-derived stem cells (Boyer-Di Ponio et al. 2014; Lippmann et al. 2012; Cecchelli et al. 2014).

The blood-brain barrier model can be improved by including cell types of the neurovascular unit in the culture as this may improve some characteristics of the brain endothelium, such as increase in cell junction tightness (Helms et al. 2016). The cells used for this co-culture can be astrocytes (Cecchelli et al. 1999; Zozulya et al. 2008), pericytes (Zozulya et al. 2008) or neurons (Stanness et al. 1999).

To conclude, the blood-brain barrier can be modelled *in vitro* which may then help to find therapeutic solutions *in vivo*. The ways to overcome the blood-brain barrier in order to deliver drugs are detailed in the following section.

1.2 Approaches to overcome the blood-brain barrier for therapeutic purposes

As mentioned above (Section 1.1), the blood-brain barrier forms not only a physical barrier between the blood and the brain but also is metabolically active. It controls which substances pass through the brain endothelium via its efflux transporters and also contains enzymes that can metabolize drugs (Begley 2004b). The existing therapeutic solutions that would be able to treat brain disorders, such as drugs, enzymes, or genes are no use since they cannot pass the blood-brain barrier (Pardridge 2005). Thus, in order to deliver or enhance the delivery of drugs, several approaches may be employed that overcome the hurdle of the blood-brain barrier. These approaches are described below and include invasive injections, or many non-invasive approaches, e.g. formulation of prodrugs, modulation of the blood-brain barrier, nasal delivery, and nano-carriers.

1.2.1 Invasive approach

Various mechanical approaches have been tried to deliver drugs into brain, such as disruption of the blood-brain barrier, using a catheter, implantable microspheres and microchips.

Disruption of the blood-brain barrier is aimed at disrupting tight junctions or facilitating paracellular movement. This may be performed using hyperosmolar mannitol (Neuwelt et al. 1991), bradykinin (Schürer et al. 1989), ultrasound (Cho et al. 2002) or electromagnetic radiation (Schirmacher et al. 2000). This approach is still considered to be risky due to entry of other substances that would not normally have access to the brain tissue, such as albumin, neurotransmitters, amino acids, xenobiotics or pathogens (Patel et al. 2009; Begley 2004b).

Alternatively, a **catheter** can be introduced into the brain to directly infuse drugs, as first reported in 1963 (Ommaya 1963). Since then, it has been successfully used to treat cancer pain by infusing morphine (Goudas et al. 1999). Another approach to reach the brain is using implantable **microspheres.** Biodegradable microspheres have been successfully implanted into brain tumours (Menei et al. 2004). Technological advances have helped the field by using an implantable **microchip**, which can have up to 1000 different compounds inside. It works on a principle of slow dissolution of the anode membrane which causes a release of compounds from different compartments of the chip (Patel et al. 2009). However, the effectiveness of this method will depend on brain compatibility and its ability to enter those brain cells which are to be treated.

The disadvantages of the invasive approach are several. Firstly, as with any surgical procedure, there is a great risk to the patient due to introduction of infection. Also, it is possible that the operation will cause damage to the brain tissue especially around the device (Begley 2004b).

1.2.2 Modifications of drugs

In order to treat the brain, drug transport across the blood-brain barrier can sometimes be achieved by changing the design of the drug. Modifications such as lipidation, use of a prodrug or attaching biological molecules to the drug have been successfully used.

Lipidation was the first drug modification that overcame the blood-brain barrier. It is based on adding lipid-like molecules to a drug and thus making it more hydrophobic to passively cross the blood-brain barrier. It has been proposed that lipophilicity corresponds to brain penetration (Levin 1980). Sometimes certain lipophilic drugs may still have poor brain penetration, perhaps due to the effect of efflux transporters (Begley 2004a). It may be possible to

inhibit efflux transporters, however more needs to be known about the mechanism by which they interact with the drug and ultimately operate (Begley 2004a). Another drawback of using lipidation is that it is not a brain-targeted approach as it allows drug diffusion across other plasma membranes in the body (Patel et al. 2009). Moreover, it may also increase the size of drugs thus lowering their effectiveness (Fischer et al. 1998).

Another way of targeting is synthesis of a **prodrug.** A prodrug is metabolized enzymatically or chemically into a drug in the cell or in the extracellular space and can affect brain parenchyma. A prodrug may transport more easily across the blood-brain barrier, however in a drug form it may become "locked" within the brain and thus unable to transport back into the blood. A typical example is heroin, which is deacetylated in the brain parenchyma into morphine which has low penetration of the blood-brain barrier and thus accumulates in the brain (Begley 2004b). Moreover, it is possible to improve targeting of a prodrug by conjugating it with a "targetor" (Han & Amidon 2000).

B**iological molecules** can be attached to the drug or can be mimicked by the drug synthesis thus giving it the advantage of a biological targetor as well as enhancing the penetration of the blood-brain barrier. This principle exploits the transport systems at the brain endothelium, whether these are carrier-mediated transport or macromolecular transport. Carrier-mediated transporters may be used by drugs mimicking amino acids, vitamins, hexoses or neuropeptides (Patel et al. 2009). However, these transporters are usually very selective and specific (Begley 2004b). Macromolecular transport can be also exploited, such as the transferrin receptor that has been targeted by monoclonal antibody OX26 (Friden et al. 1991; Pardridge et al. 1991) to deliver many therapeutically useful molecules (BDNF, NGF etc.) (Begley 2004b).

The observation of brain-penetrating viruses has led to a new system of delivery strategies for the brain. These use small penetrating peptides, such as TAT (trans-activating

transduction) peptide from HIV virus (Zhao & Weissleder 2004), or penetratin and OEGelin (Patel et al. 2009) and they can be used to deliver attached drugs to the brain.

1.2.3 Nasal delivery

The olfactory route has been discovered as a way to deliver certain molecules into the brain (Thorne et al. 1995), and certain bacteria and viruses use this route as well. The principle of this path lies in exploiting the fact that the olfactory neurons that sense molecules in the nose extend into the brain (Figure 1.4). The olfactory neurons penetrate the basal lamina and merge into nerve bundles, which penetrate the cribriform plate that separates the brain from the nose and finally reach the brain in the region of the olfactory bulb (Lochhead & Thorne 2012). The penetration of drugs via this route is also enhanced when drugs are lipophilic (Sakane et al. 1991) so not all drugs may be delivered via this route. The mechanism of transport of molecules is considered either intracellular (i.e. molecules moving through cells) or extracellular (i.e. molecules moving via extracellular spaces) (Lochhead & Thorne 2012). Successful drug delivery has been achieved in animals for insulin-like growth factor (Thorne et al. 2004) or interferon β1B (Thorne et al. 2008).

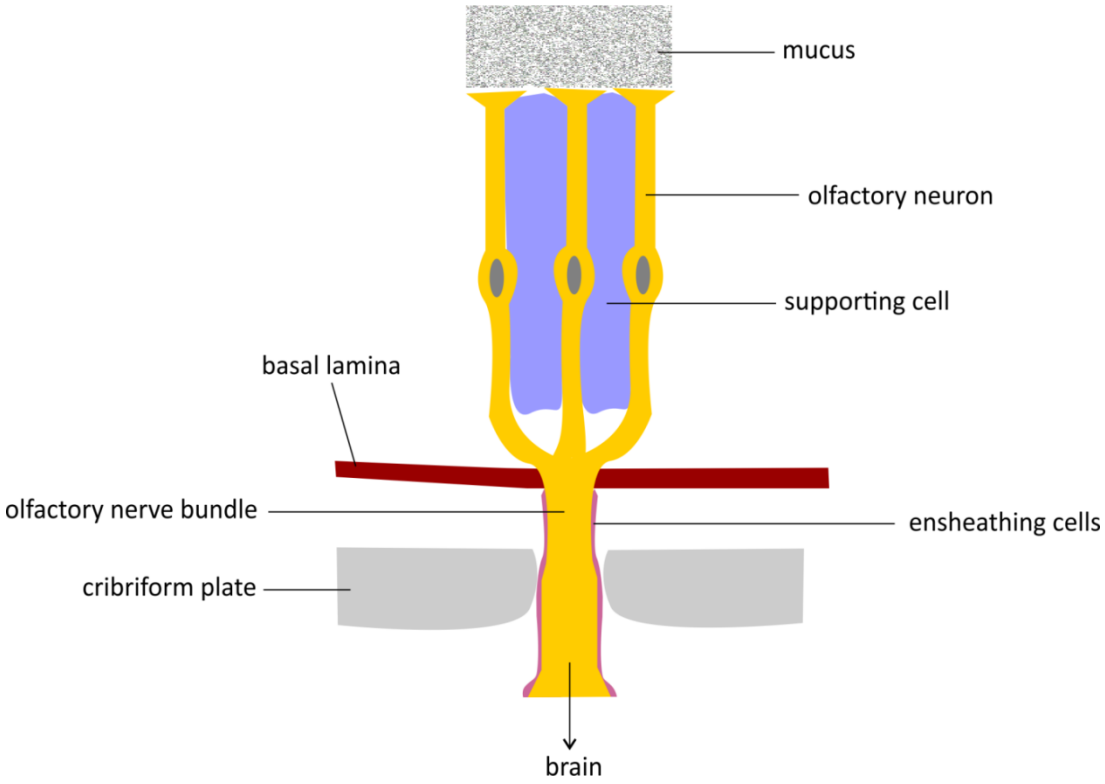

Figure 1.4. Organization of the olfactory neurons. The olfactory neurons sense within the mucus of the nose, they penetrate both basal lamina and cribriform plate where they form nerve bundles with other olfactory neurons that then reach the brain in the olfactory bulb.

Many substances have been successfully delivered into the animal models of diseases using the above invasive and non-invasive routes, such as BDNF (Yan et al. 1994), VEGF (Yang et al. 2009) or TGFβ (Ma et al. 2007). Despite this, these modes of transport have been failing in clinical trials. For example Alzheimer's disease has not had a new drug pass clinical trials for 10 years (Langley 2014) despite large research efforts. Therefore, a new proposal has emerged, to use nanoparticles as a delivery system, to improve the delivery of the drugs into the brain.

1.2.4 Nanoparticle-mediated delivery of therapeutic molecules

Nanomaterials have several applications, one of which is medicine. Nanoparticles are defined as objects in the size range between 1 and 100 nm according to International Organisation for Standardization (ISO). Nanoparticles have distinctive properties that are different from those of the bulk material; some of them will be discussed in the following section related to gold nanoparticles.

Nano-carriers for medicinal use can be made from several materials that have been found useful for many applications, such as diagnostics, therapy, or even theranostics, i.e. therapy and diagnostics combined. The list of the most common nanomaterials used in nanomedicine is listed in Table 1.2, with their advantages and disadvantages.

Table 1.2. Most common nanomaterials used in nanomedicine; their advantages and disadvantages.

Type of nanomaterial	Advantages	Disadvantages	Review article
Silica nanoparticles	Synthesis in variety of shapes and sizes Drug loading inside the pores of the material	If coating not stable, nanoparticles can cause haemolysis	(Roggers et al. 2014)
Magnetic nanoparticles	MRI agents already in medicine Theranostic application	If uncoated, can interact with proteins and lead to opsonisation	(Veiseh et al. 2010)
Gold nanoparticles	Synthesis in variety of shapes and sizes Optical properties useful for therapy and diagnosis	Ligand attachment limited to thiols and amines	(Dykman & Khlebtsov 2012)
Quantum dots	Optical properties useful for imaging	Usually only in small sizes Typically made out of heavy metals, concerning for clearance	(Drbohlavova et al. 2009)
Carbon nanotubes	Drug loading inside the material Theranostic application	Low biocompatibility and safety	(He et al. 2013)
Liposomes	Biocompatible Biodegradable Drug loading inside the material	Quick capture by reticuloendothelial system Accumulation in liver and spleen Main delivery via passive targeting	(Bozzuto & Molinari 2015; Schnyder & Huwyler 2005)
Polymeric nanoparticles and dendrimers	Can be biodegradable and biocompatible Synthesized to various sizes and complexities	Synthesis or extraction complicated and costly	(Muhamad et al. 2014; Costantino 2010)

1.2.4.1 Nanomaterials as a potential drug-delivery system for the brain

Nanomaterials may also be a useful drug-delivery system. The therapeutic potential of nanoparticles lies in their design; they may be able to regulate release of drugs and their penetration through the tissues, they may increase stability in blood-circulation, or they may improve solubility and availability of the drug. Moreover, targeting molecules can be also added to the nanoparticles, increasing their tissue specificity (Yang 2010). Due to their high surface-to-mass ratio, a potentially high number of molecules and therefore drugs can be attached to their surface (Begley 2004b).

In essence, two types of nanoparticle delivery systems can be considered: a) encapsulating system, where drug is enclosed within a nanoparticle core, or b) surface-attached system, where drug is attached to the nanoparticle surface (Figure 1.5). Molecules that may be attached to the nanoparticle surface may also include cell targeting molecules in order to enhance cell-selectivity of the delivery system. Moreover, other molecules, such as stabilizing groups, may be necessary in order to improve circulation half-life in blood and reduce capture by the reticuloendothelial system (Alyautdin et al. 2014). As a stabilizing molecule, it is possible to add OEG (polyethylene glycol) chains (this process is sometimes called OEG-ylation). This has been successfully used to coat liposomes and form OEG liposomes (Uster et al. 1996; Gabizon et al. 1994) as liposomes themselves are not very stable in the blood and are rapidly cleared by macrophages (Alyautdin et al. 2014). OEG-ylation has been used in liposomes loaded with glucocorticoids and shown to be helpful in treating multiple sclerosis in an animal study (Schmidt et al. 2003).

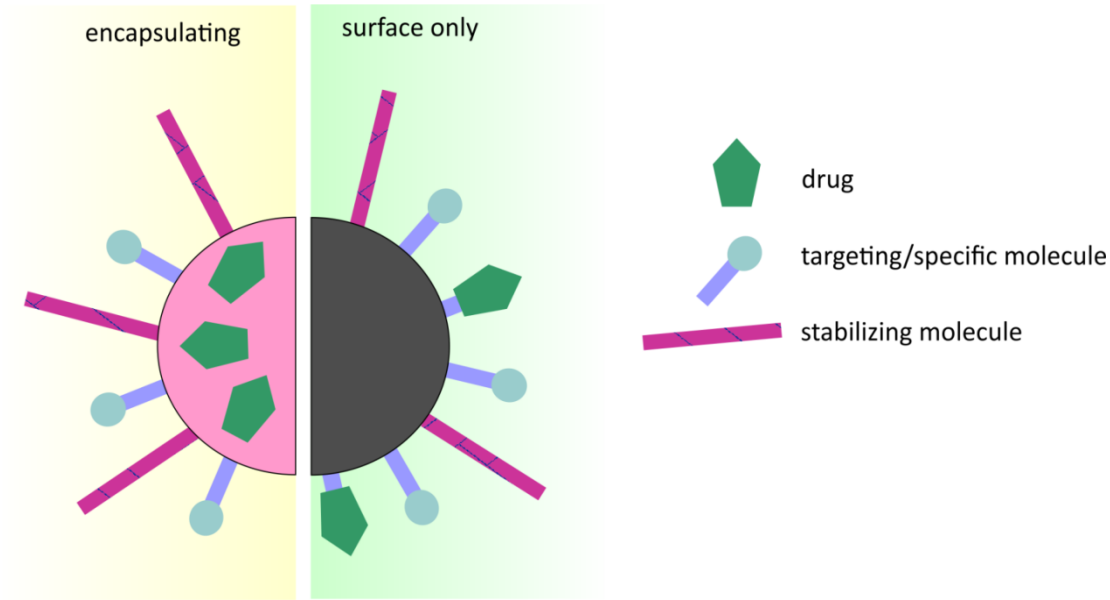

Figure 1.5. Scheme of a nanoparticle formulation for drug delivery. Nanomaterials can either encapsulate drugs or bind them on their surface. Additional molecules such as targeting or cell-specific molecules can be added to improve cell-selectivity. Moreover, stabilizing molecules that improve blood circulating half-life, such as polyethylene glycol (OEG) may be also added.

The ultimate aim of the pharmaceutical industry and research is to design a nanoparticle carrier that is able to deliver drugs into the brain without changing the properties of the blood-brain barrier. Even though an "ideal" nano-carrier has not yet been discovered, many nanomaterials have gone through large research efforts in order to bring them closer to the potential clinical applications, as discussed below.

1.2.4.1.1 Liposomes

It is known that lipidation helps to move drugs across the blood-brain barrier Therefore, whole particles based on lipids, i.e. liposomes, have been created and widely used for drug delivery into brain. Liposomes are similar to micelles. Micelles are only a single lipid layer whereas liposomes form a lipid bilayer that is in a ball form, i.e. a shell within which a substance of interest can be encapsulated.

Table 1.3 summarizes recent research using liposomes as a delivery system into the brain.

Liposomes have also found use as a general drug-release system in the blood. This may be possible when their circulation half-time in blood is designed to be high. They can then slowly release pharmaceuticals, for example irinotecan, doxorubicin, nerve growth factor, galanthamine, asialoerythropoietin, citicoline and tissue plasminogen activator (Alyautdin et al. 2014).

Table 1.3. Examples of liposomes for brain-specific targeting and drug delivery into normal and cancerous cells. Various molecules have been attached on the outside of the liposomes and some of them also have a therapeutic cargo inside the liposomes. The liposomes are used both for in vivo and in vitro studies. mAB – monoclonal antibody, hCMEC/D3 – human cerebral microvascular endothelial cell line D3, EGFR – epidermal growth factor receptor, GFAP - glial fibrillary acidic protein.

Molecule on the outside	target	cargo	cells/animals	Ref
mAb OX-26	Transferrin receptor	Gene (beta-galactosidase or luciferase)	rats	(Huwyler et al. 1996)
		none	*In vitro*, human hCMEC/D3	(Markoutsa et al. 2011)
anti-GFAP antibody	GFAP	none	*In vitro*	(Chekhonin et al. 2005)
mAB anti-GFAP and the recombinant E2 extracellular loop of connexin 43	GFAP, connexin 43	none	rats	(Chekhonin et al. 2012)
anti-transferrin receptor antibody Rl7217	Transferrin receptor	none	*In vitro*, hCMEC/D3	(E. Salvati et al. 2013)
apo100 recombinant peptide	LDL receptor	doxorubicin	hCMEC/D3 cells, human brain or epithelial tumour cells	(Pinzón-Daza et al. 2012)
p-aminophenyl-α-D-manno-pyranoside (MAN) and transferrin	GLUT transporters, transferrin receptor	daunorubicin	murine C6 glioma cells; mouse	(Ying et al. 2010).
lactoferrin	Lactoferrin receptor and other unspecified receptors	radioisotope complex 99mTc labeled N,N-bis(2-mercaptoethyl)-N',N'-diethylethylenediamine	bEnd.3 cells (murine brain endothelial cells); mouse	(Huang et al. 2013)
Anti- heparin-binding epidermal growth factor-like growth factor	heparin-binding epidermal growth factor-like growth factor	doxorubicin	Vero-H cells, MDA-MB-231 human breast cancer cells; mouse	(Nishikawa et al. 2012)
mAB anti-insulin receptor	Insulin receptor	human EGFR antisense gene	U87 human glioma cells	(Zhang et al. 2002)
TAT peptide	No specific receptor	none	Rat brain capillary endothelial cells, murine C6 glioma cells	(Qin et al. 2012)
transferrin	Transferrin receptor	5-Fluorouracil	rats	(Soni et al. 2008)
Sendai virus	unknown	Quantum dots with mAB anti-EGFR	medulloblastoma-derived Daoy cell line (pediatric brain tumor), glioblastoma-derived U251 cells (adult brain tumor)	(Dudu et al. 2012)

Apolipoprotein E-derived peptide, phosphatidic acid	Not specified		hCMEC/D3 cells; mouse	(Bana et al. 2013)
mannose-vitamin E derivative conjugate (MAN-TPGS$_{1000}$) and dequalinium-lipid derivative conjugate (DQA-OEG$_{2000}$-DSPE)	GLUT transporter, other not specified	Paclitaxel, artemether	Glioma C6 cells, murine brain microvascular endothelial cells; rats	(Li et al. 2014)
Transferrin and poly-L-arginine	Transferrin receptor, cell penetration	None or β-galactosidase plasmid for *in vivo* study	bEnd.3 cells, rat primary glial cells; rats	(Sharma et al. 2012; Sharma et al. 2013),
Folate and transferrin	Not specified	doxorubicin	C6 glioma cells, bEnd3 cells; rats	(Gao et al. 2013)

1.2.4.1.2 Polymer-based nanoparticles

Polymer-based particles and nanoparticles are another popular drug delivery system into the brain. The polymer matrix of the particles can be made of several different compounds, such as of poly(alkyl cyanoacrylates); polyesters such as polylactides (PLAs); poly (D,L-lactide-co-glycolate) (PLGA); protein albumin; chitosan; solid lipids; polyethyleneimines and polysaccharides. This category of polymeric nanoparticles also includes dendrimers, which are highly organized branched organic macromolecules, such as poly(amidoamine) or in short "PAMAM".

Polymeric nanoparticles have some similarities with liposomes but some of their properties are unique. Similarly to liposomes, proteins from the serum can adsorb on polymeric particles, which can facilitate formation of large aggregates with one another and thus be quickly cleared by phagocytic cells (Pinto Reis et al. 2006). There are several ways to increase the circulation half-life; by reducing their size (Alyautdin et al. 2014) or by addition of surfactants to their surface (Tröster et al. 1990), such as OEG, polysorbate 80 or polysaccharides (Pinto Reis et al. 2006). For example, polysorbate 80 has been found to improve blood-brain barrier penetration via endocytosis in comparison with polymeric nanoparticles not coated

with polysorbate 80 (Alyaudtin et al. 2001). A therapeutic cargo can be carried on the outside of the particle (nanosphere), implemented in the polymeric structure (nanomicelle) or in the inside compartment (nanocapsule) (Griffiths et al. 2010).

There have been a number of studies using many different polymeric nanoparticles as a drug delivery system into the brain. **Polybutylcyanoacrylate** has been loaded with the opioid dalargin and investigated for penetration of mouse brains (Alyaudtin et al. 2001; Kreuter et al. 1995). A similar design of nanoparticles has been used to deliver the alkaloid tubocurarine, a relaxant of skeletal muscles which does not normally penetrate the blood-brain barrier. These nanoparticles caused seizures when perfused into rats, which tubocurarine alone can cause only when injected into brain ventricles (Alyautdin et al. 1998). The same group also investigated loperamide on the same polymer-based nanoparticles and their transport into mice (Alyautdin et al. 1997); loperamide was also delivered into mouse brain by human serum albumin nanoparticles with attached apolipoprotein E (Michaelis et al. 2006). The drugs rivestigamine, glucitabine, tacrine or doxorubicin were delivered into the brain via polybutylcyanoacrylate particles with polysorbate 80 (Alyautdin et al. 2014).

Other types of matrices of polymers for brain delivery include polylactide or polystyrene particles coated with virus-derived peptides. **Polylactide** particles coated with TAT-peptide and loaded with the antiretroviral drug rotinavir were able to penetrate the blood-brain barrier of mice and release the drug over a period of 2 weeks (Rao et al. 2008). **Polystyrene** particles with *Herpes simplex*-derived glycoprotein gh625 used in an *in vitro* study showed increased uptake and crossing of the brain endothelial cells compared to the control particles without the protein (Guarnieri et al. 2013).

Polymer-based particles also include dendrimers, i.e. highly branched molecules. For brain delivery, the use of one type of dendrimer, PAMAM (polyamidoamine) dendrimer, became very popular. PAMAM dendrimers were developed first in 1985 (Tomalia et al. 1985).

They have a very useful property – they can electrostatically associate with DNA (Bielinska et al. 1999), which meant that they have been investigated as a way to transfect cells *in vitro* or deliver DNA/RNA *in vivo*. This delivery has been achieved by using several targeting molecules attached to OEG. For example, PAMAM dendrimer with Angiopep was able to enter brain possibly by an LRP-mediated endocytotic mechanism (Ke et al. 2009). Dendrimers with other targeting molecules were used, such as lactoferrin, transferrin (Huang et al. 2008) or peptide from rabies virus glycoprotein (RVG29) (Liu et al. 2009). However, both polymeric nanoparticles and dendrimers have a disadvantage in requiring a long process of isolation or production (Muhamad et al. 2014).

1.2.4.1.3 Other nanoparticles

Most of the research on drug delivery into brain used liposomes or polymer-based nanoparticles. Solid nanoparticles, with a hydrophobic core and phospholipid bilayer on the outside, are also mentioned in the literature (Alyautdin et al. 2014). In this section, inorganic nanoparticles such as metallic ones or made with silica are briefly described.

Iron oxide nanoparticles have been used as a potential therapeutic delivery system, for example using anti-PECAM-1 antibody as a targeting molecule. These nanoparticles crossed brain endothelial cells (cell line hCMEC/D3) and entered the brains of rats, but were also found in lungs in high levels compared to the control (IgG coated nanoparticles) (Dan et al. 2013). However, using iron oxide as a means of delivery or treatment into the brain has been discouraged by the findings of Hohnholt et al., (2013). They found that astrocytes can process metallic ions from the nanoparticles and store them intracellularly rather than export them out of the cell. The authors suggested that the reason might lie in the astrocyte's capability to protect brain from potential cytotoxic properties which these ions might possess.

Silver nanoparticles have not been used for targeted delivery as they are toxic both *in vivo* (van der Zande et al. 2012) and *in vitro* (Grosse et al. 2013), where the uptake and distribution was described using brain endothelial cells (Tang et al. 2010). However, the intrinsic toxicity of silver might be useful in using silver nanoparticles to treat brain tumours (Wang et al. 2013).

Other types of inorganic material - silica or titanium oxide nanoparticles - have been shown to enter brain endothelial cells *in vitro* (Ye et al. 2013). Their clinical application might be difficult to pursue as silica nanoparticles have shown neurotoxicity in mice and cytotoxicity *in vitro* (Wu et al. 2011), also titanium oxide nanoparticles are cytotoxic (Zhang et al. 2012).

Another type of nanoparticle, gold nanoparticles, might have a potential for drug delivery into the brain as explained in detail in the following section.

1.3 Gold nanoparticles

Gold nanoparticles have been part of our lives since the medieval times. It was well known how to colour panes of glass in churches red – using gold nanoparticles. But it is not just the optical properties that are intriguing; gold nanoparticles are red in colour rather than gold as their bulk relative. This part will show how the properties of the gold core affect nanoparticle stability. Next, the various ligands that have been attached to gold nanoparticles are briefly discussed, but gold nanoparticles cannot be used in animal models or in clinics unless toxicity is investigated as well as the mechanism of transport into the cells.

1.3.1 The properties of the gold core – from shape to chemistry

1.3.1.1 Shape, size and surface reactivity

Gold nanoparticles can be synthesized in several shapes, such as nanospheres, nanorods, nanocages and nanoshells. The most commonly used shape for drug-delivery research is nanospheres. This thesis is focused on using gold nanospheres. Information on the chemical properties of gold nanocages and nanoshells has been reviewed elsewhere (Jelveh & Chithrani 2011; Hu et al. 2006; Xia et al. 2011).

Another characteristic of the gold core is its size. The most common size of gold nanoparticles that is used for application in biology ranges between 1.5 nm to 50 nm in diameter (Guerrero et al. 2010; Sadauskas et al. 2007; Gu et al. 2009; Lin et al. 2012; Libutti et al. 2010; Sandhu et al. 2002; Prades et al. 2012; Peckys & de Jonge 2014; Elbakry et al. 2009; Fraga et al. 2013; Yang et al. 2005). The size is a very useful determinant of surface properties of the nanoparticle, i.e. how many surface atoms might have the ability to react and form a bond. This surface atom reactivity will also depend on stericity of potential ligands and can be calculated.

For example, gold nanoparticles of 2.2 nm diameter have been calculated to have about 162 surface atoms (Hostetler et al. 1998). However, Hostetler calculated that not all of them can form bonds – in this example, there would be only 92 atoms available to form bonds. Moreover, the smaller the nanoparticle, the larger the surface-to-volume area; small nanoparticles might therefore have over 50% of their surface atoms available for reaction.

1.3.1.2 Physical properties of the gold core

Gold nanoparticles have many useful properties, such as optical properties, heat-generating or magnetic properties.

Optical properties of gold nanoparticles are well studied; they are responsible for difference in colour of nano-sized gold from its bulk relative. The reason for this phenomenon is a surface plasmon resonance (SPR). It induces a strong absorption band at around 520 nm, and can be determined by a spectrophotometer in the range of UV-visible (Huang et al. 2007). The position of the SPR peak is not a given for a certain nanoparticle core, in fact surface ligand coating may change the position of the SPR peak (Hu et al. 2006). Therefore, the optical properties of gold nanoparticles are useful for detecting gold, measuring gold concentration or characterization of nanoparticle size, shape or ligand coating (Huang et al. 2007).

Gold nanoparticles are also able to quench fluorescence, especially if they are less than 40 nm in diameter (Swierczewska et al. 2011). Quenching happens when a gold nanoparticle is at a certain distance from a fluorophore (Dulkeith et al. 2005), the nanoparticle's surface plasmon resonance may change the excitation/emission property of the fluorophore, preventing it from emitting light (Kang et al. 2011).

Gold nanoparticles are also able to generate heat after absorbing light. This heat can then be dissipated to its surroundings, or can cause the nanoparticle to melt, as in case of nanorods (Link et al. 1999). Moreover, the nanoparticle-generated heat may cause a structural change and ablation of gold core. This heating property has found use in photothermal therapy (Huang & El-Sayed 2010; Day et al. 2011).

Subtle magnetic properties have been also reported in gold nanoparticles (Nealon et al. 2012). However, the explanation for magnetism of gold is still controversial (Nealon et al. 2012).

1.3.1.3 Synthesis of gold nanoparticles

Gold nanoparticles are easy to synthesize, as in principle, the formation of gold nanoparticles occurs when gold salt is reduced in the presence of a stabilizing agent. There are two general methods to synthesize gold nanoparticles, the Turkevich method and Brust-Schiffrin method.

The Turkevich method was first applied in 1951 (Turkevich et al. 1951). The reducing and stabilizing agent is sodium citrate, which yields gold nanoparticles of about 20 nm in diameter (Figure 1.6A). In order to change the nanoparticle size, the ratio of gold to sodium citrate can be varied (Frens 1973).

The "Brust-Schiffrin" method (Brust et al. 1994) revolutionised the nanotechnology field as it achieved very stable and small nanoparticles. Sodium borohydride acts as a reducing agent and alkanethiols as stabilizing agents. Due to the fact that the reaction is performed in 2 phases (water-toluene), tetraoctylammonium bromide is used as a phase-transfer reagent (Figure 1.6B). The reaction results in nanoparticles of 1 - 3 nm in diameter. Later, monolayer-protected gold clusters soluble in water were reported (Templeton et al. 1998; Ackerson et al. 2005).

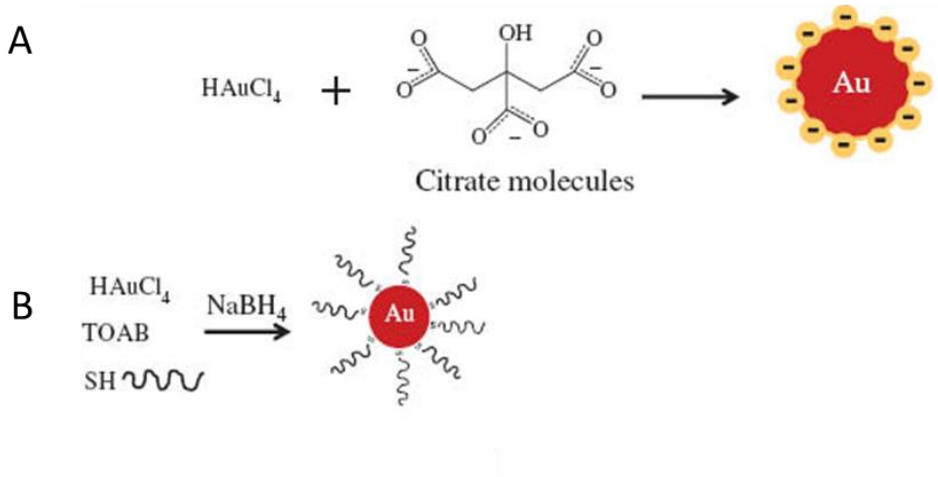

Figure 1.6. Schematic representation of two methods to synthesize gold nanoparticles. A. Turkevich method of citrate reduction creates stable negatively charged colloidal gold nanoparticles. B. Brust-Schiffrin's reaction results in nanoparticles stabilized with thiolated molecules attached to the gold core. Adapted from (Remant Bahadur et al. 2014).

1.3.2 The properties of surface ligand molecules

If gold nanoparticles were not coated or stabilized with ligands, they would retain their reactive abilities, much valued in engineering (Hvolbæk et al. 2007). Moreover, a successful nano-carrier depends on careful choice and design of ligands, i.e. molecules attached to the nanoparticle surface. As mentioned in section 1.2.4, surface molecules that can be attached include targeting molecules, therapeutic cargo, or other molecules (stabilizing, imaging/tracking) (Figure 1.5). The stability of the ligands can be modulated by the way in which they are attached, either covalently or non-covalently. Moreover, this section also introduces the ligand exchange reaction that is used for simple coating of nanoparticles.

1.3.2.1 Attachment of ligands to gold nanoparticles

The ligand molecules that have been used to stabilize and transport nanoparticles into the cells may have a charge, i.e. a neutral one (Gromnicova et al. 2013), a negative one (Schleh et al. 2012) or a positive one (Schleh et al. 2012). Moreover, gold nanoparticles may also be coated with both positively and negatively charged ligands (Elbakry et al. 2009; Wurster et al. 2013; J.-S. Lee et al. 2008). However, a specific synthetic approach must be employed to prevent nanoparticles from aggregating if the ligand addition occurs in a single reaction. Approaches to solve this issue include coating the nanoparticles layer-by-layer (Elbakry et al. 2009) or attaching polyethylene-glycol to the nanoparticle to keep nanoparticles separate and prevent aggregation (S. H. Lee et al. 2008).

Ligands can be attached to spherical gold nanoparticles either via a strong interaction (partly covalent) or by non-covalent electrostatic interaction (Figure 1.7). The strong interaction results in ligand attachment which is more stable. However, sometimes a weaker electrostatic bond is preferred as the release of the ligand is faster. The most used strong interaction to the gold core is a thiol bond and its variations, such as xanthates, disulfides, dithiols, trithiols or tetrathiols. This S-Au interaction is 35% covalent but mostly electrostatic. This interaction is widely termed as "covalent" (Ding et al. 2014). Other ligand interactions with the gold core exist, based on phosphine or amine groups (Daniel & Astruc 2004). The strength of the "covalent" bond can then be modulated by employing: (a) several thiols to attach a single ligand to the gold core, or (b) cyclic thiols such as a 1,2-dithiane end group (Letsinger et al. 2000) which increases the strength of the ligand bond.

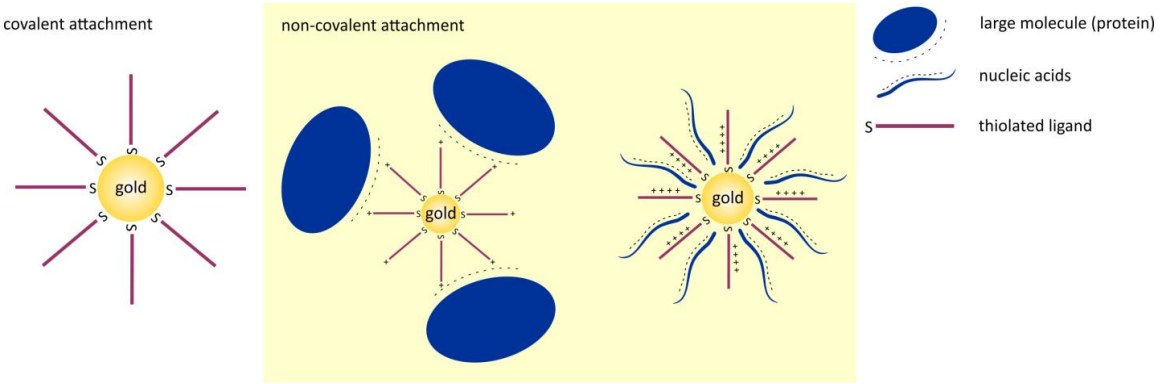

Figure 1.7. Ligand attachment to gold nanoparticles. Ligand molecules can be attached to the gold core either covalently via a thiol bond or non-covalently via electrostatic interactions. Non-covalent bond can then bind and capture molecules such as proteins or nucleic acids.

The electrostatic interactions are the basis for non-covalent attachment, where a charged group attracts an oppositely charged molecule. A thiol-bound group of nanoparticles that can carry a charge and thus bind other ligands are for example mixed alkanethiol-covered nanoparticles, termed as monolayer mixed-protected gold clusters (Templeton et al. 1998; Hostetler et al. 1998; Hostetler et al. 1996). These have been used by Rotello's group (McIntosh et al. 2001) who prepared gold nanoparticles (2 nm gold core) coated with both a neutral alkanethiol and a positively charged trimethylammoniumundecanethiol. The latter ligand contained positively charged amine groups that were able to capture DNA strands (McIntosh et al. 2001). The resulting nanoparticles have been also used to carry plasmids into human embryonic kidney cells (HEK 293T) (Sandhu et al. 2002). Another nanoparticle-attached charged ligand, polyethylenimine (PEI), has been shown effective in non-covalently holding plasmid DNA and transfecting cells (Thomas & Klibanov 2003).

1.3.2.2 Ligand exchange reaction and release of thiol-bound ligands

Murphy's group (Hostetler et al. 1996; Templeton et al. 2000) first described a very simple exchange reaction that occurs with thiol-bound ligands to the gold core. When an excess of free thiolated molecules is added to the mixture of thiol-coated gold nanoparticles, this excess of free thiols react with the gold core and some bind, exchanging for the already attached ligand (Figure 1.8). This reaction is particularly useful for ligand coating of gold nanoparticles with ligands that may be sensitive to the reducing environment of the Brust-Schiffrin reaction. In order for this the reaction to be favoured, the free thiolated ligand must be in molar excess to the gold.

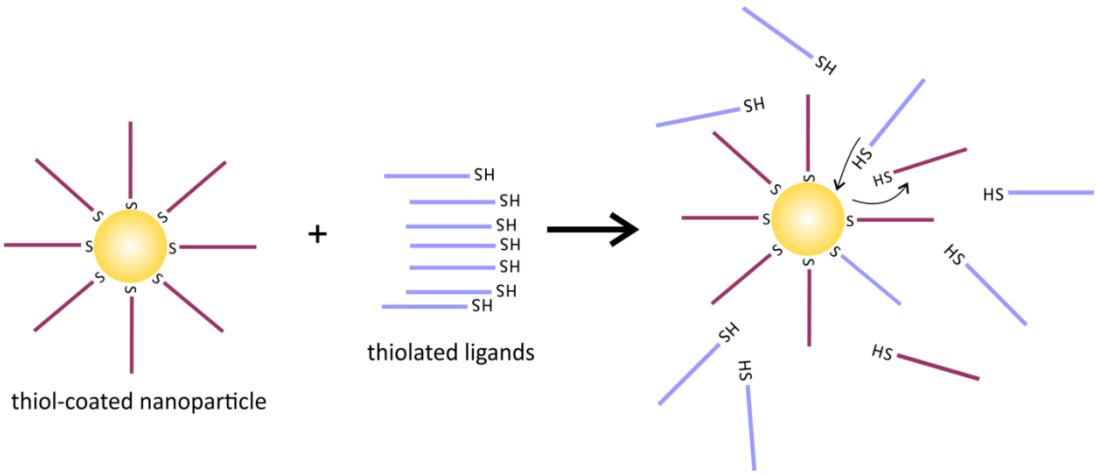

Figure 1.8. Ligand binding to gold core via ligand exchange (or place-exchange) reaction. If thiol-coated gold nanoparticles are incubated in the presence of a molar excess of free thiolated ligands, a reaction occurs which results in some free thiols binding onto the gold core, displacing and thus releasing the original thiolated ligands.

This reaction has been used both for coating nanoparticles as well as release of ligands from nanoparticles in cells. The fluorescent dye alkanethiol-BODIPY was attached using the ligand-exchange reaction to 2 nm gold nanoparticles (Atukorale et al. 2015). Furthermore, this thiol-induced release of thiolated ligands from the nanoparticle has been also demonstrated to occur within cells. Cells contain a relatively high cytosolic concentration of glutathione, which has been shown to release ligands from the gold core (Verma et al. 2004; Hong et al. 2006).

1.3.3 Gold nanoparticles in biological systems

1.3.3.1 Toxicity of gold nanoparticles in living systems

The toxicity of nanoparticles is an important consideration if they are to be used for biological or therapeutic purposes. However, as with any substance, it is highly dose-dependent and increasing dose over a certain threshold will induce toxicity. This threshold tolerance may cause cellular damage but it will highly depend on factors inherent to the nanomaterial, such as its ligand coating, preparation method, size, charge or shape, as discussed here.

1.3.3.1.1 Types of cellular damage that treatment with gold nanoparticles may cause

Several types of cellular damage caused by gold nanoparticles have been investigated, such as oxidative stress and mitochondrial damage, or DNA damage. Oxidative stress can be caused by nanoparticles coated with triphenylphosphine monosulfonate (Pan et al. 2009). Necrosis may be caused by these nanoparticles forming reactive oxygen species (ROS) which can lead to disruption of mitochondrial membranes as shown in HeLa cells. Similarly, Mateo et al. (2014) investigated gold nanoparticles of larger sizes, 30 - 90 nm in diameter, for causing cell damage. The authors correlated the nanoparticle-induced damage to leukaemia and hepatoma cell lines with a decrease in the cellular glutathione (GSH) levels and an increase in the ROS production.

The width of DNA is 2 nm so it is not surprising that small gold nanoparticles under 2 nm can bind to DNA (Tsoli et al. 2005), thus having a potentially damaging effect. However, not

all gold nanoparticles may enter the nucleus, in which case the resulting DNA damage may be caused by oxidative stress rather than by direct association with the DNA. On the other hand, very small gold nanoparticles can be effective in entering the nucleus and binding onto the DNA, such as 1.4 nm gold clusters with 55 gold atoms (Tsoli et al. 2005). This property may be useful for radiosensitizing therapy; however, a careful approach must be taken when testing nanoparticles on *in vitro* models. As the cell viability/membrane integrity decreases, it may cause false-positive nuclear localisation of gold nanoparticles. During the process of cell death, the gold nanoparticles may be able to enter the cell nucleus as the nuclear envelope starts to break down.

1.3.3.1.2 The effect of ligand or stabilizing coating on resulting nanoparticle toxicity

The toxicity of nanoparticles may depend on their coating or stabilizing agent, for example nanoparticles coated with glucose or cysteine and stabilized with citrate or biotin were non-toxic whereas nanoparticles stabilized with cetyltrimethylammonium bromide (CTAB) were highly toxic (Connor et al. 2005). Similarly, nanoparticles coated with triphenylphosphine monosulfonate were more toxic than those coated with glutathione (Pan et al. 2009).

1.3.3.1.3 The effect of synthetic methods on resulting nanoparticle toxicity

The preparation method for the synthesis and stabilization of nanoparticles may be crucial for cytotoxicity. In general, gold atoms as such are non-toxic, it is the gold salt which is toxic (Connor et al. 2005). Nanoparticles prepared by reduction using $NaBH_4$ in the presence of

sodium citrate (modified Brust-Schifrrin method) were used in a study investigating 5 nm and 15 nm citrate stabilized nanoparticles (Coradeghini et al. 2013). 5 nm nanoparticles produced decreased viability by about 50% but only after 72 hr exposure to 50 μM (Au) of nanoparticles. 15 nm nanoparticles were not toxic, however, the authors noticed a morphological change of Balb/3T3 cells at a high concentration of nanoparticles (300 μM Au) (Coradeghini et al. 2013). Another Brust-Schiffrin preparation of gold nanoparticles (3.5 nm in diameter) did not show oxidative stress in cells at a concentration of 100 μM (Au). Moreover, the nanoparticles showed an antioxidant effect on macrophages *in vitro* (Shukla et al. 2005). On the other hand, nanoparticles prepared by reduction with sodium citrate, via Turkevich synthesis, showed higher toxicity. 18 nm citrate-stabilized nanoparticles (50 μM Au) caused reduced cell viability by 35% after 24 hrs incubation with human hepatoma (HepG2) cells, and they also increased ROS (i.e. reactive oxygen species, markers of oxidative stress) in these cells (Paino et al. 2012). Similarly, 20 nm nanoparticles prepared by the same method also caused apoptosis (Choi et al. 2012). Therefore, the nanoparticle toxicity to cells depended upon the preparation method, concentration used and time of incubation.

1.3.3.1.4 Nanoparticles toxicity is affected by their size and varies between different cell lines

The size of nanoparticles or cell line tested also affects nanoparticle toxicity. Pan et al., (2009) showed that gold nanoparticles 15 nm in diameter were not toxic compared to 1.4 nm nanoparticles. Tsoli et al. (2005) also found similarly-sized nanoparticles (1.4 nm gold clusters) to be toxic in cancer and normal cell lines.

Another point to consider when evaluating nanoparticle toxicity *in vitro* is the cell line used; it was shown that the nanoparticle toxicity depended on the cells used (Choi et al. 2012). Mostly cancer cell lines have been used to study gold nanoparticle toxicity. The cells may

originate from human or animal sources; many *in vitro* studies on gold nanoparticle toxicity were reviewed in (Khlebtsov & Dykman 2011). The examples of cell lines used include mouse macrophage RAW 264.7 (Liu et al. 2013), human hepatocarcinoma HepG2 cells (Liu et al. 2013; Fraga et al. 2013), human cervical adenocarcinoma HeLa cells (Niidome et al. 2006; Tkachenko et al. 2004), or human leukaemia (K562) (Connor et al. 2005).

1.3.3.1.5 The effect of charge on nanoparticle toxicity

The charge of the nanoparticles may also be an important factor in toxicity. The charge may cause nanoparticles to aggregate (Eghtedari et al. 2009), bind different proteins from serum (Arvizo et al. 2012) and enter cells more readily (Cho et al. 2009) or even cause a very different type of toxic effect, such as mitochondrial stress, change in cell morphology or cause of DNA damage (Schaeublin et al. 2011).

Nanoparticle surface charge may also affect intracellular processes. For example, cationic nanoparticles (compared with negatively charged or neutral nanoparticles) disrupted membrane potential and led to higher intracellular Ca^{2+} levels (Arvizo et al. 2011). These findings may be updated in future studies as the understanding of this process is not clear.

1.3.3.1.6 The effect of shape on nanoparticle toxicity

Gold nanoparticles come in different shapes and these too can affect their toxicity. In general, gold nanorods are considered to be more toxic (Niidome et al. 2006), but this is probably due to the synthetic process where a stabilizing agent CTAB is used. CTAB is highly toxic for cells and thus if a ligand coating of nanorods is optimized, such as using polyethylene glycol (OEG), the toxicity can be greatly reduced (Niidome et al. 2006).

1.3.3.1.7 Investigation of nanoparticle toxicity to animals and their elimination

In vitro evaluation might be helpful to determine the basic toxicity, however, it does not give certainty that nanoparticles that appear safe *in vitro* up to a particular dose will have no negative effect on animals. For example, gold nanoparticles that were not toxic for HeLa cells showed some toxicity in animals (Chen et al. 2009). Therefore, experiments using a wider range of tested cells or *in vivo* experiments may be necessary, especially in case of future applications of gold nanoparticles in clinics.

Nanoparticle toxicity *in vivo* has some similarities to the results found *in vitro*. For example, the size of nanoparticles appeared to matter in a study of gold nanoparticles in a broad range of sizes. Nanoparticles of sizes 8, 12, 17 and 37 nm negatively influenced the animals' weight, fur colour or appetite whereas nanoparticles <8 nm and >37 nm did not cause any detrimental effects to the animals (Chen et al. 2009).

Gold nanoparticles, if they are to be used in biological systems, need to have their elimination pathway examined. As the nanoparticles enter the body, they encounter proteins (part 1.3.3.2.3) which may increase their size, termed as the hydrodynamic diameter. Nanoparticle size and surface chemistry can be changed in order to modify their blood half-life, tissue distribution and bodily clearance (Longmire et al. 2008). Renal clearance is responsible for filtration of molecules smaller than 6 nm (Longmire et al. 2008). Liver then eliminates larger molecules. In the liver, hepatocytes and Kupffer cells catabolize and process larger molecules which, if not broken down and eliminated, remain within the cells (Kuntz & Kuntz 2006). As an example, gold nanoparticles of 20 nm have been found to remain present in liver and spleen even after 2 months (Balasubramanian et al. 2010). On the other hand, fast renal clearance was reported by Hainfeld et al. (2006) where 75% of 1.9 nm gold nanoparticles were cleared from the body after 5 h. In the case of renally-cleared nanoparticles, renal filtration over a longer time

period may need to be investigated as demonstrated by Simpson et al. (2013). In their study the majority (about 2/3) of 1.2 nm gold nanoparticles were rapidly excreted via kidney, however, some were still detected in liver and spleen after 4 weeks (Simpson et al. 2013).

1.3.3.2 Cell uptake of gold nanoparticles

The nanoparticles may be taken up into cells either actively by endocytosis or passively via passive membrane penetration. Both of these mechanisms of transport are detailed in Chapter 4 (section 4.1.1). In this part, the general properties of gold nanoparticles, such as the effects of their shape and size on uptake into cells are introduced. Moreover, investigations of exocytosis of nanoparticles are also briefly mentioned here.

1.3.3.2.1 The effect of nanoparticle shape and size on cell uptake

Shape and size of nanoparticles have been investigated in regards to efficiency of nanoparticle uptake into cells. The effect of nanoparticle shape is still controversial. When studying spherical and rod shaped nanoparticles, E. C. Cho et al. (2010) found no difference in the uptake mechanism, whereas Chithrani et al. (Chithrani et al. 2006; Chithrani & Chan 2007) found a better uptake of spherical nanoparticles into HeLa cells.

The size of nanoparticles that would be most effectively endocytosed has been investigated. Jiang et al. (2008) investigated nanoparticles in a wide size range of 1- 100 nm coated with Herceptin. They found that 25 – 30 nm was optimal for uptake into cells and noted a 50 nm size as a cut-off point for endocytosis. This finding has been explained by (Zhang et al. 2009) who theorized that the 25 - 30 nm size range is probably optimal for bending rigidity of the membrane and the binding energy of ligand–receptor. Also, if a receptor mediates the

transport of the coated nanoparticles, a certain concentration of the ligand coating would cause saturation of these receptors at which point the uptake will peak (Zhang et al. 2009). Chithrani et al. (2006) used a tighter size distribution; they investigated citrate-stabilized 14, 50 and 74 nm gold nanoparticles and observed that 50 nm nanoparticles were most effective in entering the cell. A very similar result to this study was shown with quantum dot nanoparticles where 50 nm particles yielded a higher uptake compared with 15 nm and 5 nm nanoparticles (Osaki et al. 2004).

On the other hand, small gold nanoparticles of <5 nm may not only be able to be endocytosed (Verma et al. 2008), they may also use passive transport into the cell. This may be particularly useful for transport into cell types that do not have as much active transport.

1.3.3.2.2 Exocytosis of nanoparticles

Most of the research interest has been on endocytosis but exocytosis is as important. Exocytosis may depend on incubation time of nanoparticles with cells and the cell types, for example Verma et al. (2008) did not observe exocytosis for 5 nm gold nanoparticles when incubated for 6 hrs in mouse dendritic cells (clone DC2.4). On the other hand, in one of our studies we have shown transcytosis of < 5 nm gold nanoparticles from brain endothelial cells (hCMEC/D3) even after 3 hrs (Gromnicova et al. 2013).

1.3.3.2.3 The effect of physiological environment on nanoparticles

Within the body or in the cell medium, nanoparticles may change their surface property due to several factors, such as protein absorption, or glutathione-dependent ligand exchange.

1.3.3.2.3.1 Absorption of proteins onto nanoparticles

1.3.3.2.3.1.1 Characteristics of the protein corona

When nanoparticles enter the blood or culture medium with serum, proteins may adhere to the nanoparticle surface forming a protein corona. This protein corona has been classified as "hard", which stays on the nanoparticle for a longer time period and "soft" corona, which exchanges from the nanoparticle surface over time where the proteins do not stay adhered for long (Milani et al. 2012). Interestingly, the protein corona never reaches binding equilibrium (Walkey & Chan 2012).

The protein corona is also characteristic of the route which the nanoparticle takes in the body. Therefore, it will be highly dependent on the site of administration – it will differ if the nanoparticle was administered orally, inhaled or injected (Lundqvist et al. 2011).

The surface ligands attached to the nanoparticle may also affect the corona composition. In general, hydrophilic nanoparticles (which are more resistant to protein absorption) absorb mostly albumin, fibrinogen and IgG, whereas hydrophobic nanoparticles absorb mostly apolipoproteins (Cedervall et al. 2007; Gessner et al. 2000).

1.3.3.2.3.1.2 Impact of the protein corona on the nanoparticle

It has been widely investigated what impact of the protein corona might have on nanoparticles. It may shield targeting ligands bound on the nanoparticles, change the overall charge of the nanoparticle (its zeta potential) or have an effect on bodily clearance.

The fact that the targeting ligands on the nanoparticles may be shielded by a protein corona has been shown recently. 50 nm SiO_2 nanoparticles coated with transferrin lost their targeting property to the transferrin receptor after absorption of proteins which "hid" the targeting molecule (A. Salvati et al. 2013).

The protein corona may have an impact on the charge properties of the nanoparticle as a whole – their zeta potential. The zeta potential describes the charge of a particle in a liquid environment of a defined pH. The zeta potential of the nanoparticles has been shown to change upon protein absorption to being negative, between -10 mV to -20 mV (Walkey & Chan 2012). For example, for 10 nm gold nanoparticles the zeta potential has been found to increase from the original -44 mV to the average charge of serum proteins, i.e. -10 mV (Casals et al. 2010). Interestingly, the proteins prevented aggregation of nanoparticles that would have happened at this zeta potential (Casals et al. 2010).

Lastly, the protein corona may influence the interaction of the nanoparticles with the immune system, i.e. when "opsonin" plasma proteins such as IgG or complement components adsorb onto nanoparticles. As a result, the nanoparticles can be recognized and cleared via mononuclear macrophages (Walkey & Chan 2012).

1.3.3.2.3.1.3 Overcoming protein absorption onto nanoparticles

There are several ways to overcome the issue of protein absorption – we can either design nanoparticles that will avoid the absorption or we can exploit this property.

To avoid the formation of a protein corona, the design of the nanoparticle may need to be carefully considered. Using a neutral or hydrophilic nanoparticle coated with various polymers, such as polyethylene-glycol (OEG) can prevent protein absorption. OEG can effectively repulse proteins, however, it can also lead to a loss of targeting specificity (Klibanov et al. 1991).

Another way to eliminate protein corona formation is to prepare nanoparticles with a structured ligand shell morphology. These nanoparticles do not absorb proteins compared to the same nanoparticles but with unstructured ligand morphology (Verma et al. 2008). This finding points out the possibility of designing nanoparticles with highly organized ligands, similar to a viral capsid. Another way to reduce protein absorption is to decrease the size of nanoparticle. For example 5 nm gold nanoparticles have lower protein absorption than larger gold nanoparticles (60 nm and 100 nm) possibly due to a geometric property of their surface curvature (Lacerda et al. 2010).

1.3.3.2.3.2 The effect of cellular glutathione on ligand release from nanoparticles

Another point to consider when designing a nano-carrier is the reducing environment in cells. One reducing agent, glutathione, may cause gold nanoparticles to release the ligands attached to the gold core. Glutathione exists in reduced (glutathione) and oxidized (glutathione disulphide) form. Glutathione contains a reactive thiol group which may react with the gold nanoparticle and cause a ligand-exchange reaction (Figure 1.9), as described previously (Section 1.3.2.2, Figure 1.8) and shown experimentally (Verma et al. 2004). The extracellular levels of glutathione are relatively low, however, in the cytosol it is up to 1000x higher. This factor can be used in the design of the nanoparticle to control the release of a potential therapeutic cargo.

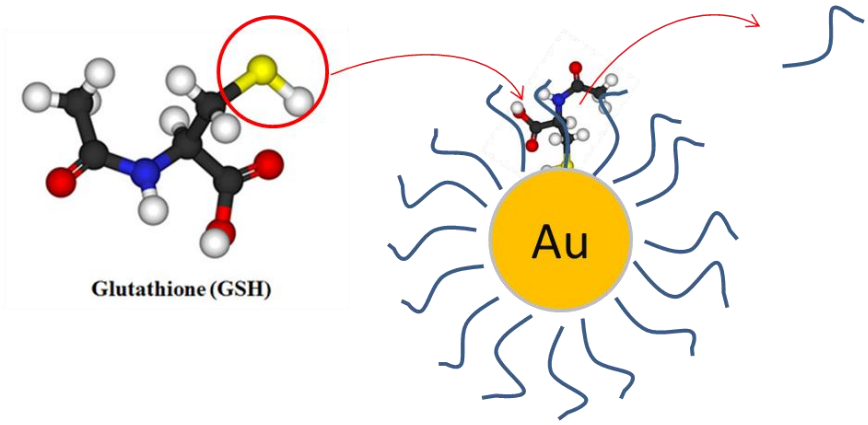

Figure 1.9. Interaction of monolayer-coated nanoparticles with glutathione. Glutathione contains a reactive thiol group (red circle) which may react with the gold core and exchange with the original ligand, causing the release of the ligand. This figure has been published elsewhere (Male et al. 2016).

1.3.4 Biological applications of gold nanoparticles

Gold nanoparticles are already used in several biological applications as introduced in this section. They are a useful tool for imaging of cellular molecules by electron microscopy but can also detect substances and thus be used in colorimetric or fluorescence-based sensing. Also, gold nanoparticles can be useful for delivery of various cargos; from oligonucleotides to drugs. This makes them a potential delivery system into tissues, such as brain, and several types of gold nanoparticles have been identified as able to cross the blood-brain barrier.

1.3.4.1 Imaging and detection

Gold nanoparticles have been traditionally used for imaging in the transmission electron microscope. Usually, a specific (primary) or non-specific (secondary) antibody is attached to the nanoparticle and labels the protein of interest inside a cell. This technique is

generally called immunoelectron microscopy; one of the examples is attaching IgG onto nanoparticles and investigating interactions of pathogens with human IgG (Ho et al. 2004).

Gold nanoparticles, due to their optical properties, have found use in dark-field microscopy. The principle is based on surface plasmon resonance scattering which is greater than the absorbed incident light and therefore it is possible to visualize objects under the detection limit of optical microscopy. This method is similar to immunoelectron microscopy as gold is conjugated to antibodies. It has been used for example in detecting cancer cells on the basis of binding to the epidermal growth factor receptor (El-Sayed et al. 2005).

1.3.4.2 Biosensing and diagnosis

Gold nanoparticles have been applied in several sensing strategies: colorimetric, fluorescent, electrochemical and catalytic. Only the first two will be briefly explained as they relate to biological applications - colorimetric sensing, which uses absorbance to detect changes in the sample, or fluorescence-based sensing measuring fluorescence from molecules released from the nanoparticles.

1.3.4.2.1 Colorimetric sensing

Colorimetric sensing uses absorbance to detect changes in the sample. The principle lies in gold nanoparticles forming larger aggregates, and thus causing a change in colour compared with dispersed nanoparticles. This type of sensing has been used to detect metal ions (such as Pb^{2+} or Hg^{2+}), anions (such as CN^{-}), small molecules (concanavalin A), proteins (platelet-derived growth factor) or oligonucleotides (Saha et al. 2012). Detection of oligonucleotides is based on hybridization of the nanoparticle DNA with the target DNA (Figure 1.10).

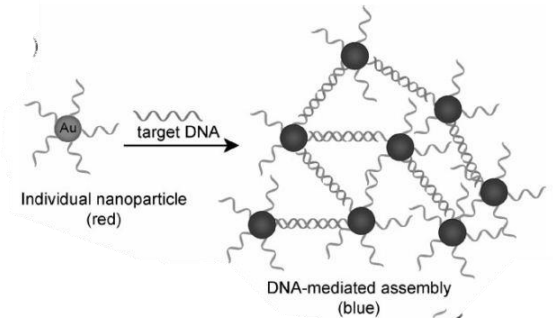

Figure 1.10. Gold nanoparticles as biosensors of oligonucleotides. DNA-attached gold nanoparticles in solution (with certain colour, such as brown) do not aggregate unless target DNA is added – this causes hybridization and formation of large aggregate which is detected by a colour change (such as blue). Adapted from (De et al. 2008).

1.3.4.2.2 Fluorescence-based sensing

The fluorescence-based sensing relies on fluorescence quenching properties of gold nanoparticles. Molecular beacon for sensing DNA is one of the uses, where a DNA strand with a fluorescent label is attached to a gold core. This DNA forms a hairpin structure, bringing the label close to the gold core which quenches it. If target DNA is present, it hybridizes with the beacon and releases the hairpin, causing the label to move away from the gold core and recover its fluorescence properties (Figure 1.11). This has been used for example in detecting a single base mismatch using gold clusters (1.4 nm) with attached ssDNA (Dubertret et al. 2001).

A hairpin DNA nanoparticle can be a useful and promising tool in **real-time imaging of mRNA**, shown in a study where the hairpin-DNA gold nanoparticle remained hybridized with the mRNA, allowing for imaging mRNA of a Respiratory Syncytial Virus inside a HEp-2 epithelial cell (derived from larynx carcinoma) (Jayagopal et al. 2010).

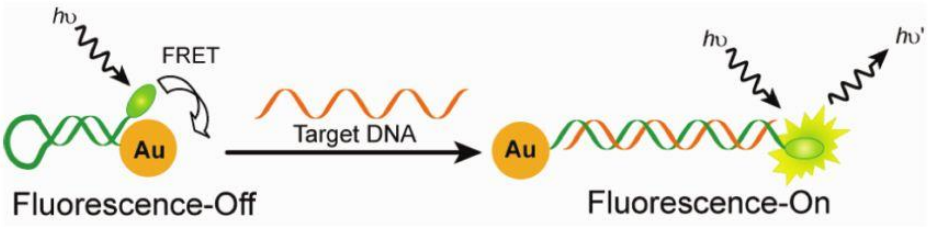

Figure 1.11. Gold nanoparticles in fluorescence-based sensing. Gold nanoparticles can function as molecular beacons, with the attached DNA self-hybridized in a hairpin structure, bringing a fluorescent label to a close proximity of the gold and therefore quenching it. However, after hybridization with target DNA, the label moves far enough from the gold core to release fluorescence. Adapted from (Saha et al. 2012).

1.3.4.3 Photothermal therapy

Photothermal therapy is based on the principle of heat generation by nanoparticles after light absorption (Dykman & Khlebtsov 2012). The gold nanoparticles transmit this heat to the surrounding environment and if they are inside a cell, such as a tumour cell, the heat can cause cell death. The laser that irradiates the focal point can be applied in pulses to avoid damage to other tissues (Pitsillides et al. 2003). The types of gold nanoparticles that can be used are for example nanospheres, nanorods, nanocages or nanoshells and all of these have been investigated in cancer therapy (Dykman & Khlebtsov 2012).

For example, gold nanorods have been used to release the drug doxorubicin after intercalating the drug into DNA attached to the nanorods (Zhang et al. 2016). The authors found greater release of doxorubicin and also its entry into the cell nucleus upon near infrared radiation.

1.3.4.4 Delivery of molecules

Drug delivery using gold nanoparticles is becoming more and more popular. It can be a very simple one or two step synthetic process to attach molecules onto the surface of gold nanoparticles as described in Section 1.3.1.3 and 1.3.2. Some examples of delivering various

molecules like proteins, drugs and nucleic acids into the cells are mentioned in the following section in more detail.

1.3.5 Therapeutic cargo molecules delivered by gold nanoparticles

Gold nanoparticles have been used to deliver several therapeutically useful molecules, such as proteins, drugs, or nucleic acids.

1.3.5.1 Proteins on gold nanoparticles

Protein delivery can be facilitated by gold nanoparticles. Proteins attached to nanoparticles can be utilised in two different ways: they can either function as a targeting molecule to facilitate the nanoparticle uptake or they can be a cargo that is delivered into the cell.

One typical example for a targeting protein is transferrin, which can be either covalently attached directly to the gold core (Yang et al. 2005) or via a linker (Choi et al. 2010). The nanoparticles with direct covalent transferrin attachment have been investigated and shown to transport into human nasopharyngeal carcinoma cells (Yang et al. 2005). Similarly, the transferrin attachment via a linker was used to target gold nanoparticles into cancer cells Neuro-2A *in vitro* as well as when implanted *in vivo* in mice (Choi et al. 2010).

Moreover, gold nanoparticles can also attach and deliver protein cargos. One such therapeutic protein is tumour necrosis factor alpha (TNFα). TNFα is a potent cytokine used in treating cancer. Gold nanoparticles carrying this cytokine have been shown to enter tumour cells *in vivo* (Visaria et al. 2006) and have since proceeded into clinical trials (Libutti et al. 2010).

Another therapeutic protein, insulin, has also been attached to gold nanoparticles. Insulin is used to treat diabetes and in general, it is injected subcutaneously. A nanoparticle-attached insulin has been investigated for alternative administration into the body – i.e. using oral, trans-mucosal (Joshi et al. 2006; Bhumkar et al. 2007) or nasal (Bhumkar et al. 2007) delivery routes. These alternative routes would make insulin delivery less invasive and more suitable for certain patients.

1.3.5.2 Drugs on gold nanoparticles

Gold nanoparticles have also been shown to deliver drugs into cells. For example, paclitaxel (Gibson et al. 2007) or doxorubicin (Kim et al. 2010) have been attached to the gold nanoparticles and delivered into cells. Nanoparticles with doxorubicin have also entered tumour cylindroids (Kim et al. 2010).

Moreover, the way the drug attaches to the nanoparticle, i.e. the type of linker used, can be modulated in order to control release of drugs. For example, the anticancer drug 5-fluorouracil has been attached to the nanoparticles via a linker containing the o-nitrobenzyl group, which can be cleaved by UV irradiation (Agasti et al. 2009), thus allowing for release of the compound.

1.3.5.3 Nucleic acids on gold nanoparticles

Gold nanoparticles have been also prepared with attached nucleic acids, including plasmids, and DNA or RNA, both single (ss) or double (ds) stranded. As nucleic acids are highly negatively charged, they cannot penetrate the cell normally. Therefore, gold nano-

carriers are a useful option, as cargo molecules can be easily attached, both covalently and non-covalently.

1.3.5.3.1 DNA-coated gold nanoparticles

Covalent attachment of ssDNA on gold nanoparticles resulted in cell uptake, despite the fact that no other surface-bound ligands were present, and the resulting nanoparticle had a negative charge (Rosi et al. 2006). It was proven that the nanoparticles were taken up into the cell by a reduction of gene expression.

DNA attached to nanoparticles can not only be used as a cargo but also facilitate delivery of other therapeutic substances. For example, gold nanoparticles with covalently attached DNA that was amine functionalized, carried platinum (IV) pro-drug (Dhar et al. 2009). Another example is the use of a certain type of DNA, termed as a proton-fuelled DNA nanomachine, which responds differently depending on pH (Liu & Balasubramanian 2003). At pH 8 it forms a duplex with a complementary strand, at pH 5, one strand folds into an i-motif, releasing the other strand (Liu & Balasubramanian 2003). This type of DNA has been shown to intercalate drugs such as doxorubicin and release them at low pH, such as in a lysosome. Gold nanoparticles have been prepared that were coated with this DNA and have been shown to enter cancer cells and release doxorubicin there (Song et al. 2013; Zhang et al. 2016).

Another advantage of using nucleic acid–coated gold nanoparticles in comparison to other types of nano-carriers is that the gold core may be dissolved and thus removed. This has been shown with gold nanoparticles that were coated with a cross-linked shell of modified oligonucleotides (Cutler et al. 2011). In this study, the gold core was then dissolved, leaving a hollow oligonucleotide nanoparticle. Use of this preparation method may be particularly relevant when treating chronic diseases that need several doses of the therapeutic oligonucleotide a day, elegantly solving the issue of clearance and gold toxicity.

1.3.5.3.2 RNA-coated gold nanoparticles

RNA delivery is also relevant for therapeutic purposes as part of RNA-therapy (see Section 6.1). Many different types of RNA have been delivered by gold nanoparticles, such as siRNAs, hairpin RNAs or RNA aptamers.

Small interfering RNA (siRNA) is part of the gene silencing machinery (Hamilton & Baulcombe 1999). It has been attached to gold nanoparticles both covalently (Giljohann et al. 2009; Oishi et al. 2006) and non-covalently (Guo et al. 2010; Zhao et al. 2012; Niikura et al. 2014). The transfection efficiency of the resulting nanoparticles was similar or higher with both types of attachment of siRNA to the nanoparticle compared to traditional transfection. For example, gold nanoparticles with covalently attached firefly luciferase siRNA had a similar silencing effect when compared with a traditional approach using Lipofectamine (Giljohann et al. 2009). Moreover, these siRNA-gold nanoparticles were more stable as they were more efficient at gene silencing 4 days post-addition of the nanoparticles. In another study, non-covalent attachment via PEI of lamin A/C siRNA showed more efficient gene silencing efficacy than Lipofectamine transfection (Guo et al. 2010).

Gold nanoshells have an advantage in delivery of nucleic acids. Upon laser irradiation, the RNA may be released from the nanoshell. For example, gold nanoshells coated with siRNA against green fluorescent protein were irradiated and released in cells (Braun et al. 2009).

Ribonucleic acids that are delivered into cells may be also modified to be more stable, for example by using locked nucleic acids (Singh et al. 1998). For example, locked nucleic acids have been covalently attached to gold nanoparticles and delivered to A549 lung carcinoma cells (Seferos et al. 2007).

1.3.6 Gold nanoparticles in the brain

So far, most of the therapeutic uses of gold nanoparticles have been aimed at treating cancer (Jelveh & Chithrani 2011). Most of the attempts to penetrate the blood-brain barrier using nanoparticles have been investigated using other types of nanoparticles, such as liposomes, polymeric nanoparticles and others mentioned above. In this section, gold nanoparticles are introduced as a potential delivery system across the brain endothelium *in vitro*. Also, gold nanoparticles have been investigated for treatment of brain cancer. Lastly, the targeting molecules that have been attached to enhance brain delivery of gold nanoparticles are shown.

1.3.6.1 Gold nanoparticles as a potential drug delivery system across the brain endothelium *in vitro*

Several studies searching for a drug-delivery system into brain have been performed *in vitro.* Rat brain endothelial cells were used to investigate transport efficiency of OEG-coated gold nanoparticles. The authors showed size dependency in transport across the cells where 4 nm nanoparticles had the highest transport efficiency compared to larger nanoparticles (16, 21 and 24 nm). Also using shorter OEG chains (M_n 1000 and 2000) achieved higher transport across the cells compared to longer OEG chains (M_n 5000 and 10000) (Etame et al. 2011).

Human brain endothelial cells (hCMEC/D3) have been used also for studies of uptake of 5 – 25 nm sized gold nanoparticles coated with human serum albumin or transferrin, but the authors did not see any dramatic uptake of either of these nanoparticles (Ye et al. 2013).

However, we have reported a study using glucose-coated gold nanoparticles < 5 nm which were able to cross human brain endothelial cells (hCMEC/D3) effectively in comparison with other nanoparticles (glutathione-coated <5 nm or 30 nm colloidal gold). These

nanoparticles were also able to enter human primary astrocytes in a 3-dimensional co-culture (Gromnicova et al. 2013).

1.3.6.2 Gold nanoparticles in treating brain cancer *in vitro* and *in vivo*

Some of the gold nanoparticles have been investigated as a useful tool in brain cancer therapy. For example, gold nanoparticles carried a photothermal drug with a targeting molecule of EGF (Cheng et al. 2011). For radiation therapy, OEG-coated 12 nm gold nanoparticles have been used in transport assays into primary brain endothelial cells and the human U251 glioblastoma cell line in xenograft implants in mice (Joh et al. 2013). Similarly, 11 nm colloidal gold nanoparticles were investigated in brain tumours in mice for radiation therapy as well as for microCT imaging (Hainfeld et al. 2013).

Gold nanoparticles carrying both a targeting molecule and a drug have been shown to enter cancer glioma cell lines (LN229 and U87) *in vitro* as well as implanted glioma cells *in vivo* (Dixit et al. 2015). This study showed increased uptake of nanoparticles with transferrin peptide (HAIYPRH) and photodynamic drug phthalocyanine 4 in comparison with nanoparticles without transferrin *in vitro* and *in vivo*. Similar to this study, another targeting molecule, trans-activating transcriptional activator (TAT) peptide, was used alongside a drug doxorubicin and both ligands were attached to a gold core of about 5 nm in diameter (Morshed et al. 2016). These nanoparticles were able to enter brain metastatic cell lines (MDA-MB- 231-Br, CN34-Br) and deliver the drug doxorubicin to both *in vitro* and also after implanting them intra-cranially *in vivo*. These targeted nanoparticles thus increased lifespan of cancer-implanted mice in comparison with the control animals.

1.3.6.3 Gold nanoparticles coated with targeting molecules to improve brain localisation

To target the brain, receptor-mediated endocytosis may be exploited, in particular the transferrin receptor or insulin receptor.

The transferrin receptor has been used as a target for nanoparticle penetration of the blood-brain barrier in two studies that exploited different strategies. Wiley et al. (2013) used 5 – 50 nm nanoparticles with transferrin attached to a OEG linker at different densities on the nanoparticle. Nanoparticles of sizes 45 nm and 80 nm localized in the brain parenchyma of mice. The authors also found better transcytotic release of nanoparticles with lower density of transferrin than those carrying higher density, thus being able to enter the brain parenchyma (Wiley et al. 2013). The same group then investigated transferrin attached to 80 nm gold nanoparticles via an acid-cleavable linker (Clark & Davis 2015). These nanoparticles had a high avidity (i.e. strength of interaction) to the receptor but as the transferrin was cleaved off within the vesicle, the resulting brain penetration was enhanced, in comparison to non-cleavable linker.

Another study (Prades et al. 2012) used a peptide sequence that interacts with the transferrin receptor, attached to 13 nm gold nanoparticles together with a cargo of amyloid-beta breaker peptide (CLPFFD). Gold nanoparticles with CLPFFD had been shown to bind to amyloid beta that was then destroyed by irradiating these gold nanoparticles as shown in an earlier study (Guerrero et al. 2010). The nanoparticles targeted to the transferrin receptor crossed an *in vitro* model of the blood brain barrier (bovine brain endothelial cells and rat astrocytes); they were also observed in brain parenchyma of mice (Prades et al. 2012).

Another interesting cellular target is the insulin receptor, as shown by (Shilo et al. 2014). It was targeted using 20 nm gold nanoparticles coated with insulin attached to a OEG

linker, which penetrated further into the brain than the control nanoparticles 2 hrs after injection into the tail vein.

1.4 Concluding remarks

In order to overcome the blood-brain barrier in an undisturbed way, a non-invasive approach is the most suitable one to use. In this case, nanoparticles can be used as they offer an advantage of controlled production and manipulation of their properties to suit their purpose. Gold nanoparticles can be a useful platform for carrying therapeutically useful molecules as they are very easy to synthesize and can attach different types of a therapeutic cargo.

1.5 Aim of the thesis

As mentioned in the introduction, there is a need for the development of a nanocarrier that can cross the blood-brain barrier. Gold nanoparticles present one such possible nanocarrier. Prior to the PhD work we have shown that gold glyconanoparticles can enter and cross the brain endothelium *in vitro* (Gromnicova et al. 2013), thus glyconanoparticles were selected to continue this work. Moreover, the development of methods to attach oligonucleotides to the nanoparticles and deliver them into the brain *in vitro* might help to advance the field of RNA-therapy for CNS diseases. Therefore, the aim of this thesis was to develop a nanocarrier to deliver oligonucleotides into the brain.

Thus the thesis may be divided into these objectives, contained within each chapter:

- **Chapter 3**: To assess uptake of gold glyconanoparticles into and across the brain endothelium and assess uptake into astrocytes, using the co-culture model of the blood-brain barrier.
- **Chapter 4**: To determine the mechanism of transport of one of the selected nanocarrier formulations in various endothelial cells.
- **Chapter 5**: To assess brain localisation and bodily distribution of gold glyconanoparticles in rats.
- **Chapter 6**: To attach an oligonucleotide cargo molecule to the nanoparticles and use a proof-of principle study to determine the delivery efficiency and release in brain endothelial cells and astrocytes *in vitro*.

In addition to these chapters, an Appendix is also included, that contains additional figures.

Chapter 2. Material and Methods

2.1 Nanoparticle-related methods

2.1.1 Gold glyconanoparticles

Gold nanoparticles of about 2 nm gold core coated with glucose, galactose, maltose, lactose, OEG-amine/galactose, OEG-amine/galactose/insulin and glutathione-FITC were obtained from Midatech Pharma. These nanoparticles were prepared as stated previously (Lund et al. 2011), similarly to the method below on preparation of DNA-coated nanoparticles. They were dissolved in water and were characterized by Midatech before their arrival using HPLC (high performance liquid chromatography) and DLS (dynamic light scattering). HPLC on a gel filtration column was used to separate and identify the nanoparticles' ligands on the basis of their size and DLS was used to determine the size of nanoparticles via light scattering. The gold concentration of the stock solution ranged between 0.7 mg/ml to 2.3 mg/ml.

For cell studies, the nanoparticles were used at concentrations of 8 - 75 μg/ml.

2.1.2 Preparation and characterization of gold glyconanoparticles coated with DNA

DNA sequences and types used in this thesis:

- attached sequence: 3′ AAT ATC GCG GAC AGA AGA CG 5′–C6-thiol (Sigma)
- Complementary sequence: 3′ CG TCT TCT GTC CGC GAT AT 5′ –biotin (Sigma)

The thiolated sequence was then attached to the gold nanoparticles in several ways described below.

2.1.2.1 Standard method of modified Brust-Schiffrin reaction in water

A mixture of 15 μmoles of ligands in total was prepared in water with several variations:

A) 0.75 μmoles thiol-DNA, 7.125 μmoles thiol C2-linker modified galactose, 7.125 μmoles disulphide OEG-amine.

B) 0.75 μmoles thiol-DNA, 14.25 μmoles thiol C2-linker modified galactose

C) 7.5 μmoles thiol C2-linker modified galactose, 7.5 μmoles OEG-amine.

D) 15 μmoles of thiol C2-linker modified galactose

Then, 1 mg (5 μmoles) of Au salt [Gold (III) chloride hydrate] prepared in water was added to the mixture to the final volume of 1 ml. Then, while vortexing the mixture, 100 μl of 1M $NaBH_4$ was quickly added which caused the nanoparticles to form. 1 hr shaking of the nanoparticles followed. To check for nanoparticle aggregation, the nanoparticles were spun at 5000 rpm for 5 min. The supernatant was kept and stored at 4 °C.

2.1.2.2 Modified Brust-Schiffrin reaction at pH 11

A similar reaction mixture as above was prepared:

A) 7.5 μmoles thiol C2-linker modified galactose, 7.5 μmoles OEG-amine

B) 0.75 μmoles thiol-DNA, 7.125 μmoles thiol C2-linker modified galactose, 7.125 μmoles disulphide OEG-amine.

C) 0.075 μmoles thiol-DNA, 14.925 μmoles thiol C2-linker modified galactose

D) 15 μmoles of thiol C2-linker modified galactose

200 mM NaOH (150 μl) was added to the galactose/OEG-amine ligand mixture prepared in water, followed by 1 mg (5 μmoles) of Au salt [Gold (III) chloride hydrate]. Then, thiol-DNA was added (final volume 1 ml) and the mixture was incubated for 2 min at room temperature. While vortexing the mixture, 100 μl of 1M $NaBH_4$ was added rapidly to cause nanoparticle formation. The mixture was then shaken for 1 hr at room temperature. To check the nanoparticle aggregation, the nanoparticles were spun at 5000 rpm for 5 min. The supernatant was kept and stored at 4 °C.

The nanoparticles were analysed using FPLC (fast protein liquid chromatography) ÄKTA pure (GE Healthcare) and separated on a size exclusion chromatography column. This technique separates molecules on the basis of their size. The Superdex 200 (10/300) column excludes molecules >300 kDa and has a separation range of 10-200 kDa. PBS was used as elution solvent.

2.1.2.3 Ligand-exchange reaction

2 variations of the reaction were performed. In the first experiment (section 6.2.2.4, 6.2.3, 6.2.4) 2.1 mg of thiol-DNA prepared in nuclease-free water was added to 58.25 μg of galactose-coated nanoparticles (batch M157-39-5, Midatech Pharma) and the mixture was incubated at 37 °C and monitored over 3 days. The nanoparticles were analysed using FPLC ÄKTA pure and separated on Superdex 200 10/300 GL column with PBS as elution solvent.

In the second experiment (section 6.2.5 and 6.2.7), ligand place-exchange reactions with the aim of producing nanoparticles with 0, 1, 2, or more DNA oligonucleotides attached to them, were performed by Dr Phil Williams in Midatech Pharma. In this case, 2.1 mg of thiol-

DNA was added to 349.5 μg galactose nanoparticles (batch M157-39-5). The reaction occurred over 4 days at 37 °C. Then, 100 μl of PBS was added to the mixture (final volume about 0.5 ml), which was then separated on FPLC ÄKTA pure (GE Healthcare) on Superdex 200 10/300 GL column with PBS as elution solvent run at 2ml/minute. Fractions of 0.5ml were collected, and we received fractions 8, 11 – 30 for analysis.

2.1.2.4 Analysis of gold concentration by spectrophotometric assay

Samples of gold nanoparticles were measured against a standard (Gold standards for AAS 1000 mg/ml, Sigma), that was applied at 3 concentrations, 1 mg/ml, 5 mg/ml, 10 mg/ml. The assay was performed in a 96 well plate, each sample was tested in triplicate. A total volume of 10 μl of sample was applied to the well. To this, 30 μl of 50% fresh cold aqua regia was applied. The liquid was mixed by gentle tapping and left to stand for 1 min. Next, 150 μl of 2 M NaBr was added. The absorbance was read on a plate reader, OPTIMA FluoSTAR, at 390 nm.

2.1.2.5 Analysis of DNA concentration in fractionated DNA/galactose gold nanoparticle samples

The DNA concentration in different fractions (15, 17, 18, 19, 20, 21, 23, 27) of DNA/galactose nanoparticles was analysed using NanoDrop (Thermo Fisher) at 260 nm. As the concentration was too high, 1 μl of the sample was mixed with 1 μl of water, then 1 μl was analysed according to manufacturer's instructions. As a blank, gold nanoparticles coated with galactose were used after they were diluted to about 0.3 mg/ml, i.e. a similar concentration of the nanoparticle fractions.

2.1.2.6 Electrophoretic mobility shift assay to analyse nanoparticles with attached DNA

Nanoparticles coated with galactose and DNA were mixed with a molar equivalent of biotinylated complementary probe and the mixture was brought to pH ~ 8 with TBE buffer, the final concentration of the TBE buffer was 0.5X or 1X (pH 8.3). The mixture was incubated for 1 h at room temperature. The DNA samples included: probe with biotin, nanoparticles with galactose/DNA/biotin at day 3, 2 and 1 of reaction with free SH-DNA; or nanoparticles with galactose/DNA/biotin at day 3 over 3 different concentrations of SH-DNA.

The nanoparticle samples were run on an 8% polyacrylamide gel. This gel was pre-run in 0.5X TBE for 1hr. The samples contained master mix (34 μl 10X TBE, 68 μl water) and water, the concentration of DNA-containing stock was around 100 nM. The sample was then prepared by mixing DNA stock (volume 1 μl), master mix (6 μl) and water (13 μl). The samples were loaded with 5 μl loading dye (6X, Fermentas) and run at 85 V for 1 hr.

The gel was then wet blotted at 100 V for 1 hr in 0.5X TBE at 4° C on a nylon membrane Amersham Hybond N+ (GE Healthcare). DNA was then cross-linked in the membrane with UV and was developed using Chemiluminescent Nucleic Acid Detection Module Kit (Thermo Fisher). The membrane was photographed using a GelDoc system.

2.1.3 TEM size determination of nanoparticles

Transmission electron microscopy was performed by air-drying 2 μl of gold nanoparticle solution (1:10) on a copper mesh grid (with pioloform film, carbon coated), left for a few seconds to adhere to the film and then blotted off with a filter paper. The grid was then

air-dried overnight. The nanoparticles were observed on a JEM 1400 or JEM 2100, with acceleration voltages of 120 kV and 200 kV, respectively.

3 images were taken of each nanoparticle sample and size distribution was analysed using ImageJ 1.49. The procedure was as follows: The scale was set using the scale bar of the TEM image. The parts of the image that were shaded were cropped off, leaving only the part with evenly lit background. The brightness was adjusted to visualise the dark nanoparticles. Then, the threshold was adjusted and applied, using function Adjust – Threshold – Apply. Then, the 2D projection of particle areas were measured, using the function Tool - 'Measure particles', with the size to measure set at 0.5 nm to infinity. The Summarized option was checked. The data of area of each nanoparticle were then saved in an Excel file. The data from 3 images were pooled together into a single Excel sheet. Here, the diameter was calculated based on a 2D projection area assuming each nanoparticle is a circle: $(\sqrt{A/\pi}) * 2$. This is based on a formula for the area of a circle ($A = \pi r^2$).

2.1.4 Investigation of release of ligands from gold core

For these studies, gold nanoparticles with glutathione-FITC (supplied by Midatech Pharma) were used and both the effect of pH and a reducing agent, glutathione, were investigated.

Different pH solutions were prepared using universal buffer mixtures made with different proportions of 0.2M Na_2HPO_4 and 0.1M citric acid. The pH was checked by pH papers. The nanoparticles at concentration 10 μg/ml were added to the solutions and incubated for either 30 min or 3 hrs. Then, the pH was brought to 7.5 for the measurement of fluorescence using 0.1M Sörenson's buffer and the mixture added into a 96 well plate in 4 technical replicates. Fluorescence was measured at 495/519 nm with a plate reader FluoSTAR Optima.

Different concentrations of glutathione (1, 2.5, 5, 10mM) were prepared in water with 1 mM EDTA, final volume 1 ml. Nanoparticles were added (10 μg/ml), the solution mixed and 100 μl of this mixture added into a 96 well plate in 4 technical replicates, the measurements were then performed at 10 min, 30 min, 1 hr, 2 hrs, 3 hrs, 4 hrs, 5 hrs, 6 hrs and 24 hrs. Fluorescence was read at 495/519 nm on a plate reader, FluoSTAR Optima.

2.2 Cell-culture –related methods

2.2.1 Cell cultures

Table 2.1. Cultivation conditions for the human cell cultures used in this study.

Cell type/name	abbreviation	Source/supplier	Culture medium/supplier¶	Serum content	Passage used	maintenance
Brain endothelial cell line	hCMEC/D3	(Weksler et al. 2005)	EBM-2 MV* (Lonza)	2.5%	24 - 34	Split at 90%, medium changed every 2-3 days
Bone marrow endothelial cell line	BMEC	Babette Weksler	Endothelial cell medium ECM (ScienCell)	5%	23 - 30	Split at 90%, medium changed every 2-3 days
Human primary astrocytes	hA	ScienCell	Astrocyte medium (ScienCell)	2%	2 - 8	Split at 70 – 80%, medium change every 2 days
Conditionally immortalized glomerular endothelial cells	ciGENC	Simon Satchell (Satchell et al. 2006)	EBM-2 MV (Lonza)	5%	24 - 27	Split at 85%, medium change every 2-3 days
Human primary microvascular lung endothelial cells	HMVEC-L	Lonza	EBM-2 MV (Lonza)	5%	1 - 3	Split at 70%, medium change every 2 days

The medium was prepared according to the manufacturer's instructions unless otherwise stated.

*EBM-2 MV medium for hCMEC/D3 contained 0.025% VEGF, IGF and EGF; 0.1% bFGF, 0.1% (v/v) rhFGF, 0.1% (v/v) gentamycin, 0.1% (v/v) ascorbic acid, 0.04% (v/v) hydrocortisone.

All cells except ciGENC were incubated at 37 °C, all cultures were kept in a humidified atmosphere with 5% CO_2.

ciGENC were kept at 30 °C in order to divide. After proliferation the cells were cultured at 37 °C for at least 3 days to allow the glomerular endothelial phenotype to develop prior to experimentation (Satchell et al. 2006).

2.2.2 Determination of cytotoxicity of gold nanoparticles with MTT assay

To assess cytotoxicity, an MTT [3-(4,5-dimethylthiazol-2-yl)-2,5-diphenyltetrazolium bromide] assay was performed on cells cultured in 96 well plates, with 4 replicates per treatment. Nanoparticles were applied to the confluent cells at varying concentrations, from 4 μg/ml up to 32 μg/ml, or in the case of OEG-amine/galactose up to 75 μg/ml. Incubation time was 22-48 hrs at 37 °C. Digitonin was used as a positive control of toxicity at 30 μg/ml for 30 min. The nanoparticles or digitonin solution were removed, the cells carefully washed once in HBSS (Hank's balanced salt solution, Sigma), fresh medium (50 μl/well) was added followed by MTT (10 μl/well of 5 mg/ml MTT) and the cultures were incubated for 3.5 – 4 hrs at 37 °C. The MTT solution was carefully aspirated, 100 μl of DMSO (dimethylsulfoxide) added per well and the plate was shaken for 5-10 min. The absorbance was read at 540 nm on a plate reader OPTIMA FluoStar.

Also, the morphology of the cells was observed after 24 hr, when cells were incubated with nanoparticles (glucose, OEG-amine/galactose, OEG-amine/galactose/insulin) at a concentration of 32 μg/ml.

2.2.3 Electron microscopy as a way to detect gold nanoparticles in cells

As gold nanoparticles are a type of metal nanoparticles, electron microscopy can easily detect such a highly electron-dense material. This makes localisation of nanoparticles within cells and tissues easy, as well as it can be used to quantitate the amount of nanoparticles.

The principle of electron microscopy lies in electron beam hitting the sample and thus creating several types of information. The transmitted electrons are used for transmission

electron microscopy (TEM). On the other hand, scanning electron microscopy (SEM) uses both secondary electrons for information on the surface topography and other types of scattered electrons for advanced imaging. Furthermore, the electrons from the beam also produce characteristic X-rays that are basis for elemental analysis by energy-dispersive X-ray spectroscopy (EDS or EDX).

In order to use electron microscopy, usually vacuum is involved in the imaging chamber and therefore the samples need to be carefully prepared. The main steps involve glutaraldehyde fixation, penetration, osmication (with OsO_4), dehydration and resin infiltration. The cells *for in vitro* work can be handled in two main ways, either the cells are pelleted (Oh & Park 2014; Thomas & Klibanov 2003; Shukla et al. 2005; Coulter et al. 2012) or they are grown on a porous transwell membrane (Gromnicova et al. 2013; Ye et al. 2015) . Moreover, as gold nanoparticles smaller than 10 nm are not visible within cells or tissues by standard TEM or SEM, their size needs to be increased. For this purpose silver enhancement is used. Silver enhancement works on the principle of deposition of silver atoms on gold, thus achieving increase in size as well as highly electron-dense particle.

The advantages of using TEM for analysis of uptake of gold nanoparticle uptake into cells and tissues are several. It can be used both qualitatively and quantitatively. The qualitative use allows for localisations within subcellular compartments that are easy to distinguish, such as mitochondria, endosomes, lysosomes, nucleus and Golgi apparatus. Furthermore, one can also investigate nanoparticle interactions with the plasma membrane. The quantitative use therefore provides large sets of data on numbers of nanoparticles in different localisations (Figure 2.1) as demonstrated previously (Gromnicova et al. 2013; Sreekanthreddy et al. 2015), Moreover, as electron microscopy is essentially non-destructive technique, it allows for repeated analysis of the fixed and processed sample.

There are also some disadvantages in using electron microscopy. Mainly, it is an expensive and time-consuming technique. Knowledgeable staff is also needed for sample preparation and operation of the microscopes. As the sample is fixed, the limitation is that this technique does not allow for real-time imaging unless modified electron microscopy is used.

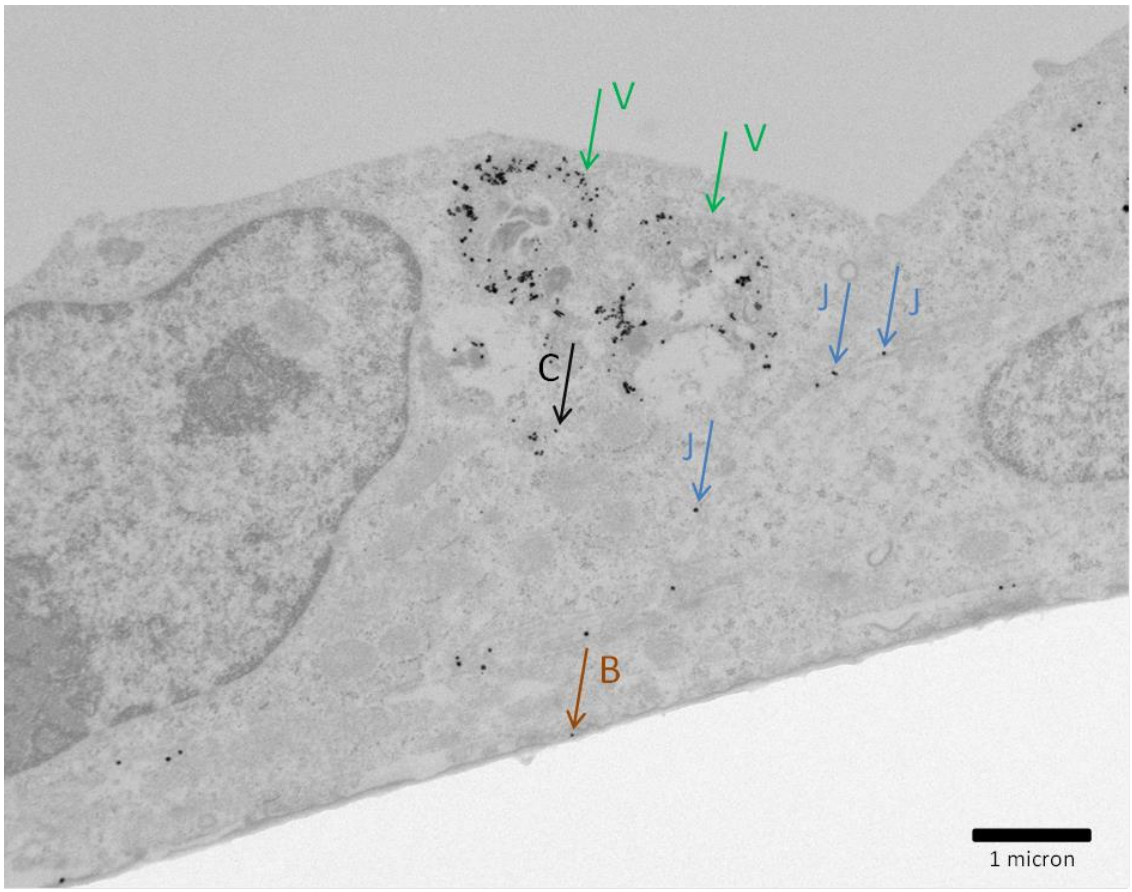

Figure 2.1. **Electron microscopy can allow us to determine numbers and localizations of gold nanoparticles in cells.** Electron microscopy provides detailed information on overall nanoparticle numbers which can be counted and sorted into different categories based on their localization, such as in vesicles (V), cytosol (C), junctions (J) and below the basal plasma membrane (B). Here shown an electron micrograph of hCMEC/D3 cells after 7 hr incubation with CLPFFD peptide-coated <5 nm gold nanoparticles (silver enhanced). (Image by the author.)

2.2.4 Nanoparticle transport assays and TEM protocol for quantification of nanoparticles

To assess the rate of transport of nanoparticles into and across the cells, the assay was performed using transwell inserts (1 cm^2, Corning Costar) on which a monolayer of endothelial cells was formed. The endothelial cells cultured in this system were hCMEC/D3, ciGENC, BMEC and HMVEC-L. The transwell system consists of the top chamber, in which the cells grow, and has a volume of 0.5 ml of cell culture medium and bottom chamber volume of 1.5 ml with HBSS. The cells were seeded at a density of 80,000 – 100,000 cells per insert and incubated for 2 – 3 days in their respective culture medium at suitable conditions (see note on ciGENC, Section 2.2.1). Only after a monolayer was formed, was the transport assay performed. The nanoparticles were applied to the top of the chamber (into the insert part) at a concentration of 8 μg/ml, unless stated otherwise. The culture temperature was usually 37 °C or 4 °C. In the latter case, the cells were kept at 4 °C for 30 min prior to application of nanoparticles. The time of incubation was dependent on the experimental design and ranged from 0.5 hrs to 8 hrs. After the incubation, the liquids from both parts of the well were removed and both chambers were washed 3x in HBSS. The cells were then fixed for 1 hr (room temperature) in 2.5% glutaraldehyde or 0.4% glutaraldehyde in the case of transport studies for DNA-nanoparticles. The fixative was removed and the chambers washed 3X in PBS (phosphate buffer saline) and stored in Sörensons phosphate buffer at 4 °C.

2.2.4.1 Preparation of samples for transmission electron microscopy

The samples of transport assays were processed for transmission electron microscopy where all the incubations were performed at room temperature and all the solutions were applied to both the insert and the bottom chamber.

Firstly, the storage buffer (Sörensons phosphate buffer, PB) was removed and cells were permeabilized in 0.01% Triton x100 for 15 minutes on a rocker. The inserts were washed 3x in 0.1 M PB and silver enhanced. Silver enhancement (Aurion) was prepared according to the manufacturer's instructions and its function tested on a dot blot. Then, the silver enhancement solution was applied to the insert and rocked for 1 hr. It was removed and washed 3x in distilled water. The cells were then osmicated in 1% (w/v) osmium tetroxide prepared in 0.1 M PB for 30 min. The insert was washed 3x in 0.1 M PB, allowing longer washes (several minutes between each wash). Then, the insert was removed from the well, its membrane cut out and cut in half, then the middle part of one half was cut into a strip (~3 mm wide), which was then cut in half and edges were removed, now 2 squared pieces were created. The part towards the edge of each piece was noted by cutting the corner off. Both pieces were directly placed in 30% ethanol as a beginning of the dehydration process, the timings and concentrations of ethanols were as follows: 30% for 5 min, 50% for 5 min, 70% for 10 min, 90% for 10 min, 100% for 10 min performed twice, 100% with molecular sieve for 10 min. After dehydration, the membrane pieces were incubated in a 50:50 mixture of 100% ethanol and Epon resin overnight and then penetrated with fresh resin twice for 2 hrs. The pieces were embedded in a cushion in fresh resin to form a block for 48 hrs at 60 °C.

2.2.4.2 Microsectioning and electron microscopy

Resin blocks were first prepared for microsectioning by removing the tip of the block to reach the pieces of insert. The prepared block face was microsectioned to 80 nm thick sections using a Diamond knife (Diatome, Switzerland). The sections were collected onto pioloform film-covered copper grids. After at least 2 hrs of air drying, they were immersed in 4% aqueous

uranyl acetate (30 min) followed by Reynolds lead citrate (10 min). Again, they were dried for at least 2 hrs prior to TEM imaging.

Sections were viewed on a Jeol JEM 1400 or 1010 at an acceleration voltage of 80 kV at various magnifications (5000x and 50x for JEOL 1400; 150x and 20000x for JEOL 1010).

2.2.4.3 TEM quantification of nanoparticle uptake

The sections had a visible insert membrane on which cells were observed. Therefore, the cells were observed for quantification at magnification of 5000x (JEM 1400) or 20000X (JEM 1010). The nanoparticles were counted and sorted into 3 – 4 categories (vesicles, cytosol, basal plasma membrane and nucleus) at the time of viewing on the electron microscope. The length of insert which was assessed (usually between 300 – 1500 microns in length) was then measured at low magnification (50x for JEM 1400 and 150X for JEM 1010) and the number of nanoparticles was recalculated per this length of insert. This method has been developed as it covers a broader range of data (there are more cells counted than in our previous method of 25 images per insert).

2.2.5 3-dimensional co-cultures for nanoparticle transport

3-dimensional co-cultures of hCMEC/D3 cells and human astrocytes were created for nanoparticle transport studies. Firstly, astrocytes of 2 - 4 $x10^6$/ml were added into a collagen solution (80% rat type I collagen 2 mg/ml, 10% 10x MEM, 10% cell suspension in medium) and plated in a 24 well plate (450 µl/well). The collagen was let to set for 10 min at 37 °C. Liquid was removed from the collagen by dropping a RAFT™ absorber (Lonza) on top of the collagen gel which absorbed the liquid for 15 min. Then the plunger was removed and astrocyte medium

was added and the culture was incubated for 24 hrs. hCMEC/D3 cells were seeded on top of the gel and grown to form tight monolayers and the co-cultures were incubated for 2-3 days in modified EBM-2 medium.

Nanoparticles were added to the co-cultures at a concentration of 8 μg/ml and incubated for 3 hrs. Then, the co-cultures were washed 3x in HBSS and fixed in 2.5% glutaraldehyde for 2 hrs in the case of studies using nanoparticles coated with glucose, OEG-amine/galactose, OEG-amine/galactose/insulin. Cultures with nanoparticles with DNA duplex (thiol DNA - biotin DNA) were fixed with 0.4% glutaraldehyde for 2 hrs. The cultures were washed x3 in PBS and gently detached from the bottom of the well with a spatula. The gel was then stored in phosphate buffer at 4 °C and processed for electron microscopy in a similar manner to that described in Section 2.2.3. The number of nanoparticles was counted in whole astrocytes and the number of cells was noted.

2.2.6 Detection of DNA ligand from dsDNA/galactose nanoparticles by electron microscopy

In order to detect DNA cargo within cells by TEM, "immuno-gold" labelling was used on cell samples that were incubated with dsDNA/galactose nanoparticles where the unbound strand of DNA contained biotin (5').

3D co-cultures of endothelial cells and astrocytes that were prepared as above and fixed in 0.4% glutaraldehyde were used. They were permeabilized in 0.05% triton X-100 for 1 hr. The samples were washed three times in 0.1 M PB buffer over 15 min. They were blocked with 100 mM glycine (0.5 ml, prepared in 0.1 M PB) for 1 hr, then washed three times in 0.1 M PB buffer over 15 min. 0.3% hydrogen peroxide solution (prepared in water) was applied to the samples for 20 min. Five washes in 0.1 M PB buffer followed over 15 min. Horseradish Peroxidase

Complex (GE Healthcare, RPN1051, 1/400) was added for 2 hrs in diluent (5 mg/ml BSA + 0.01% Tween20 in PBS). Samples were washed and rocked several times (5 or more) over 1 hr. 20 nm gold nanoparticles coated with OEG-biotin (Sigma) were added at a dilution of 1/500 (concentration not determined) and incubated overnight. Several washes (5 – 10) in 0.1 M PB followed over 4 hrs with rocking. 1% osmium tetroxide (in 0.5 M PB) was added for 45 min. The samples were then dehydrated with ethanol and resin embedded as described in see Section 2.2.3.

2.2.7 Transfection of cells with siRNA and analysis of transfection

2.2.7.1 Silencing of insulin receptor on hCMEC/D3 cells

siRNAs for insulin receptor knockdown (siRNA for INSR silencer, ID 31, on CD220, Life Technologies) as well as nonsense siRNA (Silencer® Negative Control No. 1 siRNA, 50 μM) were purchased from Life Technologies and used at 10 μM. Rapidly growing cultures of hCMEC/D3 were used. We used 12 well plates; single well values follow. The cells were seeded at a density of 200,000 cells/well in transfection medium (EBM2 without antibiotics, 800 μl) for the following day of transfection (70% of confluency). At the day of transfection, 6 μl of siRNA was added to 100 μl of warm OPTIMem (Life Technologies) and 2 μl of lipofectamine (Life Technologies) was added to 100 μl OPTIMem in separate tubes and incubated for 5 min. Then both mixtures were combined and incubated for 20 min. Then this mixture was added to cells, mixed by gentle rocking and incubated for 6 hrs at 37 °C. The mixture was removed, cells washed x3 in HBSS and standard EBM2 medium was added. The cells were cultured for 24, 48 or 72 hrs.

2.2.7.2 Transfection of human astrocytes

2.2.7.2.1 Optimization with reporter siRNA

The transfection of human primary astrocytes was optimized using a red fluorescent oligo BLOCK-iT Alexa Fluor (Life Technologies) with a transfection agent Lipofectamine RNAiMAX (Life Technologies). The cells were seeded at variable densities in a 12 well plate and transfected. The transfection mix was prepared by mixing OPTIMEM (Life Technologies) 100 µl /well and 6 µl Lipofectamine and mixing 100 µl OPTIMEM and 1 µl siRNA (20 pmoles), then combining them together. The mix was added after 5 min incubation onto the cells (200 µl) that contained 800 µl of transfection medium (medium without antibiotics). The cells were then incubated at 37 °C for 6 hrs. Then, the medium was removed and the cells washed 3x in HBSS before full astrocyte medium was added. The cells were then incubated for 1-6 days post-transfection.

2.2.7.2.2 Silencing of aquaporin 4 on human astrocytes

The transfection was performed using Lipofectamine RNAiMAX (Life Technologies), using aquaporin 4 siRNAs, keeping to the conditions of transfections with reporter siRNA.

The siRNAs tested:

1. Commercially available AQP4 siRNA s1524 (Life Technologies)
2. 2 siRNA sequences selected by us:
    a. (sense strand) 5′ AAGAUCAGCAUCGCAAGUCUUU 3′
       (antisense strand) 5′ AGACUUGGCGAUGCUGAUCUU 3′

    b. (sense) 5′ AAUCCUCUAUCUGGUCACACCUU 3′
       (antisense strand) 5′ GGUGUGACCAGAUAGAGGAUU 3′

2.2.7.3 Examination of expression of insulin receptor or aquaporin 4 by flow cytometry

The hCMEC/D3 cells that were transfected as above, trypsinized, spun (1500 rpm, 5 min) and washed x3 in wash solution (1% BSA, 100 mM HEPES in HBSS). Then they were incubated with insulin receptor primary antibody (ab44914, Abcam), transferrin receptor antibody (MAB2474, R&D Systems) or IgG2a (Mouse IgG2a Isotype Control from murine myeloma, Sigma) isotype control antibody (both 20 μg/ml in 50 μl of wash solution) for 2 hrs at 4 °C. Then, the cells were washed x3 in wash solution and resuspended in 200 μl of secondary antibody, sheep anti-mouse FITC-conjugated (Sigma) (1:100) for 1 hr in the dark at 4 °C. The cells were then washed x3 in PBS and resuspended in 400 μl of PBS for FACS analysis.

Primary astrocytes were transfected as above, trypsinized and spun (1500 rpm, 5 min) and washed x3 in HBSS. They were then fixed in 4% PFA for 5 min. Washed twice in PBS, then the cells were permeabilised with 0.05% saponin in 5% goat serum for 30 min. After spinning the cells, they were incubated with primary antibody anti-aqp 4 (H-10, Santa Cruz), 1/100, or isotype control rabbit IgG, 1/2500 in diluent (2.5% goat serum and 0.05% saponin in HBSS) for 1 h. The cells were washed x3; each wash took about 2 min. Secondary antibody anti-rabbit AlexaFluoro 488 (Life Technologies) was added at a concentration of 10 μg/ml in diluent (2.5% goat serum and 0.05% saponin in HBSS) for 45 min. 3 washes in PBS followed, then the cells were resuspended in 400 μl of PBS for FACS analysis.

FACS analysis was performed on a Facscan. Expression of insulin receptor was detected using FL1 channel at 400 - 430V; expression of aquaporin 4 was detected at 330 - 350V. The cell population was gated and 10,000 events were analysed from the gate.

2.2.8 Analysis of endothelial glycocalyx by lectin binding

hCMEC/D3 cells (seeded at a density of 20,000/well) were cultured in a 96 well plate for 7 days, and the lectin profile assessed at day 2, 4 and 7 of culture where each lectin treatment was performed in triplicate. ciGENC cells (seeded at a density of 10,000/well) were cultured at 30° C to reach confluency (3 days), then moved to 37° C and cultured for 4 more days before analysis. The cells were washed twice in HBSS, fixed in 0.1% glutaraldehyde (in PBS) for 15 min. Then they were washed twice in PBS and blocked in 0.05M Tris/HCl pH 6.8 for 20 min. The cells were washed 3x in wash buffer (0.05% Tween20 in PBS) and biotinylated lectins were added: Ulex Europaeans agglutinin 10 μg/ml, Wheat germ agglutinin 5 μg/ml, Peanut agglutinin 20 μg/ml, Wisteria floribunda lectin 20 μg/ml; all prepared in diluent (5 mg/ml BSA and 0.01% Tween20 in PBS). The lectins were incubated with the cells for 1 hr and then washed out in wash buffer three times. Streptavidin peroxidase (Streptavidin-Biotinylated Horseradish Peroxidase Complex, GE Healthcare, RPN1051) (1:700) was added to the cells for 1hr, followed by three washes in wash buffer and one wash in PBS. The chromogen was prepared: tetramethylbenzidine at a final concentration of 0.1 mg/ml in 0.1 M sodium acetate/citric acid buffer, pH 6.0. Hydrogen peroxide at a final concentration of 0.03% w/w was added. This chromogen solution was added to the wells (100 μl/well) for 10 – 15 min to develop a blue colour; the reaction was stopped by addition of 20 μl of 10% H_2SO_4 per well, producing a yellow colour. The absorbance was read at 450 nm on a plate reader OPTIMA FluoSTAR.

Also, the cells were analysed for partial removal of glycocalyx by digestion with enzymes. The enzymes were neuraminidase (50 mU/ml) and O-Sialoglycoprotein endopeptidase (25 μg/ml, Cedar Lane Labs) used for 2 hrs at 37 °C to pre-treat the confluent cells. The cells were then washed three times and fixed in 0.1% glutaraldehyde (in PBS) for 15 min. The lectin staining then followed as detailed above.

2.2.9 The effect the enzymatic removal of glycocalyx on nanoparticle uptake into hCMEC/D3 and ciGENC cells

The confluent layers of endothelial cells (hCMEC/D3 and ciGENC) were treated with enzymes [neuraminidase (50 mU/ml) and endopeptidase (25 μg/ml)] as mentioned above for 2 hrs. The cells were then washed twice with HBSS and OEG-amine/galactose nanoparticles were added (8 μg/ml) in EBM2-MV (2.5 % FBS) to the cells for 3 hrs. The cells were washed 3x in HBSS, fixed in 2.5% glutaraldehyde for 1 hr at room temperature, washed x3 in PBS, stored in 0.1 M PB buffer, and processed for electron microscopy (see Section 2.2.3).

2.2.10 Analysis of degree of endocytosis

The cells (hCMEC/D3 or ciGENC) were treated with FITC-dextran (Sigma) of 70 kDa or 10 kDa, where stated. The cells were grown in 12-well plates and FITC-dextran was applied at 0.2 mg/ml for 1 hr at 37 °C or at 4 °C (with pre-cooling for 30 min). The cells were washed with ice-cold HBSS 5x over 5 min; they were trypsinized, collected and washed 2x in HBSS + 0.1 mg/ml BSA. Then they were resuspended in PBS and analysed using flow cytometry (BD FacScan, channel FL1, 460 – 500V), where a gated cell population of 10,000 events was analysed.

2.2.11 Inhibition of active transport processes in hCMEC/D3 cells

To assess the active uptake of OEG-amine/galactose gold nanoparticles, the hCMEC/D3 cells were cultured for 3 hrs at 4 °C or for 2 hrs with inhibitors of active metabolism NaN_3 (10 mM) + 2-deoxyglucose (50 mM) prepared in EBM-2 medium with a 30 min pre-treatment and processed for TEM (see Section 2.2.3).

The possible cytotoxic effect of NaN_3 + 2-deoxyglucose on cells was assessed by staining cells with propidium iodide after 2 or 4 hr treatment, the cells were pre-treated for 30 min. Digitonin (30 μg/ml for 15 min) was used as a positive control for cell death, and fluorescence intensity was measured on a Facscan, channel FL2 set at 400V. The cell population was gated and 10,000 events analysed.

Moreover, to analyse the type of endocytosis involved in the transport of OEG-amine/galactose gold nanoparticles, specific metabolic inhibitors were used. Chlorpromazine, nystatin, nocodazole and cytochalasin D were tested at varying concentrations (Table 2.1). The cells were cultured on 12-well plates until confluent and pre-treated with inhibitors for 1 hr. Then, 70 kDa FITC-dextran was added to the cells with or without the inhibitor, for 1 hr. The cells were then washed 5x with 1.5 ml cold HBSS/wash and trypsinized, spun at 1500 rpm for 5 min, the supernatant removed, washed x1 with 1.5 ml cold HBSS + 0.1% BSA and then a final wash of 1 ml of cold PBS. The cells were then resuspended in 400 μl PBS and analysed with the Facscan at FL1 = 460 V.

TEM was used to analyse the effect of selected inhibitors, i.e. 50 μg/ml nystatin or 30 μg/ml chlorpromazine, on nanoparticle uptake. The confluent cells grown on transwell inserts were pre-treated with the inhibitors for 5 min, then the gold nanoparticles (8 μg/ml) were added to EBM-2 MV medium with nystatin or chlorpromazine. The cells were incubated for 1 h, washed x3 in HBSS and fixed in 2.5% glutaraldehyde for 2 h at room temperature, then washed x3 in PBS and stored in 0.1 M PB at 4 °C. The cells were then processed for electron microscopy as described in Section 2.2.3.

Table 2.2. Tested concentrations and incubation times of antibiotic inhibitors.

inhibitor	concentration used (µg/ml)	inhibitor incubation time*
chlorpromazine	5	2 hrs
	8	2 hrs
	10	2 hrs
	15	1 hr
	30	1 hr
	50	1 hr
cytochalasin D	10	2 hrs
	20	2 hrs
	40	2 hrs
nocodazole	10	2 hrs
	20	2 hrs
	50	2 hrs
nystatin	20	2 hrs
	50	2 hrs
	80	1 hr

* this incubation time corresponds to pre-treatment of 1 hr and treatment of 1 hr with FITC-dextran for 2 hr treatments. In the case of 1 hr treatment, only pre-treatment was used, the inhibitor was removed during incubation with FITC-dextran.

2.2.12 Analysis of vesicular diameter and cell area

3 TEM sections of hCMEC/D3 and 3 sections of ciGENC cells were used to analyse vesicular diameter and cell area. Each section corresponded to a well with a single treatment. As each treatment had 3 wells, one was randomly picked for this analysis and 3 independent experiments were analysed per cell type, resulting in 3 sections analysed altogether.

At 20,000x magnification on JEM 1010 (Jeol, Japan), about 100 vesicular diameters were measured per section in cells that were randomly picked. The data set was analysed with Microsoft Office Excel 2010 and GraphPad Prism 3.0 (USA).

Similarly, to obtain areas of hCMEC/D3 and ciGENC, 3 independent experiments were analysed for each cell type. At magnification of 2,000X on JEM 1010 (Jeol, Japan) 10 images per treatment were taken randomly. The cell area was measured using ImageJ. The data were

analysed as a distribution histogram and means of each independent experiment were calculated and analysed by GraphPad Prism.

2.3 Methods related to animal experiments

2.3.1 Animal treatment protocol

The animal experiments of injection, perfusion, fixation and organ removal were performed in Istanbul by Mehmet Kaya and colleagues; details on the procedure are in (Gromnicova, Yilmaz, et al. 2016). Briefly, nanoparticles (50 μg of Au) were infused into the left carotid of rats over 1 minute and allowed to circulate for 10 minutes after which the animals were perfused and fixed in 2% PFA and 2.5% glutaraldehyde. The organs were removed, stored at 4° C and sent to us for analysis by ICP-MS and electron microscopy.

2.3.2 Gold nanoparticle analysis in brain tissue by light and electron microscopy

The fixed rat brains were separated as cerebrum and cerebellum and both parts were sectioned at a thickness of 100 μm using a vibrating microtome, VT1000 (Leica Microsystems, Germany). A section which correlated to the start of hippocampal region was chosen from each animal in each treated group. To determine that silver enhancement does not cause nonspecific staining, a brain of an untreated animal was used (the section was kindly supplied by Igor Kraev). The animal was perfused-fixed comparably to the treated animals and a random vibratome section was picked for the comparison. All sections were permeabilized in 0.05% Triton-X100 in 0.1 M PB for 30 min. The gold nanoparticles present were silver enhanced (R-GENT SE-EM, Aurion, Netherlands) for 140 min at room temperature. The silver enhancement caused brown staining of the regions containing nanoparticles and was stopped by three washes in water. The sections were then imaged by light microscopy and processed for electron microscopy.

The brain sections were incubated in 1% (w/v) osmium tetroxide in 0.1 M PB for 30 min at room temperature. They were dehydrated in a graded series of acetone before being incubated with a 1:1 mixture of Epon resin and 100% acetone overnight. The sections were then infiltrated in Epon resin and flat-embedded between two sheets of Aclar. The regions of the brain with visual evidence of silver enhancement were attached to capsule. These were sectioned on ultramicrotome (Leica Ultracut, Leica Microsystems, Germany) at 80 nm thickness. The sections were collected on copper slot grids with pioloform/carbon support films and counter-stained with 4% uranyl acetate (30 min) and Reynolds lead citrate (10 min). The slot grids with sections were viewed on JEM 1010 (JEOL, Japan) at an accelerating voltage of 80 kV.

2.3.3 Inductively-coupled plasma mass spectroscopy (ICP-MS)

Electron microscopy can be used to analyse the tissue and cellular localisations of nanoparticles within the brain, however, the overall amount of gold present in the brain and other organs also needs to be determined in order to allow quantitative tissue distribution comparison. For this purpose, inductively-coupled plasma mass spectroscopy (ICP-MS) is used. In general, biological samples are supplied as a liquid, i.e. dissolved tissue. The liquid sample is passed into a nebulizer that transforms it into an aerosol before detection by mass spectrometry.

As mentioned, the preparation of biological samples involves transforming them into liquid. Depending on the material used, aqua regia is the most common reagent. Aqua regia, a mixture of nitric and hydrochloric acid, liquefies the sample and also breaks down gold nanoparticles. It is possible to speed up the break down process using a reaction vessel in a microwave (Yang et al. 2012). Closed environment and high pressure are created during the procedure. Another way to dissolve biological material is to use the alkali tetramethylammonium hydroxide (Gray et al. 2013). Both of these are generally used for

unfixed material. Acids at room temperature may not be able to penetrate fixed tissues easily and dissolve them in a reasonable time. We have successfully used boiling nitric acid to dissolve glutaraldehyde-fixed rat tissues (Gromnicova, Yilmaz, et al. 2016). This technique dissolved samples within 5 min of boiling and thus was comparable in speed with microwave digestion.

Quantification of gold nanoparticle content with ICP-MS has its advantages and disadvantages. The major advantage is high sensitivity of the technique, usually well under parts per billion (ppb). Another advantage over more technically demanding techniques such as TEM, is the speed of analysis (<24 hours). The type of biological samples include whole-cell lysates but also cytosolic and nuclear fractions in order to distinguish specific nanoparticle localisations (Tsoli et al. 2005). Another important advantage is quantification of gold in tissues where this technique is the best option for researchers. Fixed and unfixed tissues as well as blood, urine or faeces can all be easily analysed using ICP-MS.

There are several disadvantages of using ICP-MS for gold quantification. Experienced staff is needed to operate the instrument, which may also take time to set up for gold analysis in biological samples. The major problem is to ensure that the instrument detects consistent levels of gold over several samples as well as between analyses. Gold can adhere to tubing and instrumental sections causing drifts in detected signal levels. This can be addressed using an internal standard such as iridium. Also, gold standards may need to be run several times during sample analysis in order to detect any discrepancies during detection. During this set up process, which may take months, it is generally advisable to check results of the analysed sample with another independent ICP-MS instrument. Another disadvantage is that it is a destructive technique where the sample storage may cause discrepancies in analysis, especially if already lysed.

2.3.4 Quantification of the amount of gold by ICP-MS in liver, kidney, lung and brain

The liver, kidney and lung were digested in boiling HNO_3 for 5 – 10 min and run in 1% HCl with Ir (10 ng/ml) on a NexION ICP-MS (PerkinElmer, USA). The brain tissue was divided into ipsilateral side, contralateral side and cerebellum. Nine sections were selected from the brain; starting at exactly the same point from the bregma and taking every other section. Each of those selected sections were cut in half and collected separately as ipsilateral and contralateral side. In the case of cerebellum, 10 sections were randomly picked. The brain tissue was digested in boiling HNO_3 for 15 -20 min and run in 1% HCl with an Iridium standard (10 ng/ml) on a NexION ICP-MS (PerkinElmer, USA).

The obtained values from the ICP-MS were levels of gold (ng) per g of tissue. Each animal was administered with the same nanoparticle dose (50 μg Au) regardless of its weight. To compensate for this variation, a standardized value was calculated (50/weight of animal in g) (Table 2.3). Thus, the amount of gold found in organs by ICP-MS (ng Au/g tissue) was dividedby this standardized value to achieve comparable data. The statistics was performed using one-way ANOVA or ttest generated by GraphPad Prism.

Table 2.3. The animal weights and compensation for the dose given.

treated group	animal weight	dose/weight compensation
OEG-amine	350	0.142857
	251	0.199203
	253	0.197628
	330	0.151515
insulin	245	0.204082
	225	0.222222
	245	0.204082
	248	0.201613
glucose	235	0.212766
	239	0.209205
	208	0.240385
	213	0.234742

[I performed this procedure at Midatech Pharma in Bilbao, Spain with the help and support of Ibon Perera and Julen Barrenetxea.]

2.3.5 Determination of the blood-brain barrier integrity by immunochemistry

Brain sections corresponding to the area in the brain used for electron microscopy were selected from 4 animals. Glutaraldehyde fixation of the sections was blocked using 0.05 M Tris/HCl buffer, pH 6.8, overnight. To block non-specific binding, 5% goat serum with 0.01% Tween 20 was applied and incubated for 3 hrs. Then, primary antibody (1/100 biotinylated goat anti-mouse IgG, Dako, USA), prepared in 1% goat serum in PBS, was added and incubated overnight. Serial washes with PBS followed over 3 hrs. Biotinylated horseradish peroxidase complex (1:700 in PBS) was added to the sections for 2 hrs. After serial washes for 1 hr, the chromogen was prepared: tetramethylbenzidine at a final concentration of 0.1 mg/ml, was dissolved in 0.1 M sodium acetate/citric acid buffer, pH 6.0. Hydrogen peroxide at a final concentration of 0.03% w/w was added just before the sections were ready to image. The reaction took place within 3 min and appeared as a blue staining. The staining was stable for 20 min during which time the images were taken, using a Nikon microscope. From each brain section, 5 images were taken with the 5x objective and 5 images with the 20x objective from each cortex, including ipsilateral and contralateral sides of the corresponding region.

Chapter 3. Transport of glyconanoparticles across the blood-brain barrier *in vitro*

3.1 Introduction

Gold nanoparticles have a great potential as a delivery system across the blood-brain barrier. One such delivery system is gold nanoparticles covalently coated with sugars, or glyconanoparticles, which are introduced here.

3.1.1 Glyconanoparticles as a type of therapeutic nanoparticles

Glyconanoparticles, as the name suggests, combine the worlds of glycoscience and nanotechnology. A variety of nanomaterials, such as gold nanoparticles, quantum dots, carbon nanotubes or fullerenes, and silica nanoparticles, can be used for attaching glycans (Reichardt et al. 2013). We will focus on gold glyconanoparticles here, which can be very useful in biological and therapeutical context. For example, they can be used to investigate carbohydrate interaction in basic science research; create vaccines, function as an anti-adhesive treatment against cancer or infections, or be used as biosensors and in diagnosis (Reichardt et al. 2013), see Figure 3.1. There are several advantages of using glycans as ligands for gold nanoparticles. Firstly, glycans are a natural substance, in comparison with synthetic polymers. Secondly, the resulting nanoparticles are very stable and soluble in water. Thirdly, the glycan interactions are specific, even though with lower affinity or monovalency when compared to antibodies.

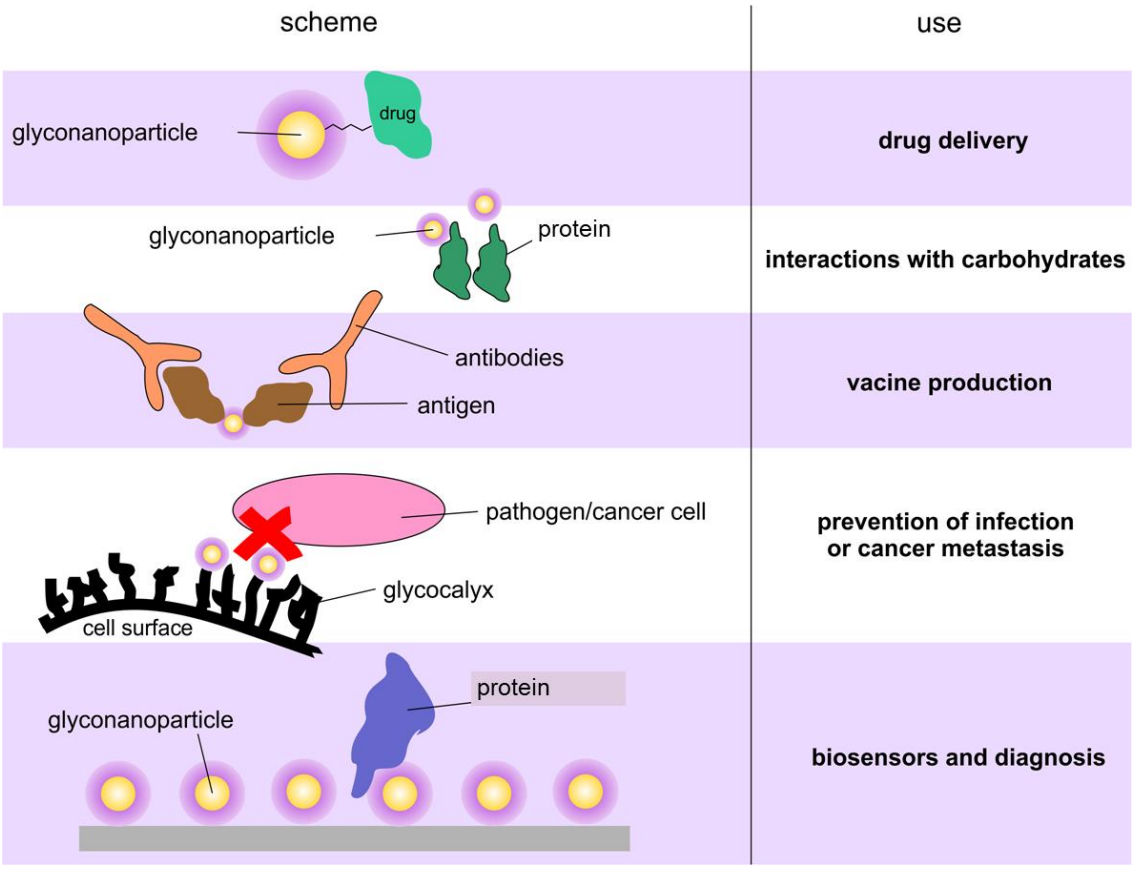

Figure 3.1 Uses of glyconanoparticles relevant to biology and therapy. The multiple uses of the nanoparticles (right column) are depicted in schemes (left column).

Glycan-protein interactions can be therapeutically useful. Pathogens usually firstly bind to host cells by identifying specific proteins on the cell surface. If this interaction is interrupted, by binding and "neutralizing" a protein either on the pathogen or on the host cell, this may halt the infection (Bernardi et al. 2013). One example of these interactions with pathogens is preventing mannose-rich glycoprotein on HIV virus (gp120) from adhering to glycosphingolipids on cells of the mucosal membranes, by using nanoparticles coated with galactosyl- and glucosyl-β-*C*-glycosides (Nolting et al. 2003). Moreover, mannose-coated gold nanoparticles have been shown to inhibit HIV attachment to specific dendritic cells (García et al. 2010). Furthermore, adhesion of cancer cells to endothelial cells, the key step of spreading metastasis and its seeding into target tissue may be interrupted with glyconanoparticles. For

example, lactose-coated gold nanoparticles prevented adhesion of cancer cells to endothelium (Rojo et al. 2004).

Moreover, glyconanoparticles can also form a platform for drug delivery, even though this function has not been as widely researched as the carbohydrate-carbohydrate interaction. One of the examples of drug delivered to derived HeLa cells was HIV pro-drug (Chiodo et al. 2014). This dissertation is also aimed at finding a way to use glyconanoparticles to carry nucleic acids, as will be detailed in Chapter 6.

3.2 Results and Discussion

This study has evolved from our initial finding (Gromnicova et al. 2013) that small gold glyconanoparticles, of 2 nm core coated with glucose, were taken up into human brain endothelial cells (hCMEC/D3). We proposed that this type of nanoparticle had potential as a therapeutic delivery system into the brain.

For the purpose of this work, we made a choice about the cell line used as well as the nanoparticle formulations. To choose the appropriate human brain endothelial cell line the factors and priorities in the investigations needed to be considered. Not a single cell line satisfies all aspects compared to an *in vivo* blood-brain barrier. From the several human cell lines established, hCMEC/D3 (human cerebral microvascular endothelial cells) (Weksler et al. 2005) is the most characterized and widespread model (Weksler et al. 2013; Helms et al. 2016). At the time of starting this doctoral project, a new source of human brain endothelial cells have emerged – stem cells (Boyer-Di Ponio et al. 2014; Lippmann et al. 2012; Cecchelli et al. 2014). However at the time, stem cell-derived brain endothelial cells had not been as well established and characterized, thus a cell line was more suitable.

As possible nanoparticle formulations to cross the blood-brain barrier *in vitro* we selected 3 formulations (See Foreword on motivation for this work). These nanoparticles were compared for their uptake efficiency into brain endothelial cells hCMEC/D3 and in a co-culture model of the blood-brain barrier as detailed below; the cytotoxicity of these nanoparticles is also shown here.

3.2.1 Single-ligand glyconanoparticle formulation

The first nanoparticle formulation with a single ligand, a glyconanoparticle coated with glucose, was based on our initial work (Gromnicova et al. 2013). This type of nanoparticle functioned as a reference for the effectiveness of nanoparticle uptake. Glucose (Figure 3.2A) was attached to the nanoparticle core via a two carbon linker that had a thiol bond attaching it to the gold core (Figure 3.2B). The diameter of this nanoparticle formulation was 1.7 ±0.83 nm, this size distribution can be seen in a histogram in Figure 3.2C and in a representative electron micrograph in Figure 3.2D. Electron microscopy was used to quantify and localise gold nanoparticles inside brain endothelial cells. As mentioned in the introduction, this technique allowed us to quantify non-destructively the amount of gold nanoparticles in cytosol, vesicles and other locations, such as junctions and nucleus; very few nanoparticles were found in junctions and nucleus and thus these compartments were not used for comparative analysis of nanoparticle uptake.

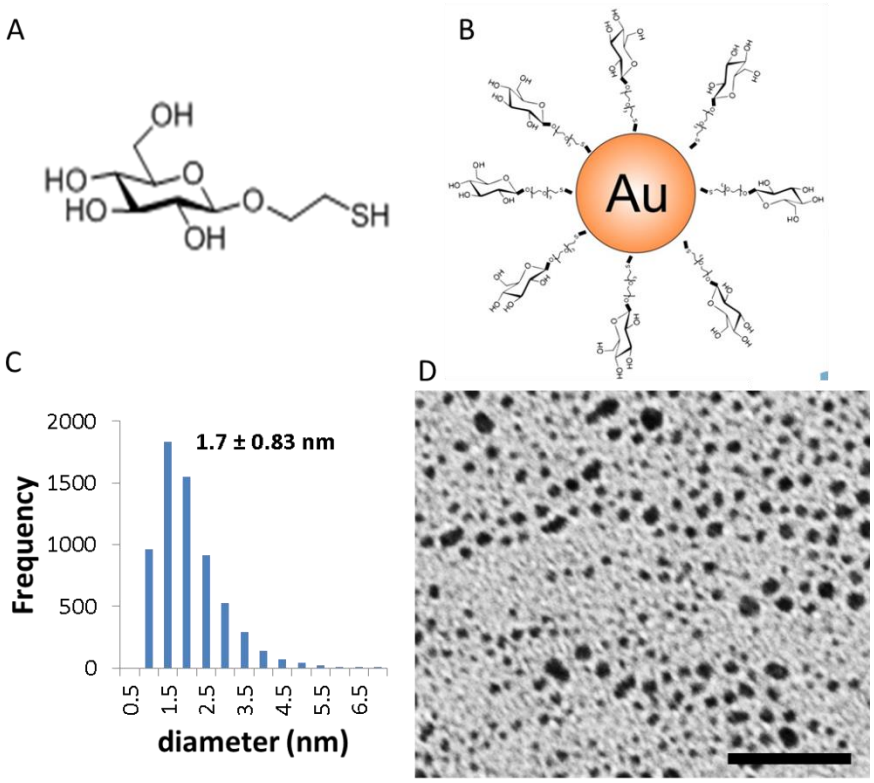

Figure 3.2 **Characterisation of glucose-coated gold nanoparticles.** A. The chemical structure of ligand glucose used to coat these nanoparticles. B. Scheme of the nanoparticles, glucose has a 2-carbon link with a thiol bond, attaching it covalently to the gold core. C. Size distribution of the nanoparticle core with mean ± standard deviation. Data analysed from 3 TEM images. D. Representative transmission electron micrograph of the nanoparticles, one of which was used for the size-distribution analysis. Scale bar = 25 nm.

We also tested glyconanoparticles coated with lactose, maltose and galactose in order to compare their uptake into brain endothelium. The uptake was tested after 8 hr incubation with brain endothelial cells. The tested sugars have a similar charge and corresponding nanoparticles were prepared in a similar way to glucose-coated nanoparticles. Because of this, we did not expect dissimilar cell uptake. However, in a pilot experiment (Figure 3.3) we found that uptake of maltose and lactose-coated nanoparticles by brain endothelial cells was about 10% of that of glucose-coated ones. Only galactose-coated nanoparticles had very similar cell uptake profile. Both maltose and lactose are disaccharides whereas glucose and galactose are monosaccharides which may cause a different stoichiometry of the ligand shell on the nanoparticles. If the ligand

arrangement on the nanoparticle surface is random rather than orderly, this may reduce nanoparticle uptake by the cell (Lund et al. 2011; Verma et al. 2008).

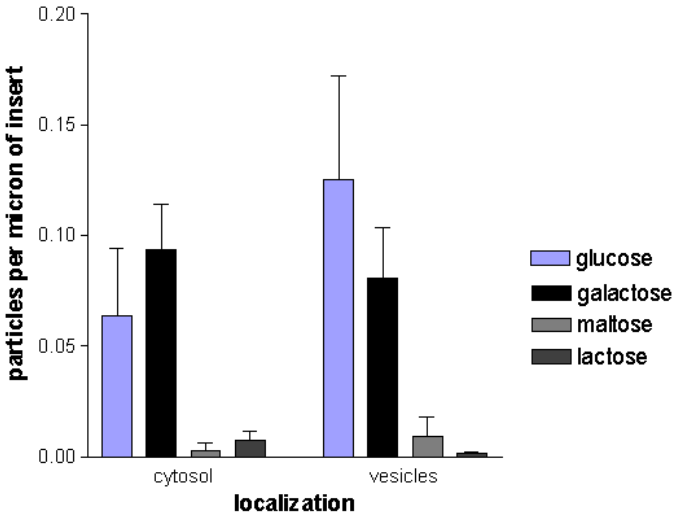

Figure 3.3. Comparison of uptake efficiency of gold glyconanoparticles into brain endothelial cells. Glyconanoparticles coated with glucose, galactose, maltose or lactose were assessed for their uptake efficiency into hCMEC/D3 cell after incubating them for 8 hrs at a concentration of 8 µg/ml. A pilot experiment was performed, data show mean ± SEM of three technical replicates.

3.2.2 Double-ligand glyconanoparticle formulation

The selection of another type of glyconanoparticle was based on the finding that an orderly structure of two surface ligands enhances uptake of nanoparticles (Lund et al. 2011; Verma et al. 2008). Thus, a dual-ligand nanoparticle was used. One ligand may be glucose or galactose, as their uptake properties to brain endothelium were similar. The other ligand was thought to add structured morphology to the resulting ligand shell. OEG-amine [oligo(ethylene glycol) amine] was selected as it contains hydrophilic OEG and an amine group which gives positive charge to the resulting nanoparticle at pH 7.4. The OEG-amine chain was 17-amino-3,6,9,12,15-pentaoxaheptadecane-1-thiol (Figure 3.4A). It is possible to control the ligand ratio of sugar : OEG-amine, however 50:50 ratio has been previously shown to be the most efficient for

nanoparticle entry in cells (Lund et al. 2011; Verma et al. 2008). Therefore, a nanoparticle with OEG-amine/galactose at 50:50 ratio was formulated and selected (Figure 3.4B), with the core size of 2.24±0.77 nm (Figure 3.4C). The chemical structure of galactose ligand used to coat this nanoparticle is shown in Figure 3.4D. A representative electron micrograph of these nanoparticles is shown in Figure 3.4E. Another useful property of this nanoparticle is that its positive charge can interact with negatively charged molecules in a non-covalent way.

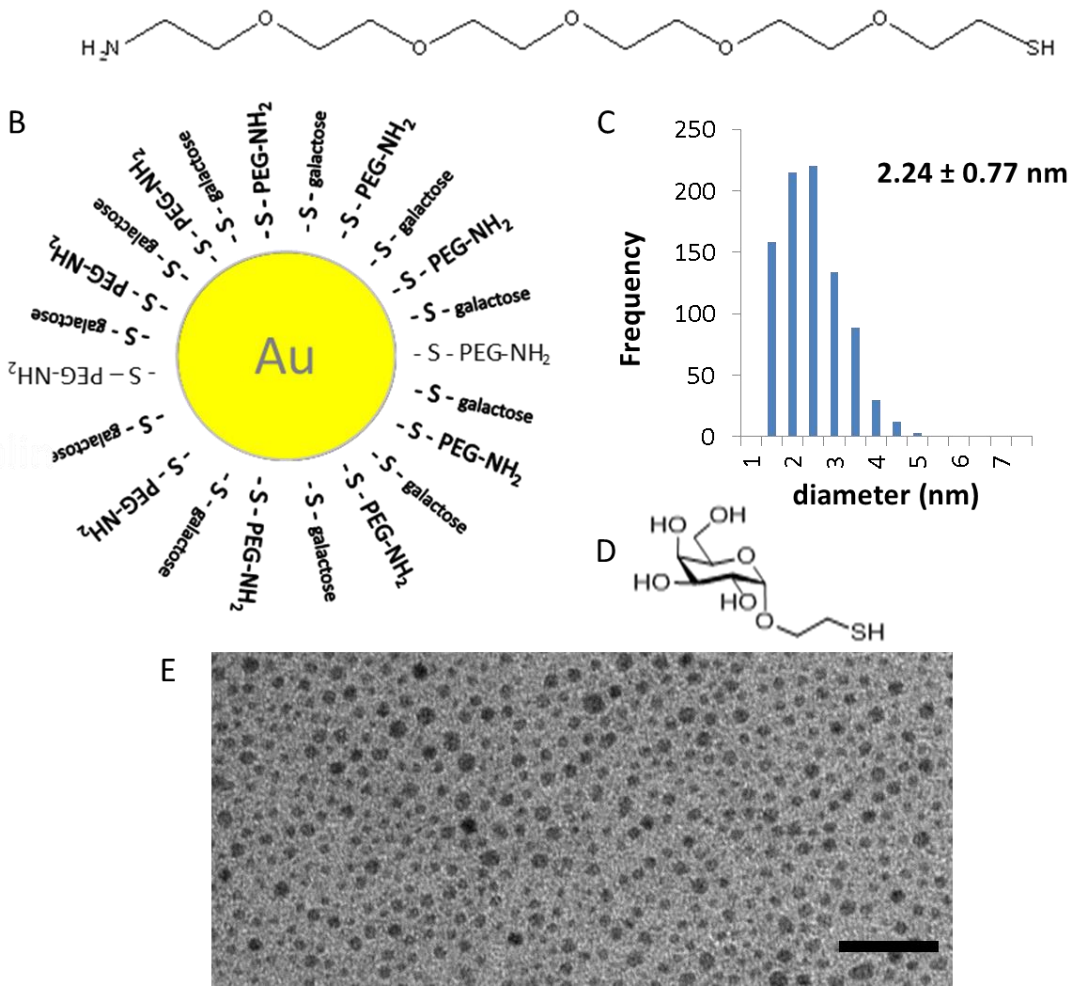

Figure 3.4 **Gold nanoparticles coated with OEG-amine/galactose.** A. The chemical structure of attached OEG chain. B. The schematic ligand organization of thiol-OEG-amine and thiol-C2 galactose (C2 stands for a carbon linker) in equal ratio on the nanoparticle. C. size distribution of the gold nanoparticles with mean ± standard deviation. Data analysed from 3 TEM images. D. chemical structure of ligand galactose used to coat these nanoparticles. E. electron microscopy of the nanoparticles (scale bar = 20 nm).

3.2.3 Triple-ligand glyconanoparticle formulation

Another formulation of glyconanoparticle that we used contained three ligands. Ligands OEG-amine and galactose as in the previous formulation were attached to the gold core in a 50:50 ratio and insulin was attached non-covalently to amine groups (Scheme in Figure 3.5A). On average, each nanoparticle contained about 7 insulin molecules (Midatech Pharma, personal communication). Insulin molecules interacted electrostatically with amine groups on the OEG chains as insulin is negatively charged at a neutral pH (pI = 5). The evidence of this interaction was analysis of protein content in the supernatant of isolated nanoparticles. This type of nanoparticle was also observed to sediment, perhaps due to crosslinking between insulin and the amine groups.

This type of nanoparticle had a core diameter of 1.5 ± 0.6 nm (Figure 3.5B). The electron micrograph of these nanoparticles is shown in Figure 3.5C. The selection of insulin was based on the fact that it may enhance brain transport. Brain endothelium and other cells of the brain have insulin receptors (Havrankova et al. 1981). Insulin can be transported across the brain endothelium using receptor-mediated transcytosis. Transferrin is also used as a targeting molecule for brain transcytosis, however, the transcytosis using transferrin receptor is less efficient. When compared with insulin receptor using corresponding antibodies in rhesus monkey (anti-transferrin receptor and anti-insulin receptor), insulin receptor showed 10-fold higher transcytosis (Friden et al. 1996; Pardridge et al. 1995).

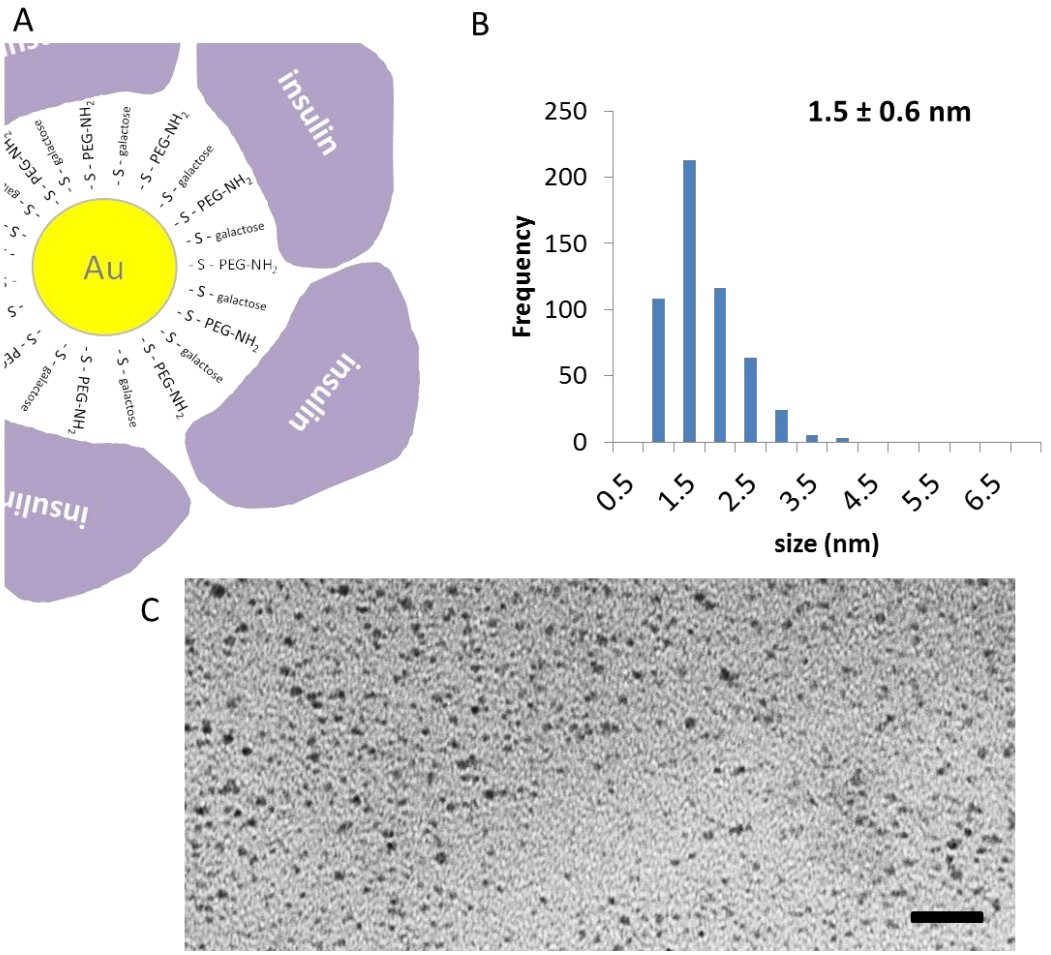

Figure 3.5 **Characterisation of nanoparticles coated with OEG-amine/galactose/insulin.** A. Scheme of ligand organisation with insulin non-covalently attached to OEG-amine. B. Size distribution of the nanoparticles with mean ± standard deviation. Data analysed from 3 TEM images. C. Electron micrograph of the nanoparticles. Scale bar = 20 nm.

3.2.4 Comparison of uptake efficiency of the three glyconanoparticle formulations on brain endothelium

All three formulations were compared for their uptake efficiency to brain endothelial cells (hCMEC/D3). We hypothesised that OEG-amine may enhance the uptake due to its positive charge, which may promote interaction of the nanoparticle with the negatively-charged membrane. Indeed, nanoparticles coated with OEG-amine/galactose with or without insulin were most efficiently entering the cells as they had the highest count of nanoparticles in vesicles

(Figure 3.6 and Appendix Figure 1: Representative electron images of analysed samples of hCMEC/D3 cells treated with different types of nanoparticle formulation (i.e. coated with glucose, insulin or OEG-amine).). Insulin on OEG-amine/galactose nanoparticles did not significantly increase cell uptake into the vesicles or cytosol compared to OEG-amine/galactose nanoparticles only.

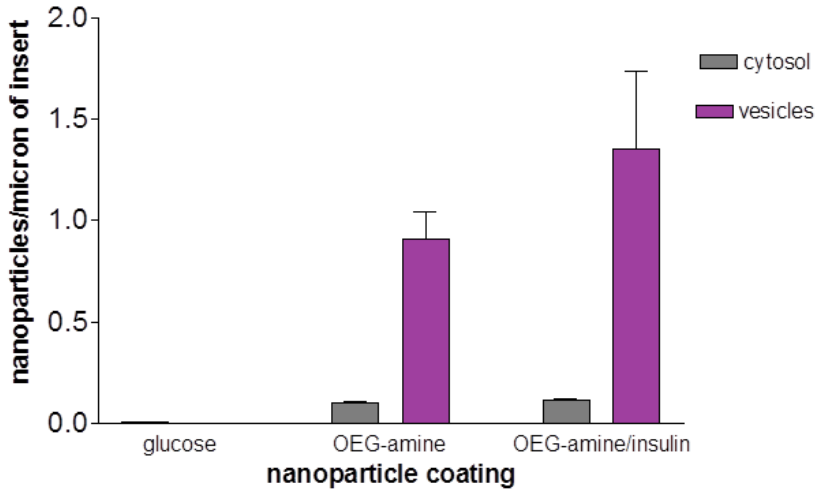

Figure 3.6 **Comparison of uptake of selected formulations of gold nanoparticles into brain endothelium.** Data show mean ± SEM from 3 independent experiments, incubation time 3 hrs, nanoparticle concentration 8 µg/ml. One-way ANOVA, **P<0.01, ***P<0.001.

Therefore, we considered whether the insulin receptor was involved in the uptake of OEG-amine/galactose/insulin nanoparticles. *In vitro* cultures may sometimes change their phenotype compared to their in vivo counter parts. Thus we used flow cytometry to determine whether that the insulin receptor was present on hCMEC/D3 cells (Figure 3.7A). The insulin receptor was then knocked down with corresponding siRNA (Figure 3.7B) and the nanoparticle uptake analysed (Figure 3.7C). Contrary to the hypothesis, the knockdown of the receptor did not decrease the nanoparticle uptake, but significantly increased it. One of the explanations for this phenomenon may be increase of the rate of endocytosis upon transfection, explaining the higher number of nanoparticles in vesicles. It may be also possible that the insulin is released

from the nanoparticle in the culture medium before it reaches the cell and thus is not actually functioning as a targeting molecule. Insulin nanoparticles have been shown as a promising nano-carrier system before (Shilo et al. 2014). The authors linked insulin to OEG via an Au-S bond and tested the difference in uptake *in vivo*. However, no evidence was shown to confirm that the insulin receptor was actually involved in the transcytosis of these 30 nm gold nanoparticles into the brain. However when compared to our results, perhaps stronger attachment of insulin to nanoparticles may result in better insulin receptor involvement in comparison with the non-covalent approach.

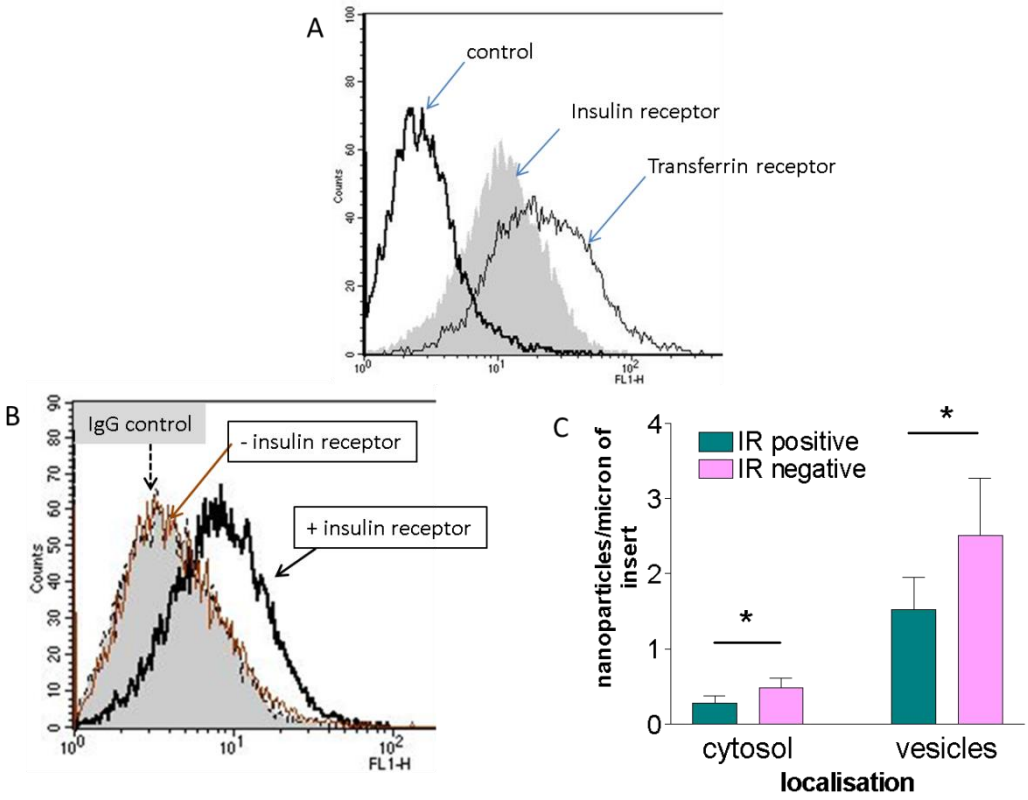

Figure 3.7 **Insulin receptor and its knockdown to test involvement of insulin receptor on uptake of insulin/OEG-amine nanoparticles.** A. The expression of insulin receptor in hCMEC/D3 cells as compared to the expression of transferrin receptor. Cells stained with no antibodies (control) or antibodies against insulin receptor or transferrin receptor. B. The representative FACS histogram of knockdown of insulin receptor on hCMEC/D3. The control population of unstained cells (IgG control cells), cells with siRNA knocked-down insulin receptor (- insulin receptor) and cells expressing insulin receptor (+ insulin receptor), silenced with a scrambled siRNA control. C. The uptake of insulin/OEG-amine nanoparticles into hCMEC/D3 cells with insulin-knockdown (IR negative) at 3 hrs. Data show mean ± SEM from 3 independent experiments, t-test, * P< 0.05.

Moreover, insulin/OEG-amine nanoparticles were also observed to sediment, thus possibly having a larger hydrodynamic diameter. Therefore, the interaction of these nanoparticles with cells might have been different in comparison to OEG-amine alone, which did not sediment. Also, we did not determine the rate of insulin release from the nanoparticle; it is possible that some insulin molecules detached from the amines on the nanoparticles since the electrostatic bond is not as strong and the Au-S bond.

3.2.5 Transport of glyconanoparticles across a 3-dimensional blood-brain barrier model

The ultimate function of nanocarriers used for brain therapy is to cross blood-brain barrier and enter cells of brain in order to deliver a potential treatment. Therefore, we tested our 3 selected formulations of gold nanoparticles for their efficiency to enter astrocytes after passing through the brain endothelium in a 3-dimensional co-culture model. In this model (Figure 3.8), human astrocytes are cultured inside a collagen gel and brain endothelium is cultured on top of the gel (Sreekanthreddy et al. 2015). The gel is also compressed to remove surplus water from the gel matrix and to increase density of astrocytes.

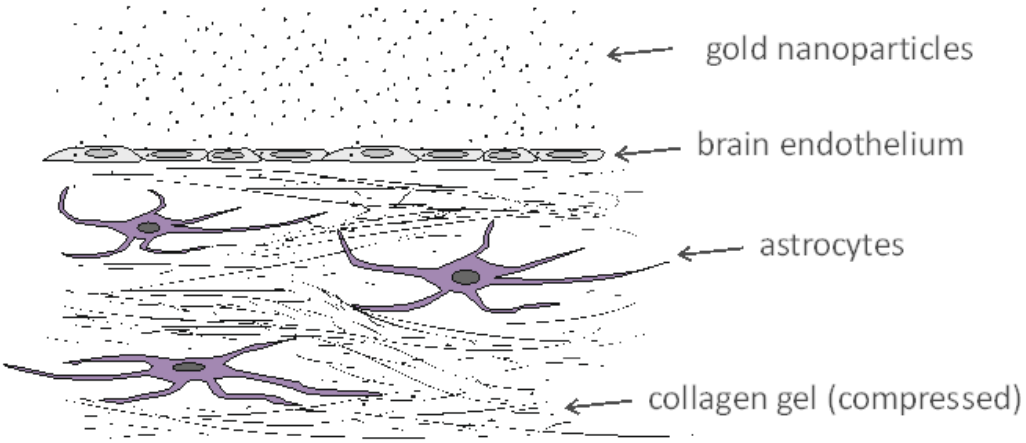

Figure 3.8 **Scheme of 3-dimensional model of the blood-brain barrier used for the nanoparticle uptake.** Human primary astrocytes are cultured in a collagen gel and compressed to remove over 90 % of liquid from the gel to increase the density of astrocytes. On top of this gel surface, brain endothelial cells (hCMEC/D3 cells) form a monolayer. When gold nanoparticles are applied, they can cross the brain endothelium and enter the gel below containing astrocytes.

This model was used for testing transport of gold glyconanoparticles. Electron microscopy showed clearly that all 3 nanoparticles were able to transport across the brain endothelium and enter astrocytes, as nanoparticles were observed in both cell types (Figure 3.9). We have reported on using this model for assessing transport of glucose-coated gold nanoparticles in our previous work (Gromnicova et al. 2013).

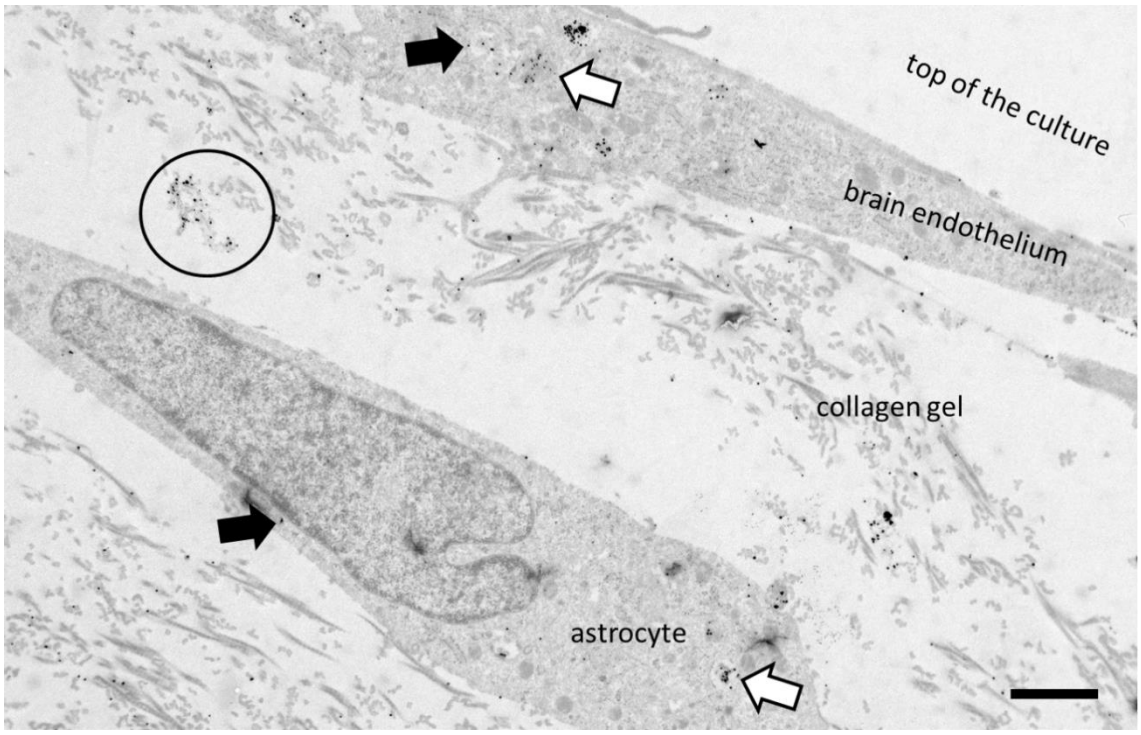

Figure 3.9 **Co-cultured 3-dimensional model of the blood-brain barrier used in the nanoparticle transport.** Silver-enhanced insulin-coated gold nanoparticles were found in brain endothelium, astrocytes and in the collagen gel (3 hr incubation). Different types of localisation are shown: in cytosol (black filled arrow), in vesicles (white arrow), in collagen (circled).

The uptake of nanoparticles into astrocytes was quantified. We found that nanoparticles coated with OEG-amine/galactose and OEG-amine/galactose/insulin had a significantly higher transport into vesicles compared to nanoparticles coated with glucose (Figure 3.10). This finding is similar to the observation of higher uptake rate of nanoparticles coated with OEG-amine/galactose and OEG-amine/galactose/insulin into brain endothelium in comparison to glucose-coated nanoparticles (Figure 3.6). Similarly to the finding on brain endothelial cells where insulin receptor was not involved in the uptake of OEG-amine/galactose/insulin nanoparticles into the cells (Figure 3.7), here also insulin did not increase OEG-amine/galactose nanoparticle transport rate across the brain endothelium.

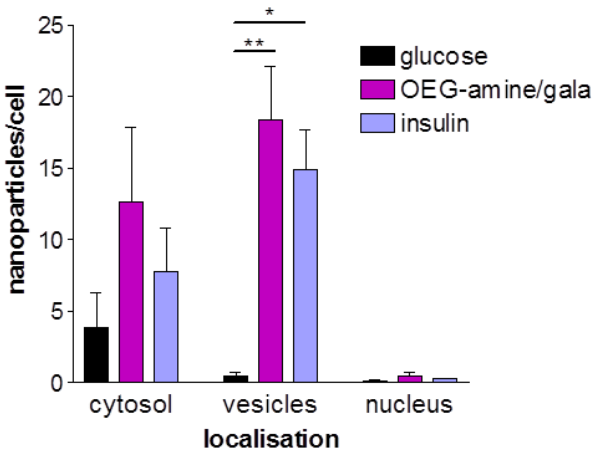

Figure 3.10 **Gold nanoparticle uptake into co-cultured astrocytes.** Gold nanoparticles coated with glucose, OEG-amine/galactose (OEG-amine/gala) and OEG-amine/galactose/insulin (insulin) were investigated for their uptake at 8 µg/ml for 3 hrs. 3 independent experiments, Data show mean ± SEM from 3 independent experiments. ANOVA, Tukey post test, *P<0.05, **P<0.01. Note the difference in the quantification method - here the nanoparticles are counted per cell rather than in cells at a certain length of an insert membrane. This is due to astrocytes being in a 3D environment whereas cells grown on a support are in a 2D environment.

The next step was to investigate cytotoxicity of these nanoparticles, as detailed below, and the mechanism of transport that is responsible for this efficiency in uptake of OEG-amine/galactose nanoparticles, which is detailed in the next chapter.

3.2.6 Investigation of cytotoxicity of three formulations of glyconanoparticles on brain endothelial cells

As these nanoparticles seemed to be effective in their transport into and across cells, we needed to establish that they are not cytotoxic. An MTT assay was used; in this assay viable cells metabolize insoluble yellow tetrazole salt to soluble purple formazan with their dehydrogenase enzymes (Mosmann 1983). MTT assay was performed on various concentrations of the nanoparticles at 24 hrs and no reduction of viability was found (Table 3.1).

Table 3.1 Investigation of cytotoxicity of gold nanoparticles to brain endothelium. Summary of MTT assays investigating cytotoxicity of gold nanoparticles at 22 – 24 hr incubation, 4 technical replicates, NS not significant difference, as analysed by one-way ANOVA. All experiments are summarized with concentrations used on hCMEC/D3 cells.

Nanoparticle	Concentrations investigated	Reduction in cell viability	No. of independent experiments performed
Glucose, 3 batches	4 μg/ml to 32 μg/ml	NS	3 (1 per batch)
OEG-amine /galactose	4 μg/ml to 32 μg/ml	NS	3
galactose	4 μg/ml to 32 μg/ml	NS	1
Lactose	4 μg/ml to 32 μg/ml	NS	1
Mannose	4 μg/ml to 16 μg/ml	NS	1
OEG-amine/gala/Insulin	4 μg/ml to 16 μg/ml	NS	2

Investigation of longer incubation times was also performed. Out of the four selected formulation of nanoparticles, OEG-amine/galactose decreased viability by about 30% after 2 days of incubation (Figure 3.11A). We then investigated toxicity concentration threshold of OEG-amine/galactose nanoparticles from 8 μg/ml (concentration used in cell studies) to 75 μg/ml (Figure 3.11B). The concentrations up to 32 μg/ml showed no cytotoxicity, however from 50 μg/ml the viability dropped. This concentration-dependency of toxicity might be due to the charge the nanoparticles have. We have found these nanoparticles stick to the insert membrane that the cells grow on, and which is slightly negatively charged (Sreekanthreddy et al. 2015). Thus, as the nanoparticles transported across the cells in higher numbers, more nanoparticles could bind to the insert's surface, perhaps causing cells to detach and die. On the other hand, this effect would not be relevant in a dynamic environment *in vivo* where the nanoparticle concentration would soon be dispersed away from the vessels into the tissues (See Chapter 5 for *in vivo* work).

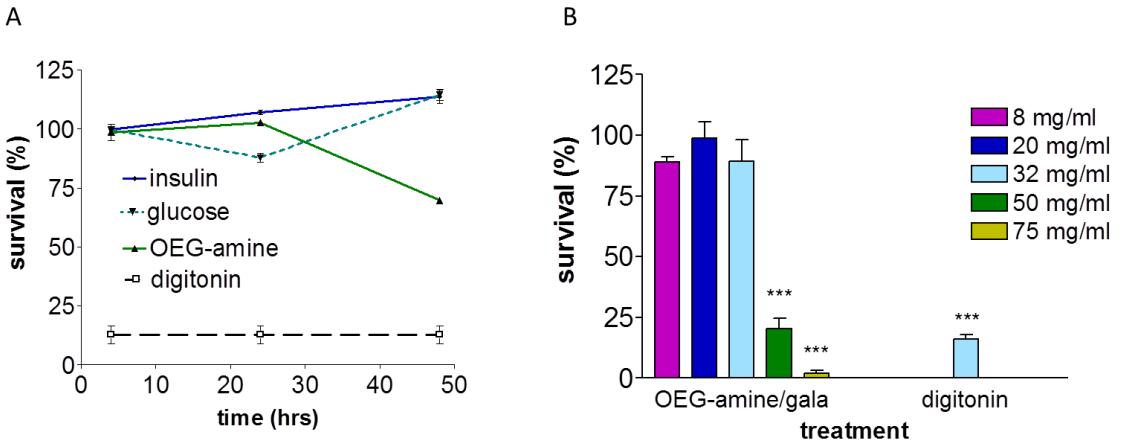

Figure 3.11 Investigation of toxicity of OEG-amine/galactose gold nanoparticles to brain endothelial cells (hCMEC/D3). A. MTT assay of the nanoparticles over time coated with OEG-amine, insulin and glucose at 32 µg/ml during 48 hr, positive control is 30 µg/ml digitonin, extended as a dotted line. Data shown as mean ±SEM of 2 independent experiments. B. MTT assay of the nanoparticles testing its different concentrations at 48 hrs exposure to the cells. Positive control of cell death is 30 µg/ml digitonin (30 min treatment), indicated as a dotted line. Data shown as mean ±SEM of 3 independent experiments. One-way ANOVA, Dunnett's multiple comparison test (treatments compared to the control) ***P < 0.001.

Other assays can be used as well to determine cytotoxicity. Apoptosis and necrosis can be determined by measuring levels of annexin V and 7-amino-actinomycin D by flow cytometry. For example these have been used by other groups to establish that gold nanoparticles (10 nm) stabilized with sodium citrate and poly-(N-vinyl)-2-pyrrolidone) induced apoptosis or necrosis in mouse dendritic cells at nanoparticle concentration of 500 µM for up to 48 hrs (Villiers et al. 2010). However, MTT assay can be useful way to determine toxicity of a very wide range of nanoparticles. Other methods can then be used if a specific toxicity issue is detected. Also transmission electron microscopy can be initial indicator of other types of cellular damage that may be caused by nanoparticles, such as oxidative stress and mitochondrial damage, or DNA damage. Specific assays that determine these can then be employed and the cell death specifically determined. For example, oxidative stress can be caused by nanoparticles coated with triphenylphosphine monosulfonate (Pan et al. 2009). Necrosis may be caused by these nanoparticles forming ROS (reactive oxygen species) which then can disrupt

mitochondrial membrane. Similarly to this study, Mateo et al. (2014) investigated gold nanoparticles of larger sizes, 30 -90 nm, for causing cell damage. The authors correlated the nanoparticle-induced damage to leukaemia and hepatoma cell lines with decrease in cellular glutathione (GSH) and increase in ROS production.

3.2.7 Summary and conclusion

Gold nanoparticles <5 nm hold a great potential to be used as nano-carriers into the brain as shown *in vitro* both on brain endothelial cells and in a co-culture model. 3 formulations of nanoparticles were used for these studies: gold nanoparticles coated with glucose, OEG-amine/galactose or OEG-amine/galactose/insulin. Glucose and galactose had similar transport efficiency into brain endothelium, but addition of positive charge in the ligand OEG-amine enhanced uptake of this glycan-coated nanoparticle. By contrast, insulin molecules, that were non-covalently attached to OEG-amine/galactose nanoparticles, did not enhance their ability to enter brain endothelium over its control OEG-amine/galactose nanoparticles. The way insulin interacts with OEG-amine and the strength of the interaction in the cell medium may need investigation since the resulting nanoparticle sediments and thus may have a larger hydrodynamic diameter.

Investigations of toxicity confirmed no toxicity of up to 4x higher concentrations than those used in transport studies, and more than 10x longer nanoparticle incubation times. These nanoparticles are safe to use on brain endothelial cells and may be safe for other cell types and cell lines due to their low toxicity.

In the following chapter, investigations into highly efficient transport of OEG-amine/galactose nanoparticles into cells will uncover some of the factors that may contribute to this phenomenon.

Chapter 4. Transport mechanisms of gold nanoparticles coated with OEG-amine/galactose in various endothelial cells

4.1 Introduction

4.1.1 Mechanism of transport of gold nanoparticles into cells

Gold nanoparticles can be taken up by the cells in two main ways. The first way, active transport, involves endocytosis whereas the second way, passive transport, does not need energy and involves nanoparticles moving through the plasma membrane. Moreover, if gold nanoparticles were required to cross the brain endothelium to achieve their therapeutic potential, they should be able to do this either actively by endocytosis and exocytosis (i.e. transcytosis) or passively through cytosolic transport (Figure 4.1).

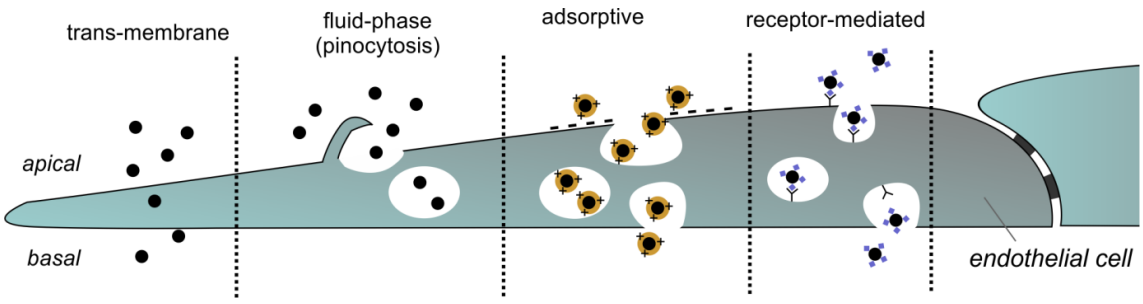

Figure 4.1 The mechanism of transport of small gold nanoparticles into and across brain endothelium. Passive transport (trans-membrane) involves nanoparticles passing across the plasma membranes. The active transport involves fluid-phase (pinocytotic), adsorptive and receptor-mediated endocytosis. Transcytosis occurs via adsorptive or receptor-mediated endocytosis at the brain endothelium.

4.1.1.1 Active transport of gold nanoparticles

Active transport is a way for cells to take up nutrients, vitamins or signalling molecules using energy. This transport can be very efficient, carrying large quantities of material into cells. Endothelial cells use active transport to transcytose material across the cell and release it on the basal side.

Nanoparticles may be able to enter the cells via endocytosis. This can be linked to a specific receptor ("receptor-mediated" endocytosis), be non-specific by adsorbing onto the cell surface, i.e. "adsorptive" endocytosis, or can be taken up as part of larger volume of liquid by the cell, i.e. fluid phase endocytosis (pinocytosis) (Figure 4.1). These categories may include distinctive structural molecules that may coat the vesicle, such as clathrin, caveolin, or be uncoated (Iversen et al. 2011). From a therapeutic point of view, "receptor-mediated" endocytosis can be very useful if a specific receptor is targeted by the nanoparticle ligand formulation such as transferrin receptor (Prades et al. 2012), insulin receptor (Shilo et al. 2014), or LDL receptor, to name just a few present on brain endothelium.

Transmission electron microscopy can be used to determine whether the nanoparticle uses active transport mechanism to enter a target cell. At the ultrasctructural level, the nanoparticles can be detected in various types of vesicles or at different stages of endocytosis. Then, the involvement of active transport in nanoparticle cell transport can be examined by two methods. Firstly, cell cultures can be incubated at 4 °C (Gu et al. 2009; Verma et al. 2008; Jiang et al. 2008; Hao et al. 2012), or secondly, specific pharmacological inhibitors can be used to either inhibit whole cellular metabolism (Verma et al. 2008) or to act on a narrower range of cellular processes. The example of the latter ones are antibiotic inhibitors, that have been previously shown to block endocytosis (Lund et al. 2011).

4.1.1.2 Passive transport of gold nanoparticles

Passive transport involves passive diffusion of nanoparticles into the cell. Therefore, this process can be less efficient than endocytosis, carrying lower amounts of nanoparticles into the cell at any one time. If the therapeutic aim is to deliver cargo across the cell, such as drug delivery across the brain endothelium, the process will be influenced by the fact that the nanoparticles should pass across two plasma membranes – the apical and basal – to reach their target. As a result, the physical properties of the membrane may be critical.

4.1.1.2.1 Simulation models of cell membrane penetration by gold nanoparticles

The passage of small gold nanoparticles into cells by crossing the plasma membrane has been modelled *in silico* (Figure 4.2). Several models of this phenomenon have emerged and understanding of this process has been improving since it was first described (Ginzburg & Balijepalli 2007; Leroueil et al. 2008; Lin et al. 2010).

One of the earlier models of membrane penetration used cationic, anionic and hydrophobic 2.2 nm gold nanoparticles. The nanoparticle was enveloped by the membrane resulting in the cytosolic lipid layer to be forced downwards (Figure 4.2B). After the nanoparticle penetrated, a hole in the lipid bilayer formed, especially in the case of cationic nanoparticles (Lin et al. 2010) and other highly charged nanoparticles (Ginzburg & Balijepalli 2007). Using this model, Leroueil et al. (2008) found that slightly larger cationic nanoparticles (5 – 6 nm) used existing holes in the membrane to enter the cell, not causing membrane holes themselves.

An improved simulation by Lin & Alexander-Katz (2013) used 2.2 nm cationic nanoparticles (Figure 4.2C). When these nanoparticles approach the plasma membrane, they bind to the bilayer and translocate through it. This allows the nanoparticles to penetrate the membrane using passive transport up to a level before transmembrane potential is depleted, after which the nanoparticles can enter via active transport. Once the membrane potential is re-established, both transport mechanisms can take place. Holes in the membrane close behind nanoparticles, leaving no permanent membrane damage. The authors suggest that these nanoparticles may use a similar mechanism to enter the nucleus as well (Lin & Alexander-Katz 2013).

Another model was based on <5 nm monolayer-protected gold nanoparticles whose ligands have both hydrophobic and hydrophilic regions (Van Lehn et al. 2013; Van Lehn & Alexander-Katz 2014; Gkeka et al. 2014). The process of membrane penetration by these nanoparticles was named as "snorkeling" (Figure 4.2A). While the nanoparticle is inserting into the membrane, the flexible backbone of ligands can change in order to mimic the lipid bilayer. The hydrophilic regions of the ligands move to the outside of the membrane while hydrophobic regions stay inside of the bilayer, parallel to phospholipids. The plasma membrane responds to this nanoparticle insertion by slightly deforming its phospholipids to a size of the coated nanoparticle in a spring-like fashion. In this model, both cationic and anionic nanoparticles of around 2 nm in size can penetrate the membrane passively without causing holes in the plasma membrane.

The described models are important for understanding of the passive uptake of gold nanoparticles through the plasma membrane. However, in a living system there are additional factors to be taken into account such as proteins that can associate with the nanoparticles (Casals et al. 2010; Walkey & Chan 2012). Thus, it remains to be seen how well the current models can represent the nanoparticle interaction with a living cell.

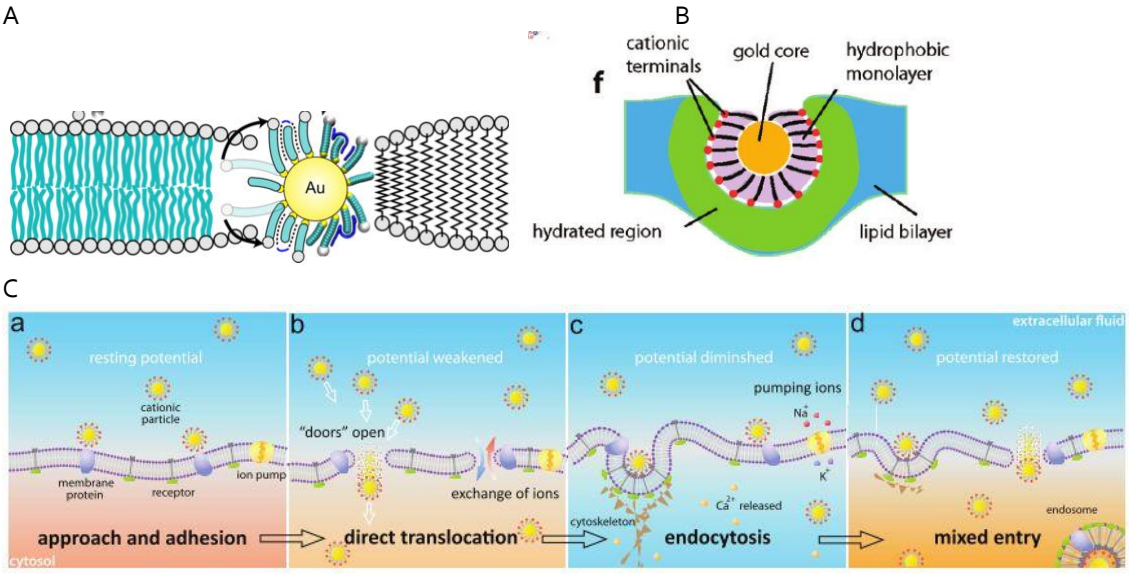

Figure 4.2 Models of passive transport of small gold nanoparticles into cells, i.e. their membrane penetration. A. Monolayer-protected gold nanoparticles penetrate through the plasma membrane via a process termed as "snorkeling" where ligands deform and rearrange themselves to mimic the lipid bilayer when inserting inside it (Van Lehn et al. 2013). B. Highly charged cationic nanoparticle penetrating through the cell membrane as the lower leaflet of the bilayer protrudes. The process forms a hole in the membrane which is water-permeable (Lin et al. 2010). The same group later showed that the process of uptake of cationic nanoparticles depends on local membrane depolarization (C). Here, nanoparticles attach to the plasma membrane as they approach it (a). At a certain concentration of cationic nanoparticles, the local membrane surface changes the transmembrane potential thereby opening the membrane for the already attached nanoparticles (b). The process carries on until the membrane potential is diminished, at which point the nanoparticles can enter only via endocytosis (c). Once the membrane potential is restored, the nanoparticles can use both types of entry (passive penetration or endocytosis)(d) (Lin & Alexander-Katz 2013).

4.1.2 Gold nanoparticles and their interaction with endothelial cells

In order for nanoparticles to be used as a specific nano-carrier into a certain cell type, we need to understand how cells respond to nanoparticles. The properties of nanoparticle, i.e. their size, charge and ligands, are investigated in how they interact with a cell. The same nanoparticle formulation may cause a different response by different cell types, leading to cell-selectivity. For example, it has been found that the same gold nanoparticle formulation can be taken up at different rates by various endothelial cells or epithelial cells (Freese et al. 2012).

Several key cell characteristics that may explain this difference are briefly introduced here, one of which is the cell surface - glycocalyx.

4.1.2.1 The role of glycocalyx in nanoparticle transport

When nanoparticles move through the blood, they may bind to the proteins or glycoproteins on the endothelial surface to enter the endothelium or directly pass through the membrane. But before nanoparticles can access the endothelium itself, they have to diffuse through the glycocalyx.

The glycocalyx is a brush-like structure that is located on the apical side of vascular endothelial cells with a variable size of 0.5 microns (van den Berg et al. 2003), 3 microns (van Haaren et al. 2003) up to 11 microns in bovine aortic endothelial cells (Ebong et al. 2011), depending on the type and size of blood vessel and species origin. The glycocalyx is composed of core molecules such as proteoglycans with a sulphated glucosaminoglycan (Table 4.1), glycoproteins and plasma-derived substances which interact with this network and bind reversibly (enzymes or their inhibitors, plasma proteins, growth factors and cytokines).

Table 4.1 Glucosaminoglycans usually found on endothelial surface and their targeting enzyme.

glucosaminoglycan	Targeting enzyme
Chondroitin sulphate	Chondroitinase
Heparan sulphate	heparinase
Hyaluronic acid	hyaluronidase

Endothelial glycocalyx has several functions in the body (Reitsma et al. 2007; VanTeeffelen et al. 2007). It is able to control penetration of several substances, based on their size and charge, as shown in experiments with dextrans. Protein permeation follows a different route as the glycocalyx appears to interact for example with albumin, as investigated in respect

to albuminaria, a kidney disease. Next, glycocalyx repels red blood cells and platelets; it also controls leukocyte adhesion via access to adhesion molecules present on the endothelial surface. Moreover, glycocalyx can transmit blood flow-induced mechanical forces such as sheer stress to endothelial cells. Plasma-derived molecules can also localise within the glycocalyx, resulting in signalling or enzymatic response (Reitsma et al. 2007; VanTeeffelen et al. 2007).

As the glycocalyx is the first structure which nanoparticles will interact with, studying the nanoparticle-glycocalyx interactions could help us to improve the design of nanoparticles. The interaction may involve several factors that can be theoretically modelled, such as osmotic pressure, electrostatic repulsion, steric repulsion between nanoparticles and glycocalyx, and entropic forces (Agrawal & Radhakrishnan 2007). This model was used to predict glycocalyx interaction with nanoparticles of diameter of 100 and 200 nm (antibody-coated) (Agrawal & Radhakrishnan 2007; Liu et al. 2011; Liu et al. 2010). Experimentally, 2.3 nm gold nanoparticles have been investigated for their attachment to human erythrocytes. In this study, glycocalyx has been found to be involved in this process (Atukorale et al. 2015).

4.1.2.2 Other cellular properties involved in nanoparticle transport

Other factors may be also involved in the differences in uptake rates of the same formulation of nanoparticles by different endothelial cells. This can be morphological differences between endothelial cells, such as when one cell is larger, accounting for higher amounts of nanoparticles, or the rate of active transport.

In the next section of this chapter, the uptake mechanisms of OEG-amine/galactose nanoparticles, whether active and passive, were investigated. Moreover, we screened these

nanoparticles on endothelial cells from vascular beds of different origin, and observed difference in uptake profile. This phenomenon may be explained by size of the respective endothelia, degree of endocytosis or their surface glycocalyx as introduced here.

4.2 Results and Discussion

This chapter investigates the mechanism of transport gold nanoparticles coated with OEG-amine/galactose, shortened as OEG-amine/galactose nanoparticles. Based on previous work shown in Chapter 3, OEG-amine/galactose nanoparticles showed the highest uptake rates by brain endothelial cells in comparison to other nanoparticle formulations. Moreover, OEG-amine/galactose nanoparticles were also able to enter brain, kidney, lung and bone marrow endothelial cells at different rates, a phenomenon that requires further investigation.

In the previous chapter we showed that the uptake of small gold nanoparticles into the brain endothelium depends on the type of ligand coating of the nanoparticle. What is the mechanism of transport that predisposes OEG-amine/galactose nanoparticles to be taken up more than glucose-coated nanoparticles? OEG-amine/galactose/insulin nanoparticles had similar uptake rate as OEG-amine/galactose nanoparticles; therefore, the comparison of uptake mechanism was largely focused on comparing OEG-amine/galactose nanoparticles with glucose-coated nanoparticles. In addition, as noted in Chapter 3, glucose- and galactose-coated nanoparticles appeared be taken up by similar uptake mechanism and thus we formed our investigations on uptake of glucose-coated nanoparticles.

4.2.1 The effect of incubation temperature on uptake of OEG-amine/galactose nanoparticles into brain endothelial cells

The subcellular localisation of glucose and OEG-amine/galactose nanoparticles by brain endothelial cells appeared different following analysis of TEM data of their uptake. Glucose-coated nanoparticles did not show a significant difference in nanoparticle numbers in the cytosol in comparison with those in vesicles (Figure 3.6). On the other hand, the number of OEG-amine/galactose nanoparticles was significantly higher in vesicles than in cytosol. The

percentage of uptake into vesicles was calculated as 89.7±3.4 % of the overall uptake of OEG-amine/galactose nanoparticles. This observation suggested that each of this nanoparticle formulation may have used a different nanoparticle transport mechanism.

We then hypothesised that glucose-coated nanoparticles entered cells by a passive transport mechanism whereas OEG-amine/galactose uptake mechanism may be active. Thus, we tested whether 4 °C cell incubation, which reduces cell metabolism, leads to a decrease in nanoparticle uptake by brain endothelial cells. Indeed, the number of OEG-amine/galactose nanoparticles in vesicles dropped by about 97% (Figure 4.3A).

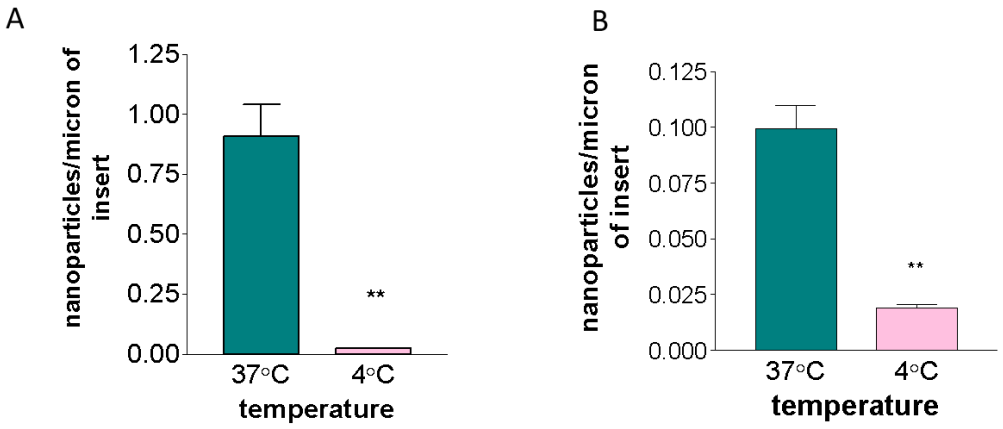

Figure 4.3. The effect of temperature on uptake of OEG-amine/galactose nanoparticles into vesicles (A) and cytosol (B). The cells were incubated at 4 °C with nanoparticles for 3 hrs. 3 independent experiments, unpaired ttest, ** P<0.01, data show mean ± SEM. Note the scale difference. A representative image used for this analysis is in the Appendix (Appendix Figure 2).

Active transport, endocytosis, has been previously proposed as a possible mechanism for cellular uptake of nanoparticles of different composition (Iversen et al. 2011; Alkilany & Murphy 2010; Chithrani & Chan 2007; Zhang et al. 2009). In addition, small gold nanoparticles have been shown to be transported via endocytosis (Verma et al. 2008). Verma et al. (2008) have also showed that gold nanoparticles with structured ligand morphology were taken up into the cell even at 4 °C incubation. In our work, the numbers of OEG-amine/galactose nanoparticles observed in the cytosol were still present in the cell even though their number was reduced

(Figure 4.3B). Alternatively, incubation of cells at 4 °C can change membrane fluidity and thus passive transport of OEG-amine/galactose nanoparticles cannot be excluded. Indeed, small gold nanoparticles have been previously shown to enter cells passively by moving through the membrane (Van Lehn et al. 2013; Van Lehn & Alexander-Katz 2014; Lin et al. 2010; Gkeka et al. 2014). Thus, a decrease in membrane fluidity may also reduce this mechanism to a degree. Therefore, in order to inhibit only active transport, we next used chemical inhibitors of active metabolism.

4.2.2 The effect of inhibitors of cell metabolism on uptake of OEG-amine/galactose nanoparticles into brain endothelial cells

The active metabolism of a cell can be inhibited by treatment with sodium azide and 2-deoxyglucose (sodium azide inhibits the electron transport chain and 2-deoxyglucose inhibits glycolysis). This treatment should only target the active transport, not changing the membrane fluidity. Thus, we treated our cultures with these inhibitors and exposed them to OEG-amine/galactose nanoparticles. As expected, we observed that nanoparticle numbers in cytosol remained the same whereas the ones in vesicles were significantly reduced (Figure 4.4A), thus allowing us to calculate percentage of involvement of active transport, which was 75.5±13 %. We confirmed that our treatment does not decrease integrity of the membrane, thus allowing for non-specific entry of nanoparticles. The reduction of membrane integrity was only around 5% after 4 h treatment (Figure 4.4B), as measured by penetration of propidium iodide. The time of pre-treating the cells (30 min) and incubating the nanoparticles in presence of the inhibitors was less than 3 h. Therefore, the effect of cell metabolism inhibition showed clearly the involvement of the active transport in uptake of OEG-amine/galactose nanoparticles. Also, the numbers of nanoparticles in the cytosol remained unchanged, suggesting that the mechanism of

passive transport of nanoparticles was not affected, perhaps as the fluidity of the membrane was intact. Both of these experiments imply that the transport of OEG-amine/galactose nanoparticles was both active and passive, even though the active transport can take up larger amounts of nanoparticles.

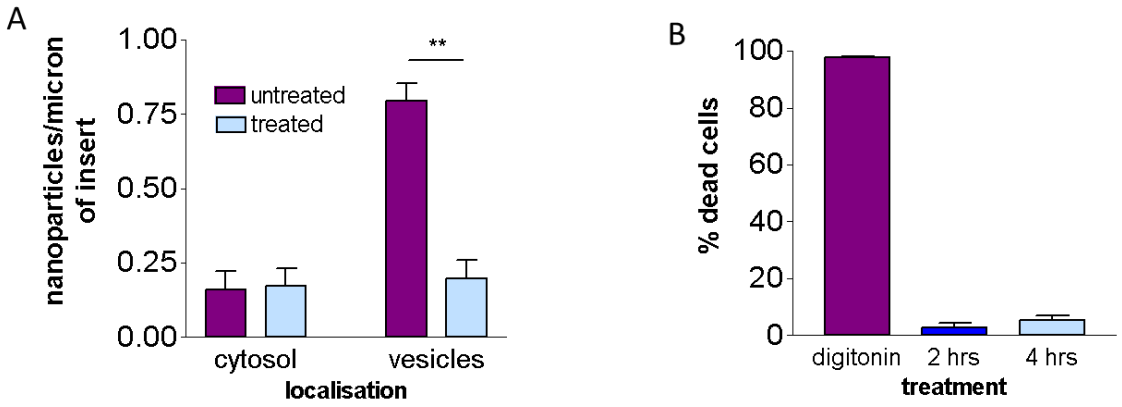

Figure 4.4. Inhibition of active transport of OEG-amine/galactose nanoparticles into brain endothelial cells (hCMEC/D3) by sodium azide/2-deoxy glucose. (A) The effect of sodium azide/2-deoxy glucose (10 mM and 50 mM respectively) on uptake of nanoparticles after 2 h incubation (one-way ANOVA, Tukey post test ** P<0.001, 3 independent experiments, error bars show mean ± SEM). (B) Test of cell membrane integrity after treating of cells with sodium azide/2-deoxy glucose for 2 h and 4 h, digitonin functions as a positive control of dead cells (3 independent experiments, error bars show mean ± SEM).

4.2.3 Investigation of involvement of specific types of endocytotic pathways in nanoparticle uptake by brain endothelial cells using antibiotic inhibitors

The next question was more specific - what endocytotic pathways were involved in the uptake of OEG-amine/galactose nanoparticles. There are different categories of endocytosis as mentioned in the introduction, i.e. "adsorptive", "receptor-mediated" or fluid-phase endocytosis. The resulting vesicle is then moved through the cell along the cytoskeleton (i.e. microtubules or actin filaments) using motor proteins.

We thus investigated the effects of (a) chlorpromazine, acting on clathrin-mediated endocytosis; (b) nystatin acting on lipid-raft endocytosis with caveolin; (c) nocodazole acting on microtubules and (d) cytochalasin D acting on actin filaments, caveolin and fluid phase endocytosis. The first step was to establish whether each of these inhibitors affect endocytosis in brain endothelial cells. This can be tested by loading cells with a fluorescent molecule such as FITC-dextran that the cells endocytose. The quantification of fluorescence intensity can be performed by flow cytometry which can easily determine intracellular levels of 70 kDa FITC-dextran (Figure 4.5A). Here, the cell population that contains FITC-dextran has higher fluorescence than untreated cells. We also established that the fluorescence of FITC-dextran was indeed a result of active transport, detecting fluorescence inside the cell rather than molecules attached to the outside of the cells. Thus, to test for non-specific binding, the treated cells were incubated at 4 °C to halt endocytosis. Indeed, the uptake of FITC-dextran was reduced, suggesting a dependence on active transport of the cell (Figure 4.5B).

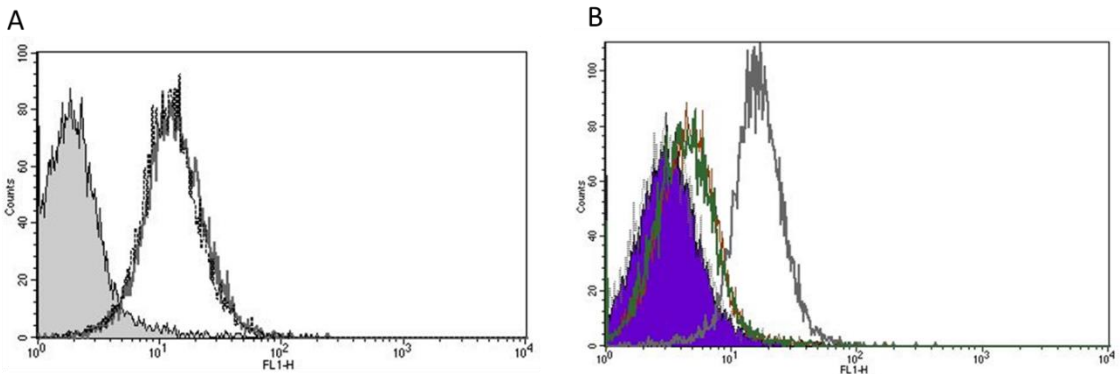

Figure 4.5. The rate of active transport assessed by quantification of FITC-dextran by flow cytometry. The assay was performed on brain endothelial cells loaded with 0.2 mg/ml 70 kDa FITC-dextran for 1 hr. (A) Grey filled - untreated cells, brown and grey – treated cells with FITC-dextran. (B) Purple - untreated at 37 °C, dotted grey left - untreated at 4 °C, brown and green line - FITC-dextran treated at 4 °C, grey line right - FITC-dextran treated at 37 °C. The experiment was performed twice, a representative image is shown.

The next step was to identify which selective inhibitors of active transport can lead to reduction of rate of endocytosis as determined by uptake of FITC-dextran. This was a necessary

step as it is not known which inhibitors reduce endocytosis in brain endothelial cells as well as their effective concentration. In other studies, this is not always determined for the specific cell type (Lund et al. 2011; dos Santos et al. 2011; Jiang et al. 2015). We found that only nystatin and chlorpromazine reduced fluorescence intensity of FITC-dextran in brain endothelial cells by 31 % and 53 %, respectively, and therefore decreased the degree of endocytosis (Figure 4.6) Moreover, these inhibitors may cause the cell to die depending on their concentration. Therefore, the rate of cell death was assessed; including tolerance of the cells to the inhibitor in respect to incubation time and concentration (see Table 4.2). Based on these observations, the effective concentration and incubation time of 1 h were selected, with pre-treatment of only 5 min.

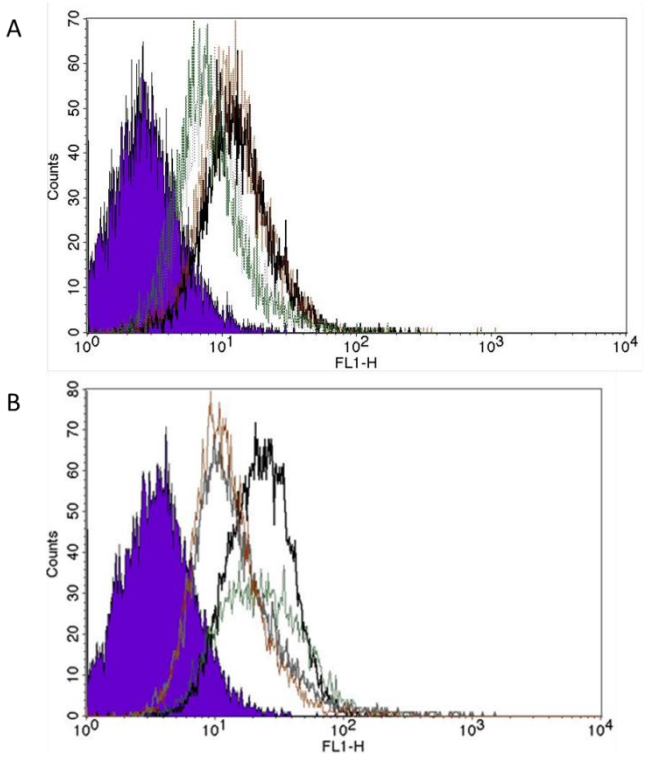

Figure 4.6. The effect of nystatin (A) and chlorpromazine (B) treatment on uptake of FITC-dextran into hCMEC/D3 cells. The cells were pre-treated for 1 hr with these inhibitors, the treatment alongside FITC-dextran application was for 1 hr. Purple population shows FITC-dextran untreated cells. The rest of the populations are as follows: A. Black line: nystatin untreated, brown 20 µg/ml nystatin, grey 50 µg/ml nystatin, green 80 µg/ml nystatin. B Black: chlorpromazine untreated, green: 15 µg/ml chlorpromazine, grey: 30 µg/ml chlorpromazine, brown 50 µg/ml chlorpromazine. Single experiment performed.

Table 4.2. The effect of chlorpromazine and nystatin treatment on hCMEC/D3 cells over 3 hr incubation.

Incubation time or recovery	Assessment of cells after inhibitor treatment	
	Chlorpromazine (30 µg/ml)	Nystatin (50 µg/ml)
30 min	Cells shrunk, looking like will detach soon	Cells changed slightly – more cubical shape
30 min recovery after 30 min treatment	Cells recovering, cubical shape, some detached	Cells nearly normally shaped
1 h	Cells round, starting to detach, similar appearance to trypsin treatment	Cells cubical shape, only slight change
Recovery 1 h after 1 h treatment	Cells not recovering, very round, only 10% returning to attached state	Cells nearly normal
2 h (trypan blue)	50% dead	No dead
3 h (trypan blue)	90% dead	Starting to shrink, 1% dead

Since the effective inhibitors of active transport have been determined, their effect on the uptake of OEG-amine/galactose nanoparticles was assessed. We expected to see a change in nanoparticle numbers in vesicles but not in cytosol as, in general, these inhibitors do not change the membrane fluidity. We found that nanoparticle numbers located in cytosol were not affected by treatment with either nystatin or chlorpromazine (Figure 4.7A, for representative images of treated cells with nystatin see Appendix Figure 6). The number of nanoparticles in vesicles showed a tendency to decrease when treated with chlorpromazine, but this decrease was not statistically significant. Unexpectedly, the number of nanoparticles observed in the nucleus tended to be higher in chlorpromazine-treated cells than in nystatin-treated or control cells. This may be due to early stages of damage to the nuclear membrane in chlorpromazine-treated cells. Indeed, electron microscopy analysis showed clear changes in the shape of the nucleus (compare Figure 4.7B with Figure 4.8) of chlorpromazine-treated cells. These nuclei appeared to have more rugged shape of the nuclear membrane, heterochromatin that condensed at the nuclear membrane, as well as they had gaps in the nuclear membrane. The tendency in reduction of nanoparticle uptake by chlorpromazine may be either a result of inhibition of clathrin-coated endocytosis, or an effect on other cellular pathways. In contrast,

other studies using these inhibitors do not report reduced cell viability or changes in the rate of transport upon treatment.

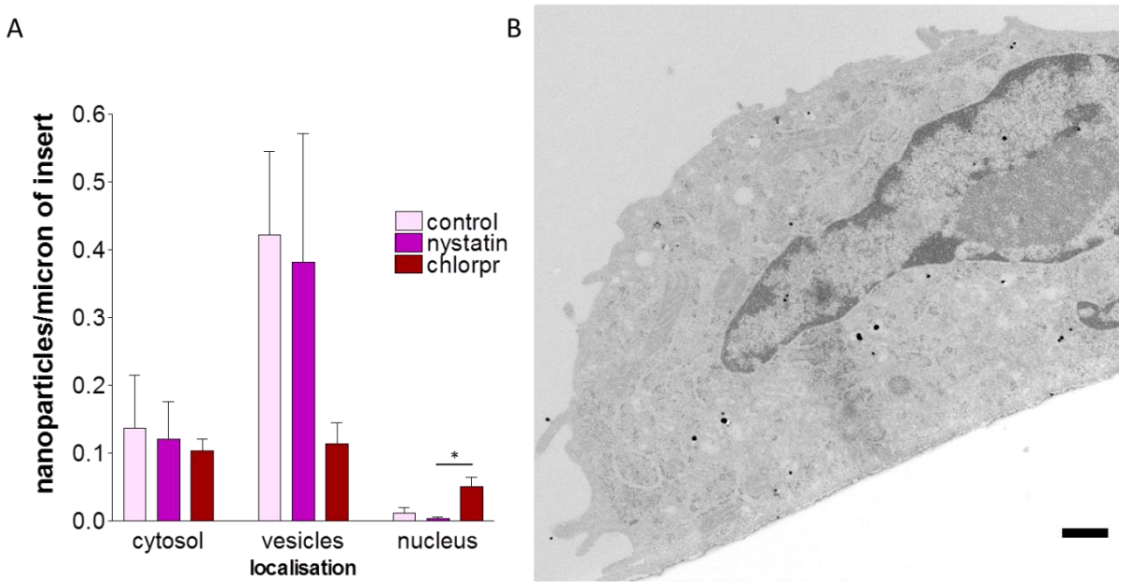

Figure 4.7. The inhibition of active transport using specific antibiotics in order to change uptake of OEG-amine/galactose nanoparticles. (A) Brain endothelial cells (hCMEC/D3) treated with both inhibitors 50 µg/ml nystatin and 30 µg/ml chlorpromazine (chlorpr) and the nanoparticles for 1 hr. 3 independent experiments, data show mean ± SEM. One-way ANOVA, *P<0.05. B. A representative micrograph of chlorpromazine-treated brain endothelial cell for 1 hr. Scale bar = 0.5 microns.

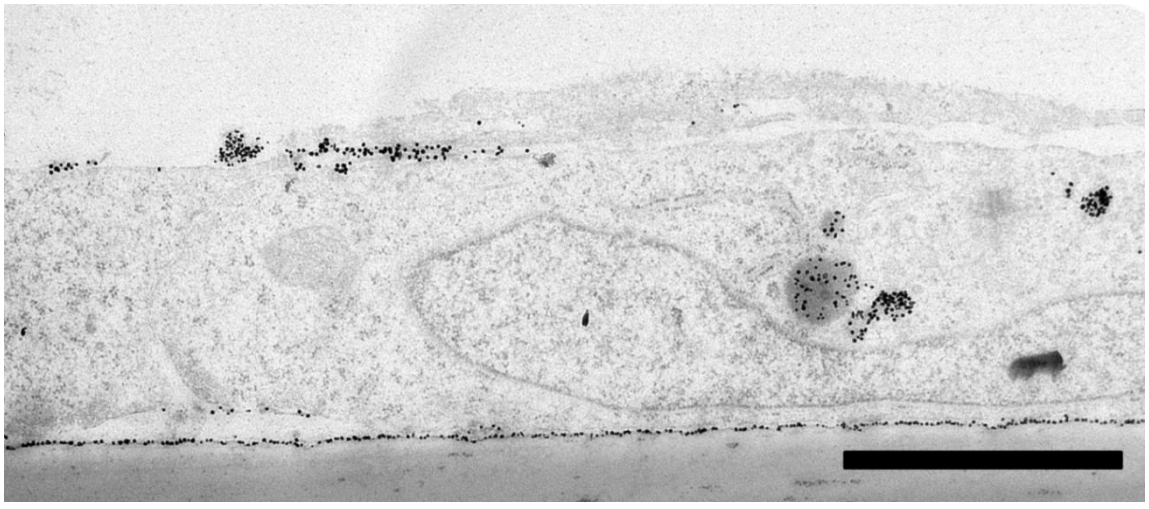

Figure 4.8. Electron micrograph of a brain endothelial cell (hCMEC/D3) containing OEG-amine/galactose nanoparticles. The nanoparticles are silver enhanced to about 20 nm size. Scale bar = 2 microns.

4.2.4 Nuclear localisations of gold nanoparticles

In previous studies, sometimes a nuclear localisation of gold nanoparticles has been observed in live cells (Gu et al. 2009) and thus a nuclear transport of gold nanoparticles has been suggested. Correspondingly, in the present study some gold nanoparticles were also observed in the nucleus of vital brain endothelial cells (Figure 4.7A). The scale of this nuclear transport was very little in comparison to endocytotic or cytosolic transport and thus the mechanism of this transport would have been difficult to investigate. In general, the mechanism of nuclear transport of gold nanoparticles is not understood and it may be because of the similar difficulties where the nuclear uptake is too low. There are two possible routes that small gold nanoparticles (<5 nm) can use to enter cell nucleus. Firstly, they can go through the nuclear pore complex, as the size of the pore complex (120 nm) may theoretically allow for their passage. The pore allows passage of molecules up to 40 kDa, whereas the nanoparticles tested here were around 30 kDa size. Secondly, they can pass through the double membrane in a mechanism similar to the one used to pass the plasma membrane (Van Lehn et al. 2013). The nuclear entry is particularly important for cancer therapy by radiosensitizing the cells loading their nucleus with gold nanoparticles. One may speculate, for example, that if the proportion of nanoparticles entering the nucleus is 1% from all nanoparticles present in the cytosol at any one time, then it may be perhaps possible to increase the nuclear entry by increasing the amount of nanoparticles entering the cytosol. However, whether an increasing amount of nanoparticles has a negative effect on the cell function would need to be established first.

4.2.5 Uptake of OEG-amine/galactose nanoparticles in microvascular endothelial cells from three vascular beds

Nanoparticles coated with OEG-amine/galactose entered the brain endothelial cells via both active and passive transport and we concluded that the active transport was predominant, since we calculated that around 75.5±13 % of nanoparticles enter the cell via an active transport. But how specific is this nanoparticle transport to the brain endothelium? We tested nanoparticle uptake in 3 other types of endothelial cells – glomerular (ciGENC), bone marrow (BMEC) and lung primary (hMVEC-L). Again, the 3 selected nanoparticle formulations were tested (Figure 4.9). Similarly to brain endothelial cells (Figure 3.6), glucose-coated nanoparticles showed the lowest uptake whereas OEG-amine and insulin showed the highest uptake by endothelial cells at similar rates. OEG-amine and insulin were mostly similar. Moreover, the nanoparticle numbers in vesicles were higher than those in the cytosol, suggesting a very similar kind of uptake mechanism in all types of endothelia. Thus, the endocytotic pathways of nanoparticle uptake may be non-specific to the type of endothelial cells while uptake rate may be dependent on other cell type-specific properties detailed below.

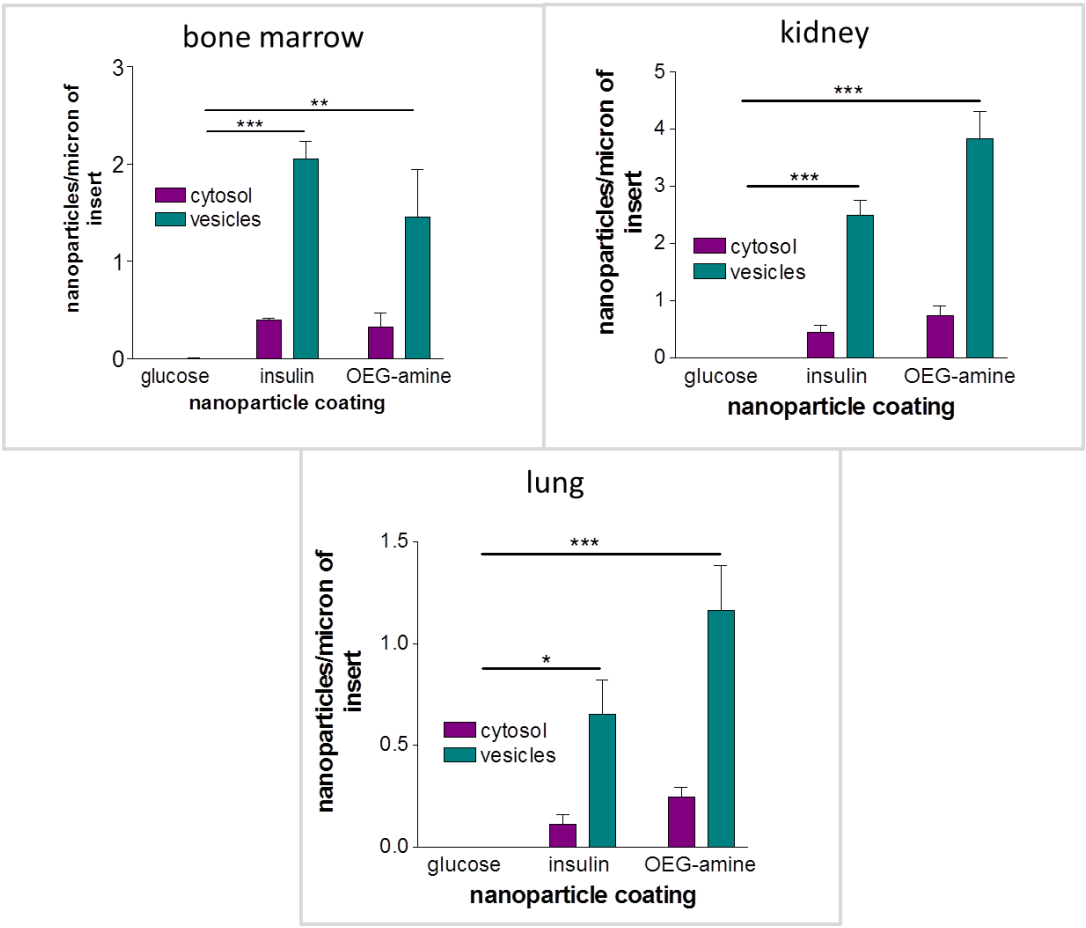

Figure 4.9. The uptake of three selected gold nanoparticle formulations into different types of vascular endothelial cells. Uptake into bone marrow (BMEC), kidney (ciGENC) and lung (primary HCMEC-L) endothelial cells is shown. Data are shown as mean ±SEM of 3 independent experiments (one-way ANOVA, Tukey post test, *P<0.05, ** P<0.01, *** P<0.001, 3 h incubation). Representative images of ciGENC cells are in Appendix Figure 3, BMEC cells in Appendix Figure 4 and HMVEC-L cells in Appendix Figure 5.

Moreover, previous studies have shown that different endothelial cells take up nanoparticles at different rates (Freese et al. 2012; Freese et al. 2013; Albanese & Chan 2011). Also nanoparticle uptake into endothelial and epithelial cells differed (Freese et al. 2012). Therefore, we compared the nanoparticle uptake of both OEG-amine/galactose and insulin in all four types of endothelial cells and found that indeed, the rate of transport differed, depending on cell type (Figure 4.10). Glucose-coated nanoparticles were not taken up in sufficient numbers to perform a comparison and thus are not shown. In comparison, using OEG-amine/galactose nanoparticle we found that in cytosol, all endothelial cells had a similar

nanoparticle numbers, even though there was a tendency for brain endothelial cells and lung primary cells to have lower numbers. This observation suggests that the mechanism for passive transport is similar in all tested endothelial cells and thus does not have an impact on nanoparticle uptake. OEG-amine/galactose/insulin nanoparticles were taken up in similar numbers in the cytosol in all endothelial cells as well. On the other hand, when comparing the nanoparticle numbers in vesicles, a difference was observed. Kidney endothelial cells showed the highest numbers of OEG-amine/galactose nanoparticles in vesicles, and had a similar uptake profile with OEG-amine/galactose/insulin nanoparticles. Although differences in nanoparticle uptake rates have been noted in other studies investigating various cell types (Freese et al. 2012; Freese et al. 2013; Albanese & Chan 2011), the explanation for this phenomenon has been lacking. Most efforts have been focused on understanding how properties of nanoparticles affect cell uptake rather than how properties of cells modulate this uptake. Understanding of cell-nanoparticle interactions is crucial for the future of nanomedicine. The ideal nanoparticle carrier would only selectively enter specific tissues, however, without the knowledge of transport characteristics into a certain cell type, this goal would be difficult to achieve. At the moment, the process of nanoparticle selection is based on observation of which cell type and how effectively are nanoparticles taken up as based on the intrinsic properties of the nanoparticles. Another approach may be to be able to fine-tune the specific properties of nanoparticles based on cellular response and thus enhance the uptake of nanoparticle by a certain cell type.

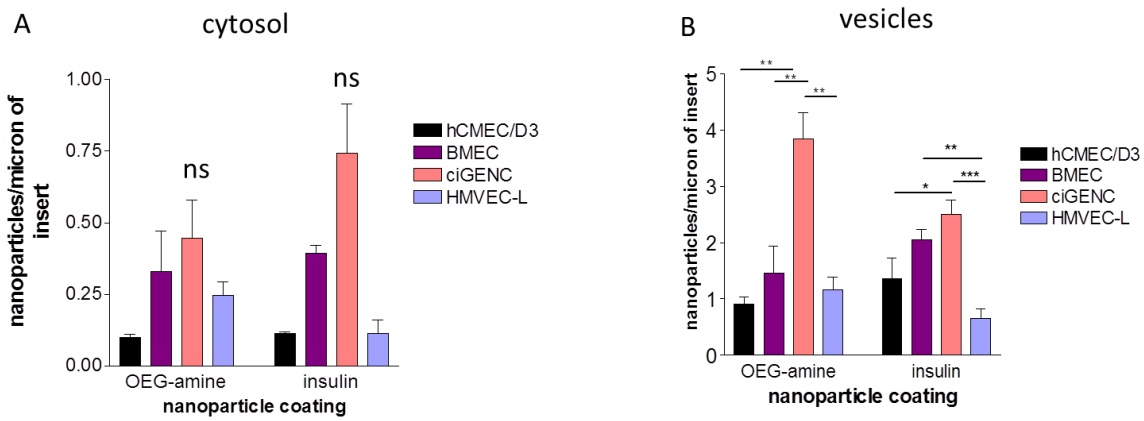

Figure 4.10. The comparison of uptake of OEG-amine/galactose and OEG-amine/galactose/insulin nanoparticles into different endothelial cells. Brain (hCMEC/D3), bone marrow (BMEC), kidney (ciGENC) and lung (HMVEC-L) are incubated with the nanoparticles for 3 hrs. Comparison of nanoparticle transport in cytosol (A) and in vesicles (B). Data are shown as mean ±SEM of 3 independent experiments (One-way ANOVA Tukey's multiple comparison test, *P<0.05, **P< 0.01, ***P<0.001, ns – not significant).

Possible cellular properties underlying differences in endothelial-specific uptake of gold nanoparticles may include:

- the endothelial cells are morphologically different;
- the rate of endocytosis is different;
- larger size of vesicles can lead to higher nanoparticle count;
- differences in the endothelial glycocalyx may be sufficient enough to promote or inhibit access of nanoparticles to the plasma membrane.

In order to determine whether these cellular processes were accounted for the differences in uptake by different endothelia, we compared uptake of OEG-amine/galactose nanoparticles in kidney endothelium with brain endothelium.

4.2.5.1 Morphological comparison between brain and kidney endothelial cells

The first possible cellular property accounting for higher numbers of nanoparticles in kidney endothelial cells compared to brain endothelial cells may simply be that they are larger cells. In this study, gold nanoparticles were quantified by counting them in cells not taking into account their cell volume, which may be larger in kidney endothelial cells. Thus, the cell volume was analysed in both kidney and brain endothelia but no difference was found (Figure 4.11). The analysis was performed using electron microscopy where cell area was measured regarding to certain length of cells along the insert membrane on which the cells were cultures.

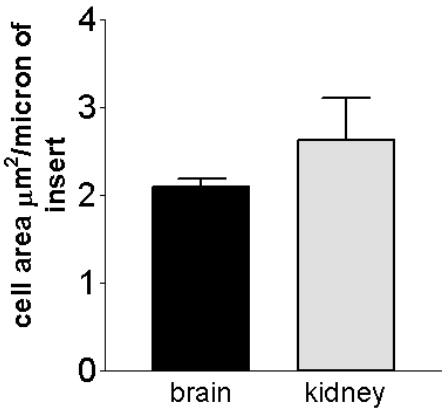

Figure 4.11. The comparison of cell area of brain (hCEMC/D3) and kidney (ciGENC) endothelial cells. The cell area (μm^2) was analysed from sections on the electron microscope measuring area of cells as they were observed along insert membrane. 3 independent experiments, unpaired ttest, result not significant, data shown as mean ±SEM.

4.2.5.2 Analysis of degree of endocytosis in brain and kidney endothelial cells

Another reason for higher nanoparticle transport may be higher endocytosis of kidney endothelium compared to brain endothelium. As mentioned previously, the degree of fluid-

phase endocytosis can be assessed by cell uptake of FITC-dextran. Indeed, we observed that kidney endothelium showed higher fluorescence intensity than brain endothelium (Figure 4.12A) suggesting a higher degree of vesicular uptake. This may be because either the kidney endothelium has higher vesicular content or its vesicles are larger. Thus, the size of vesicles was assessed in both endothelial cells by electron microscopy (Figure 4.12B) but no difference was found. Moreover, the size profile of vesicles was similar between the endothelia when we assessed their size distribution (Figure 4.13). Here, the vesicular sizes were binned and the histogram of distribution was generated, however, none of the size categories was more prominent in either of the endothelial cells. Therefore, kidney endothelium appeared to have a higher degree of endocytosis than brain endothelium, which can perhaps explain higher numbers of nanoparticles observed in the cells.

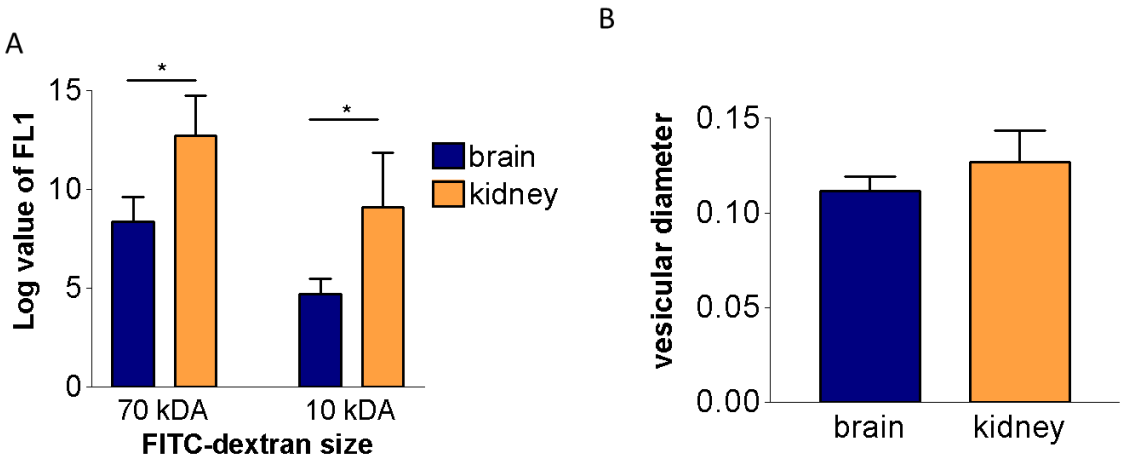

Figure 4.12. The cellular uptake of FITC-dextran into brain and kidney endothelial cells and their size of vesicles. (A) The degree of vesicular uptake as measured by uptake of FITC-dextran of different size after 1 hr of incubation (repeated-measures ANOVA with Bonferroni multiple comparison post test, * P< 0.05, data shown as mean ± SEM, 3 independent experiments). (B) Difference of vesicular diameter (μm) in the brain and kidney endothelial cells (data shown as mean ± SEM, unpaired ttest - non-significant, 3 independent experiments).

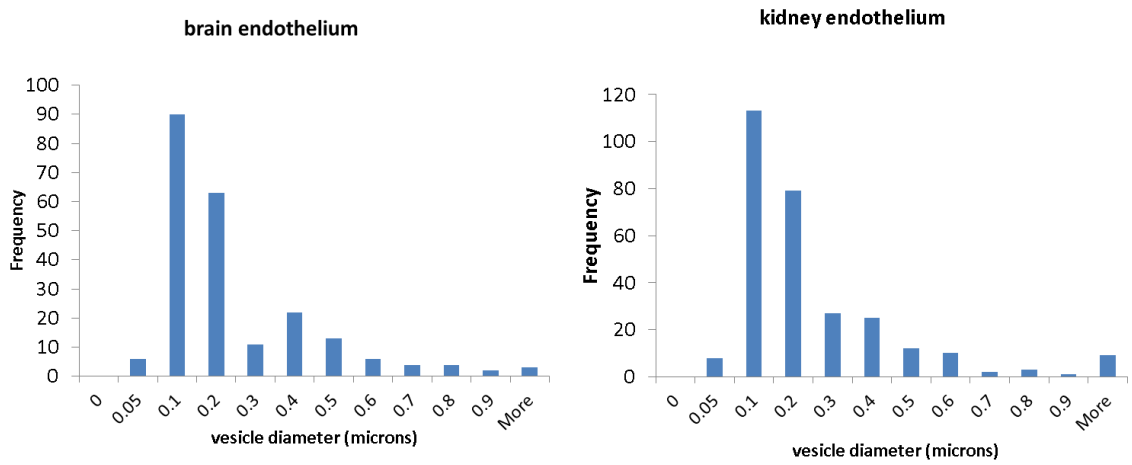

Figure 4.13. Comparison of distributions of vesicular diameters in brain and kidney endothelium. Vesicular diameter of over 300 vesicles was measured in brain endothelial cells hCMEC/D3 and kidney endothelial cells ciGENC using electron microscopy. Data are from 3 independent experiments.

The evidence for differences in endocytosis between endothelial cells from different vascular beds has been documented. For example, the expression of certain molecules typical of caveolae, i.e. lipid raft invaginations of plasma membrane, has been assessed in endothelia from various tissues (McIntosh et al. 2002) and a difference has been observed. In general, endothelia can be categorized as continuous, discontinous or fenestrated (Aird 2012). It has been shown that they have different vesicular characteristics, such as number of vesicles, between the categories as well as within them (Simionescu et al. 2002; Simionescu et al. 1974). Brain endothelium, categorized as a continuous endothelium, has the lowest density of vesicles in comparison to other continuous endothelia (e.g. lung, intestine, pancreas, skeletal muscle) (Stewart 2000). Thus, the difference in degree of endocytosis that we observed in kidney endothelium in comparison with brain endothelium may be attributed to their phenotypic difference, given that one is continuous and the other fenestrated endothelium. However, it has been observed that cells in vitro loose much of their phenotypic heterogeneity that they once had in a tissue (Aird 2012). Therefore, our findings might be restricted to the phenotype the cell

lines express and perhaps the difference in degree of endocytosis might be larger if investigated in vivo.

However, another factor that may account for difference in nanoparticle uptake to brain and kidney endothelium may be their glycocalyx, the first barrier to nanoparticle binding to the cell surface.

4.2.5.3 Involvement of glycocalyx in nanoparticle uptake

Glycocalyx, the extracellular matrix on the apical surface of the cells, is the first interface for the cell-nanoparticle interactions. Thus, we investigated whether the glycocalyx is involved in the nanoparticle uptake. It has been found that certain parts of glycocalyx may be crucial for attachment of gold nanoparticles to erythrocytes (Atukorale et al. 2015). However, whether the glycocalyx plays a role in nanoparticle uptake into other cells has not yet been established.

The first step in this investigation was to establish whether the glycocalyx in kidney endothelium appears different in composition from brain endothelium. Different approaches may be used as outlined in the introduction; we used a lectin-based assay, since it is a simple and very versatile assay. Lectins, proteins binding to specific carbohydrates, are a perfect tool to assess different parts of glycocalyx. The lectins that we used are listed in Table 4.3. Our selection was based on previous work in our group that involved screening of many lectins to establish the ones that bind most strongly to endothelial cells (Hillyer 2003). We found that lectins differ in how much binding they show (Figure 4.14). In brain endothelium, wheat germ agglutinin showed the strongest binding in comparison to the other lectins. However, in kidney endothelium this effect was not as pronounced. We also tested whether the endothelial glycocalyx changes over time in culture as the cells become more confluent (Figure 4.14). This is

particularly relevant for choosing the time to perform nanoparticle uptake experiments and also to confirm that the glycocalyx does not change in composition over time. One would assume that it may change over time in culture, however, brain endothelial cells did not show any change of glycocalyx composition up to 7 days in culture. Kidney endothelial cells did show some change in lectin binding detected by differences in binding of lectins *Wisteria Floribunda* and *Ulex Europaeus*. Unfortunately, the culture time of brain and kidney endothelial cell cannot be directly compared. This is due to differences in the cell culture conditions. Kidney endothelium grows progressively at 33 °C but develops a glomerular endothelial phenotype after 3-5 days of growing at 37 °C whereas brain endothelium both grows and develops its phenotype at 37 °C. The effect of temperature on development of glycocalyx has not been investigated and to our knowledge it is not known in general. However, as the kidney endothelial cells are grown at 37 °C for 3 or more days, the glycocalyx might have time to develop and be characteristic of this endothelium.

Table 4.3. The lectins used in this study to characterize endothelial glycocalyx

Lectin	Sugar specificity* (Rüdiger & Gabius 2002)
***Ulex Europaeus* agglutinin (UEA)**	-αL-fucose
Peanut agglutinin (PNA)	Gal-β(1-3)-GalNAc
***Wisteria Floribunda* lectin (WFL)**	GalNAc
Wheat germ agglutinin (WGA)	GlcNAc

* Gal=galactose; GalNAc=N-acetyl-galactosamine; GlcNAc=acetyl-glucosamine

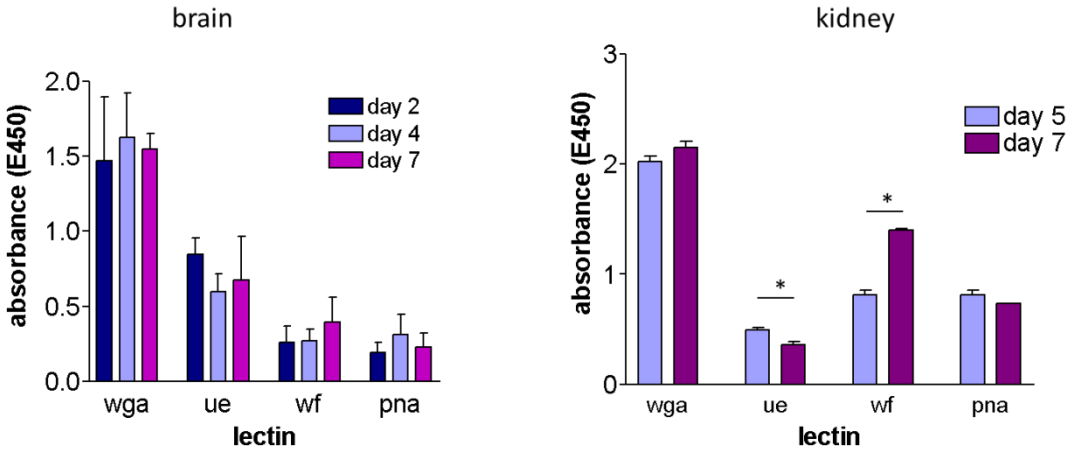

Figure 4.14. Lectin binding of glycocalyx on brain and kidney endothelial cells. Lectin-binding is used to show differences in glycocalyx composition. Lectins Wheat germ agglutinin (wga), Ulex Europaeus (ue), Wisteria floribunda (wf) and peanut agglutinin (pna) are used in cultures over time. Data shown as mean ± SEM from 3 independent experiments. Statistical tests were performed: one-way ANOVA Tukey's Multiple comparison test (brain), unpaired t-test (kidney) *P< 0.05.

We then compared whether composition of glycocalyx in brain and kidney endothelium differ by assessing various parts of glycocalyx with lectin binding. For this purpose, the lectin *Ulex Europaeus* can be used as an endothelial marker as it binds endothelium from different vascular beds (Holthöfer et al. 1982). We observed that kidney endothelium showed higher lectin binding to specific parts of glycocalyx (Figure 4.15). The glycocalyx of glomerular endothelial cells ciGENC has been imaged and stained for electron microscopy, and its size has been observed to be about 200 μm (Singh et al. 2007). Moreover, when parts of the glycocalyx were removed, the passage of albumin have increased, pointing to the possibility of the glycocalyx to be involved in glomerular filtration (Singh et al. 2007). The filtration of albumin by glomerulus is not restricted to glomerular endothelial glycocalyx only as renal filtration may be also involved (Comper 2014).

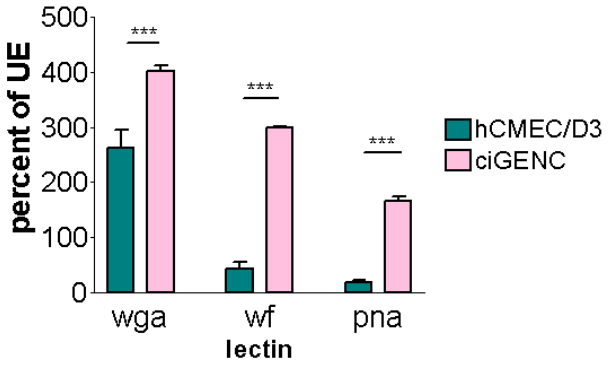

Figure 4.15. Lectin binding to glycocalyx of brain (hCMEC/D3) and kidney (ciGENC) endothelial cells. Lectin binding of Wheat germ agglutinin (wga), Wisteria floribunda (wf) and peanut agglutinin (pna) are standardized towards lectin Ulex Europaeus (ue), a standard marker of endothelium. Data shown as mean ± SEM from 3 independent experiments, one-way ANOVA, Tukey post test, ***P>0.001.

The differences between species and tissues have been analysed by lectin binding which is also becoming a more popular biological tool (Dan et al. 2016). Histochemical lectin profile of vascular beds in many different mammal species (cat, cow, dog, goat, horse, human, mouse, pig, rat and sheep) were compared (Alroy et al. 1987). The results have showed differences in species-selective staining, for example Ulex Europaeus agglutinin stained only human tissue, pointing to presence of non-reducing α-L-fucosyl residues. Moreover, new use of lectins in lectin microarrays have been used for example in characterizing stem cells and their discriminating differentiated cells from undifferentiated stem cells (Tateno et al. 2011).

To investigate whether transport of OEG-amine/galactose nanoparticles is influenced by the endothelial glycocalyx, it is possible to use enzymes to remove parts of the glycocalyx and assess the effect on nanoparticle numbers in the cells after the treatment. The enzymes must be selected carefully and be tested for their effect on glycocalyx composition. Previous work in our laboratory (David Male, personal communication) examined four enzymes: heparinase, chondroitinase, neuraminidase and O-sialoglycoprotein endopeptidase - only the latter two enzymes were the most effective in changing the binding profile of the four selected lectins. O-

sialoglycoprotein endopeptidase removes core O-sialoglycoproteins and sulfated glycoproteins (Abdullah et al. 1992). Neuraminidase removes sialic acid residues (Figure 4.16).

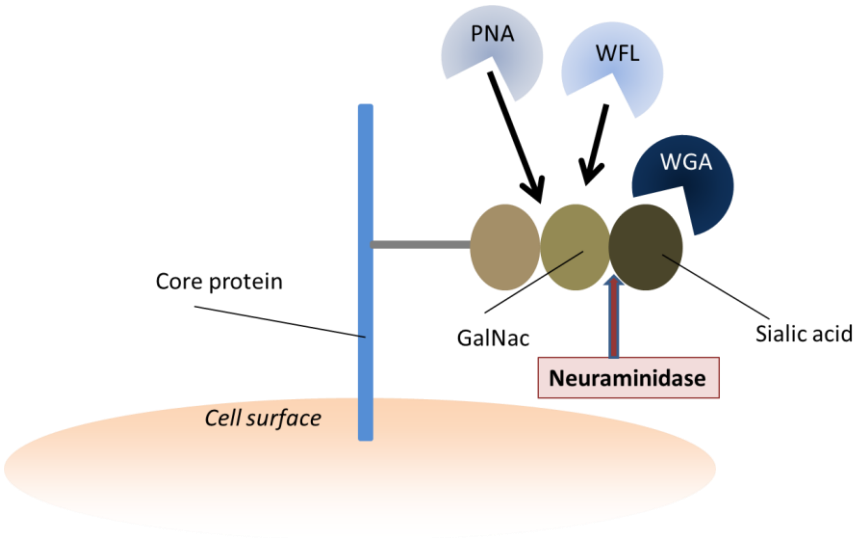

Figure 4.16. A scheme for one of the lectin binding sites on endothelial cells. PNA = peanut agglutinin, WFL = Wisteria floribunda lectin, WGA = Wheat germ agglutinin. Neuraminidase removes the terminal sialic acid to reduce binding of WGA and enhance binding of PNA and WFL. (Adapted from (Gromnicova, Kaya, et al. 2016))

Treatment with enzymes in both types of endothelial cells decreased their lectin binding profile of peanut agglutinin and slightly that of wheat germ agglutinin (Figure 4.17). This difference is more pronounced in kidney endothelial cells but this may be again because these cells have a higher composition of certain parts of glycocalyx as shown above. Therefore, we were confident that these two enzymes remove parts of glycocalyx and can thus be used to assess their effect on nanoparticle transport.

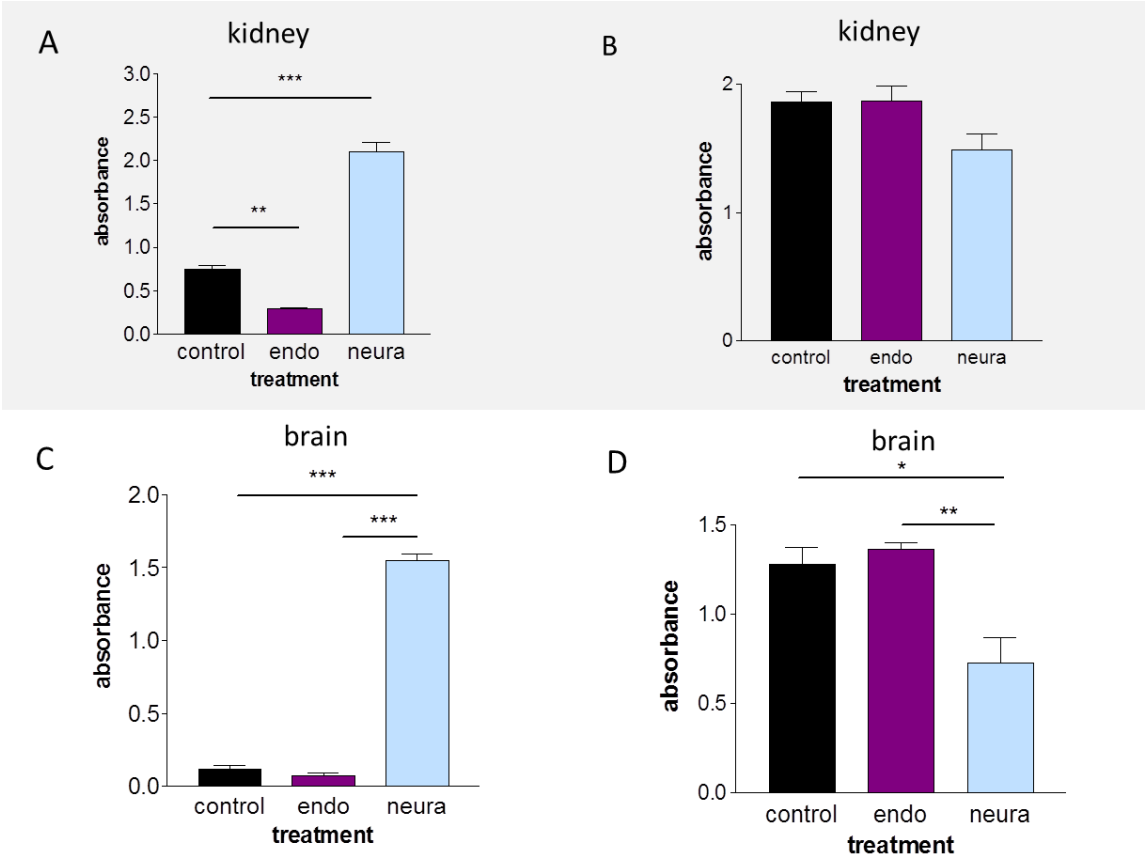

Figure 4.17. Effect of enzymatic removal of glycocalyx on lectin binding to kidney and brain endothelial cells. Binding of lectin peanut agglutinin (A and C) to glycocalyx of kidney (A) and brain endothelial cells (C) after enzymatic removal with O-sialoglycoprotein endopeptidase (endo) and neuraminidase (neura). Binding of lectin wheat germ agglutinin (B and D) to kidney (B) and brain endothelial cells (D) after enzymatic removal with O-sialoglycoprotein endopeptidase (endo) and neuraminidase (neura). One-way ANOVA Tukey's multiple comparison *P<0.05, **P<0.01, ***P<0.001. Data shown as mean ± SEM from 3 independent experiments.

In order to determine whether OEG-amine/galactose nanoparticles interact with the glycocalyx, cells were treated with O-sialoglycoprotein endopeptidase and neuraminidase. We hypothesised that removing part of the glycocalyx may increase the nanoparticle uptake by cells. It is known that the glycocalyx mesh has 20 nm gaps (Squire et al. 2001), thus potentially allowing for passage of small nanoparticles. Also, the charge of the glycocalyx may be crucial, in particular as OEG-amine/galactose nanoparticles were positively charged. We found that partial removal of brain endothelial glycocalyx did not affect the nanoparticle uptake (Figure 4.18A). On the other hand, nanoparticle uptake was affected by the enzymes in kidney

endothelial cells (Figure 4.18B). The partial removal of core polypeptides decreased uptake of OEG-amine/galactose nanoparticles rather than increased it. Therefore, the glycocalyx itself was not a barrier to the nanoparticles moving towards the cell membrane rather the results suggest that the glycocalyx facilitates nanoparticle uptake. There may be a possible mechanism by which enzymes decrease nanoparticle uptake in kidney endothelial cells. The core glycoproteins, some of which are removed by endopeptidase, have been found to be important for differentiation of vesicular "microdomains" that establish before formation of vesicles as shown by lectin binding to pancreatic capillaries (Simionescu et al. 1982). Thus, O-sialoglycoprotein endopeptidase may perhaps indirectly affect endocytotic pathways, which may be responsible for the large differences in nanoparticle uptake in different endothelia.

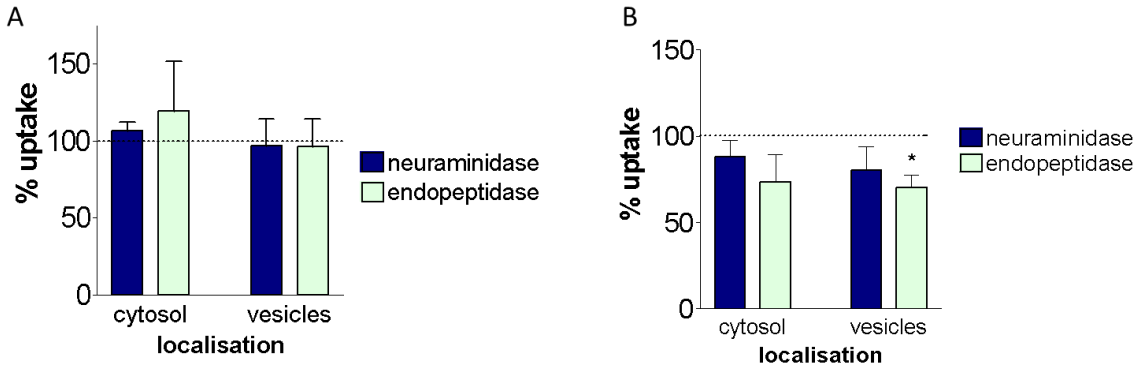

Figure 4.18. The effect of partial glycocalyx digestion on uptake of OEG-amine/galactose nanoparticle into brain (A) and kidney (B) endothelium. Enzymes neuraminidase and O-sialoglycoprotein endopeptidase partially affected glycocalyx composition, then cells were incubated with nanoparticles for 3 h and nanoparticle uptake assessed by electron microscopy (3 independent experiments, data shown as mean ± SEM, unpaired ttest, *P<0.05).

These results show that the glycocalyx may be important for nanoparticle transport, a first evidence of glycocalyx involvement in cell-nanoparticle interactions. Even though the mechanism of this interaction is not clearly understood, it may be more pronounced *in vivo*, where the glycocalyx is much more developed than *in vitro* (Potter & Damiano 2008).

4.2.6 Summary

This chapter focused on understanding the reasons for higher OEG-amine/galactose nanoparticle uptake into endothelial cells in comparison with glucose-coated nanoparticles. We have concluded that nanoparticle uptake is mainly but not exclusively an active transport process as it can be inhibited when treating with drugs to halt whole cell metabolism as well as when incubating cells at low temperature. The partial passive transport is reduced slightly by cell incubation at low temperatures which may be due to reduced membrane fluidity.

Moreover, we also tried to understand the mechanisms behind cell-selective nanoparticle transport that we observed when comparing uptake of OEG-amine/galactose nanoparticle into different types of endothelial cells. Here, we noted that kidney endothelial cells were taking up more OEG-amine/galactose nanoparticles than brain, lung and bone marrow endothelia. Thus we compared kidney and brain endothelium to determine the reason for this cell-selectivity. We first assessed the morphological difference of these two endothelia, but found no difference in their cell area. However, when we examined the degree of endocytosis, we found higher uptake in kidney endothelial cells. Another endothelial-specific property is the glycocalyx. We found it to differ between the two endothelia and when we used partial enzyme digestion, we observed a decrease in uptake of OEG-amine/galactose nanoparticle in kidney endothelial cells but not in brain endothelial cells.

Chapter 5. *In vivo* uptake of gold glyconanoparticles

5.1 Introduction

Gold nanoparticles have been assessed for their tissue distribution depending on their size or charge. Gold nanoparticles have been administered in various routes, however, a direct comparison study has not yet been done and thus only individual studies using a single route of administration are introduced here.

5.1.1 Distribution of gold nanoparticles in animal tissues

Gold nanoparticles have been administered in various routes to assess bodily distribution. One of the most commonly used routes of administration is a tail vein injection, in which the nanoparticles are administered directly into the blood stream (Wiley et al. 2013; Sousa et al. 2010; Lee et al. 2014). Intra-peritoneal injection has been also used in some cases (Prades et al. 2012; Lasagna-Reeves et al. 2010), and also directs nanoparticles into the blood stream following the infusion at the site of administration. Gold nanoparticles have also been administered orally (Hillyer & Albrecht 2001) as well as esophageally (i.e. by gavage) (Schleh et al. 2012). In both cases, some differences in tissue distribution were found, mainly with respect to the distribution of 18 nm nanoparticles depending on the route of administration. For example, 18 nm particles accumulated in the brain after gavage in large quantities in comparison to other sized particles (1.4 – 200 nm) but when administered into a tail vein, these nanoparticles did not show this pattern (Hirn et al. 2011). This example demonstrates how nanoparticle tissue distribution profile can be affected by the routes of administration.

Gold nanoparticles have been widely assessed for the size-dependence of their tissue distribution. It has been found that very small nanoparticles (under 4 nm) are more likely to

penetrate tissues and cells (Skotland et al. 2010). For example, Hillyer & Albrecht (2001) showed that orally fed 4 nm gold nanoparticles were present in all mice organs in highest amounts in comparison with 10 nm and 28 nm nanoparticles. Smaller gold nanoparticles were tested by Schleh et al. (2012), who demonstrated that 1.4 nm gold nanoparticles were present at high levels in all investigated rat organs, whereas 2.8 nm, 18 nm or 200 nm were in present in lower amounts after gavage administration. This was confirmed in a study by Hirn et al. (2011) that found correlation of size and retention of gold in tissues following intravenous administration of nanoparticles in rats. In this study, nanoparticle ranges from 1.4 to 5 nm had higher tissue accumulation the smaller the size. In summary, the smaller the gold nanoparticles, the higher the tissue accumulation they have.

The charge of the nanoparticles has also been found to play a role in their tissue accumulation. Following gavage administration of positively and negatively-charged 2.8 nm gold nanoparticles it was found that negatively charged nanoparticles accumulated in organs to a higher extent than positively-charged ones (Schleh et al. 2012). The authors suggested that this may be explained by the fact that negatively charged nanoparticles attract and bind positively-charged proteins from the plasma, thus resulting in a positively-charged nanoparticle that would be more likely to enter tissues. A different study (Lee et al. 2014) investigated larger nanoparticles, 15 nm, intravenously injected into rats. That study also compared charged nanoparticles (either with carboxyl or amine group giving them negative or positive charge, respectively) with neutral nanoparticles coated with the ligand OEG. They found fast tissue penetration and accumulation of both charged nanoparticles in comparison to OEG-ylated ones.

Can gold nanoparticles enter the brain? In a study using a range of gold nanoparticles between 1.4 nm and 200 nm, nanoparticles of 18 nm size showed the highest accumulation in in the brain (Schleh et al. 2012) On the other hand, Hirn et al. (2011) discovered higher retention

of 1.4 nm nanoparticles in brain, in comparison to other nanoparticles also up to 200 nm. Thus in general, nanoparticles under 50 nm were found to penetrate the brain to a higher extent.

If gold nanoparticles can enter the brain, in which regions can they be found? A study of Sousa et al. (2010) has shown localisation of 15 nm gold nanoparticles in the cortex, hippocampus, thalamus and hypothalamus of mice injected intravenously. Electron microscopy revealed 13 nm gold nanoparticles in the cortex and hippocampus (Prades et al. 2012). Larger sized nanoparticles of 80 nm were shown in the cortex in another study (Wiley et al. 2013).

In the following section, ICP-MS as well as electron microscopy are used to provide information on bodily distribution of gold as well as tissue and cellular localisation of gold nanoparticles in the brains of rats 10 min after injection into the carotid artery.

5.2 Results and Discussion

The previous chapters examined the uptake efficiency of selected nanoparticle formulations in brain endothelial cells *in vitro*. However, the situation *in vivo* may be very different. Therefore, we investigated whether these small gold nanoparticles enter the brain *in vivo* and if they can, whether we can locate them within the cells of brain. This would allow us to make a better correlation with the results observed *in vitro*. Small gold nanoparticles <5 nm are cleared via kidney (Longmire et al. 2008), thus we also analysed the gold content in excretory organs such as kidney and liver as well as in the lung by ICP-MS. Our hypothesis was that each nanoparticle formulation may have different abilities to accumulate in different organs, due to different ligand molecules and charge, as previously shown (Hirn et al. 2011; Schleh et al. 2012; Lee et al. 2014).

Gold nanoparticles have been found to enter the brain (Sonavane et al. 2008; De Jong et al. 2008; Sousa et al. 2010; Lee et al. 2014; Lasagna-Reeves et al. 2010; Hirn et al. 2011) but in lower quantities in comparison with other organs. Therefore, in order to increase the number of nanoparticles entering the brain, we considered 2 options:

- increase the dose so that the percentage of nanoparticles in the brain would be detectable by the electron microscopy;
- inject the nanoparticles into a carotid artery, which directly supplies the brain.

Both approaches have their advantages and disadvantages. The higher dose approach is very simple to administer via tail vein injection. On the other hand, this approach might lead to some toxicity, overloading the organs, such as kidney, that clear the nanoparticles from blood. Moreover, this higher dose would not correspond with what would be achievable in the clinic and thus would have little relevance as a therapeutic treatment. Intra-carotid injection uses a low dose, similar to one tested *in vitro*, however, the full dose enters the brain first before being distributed throughout the body and diluted in the blood. The disadvantage of this

approach is that a skilled surgical procedure is involved. Also intra-carotid injections may lead to inconsistent distribution of the substance in the brain (Saris et al. 1988). We decided to use intra-carotid injection for testing our nanoparticles, which was performed in collaboration with Istanbul University by Mehmet Kaya's group.

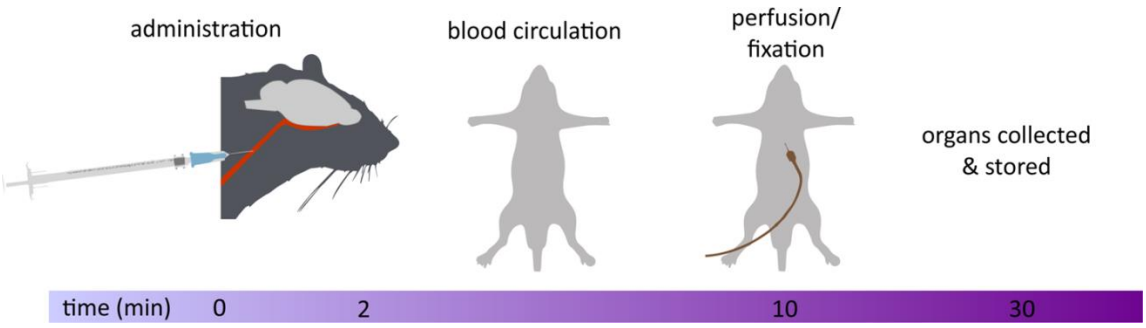

Figure 5.1. The timeline of the *in vivo* experiment. 50 µg of gold nanoparticles (Au concentration) were infused over 2 min into the left carotid artery. Animals were then perfused and fixed after 10 min of nanoparticle circulation and the organs were collected and stored at 4 °C.

We set out to administer the nanoparticles into rats and leave them circulate for 10 min (Figure 5.1). This time was selected in order to detect the first encounter of nanoparticles with the brain endothelium and possibly with brain parenchyma. Next, the animals were perfused, fixed and organs collected, namely brain, kidney, liver and lung. Electron microscopy and ICP-MS were used to analyse particle distribution in the brain, while the rest of the organs were analysed by ICP-MS.

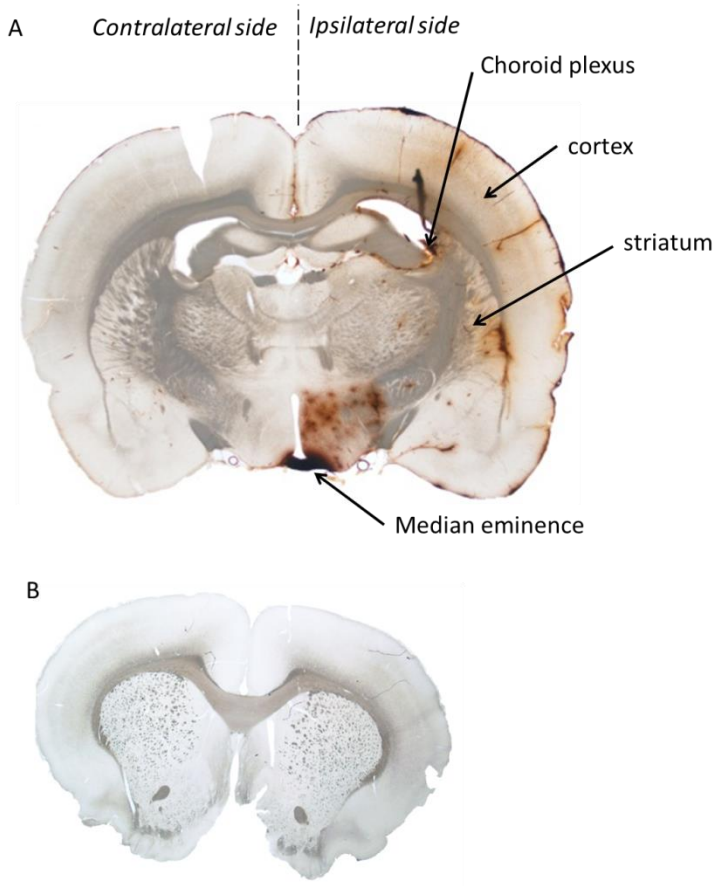

Figure 5.2. Brain section of rats treated with silver-enhancement. A Section of a rat injected with gold nanoparticles where the areas with gold nanoparticles are showing as a brown staining. The different regions of the brain are described. B control silver-enhanced section of an animal not treated with nanoparticles. Part B has been already published elsewhere (Gromnicova, Yilmaz, et al. 2016).

5.2.1 Localisation of gold nanoparticles in different regions of the brain

To determine the overall distribution of the nanoparticles in the brain, tissue sections were treated with silver enhancement, which showed localized brown staining (Figure 2A). We hypothesized that this corresponded to localization of gold nanoparticles, showing clearly the brain regions where they were located. We also tested the specificity of silver enhancement to gold nanoparticles by silver-enhancing a section from an animal that was not injected with nanoparticles (Figure 5.2B). In this case, no brown staining was observed. The sections containing gold nanoparticles had more intensive brown staining on the ipsilateral side (same

as injected) than on the contralateral side (opposite to injected) of the treated sections (Figure 5.2A). This can be explained by the anatomy of the blood vessels. The left internal carotid artery, a continuation of the common carotid artery (i.e. the administration site), supplies mostly left side of the brain despite the presence of the Circle of Willis. Thus, the contralateral side received the same or very similar dose of nanoparticles as the rest of the organs. The nanoparticle dose of the contralateral side may be also comparable to other types of administrations such as intra-venous where the brain would receive a dose after the nanoparticles have passed through the lung capillaries.

Silver enhancing of the brain sections also allowed comparison of the groups of treated animals with the same nanoparticle formulation as well as the formulations between each other (Figure 5.3). We found that within each group of treated animals there were differences in localisation and amount of brown staining. For example, in glucose nanoparticle-treated group there was one animal with brown staining in the cortex; two animals did not show brown staining in any of their regions. As mentioned previously, one of the possible disadvantages of intra-carotid injections is irregular distribution of administered substance within the brain (Saris et al. 1988). This has been described as intravascular streaming where the substance is distributed based on which part of brain the stream of blood flow will carry it into, which can result in random distribution into brain regions, showing as a disparity in regional distribution between animals of the same group.

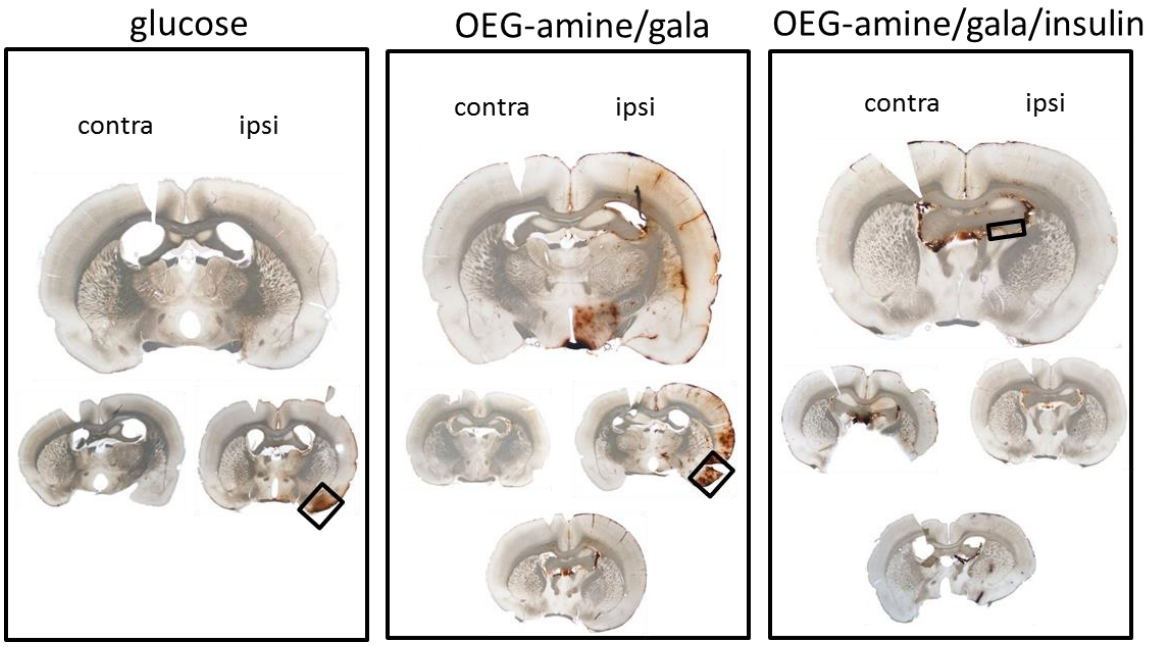

Figure 5.3. The localisation of gold nanoparticles in regions of rat brain of three treated groups. Brown staining in the coronal sections corresponds to the presence of gold nanoparticles in the brain tissue. Each section corresponds to the same brain region of each animal. Each group, i.e. treated with gold nanoparticles coated with glucose, OEG-amine/galactose and OEG-amine/galactose/insulin consisted of 3-4 animals. Rats were injected intra-carotid, the injected side is noted as ipsilateral (ipsi), opposite to injected as contralateral (contra) side.

5.2.2 Analysis of integrity of the blood-brain barrier in treated animals

Another reason for this inter-animal variation may be that the blood-brain barrier was compromised in some animals that show intensive staining. Therefore, we used immunohistochemistry to stain for immunoglobulins. If the blood-brain barrier had been disturbed and was leaking, then serum molecules would be present, such as immunoglobulins that would not normally be found in the brain. However, we did not find any evidence of immunoglobulin infiltration, when comparing the ipsilateral side with contralateral side, (Figure 5.4). Therefore, the variation between the animals was best explained by intravascular streaming as mentioned in the literature (Saris et al. 1988).

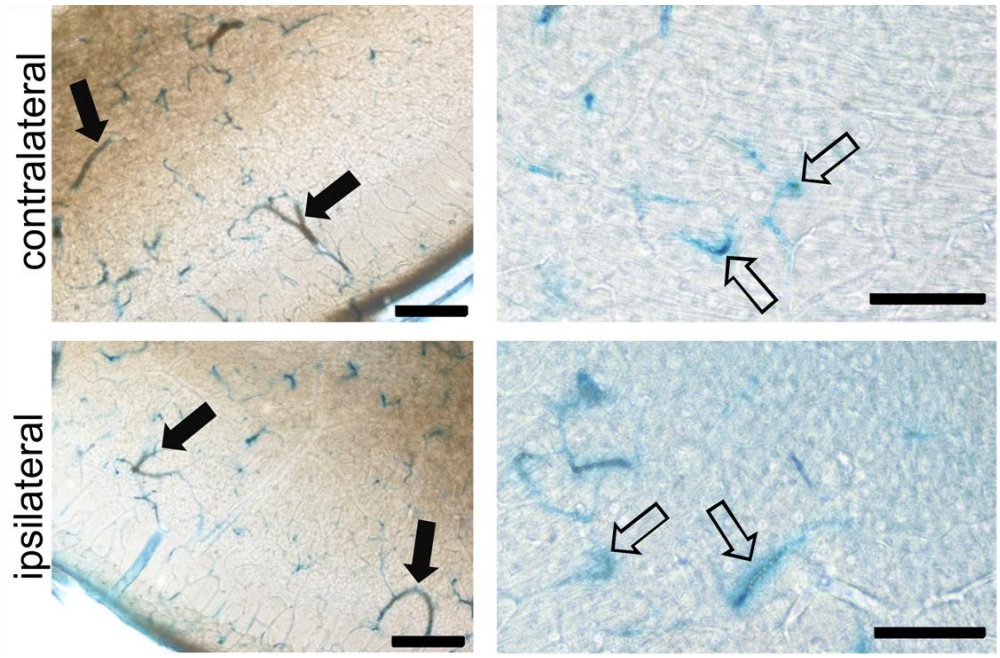

Figure 5.4. Determination of blood-brain barrier integrity by immunohistochemistry. Immunoglobulins were stained (blue) in coronal sections. Nanoparticle staining appeared in poorly perfused blood vessels (full arrows). Slight leakage of the immunoglobulin (outlined arrows) was observed in both hemispheres of the brain indicating that the leakage itself could not be caused by the injection procedure. Scale bars on the left 500 µm, on the right 100 µm. Representative images are shown, images from 1 animal representative of 3-4 rats are shown. This figure has been published elsewhere (Gromnicova, Yilmaz, et al. 2016). Reprinted with permission of Nanomedicine.

Due to these animal-to-animal variations it may be difficult to compare the groups of nanoparticle formulations between each other. However, some observations can be made (Figure 5.3). The OEG-amine/galactose –treated group had the most intensive staining in 2 animals out of 4 and that OEG-amine/galactose/insulin was mostly localised to the choroid plexus.

5.2.3 The amount of gold in the brain as analysed by ICP-MS

ICP-MS was used to quantify the differences in the amount of gold in the brain following administration of different nanoparticle formulations (Figure 5.5). We found that

although levels were generally lower in the contralateral side this decrease was not significantly different from the ipsilateral side, due to the large variability between animals. This observation can be correlated to the observations of intensity of silver enhancement, described in section 5.2.2. The reason why the ipsilateral and contralateral side did not differ from each other may lie in the large amounts of nanoparticles observed in choroid plexus and median eminence by electron microscopy (see section 5.2.7 and 5.2.8). Perhaps if these areas were removed prior to ICP-MS analysis, a better comparison might have been found between ipsilateral and contralateral side as well as between treated groups of rats. The amount of gold present in the brain did not differ between the different nanoparticle formulations. This finding contrasts with a previous study, where it has been found that the ligand coating made a difference in the brain distribution when using 15 nm gold nanoparticles (Lee et al. 2014). In that study, neutral nanoparticles (coated with OEG) accumulated in the brain to a larger extent than nanoparticles with amine or carboxylate groups. However, that study used a different method of administration, intravenous tail injection and also longer time points (over 6 months).

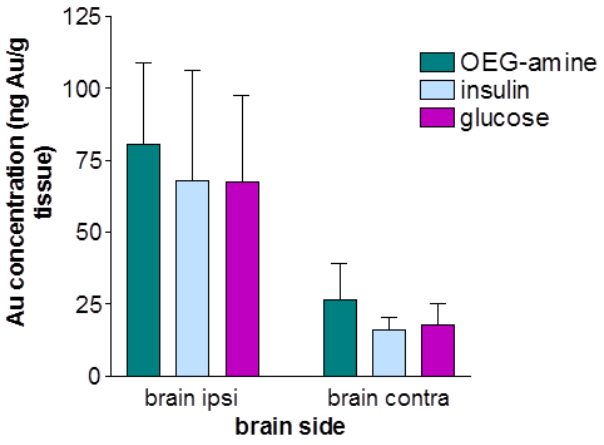

Figure 5.5. The amount of gold in the brain analysed by ICP-MS. The gold concentration in tissue (ng Au/g tissue) was compensated for variations in the dose administered (mg Au/kg animal). 3-4 animals in each group. No significant difference was detected the between the ipsilateral side and contralateral side (unpaired ttest, one-tailed). Data shown as mean ±SEM.

5.2.4 Nanoparticle localisation in cells of the cortex

The next step was to find out the cellular and intracellular localisations of our gold nanoparticles within the brain. Based on our previous finding from ICP-MS that these nanoparticles entered the brain similarly despite their ligand coating, we compared the localisation of OEG-amine/galactose nanoparticles (Figure 5.6A) with glucose nanoparticles (Figure 5.6B) within the cortex by TEM. It was important to note that the silver-enhanced gold nanoparticles were clearly distinguishable from other objects present in the cells, due to their high electron-dense contrast. We observed that indeed the nanoparticles were able to penetrate the brain endothelium and enter the brain parenchyma. Moreover, as suggested by the ICP-MS, the nanoparticle location also appeared similar for both types of nanoparticles (OEG-amine/galactose nanoparticles and glucose nanoparticles) within cells of cortex as well as within their subcellular locations.

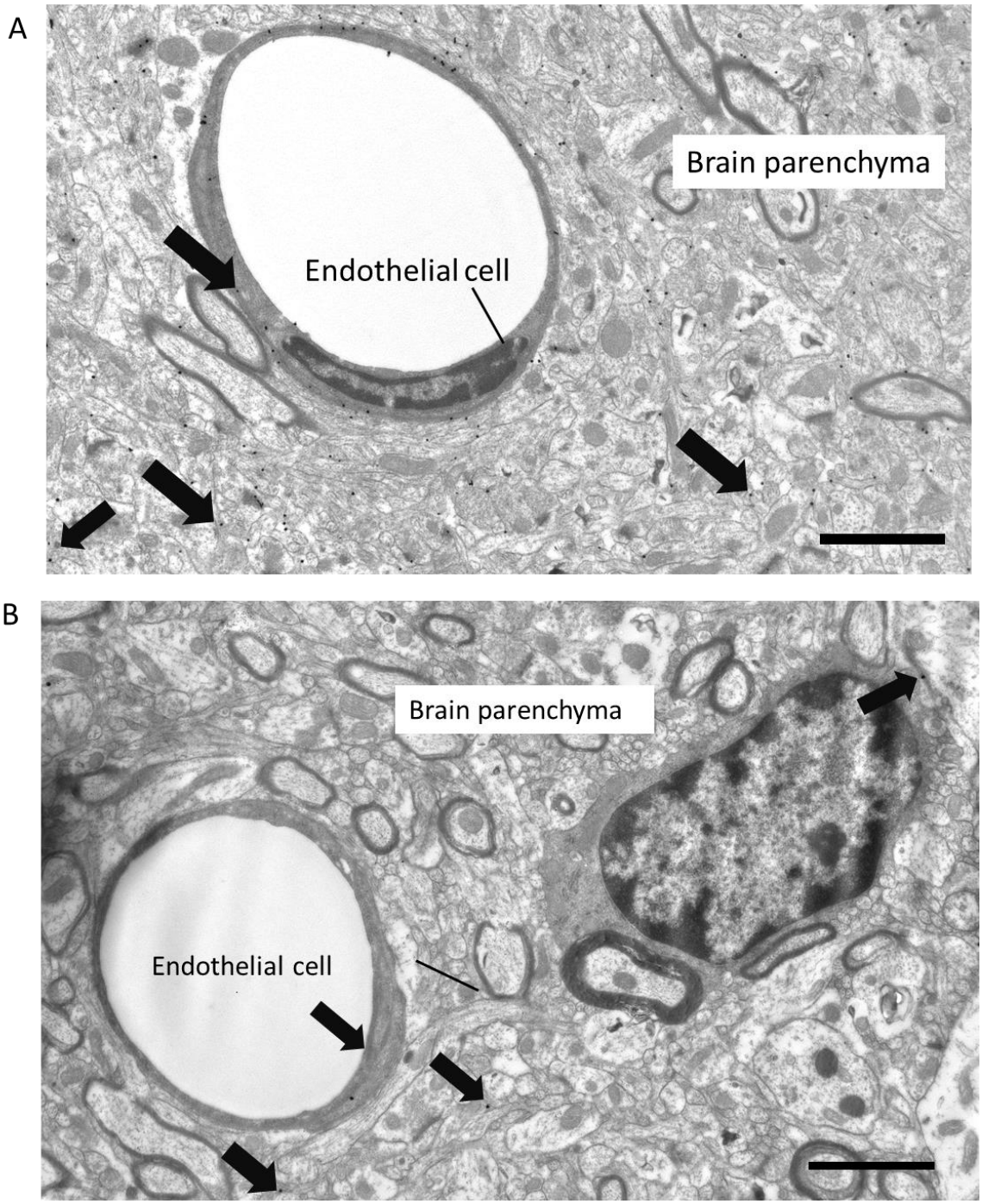

Figure 5.6. A. Gold nanoparticles coated with OEG-amine/galactose in the cortex. Some of the silver-enhanced gold nanoparticles are identified with black arrows. Scale bar = 2 microns. One animal was imaged for this brain region. B Gold nanoparticles coated with glucose in rat cortex. The silver enhanced nanoparticles are identified with arrows. Scale bar = 2 microns.

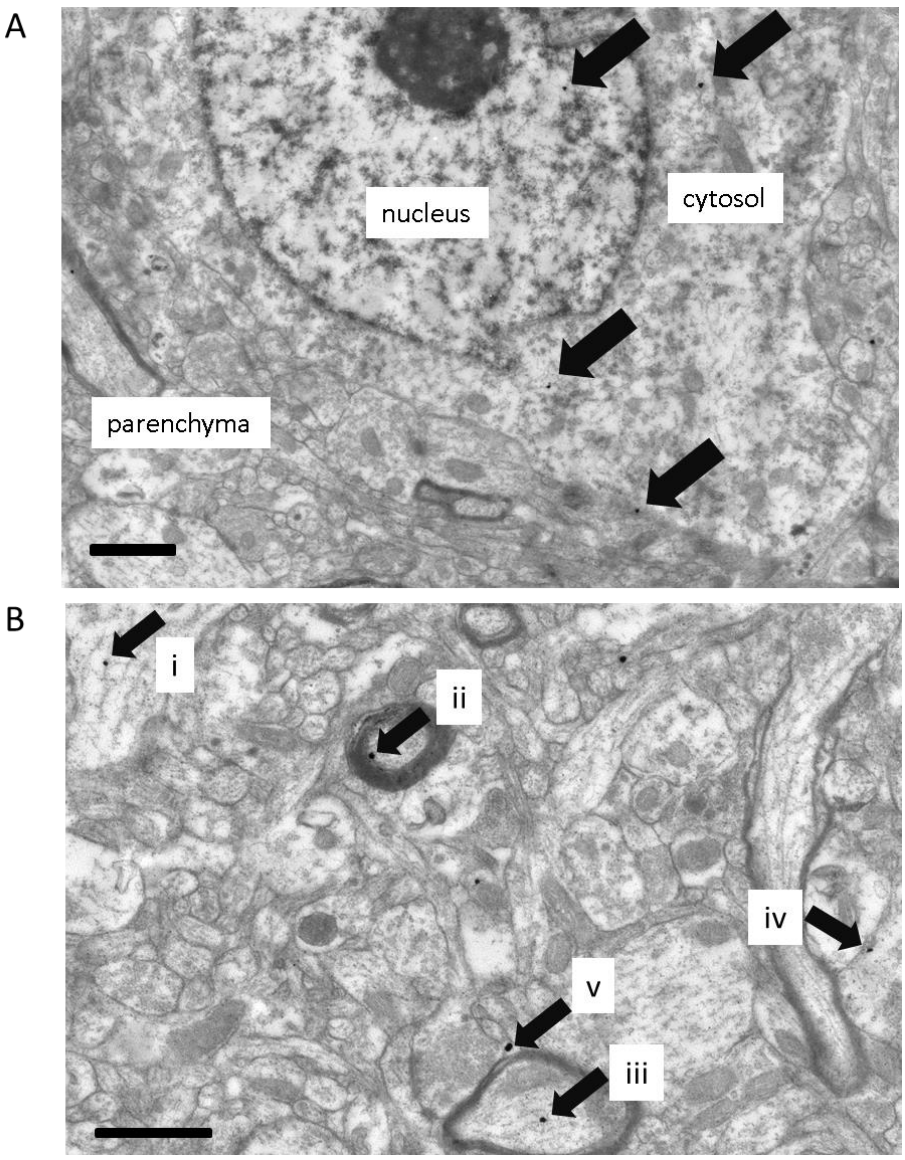

Figure 5.7. Glucose-coated gold nanoparticles in neurons. A. Nanoparticles (arrows) in nucleus and cytosol of a neuronal cell body. B Nanoparticles in myelinated axons (ii & iii), unmyelinated axons/dendrites (i & iv) and in extracellular space. Scale bars = 1 μm. This figure has been published elsewhere (Gromnicova, Yilmaz, et al. 2016). Reprinted with permission of Nanomedicine.

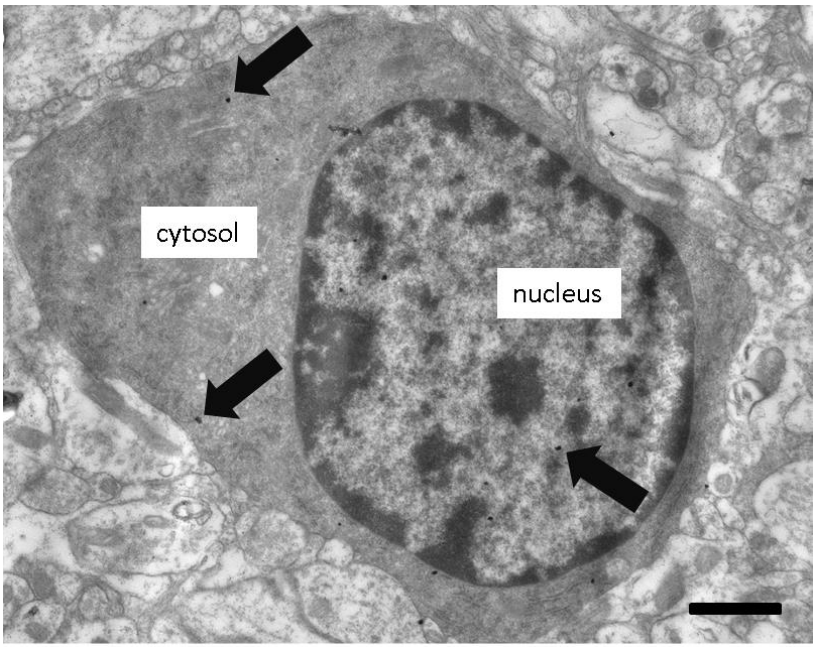

Figure 5.8. Glucose-coated gold nanoparticles in a glial cell of the rat cortex. Silver-enhanced gold nanoparticles (arrows) in both cytosol and nucleus of a glial cell. Scale bar = 1 µm. This figure has been published elsewhere (Gromnicova, Yilmaz, et al. 2016). Reprinted with permission of Nanomedicine.

As an illustrative example, sections from animals treated with gold nanoparticles coated with glucose are shown in Figure 5.6A and Figure 5.6B, as the group treated with OEG-amine/galactose nanoparticles showed comparable localisations in brain tissue. As we predicted, we were able to detect glucose-coated gold nanoparticles in the cells of the blood vessels, i.e. in endothelial cells and pericytes (Figure 5.6A and Figure 5.6B). Next, the nanoparticles were also observed in neurons; in both the cell body and axons and dendrites (Figure 5.7). We also observed nanoparticles in glial cells (Figure 5.8). Such detailed analysis of nanoparticle distribution within the brain had not been shown before, thus we published results on brain localisation of glucose-coated nanoparticles (Gromnicova, Yilmaz, et al. 2016).

5.2.5 Gold nanoparticles in the striatum and hippocampus

Gold nanoparticles coated with OEG-amine/galactose were also present in the striatum (Figure 5.9A) and hippocampus (Figure 5.9B). The nanoparticles were observed in blood vessels, extracellular spaces within the brain, in axons and dendrites. However, both regions showed much lower nanoparticle density. Thus, no nanoparticles were observed in astrocytes and nerve bodies, which may be due to this lower nanoparticle density. Figure 5.9A shows nanoparticles in the blood vessels of the striatum.

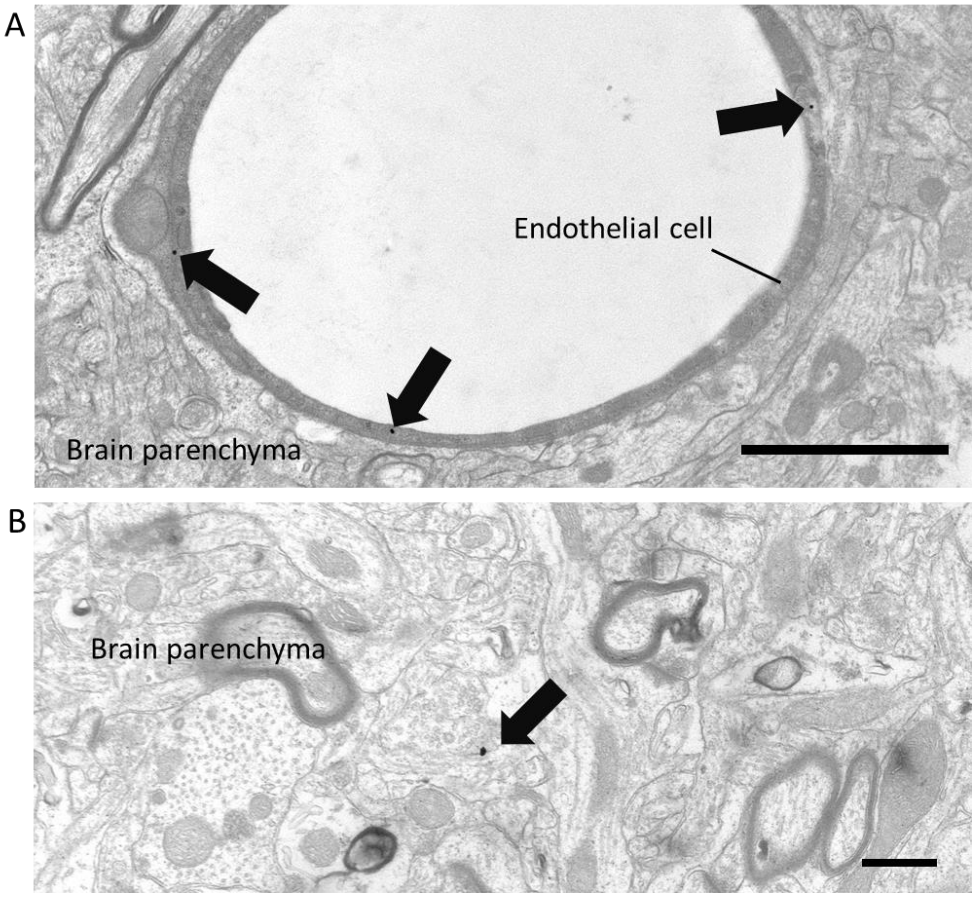

Figure 5.9. A Gold nanoparticles coated with OEG-amine (arrows) in the blood vessel of the striatum. Scale bar = 2 µm. B Gold nanoparticle (arrow) coated with OEG-amine/galactose in rat hippocampus. Scale bar = 500 nm.

5.2.6 Nanoparticles located at more than 10 micron distance from the blood vessels

Within the short-time scale of the experiment, some gold nanoparticles were found to be located over 10 microns away from the nearest vessel (Figure 5.10). In order for them to have reached this far away from the vessel, they probably penetrated through cells rather than diffusing through the tortuous extracellular space as this way would be a slower process (Sykova & Nicholson 2008). Therefore, the nanoparticles penetrated the cortex rather quickly. We have considered the possibility that the nanoparticles seen in our images might have moved there from another vessel lying closer. However, the cortical blood vessels are 50 μm apart (Nicholson 2001). In the present study, we analysed this distance in rat cortex and found that the blood vessels were 50.6 +- 25.5 μm apart (106 measurements from one animal). Our sections were 80 nm thick. Therefore, the density of the blood vessels would have to be higher in order for the nanoparticles to appear on the picture by moving from another closer vessel. Thus, if the nanoparticles can permeate the cortex at a rate of 10 μm in 10 min, then they might be able to permeate the whole cortex in 50 min if they achieve a steady state concentration in the plasma.

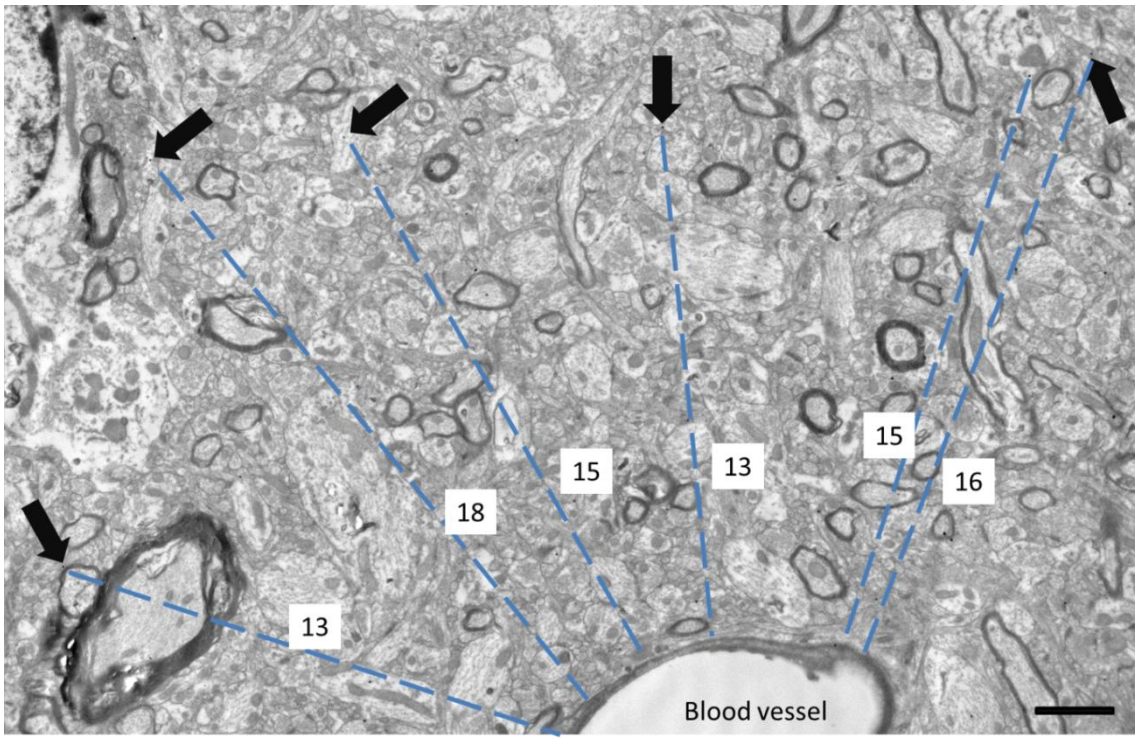

Figure 5.10. Distance from the blood vessel travelled by glucose-coated gold nanoparticles in cortex. Each nanoparticle (arrow) has its path length measured from the blood vessel with the number specifying the distance in microns. Scale bar = 2 µm. This figure has been published elsewhere (Gromnicova, Yilmaz, et al. 2016). Reprinted with permission of Nanomedicine.

5.2.7 Gold nanoparticles in cells of choroid plexus

Another formulation of nanoparticles, OEG-amine/galactose/insulin nanoparticles, was useful in determining localisations in the choroid plexus (Figure 5.11A). Here, we noted that some of the blood vessels contained residual red blood cells as well. The red blood cells had a smaller percentage of nanoparticles than the rest of the blood plasma. This showed the importance of perfusing the animals for analysis of gold content by ICP-MS. In most previous studies, the tissue has been analysed unperfused (Sonavane et al. 2008; De Jong et al. 2008), still containing blood. This may cause false positives in organs that may have very low nanoparticle localisations, such as brain. In the choroid plexus, we found the gold nanoparticles within epithelial cells and in their intracellular junctions. As the blood vessels of choroid plexus are fenestrated, the endothelium allows passage of gold nanoparticles freely into the underlying

parenchyma. Here, the choroid plexus epithelial cells form a barrier and thus may slow down the movement of nanoparticles through this tissue. We also noted some nanoparticles in the villi of choroid plexus cells which may be the result of the nanoparticles passing through the choroid plexus cells from the blood vessels or from the ventricles. The choroid plexus also has resident phagocytic and dendritic cells which also contained some nanoparticles (Figure 5.11B).

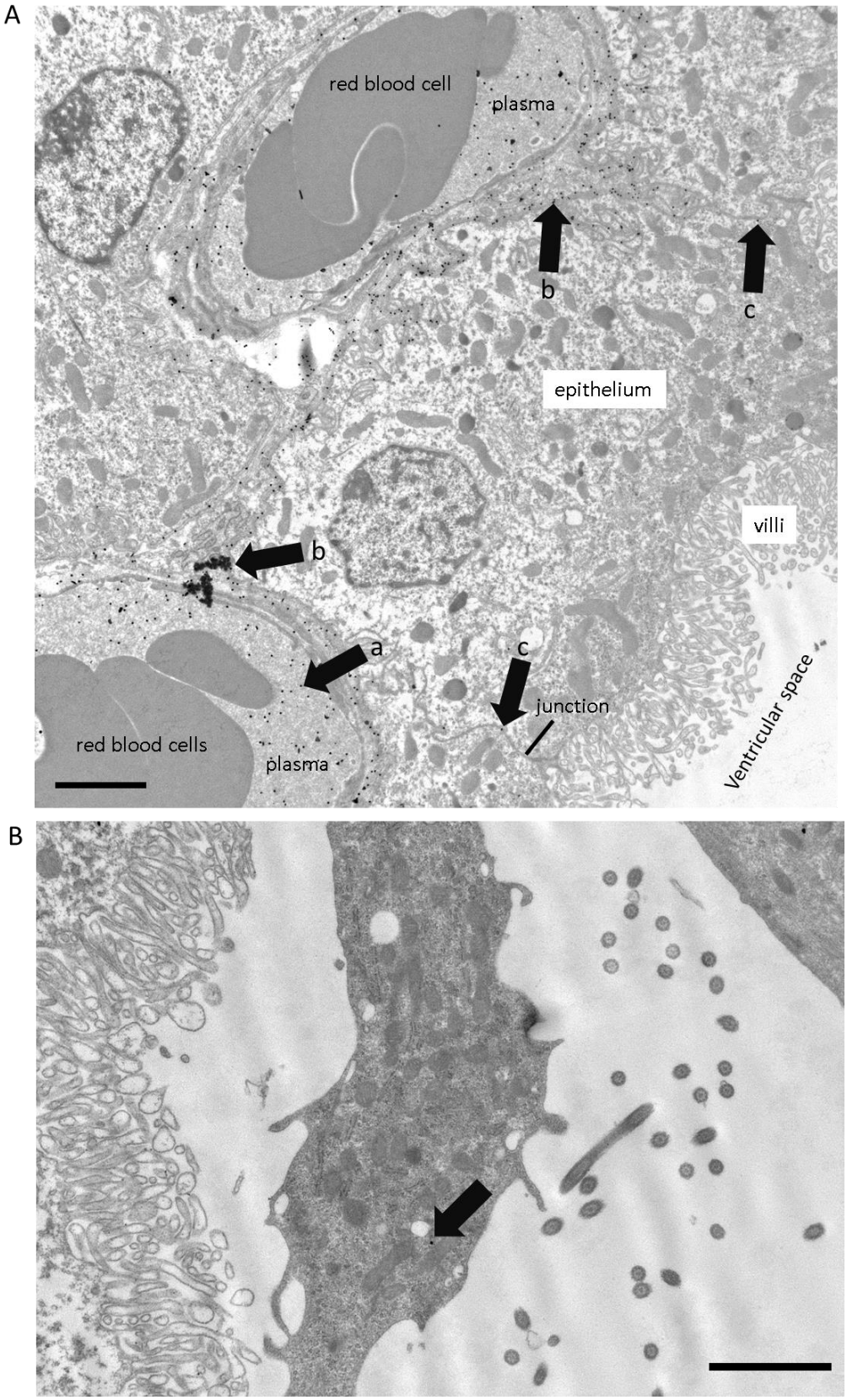

Figure 5.11. Gold nanoparticles coated with OEG-amine/galactose/insulin in rat choroid plexus. A Nanoparticles (arrows) in blood vessels (a), in the extracellular spaces beyond the blood vessels (b) and in intercellular junctions between epithelial cells (c). B A nanoparticle in a phagocytic cell of a choroid plexus (arrow). Scale bar = 2 microns

5.2.8 Gold nanoparticles in blood vessels of median eminence

Blood vessels in the median eminence of the brain also have a greater permeability than vessels in other brain regions. The median eminence is located at the bottom of the hypothalamus. This part is sometimes classified as a circumventricular organ with a secretory function. Therefore, fenestrated brain endothelium is present. We have analysed the median eminence in one of the brain sections of animals treated with OEG-amine/galactose nanoparticles (Figure 5.12). We observed that indeed the gold nanoparticles passed the fenestrated endothelium and gathered in the basal lamina of the vessels. The large vessels had the highest amounts of accumulated nanoparticles, as they slowed down their progression into the tissue. The nanoparticles were observed within the tissue as well.

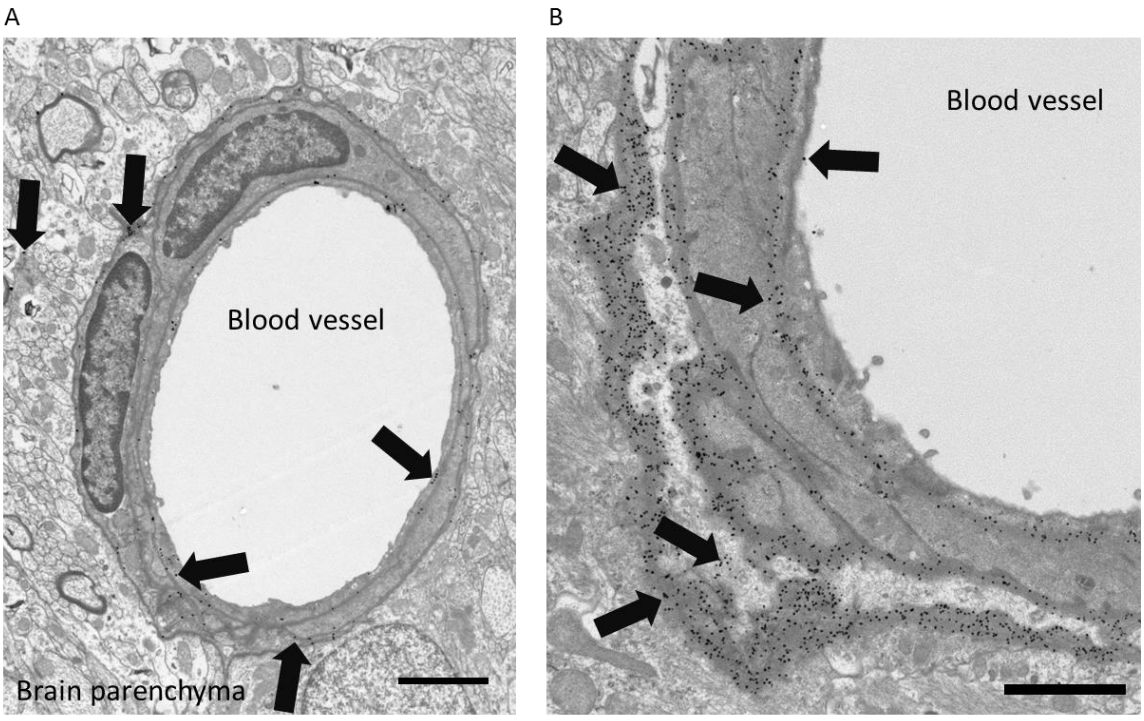

Figure 5.12. Gold nanoparticles coated with OEG-amine/galactose in median eminence. Nanoparticles (arrows) in a small (A) and a large (B) blood vessel of this circumventricular organ with fenestrated brain endothelium. Scale bar 2 µm.

5.2.9 Analysis of gold nanoparticles in cerebellum

The three nanoparticle formulations had a similar uptake profile into the brain cerebrum. The cerebellum was analysed separately from the cerebrum. In cerebellum, the three nanoparticle formulations were compared but we found no statistical difference in the amount of nanoparticles present (Figure 5.13A). When we used silver enhancement to assess regional localisation of the nanoparticles, mainly blood vessels were stained. It is possible that the majority of the nanoparticles remained in the vessels, particularly if they were not fully perfused (Figure 5.13B).

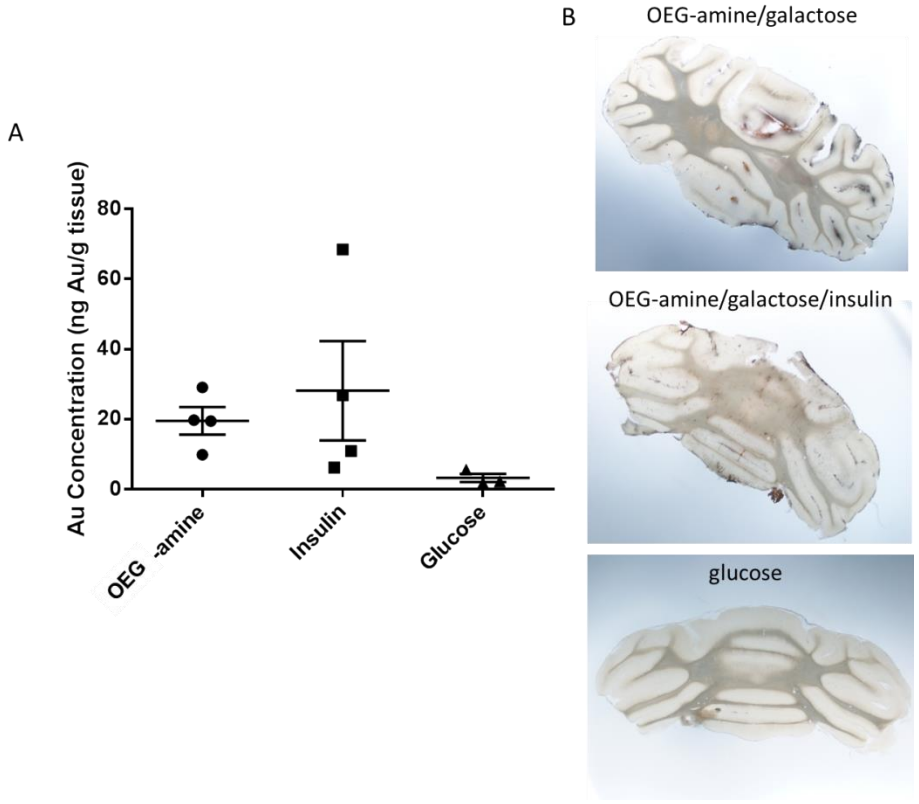

Figure 5.13. Gold nanoparticles in the cerebellum. A. The amount of gold is shown as a concentration of gold in g tissue compensated for the weight of the animals. 3-4 animals in each group. Gold nanoparticles coated with glucose, OEG-amine/galactose (OEG-amine) and OEG-amine/galactose/insulin (insulin). The amount of gold is recalculated relative to the weight of the animal. 4 animals in each group. No significant difference between groups (one-way ANOVA, Tukey post-test). Data shown as mean ±SEM. B silver-enhanced sections of the cerebellum, a representative animal shown from each group. The staining and sectioning of cerebellum was performed by Ayse Gungor.

5.2.10 The amount of gold present in liver, kidney and lung

The last part of this work was to analyse the overall distribution of all three formulations in kidney, liver and lung and compare them to those in the brain (Figure 5.14). We used ICP-MS for this purpose. We found that most of the nanoparticles accumulated in the kidney, which is a typical observation for <5 nm sized nanoparticles (Skotland et al. 2010; Hillyer & Albrecht 2001) as they are cleared via this organ. Apart from liver, there was no difference in the amount of nanoparticles with different ligand coatings. In liver, glucose-coated nanoparticles had the lowest accumulation; this was significant when comparing glucose nanoparticles with OEG-amine/galactose/insulin. Perhaps the positive charge of the ligand OEG-amine may have facilitated the nanoparticle penetration into the liver or into the phagocytic cells of the liver (Kupffer cells). Unfortunately, as the ICP-MS is a destructive method, we were not able to perform TEM analysis on livers and kidneys to see the cellular localisations of gold nanoparticles. This was because the ICP-MS analysis was performed prior to TEM investigations.

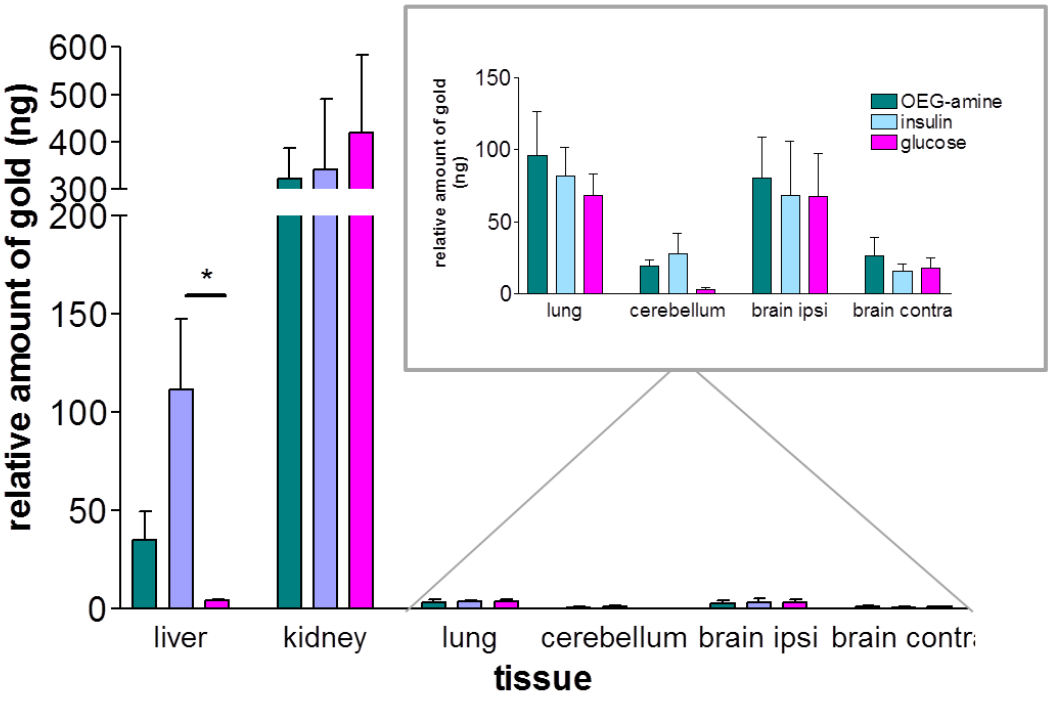

Figure 5.14. The gold content in liver, kidney, lung and brain as analysed by ICP-MS. Three formulations of nanoparticles were tested: those coated with OEG-amine/galactose (OEG-amine), OEG-amine/galactose/insulin (insulin) and glucose. Brain tissue is divided into cerebellum, ipsilateral side (brain ipsi) and contralateral side (brain contra) of the cerebrum. The amount of gold is shown as a concentration of gold in g tissue compensated for the weight of the animals. The inset shows an expanded area of the data set. 3-4 animals per group. One-way ANOVA, Tukey post-test, * P<0.01. Data shown as mean ±SEM.

5.2.11 Summary and conclusion

In conclusion, we did not observe large differences in the nanoparticle penetration of organs based on their ligand coating. According to our *in vitro* results we hypothesized that there would be a difference because the rate of uptake of the glyconanoparticles by the endothelial cells was increased due to the presence of the OEG-amine ligand. The fact that we did not find a difference does not mean that none exists; only that our 10 min experimental set up was not sufficient to find it. Therefore, a time-course study would be necessary to investigate whether the ligand coating for this type of glyconanoparticle changes the characteristics of the

nanoparticles with respect to brain entry, penetration, accumulation and clearance from different organs in the body. Moreover, as all of the kidney and liver tissue was used for ICP-MS unfortunately they could have provided us with important information on where these nanoparticles locate within these organs and whether there is a difference on their cellular accumulation between the treated groups.

Nevertheless, this work showed novel findings about the location of small gold nanoparticles in the rat brain. Some of the work on larger gold nanoparticles (80 nm and 13 nm) has been reported previously (Prades et al. 2012; Wiley et al. 2013), however, a detailed ultrastructural analysis has not been performed. Using transmission electron microscopy, we were able to gain an insight into the nanoparticle distribution characteristics in various regions of the brain. In the cortex we observed the nanoparticles within the cell bodies of neurons and glial cells as well as in their nucleus. This is a particularly important finding for therapeutic use of these nanoparticles. Moreover, the regions of the brain that contain an atypical blood-brain barrier, pointed to possible distribution characteristics of these nanoparticles that may be relevant to areas with compromised blood-brain barrier such as in certain neurological disorders.

Chapter 6. DNA-coated gold glyconanoparticles

6.1 Introduction

The previous chapter showed that gold glyconanoparticles can enter the rat brain and thus have potential as a delivery system of therapeutic molecules into the brain. One such class of therapeutic molecules are nucleic acids.

6.1.1 RNA interference

Short strands of RNA have been proposed for therapeutic use to modulate gene expression and thus treat "undruggable" diseases. This is because they can silence potentially any gene in the body (Wu et al. 2014). RNA interference has become widely known since 1998. Short strands of dsRNA (i.e. siRNA, short interfering RNA) were found to silence gene expression in *C. elegans* (Fire et al. 1998). Since then, the process of RNA interference has been elucidated. It begins with long strands of dsRNA, that are cleaved by Dicer into 21-23 nucleotide fragments of siRNA (Bernstein et al. 2001). siRNA then incorporates into the RISC complex (RNA-induced silencing complex). Here, Argonaut 2 protein unwinds siRNA, recognizes one strand as sense (or passenger), which is cleaved off, and second strand as antisense (or guide), which is retained (Matranga et al. 2005). The RISC complex then seeks, cleaves and therefore deactivates target mRNA (Ameres et al. 2007).

Another type of regulatory RNAs also exists, miRNAs, which use similar cytosolic machinery (Dicer and RISC). Unlike siRNAs, sense and antisense strands of miRNAs are not perfectly complementary (Burnett & Rossi 2012)

6.1.2 siRNA delivery modes and current progress

For therapeutic purpose, two main ways to deliver siRNA have been investigated: localized or systemic delivery. In a localized delivery, siRNA is administered to the specific site directly, whereas in a systemic delivery it is injected intravenously (Whitehead et al. 2009; Burnett & Rossi 2012). Neurological disorders mostly require systemic delivery, even though some, such as Huntington's disease, has been treated by local siRNA application (Whitehead et al. 2009).

Using siRNA for therapy is a difficult task, since oligonucleotides are prone to degradation by nucleases (Whitehead et al. 2009) and thus a delivery system is needed. Liposomes and polymeric nanoparticles are one of the most investigated systems for siRNA delivery (Whitehead et al. 2009; Wu et al. 2014). Several potential therapeutics involving these carriers have gone through clinical trials, but many have been terminated due to low therapeutic impact on patients or side-effects (Burnett & Rossi 2012). Moreover, the neurological conditions targeted by the pharmaceutical industry with siRNAs include usually Huntington's disease (Whitehead et al. 2009) even though experimentally, Alzheimer's and Parkinson's disease have been targeted in cell and animal models (Boudreau et al. 2011).

There is a great need to find new ways to deliver oligonucleotides into the brain. Gold nanoparticles have been shown to carry and deliver DNA and RNA into cells (Rosi et al. 2006; Dhar et al. 2009; Cutler et al. 2011; Giljohann et al. 2009; Guo et al. 2010; Seferos et al. 2007). Moreover, Mirkin's group (Jensen et al. 2013) has shown that 13 nm gold nanoparticles coated with a dense layer of RNA duplexes (termed as spherical nucleic acids) were able to decrease gene expression *in vivo*. In this study, explanted gliomas underwent apoptosis upon silencing gene Bcl2Like12 with their nanoparticles. The authors demonstrated the possibility of using RNA-therapy delivered by gold nanoparticles for treating a brain tumour.

As we demonstrated in previous chapters, our small gold glyconanoparticles were able to enter the brain. This chapter focuses on whether gold nanoparticles may be able to carry and deliver nucleic acids into brain endothelium.

6.2 Results and Discussion

Since we found that gold glyconanoparticles <5 nm in size can be a potential delivery system of therapeutic molecules into the brain, we investigated oligonucleotides as a potential cargo attached to these nanoparticles. Firstly, we established the rate of release of covalently-attached ligands/cargo. Then, we prepared stable DNA-attached gold glyconanoparticles and assessed the uptake of dsDNA -coated gold nanoparticles by brain endothelial cells.

6.2.1 Release of covalently-attached ligands from small gold nanoparticles

The ligands and cargo molecules were attached covalently to the gold core. Therefore, the stability of the ligand/cargo attachment was determined for <5 nm gold nanoparticles, in both a reducing environment and at different pH.

It has been shown that reducing agents present within the cell cytosol, such as glutathione (GSH), cause ligands to be released from gold nanoparticles (Verma et al. 2004); this process is explained in Section 1.3.2.2. Thus, we tested the effect of varying concentrations of glutathione on ligand release. For the purpose of these investigations we used a gold nanoparticle with a small fluorescent ligand (glutathione-fluorescein) that was attached to the gold core via a thiol bond. Gold nanoparticles can quench fluorescence, thus if the fluorescent ligand detaches, an increase in fluorescence in the solution will occur.

We tested a concentration range of reduced glutathione (GSH) from 1 mM to 10 mM, a range found within cells (Anderson 1998). The rat brain has been found to contain as little as 2 mM in cortex and cerebellum (Folbergrova et al. 1979). The concentration of glutathione may

depend on the cellular stress the cells might have been exposed to, as determined by the ROS levels (Li et al. 2012). We did not determine level of GSH in hCMEC/D3 cells used in this study.

As is shown in Figure 6.1, ligand release depended on glutathione concentration, the higher the concentration, the higher the release. Concentrations of 10 mM and 5 mM had a very similar effect on the release. The fluorescence was measured at regular intervals from 10 min to 6 h. The half-life (t ½) of ligand release from the nanoparticles was then calculated. For 1 mM GSH, t ½ was 3 h; for 2.5 mM GSH t ½ was 2 h; for 5 and 10 mM GSH t ½ was 1 h. Therefore, if gold nanoparticles were to efficiently deliver a therapeutic cargo to its target tissue across brain endothelial cells, the transit across the cell cytosol would have to be less than 1 h. Another mechanism for the nanoparticle to transit across endothelial cells is via transcytosis where lower concentrations of GSH would be encountered than those in the cytosol.

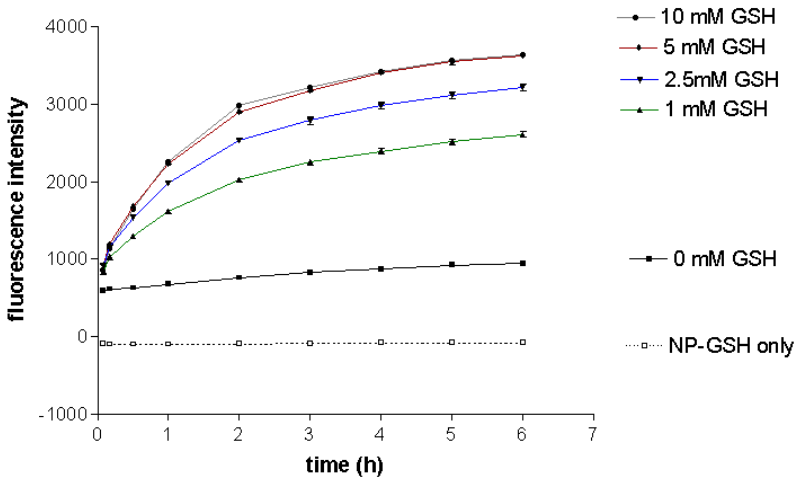

Figure 6.1. Effect of reduced glutathione on release of fluorescent ligand from gold nanoparticles. Gold nanoparticles with glutathione-FITC were used in the study. Glutathione (GSH) concentrations were tested in the range of 1 mM to 10 mM. As a control of background fluorescence of nanoparticles, nanoparticles with ligand glutathione only (NP-GSH only) were used. 2 independent experiments performed, representative graph is shown here, the points are means ± SEM of 4 technical replicates; fluorescence intensity is on an arbitrary scale.

However, vesicles such as lysosomes have a low pH (Sorkin & von Zastrow 2002) and thus we tested whether this may affect release of ligands. Nanoparticles coated with

glutathione/fluorescein were incubated in buffered solutions of pH 5, 6 and 7.5 (Figure 6.2). However, no significant release of the fluorescent ligand was observed. Moreover, not all vesicles have low pH, some, such as caveosomes, have a neutral pH (Parton & Simons 2007). This contrasts with early endosomes (pH 6.5 – 6.0), late endosomes and lysosomes (pH 5.5 – 4.6) (Sorkin & von Zastrow 2002).

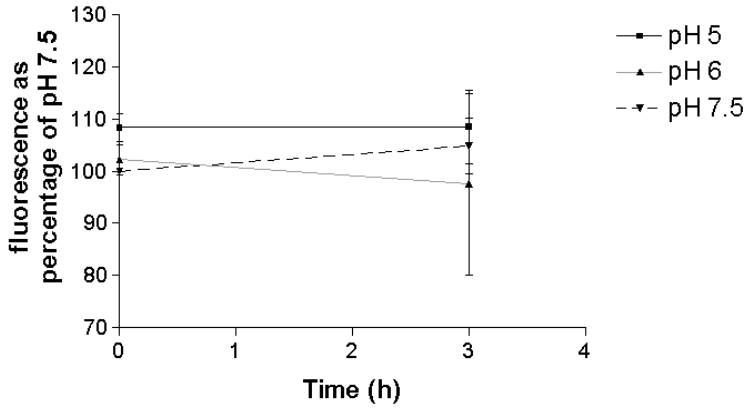

Figure 6.2. Effect of pH on release of fluorescent ligand from gold nanoparticles. Gold nanoparticles with attached glutathione-FITC were incubated in different physiological pH (5 – 7.5) for a period of 30 min to 3 h to monitor time-dependent release of fluorescent ligand from quenching by the gold core. The data (mean ± SEM) are a combination of 2 independent experiments and normalized to pH 7.5 due to pH-dependent variations in fluorescence intensity of FITC. Time 0 equals incubation of nanoparticles in solutions for 20-30 min prior to fluorescence reading.

Thus, the cargo release from gold nanoparticles in a target cell type would be cell-location dependent (cytosol x vesicles) and time-dependent. It would therefore depend highly on uptake characteristics of cargo-gold nanoparticles. As we decided to deliver oligonucleotides into the cell, the next step was to prepare oligonucleotide-coated gold nanoparticles.

6.2.2 Synthesis of small gold nanoparticles with DNA

Glyconanoparticles with covalently-attached nucleic acids have not been prepared before. However, cationic gold glyconanoparticles have been used for DNA transfection inti

cultured cells with non-covalently held DNA on their cationic glycopolymer (Ahmed et al. 2009). The nanoparticles used in that study were much larger in size, from 10 nm to 100 nm.

In order to prepare covalently-attached DNA glyconanoparticles, we used thiol-DNA and other thiolated ligands such as galactose and OEG-amine in the synthetic mixture in different proportions. Three synthetic approaches were investigated:

1. Standard method of modified Brust-Schiffrin reaction
2. Alkali synthesis using Brust-Schiffrin method as above, keeping the pH of the ligand mixture at pH 11.
3. Ligand exchange reaction, where stable galactose-coated nanoparticles are incubated in an excess of thiol-DNA.

6.2.2.1 Selection of DNA sequence

For sequence of thiol-C6-DNA (referred to as thiol-DNA in the rest of the text) we selected a 20 nt sequence (AAT ATC GCG GAC AGA AGA CG), which was not normally present in the genome of mammalian cells. Thus, this sequence may be used in future studies in rats or mice. The sequence was derived from a GFP gene (green fluorescence protein) in this proof-of-principle study for delivering DNA into cells. The GFP nucleotide sequence was obtained from a plasmid of a bacteria *Neisseria gonorrhoeae* (pCmGFP) (GenBank: FJ172221.1). The selected sequence had ≤13 nt homology by BLAST search (NCBI) with any gene in the human genome, as we were using human brain endothelial cells and astrocytes.

6.2.2.2 Standard method of modified Brust-Schiffrin reaction in water

We intended to prepare variations of DNA-coated nanoparticles with other ligands such as galactose and/or OEG-amine based on our findings shown in chapter 2, 3 and 4. The

synthetic process is based on the one patented by Midatech Pharma Plc and was performed at their laboratory. The synthesis is modified from the Brust-Schiffrin method of preparing small gold nanoparticles (Gromnicova et al. 2013). It involves mixture of gold salt (5 μmoles) and ligands (15 μmoles) in methanol and water or water only. Reducing agent, sodium borohydride, is then added, resulting in instant formation of small gold nanoparticles. The colour of the mixture changed from transparent yellow liquid to deep brown as the nanoparticles formed. DNA does not dissolve in methanol; therefore the reaction was prepared purely in water. We tested several combinations of ligands:

a) 0.75 μmoles thiol-DNA, 7.125 μmoles thiol C2-linker modified galactose, 7.125 μmoles disulphide OEG-amine,
b) 0.75 μmoles thiol-DNA, 14.25 μmoles thiol C2-linker modified galactose,

and their respective controls:

c) 7.5 μmoles thiol C2-linker modified galactose, 7.5 μmoles OEG-amine,
d) 15 μmoles of thiol C2-linker modified galactose.

However, after the reaction, all of the preparations aggregated, i.e. formed large nanoparticles. Therefore, this preparation method did not achieve any stable ultrasmall nanoparticles with DNA. Also, the control nanoparticles prepared without DNA were not stable and aggregated. Thus, we decided to modify the protocol for nanoparticle preparation as described in the next section.

6.2.2.3 Modified Brust-Schiffrin reaction at pH 11

Thiol-DNA may not have been able to form stable nanoparticles as it may have degraded in the acidic environment of the reaction. Therefore, the pH of the reaction mixture was increased to 11 and the same ligand preparations were tested as above.

The control nanoparticles with galactose and OEG-amine (combination c) did not aggregate immediately and appeared stable; however, they formed visible aggregates after one week at 4°C. In contrast, nanoparticles with only galactose (combination d) remained stable, hence the synthetic process appeared to work efficiently. Nanoparticles with DNA and galactose/OEG-amine (combination a) also aggregated immediately, possibly due to the interaction of negatively charged DNA and positively charged amine groups. On the other hand, nanoparticles with a low DNA concentration and galactose (0.075 μmoles thiol-DNA, 14.925 μmoles thiol C2-linker modified galactose) did not aggregate immediately. However, after a few weeks of being stored at 4 °C some aggregation was observed.

Therefore, the alkali method of preparation produced more stable nanoparticles than the previous reaction. In this way we were able to prepare DNA/galactose-coated nanoparticles, even though the amount of DNA used in this method was 1/10 of that used in the modified Brust-Schiffrin reaction in water.

We were able to analyse the different preparations of nanoparticles by size exclusion chromatography (SEC) on FPLC (fast protein liquid chromatography). The readings were taken at 400 nm for the gold nanoparticle peak and 260 nm for the DNA peak. Figure 6.3 shows a typical elution pattern of galactose-coated nanoparticles, prepared at alkaline pH. The nanoparticles can be characterized best by detecting the 400 nm peak, which elutes at 18.24 ml. As gold nanoparticles also absorb at 260 nm, a 260 nm peak occurred at the same elution volume. In Figure 6.4, thiol-DNA is shown for comparison. DNA is eluted mostly at 17.15 ml, even though there are also other peaks present (15.6 ml and 14.7 ml) pointing to perhaps slight impurity of the purchased thiol-DNA or oxidised dimer formation. Figure 6.5 shows gold glyconanoparticles prepared in an alkaline environment with a low amount of thiol-DNA in the presence of thiol-C2-galactose, thus forming galactose/DNA nanoparticles. Here, the results

indicate that aggregates were formed. This was later confirmed by formation of visible aggregates after a few weeks of storage.

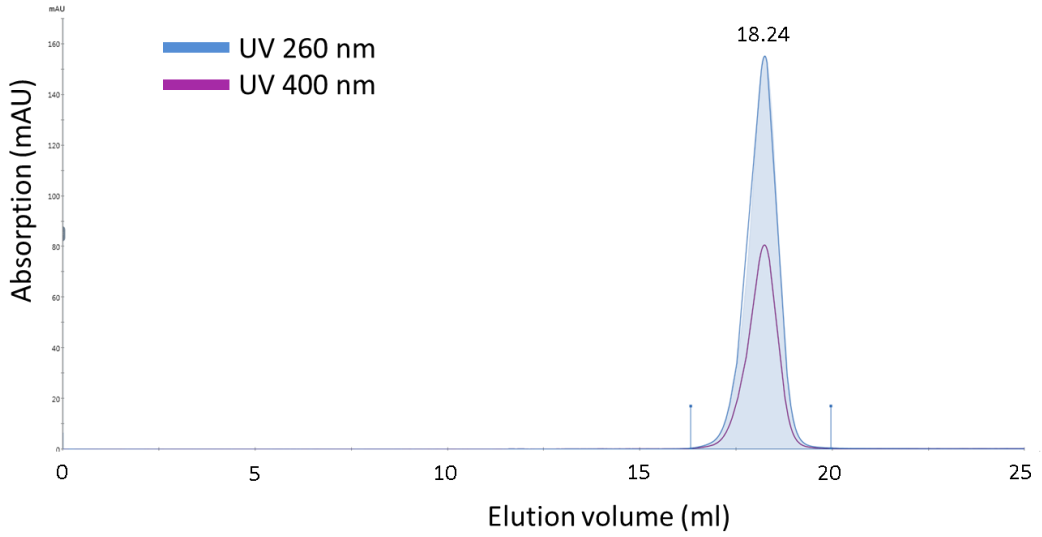

Figure 6.3. SEC profile of control nanoparticles with galactose synthesized in alkaline environment. The nanoparticle peak elutes at 18.24 ml.

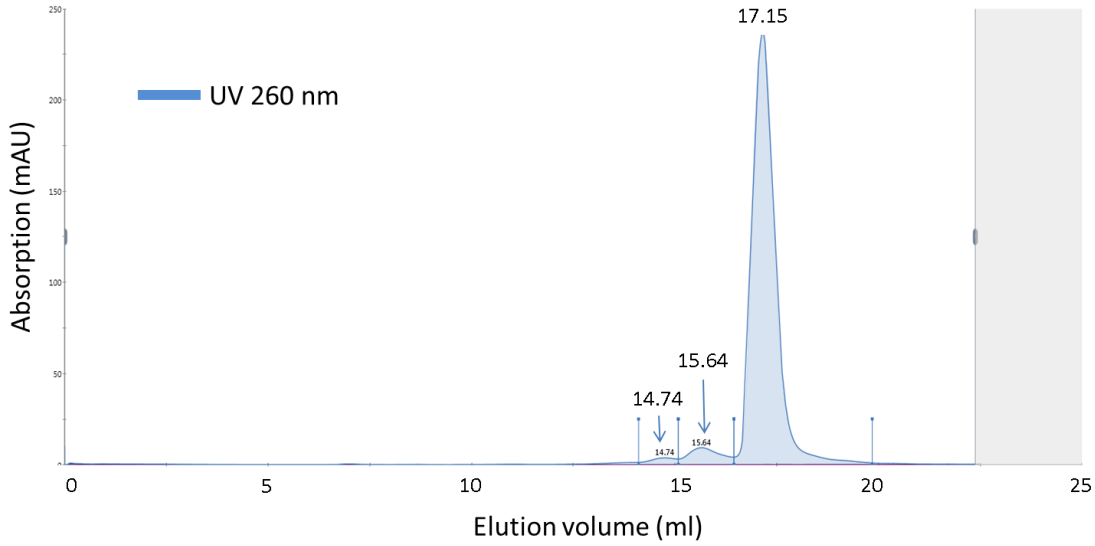

Figure 6.4. SEC profile of thiol-C6-DNA in the absence of gold nanoparticles. A large peak of DNA is observed at 17.15 ml, smaller peaks of larger fractions are present as well. The experiment was performed once.

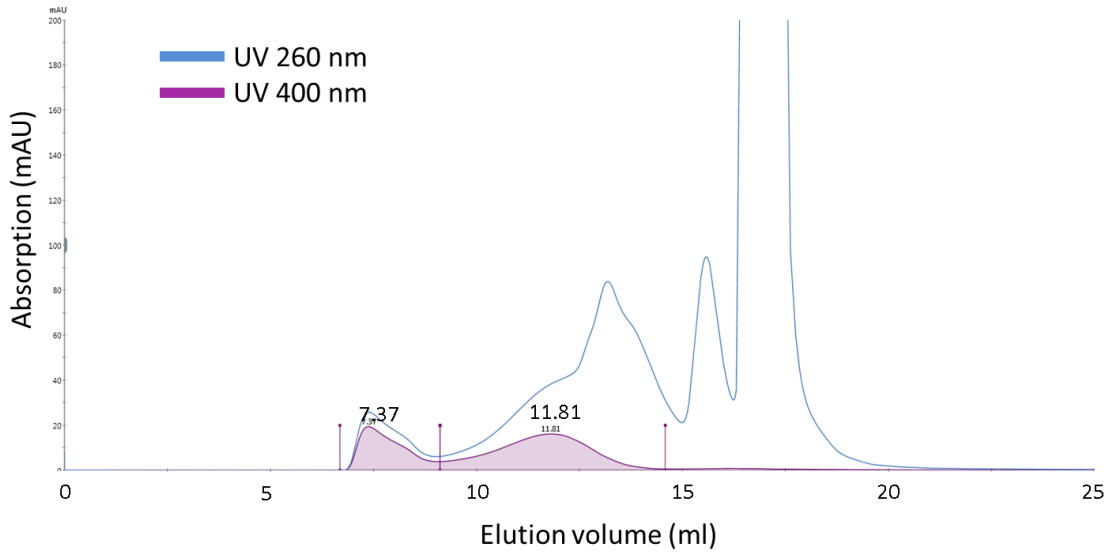

Figure 6.5. SEC profile of formulation of nanoparticles with DNA and galactose synthesized in alkaline environment. 2 distinct populations of nanoparticles are present with peaks at 11.81 and 7.37 ml. The experiment was performed once.

6.2.2.4 Attachment of DNA to stable galactose nanoparticles via ligand-exchange reaction

Another method to attach thiol-DNA to gold nanoparticles is to exploit the ligand-exchange reaction. Here, the excess of thiolated ligand A (thiol-DNA) attaches to the already formed and stable nanoparticle coated with thiolated ligands B (galactose), thus releasing ligand B. In our case, stable galactose-coated gold glyconanoparticles were incubated over several days with molar excess of thiol-C6-DNA at 37° C. The resulting nanoparticles were analysed using SEC on FPLC. Figure 6.6B shows a reading of these nanoparticles after 1 day of incubation; fractions of excess DNA are shown in Figure 6.6A. Here, thiol-DNA is exchanging with galactose as well as forming larger DNA molecules (peak of 15.59 ml, compare with Figure 4). Also other larger peaks containing DNA molecules are increasing the peak areas (peaks at 14.10 ml, 13.49 ml and 12.77 ml).

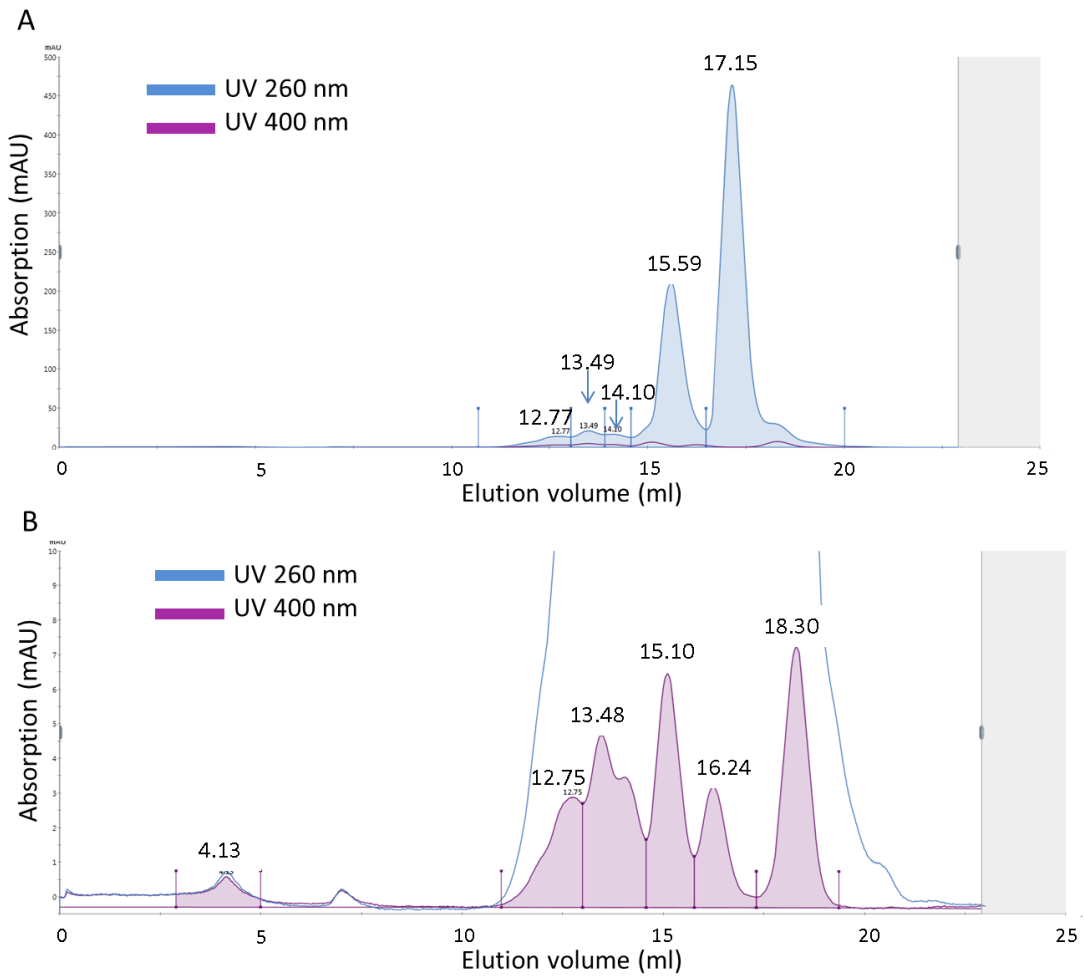

Figure 6.6. Formation of DNA-attached galactose-coated nanoparticles via ligand exchange reaction, after incubation for 1 day with excess of thiol-C6-DNA. A. SEC profile of DNA in the nanoparticle sample, B. SEC profile of nanoparticles formed by this reaction. The experiment was performed once.

When assessing the size-exclusion profile with nanoparticles (Figure 6.6B), the standard peak of nanoparticles with galactose only is present (18.3 ml, compared to 18.24 ml in control nanoparticles in Figure 6.3) as well as other peaks. These peaks of other detected nanoparticles (16.24 ml, 15.1 ml, 13.47 ml, and 12.75 ml) may thus correspond to galactose-nanoparticles with increasing numbers of DNA molecules attached to them, as the resulting nanoparticle is increasing in size. The peak at 4.13 ml is probably an artefact since the separation range of the column used is between 8 and 24 ml.

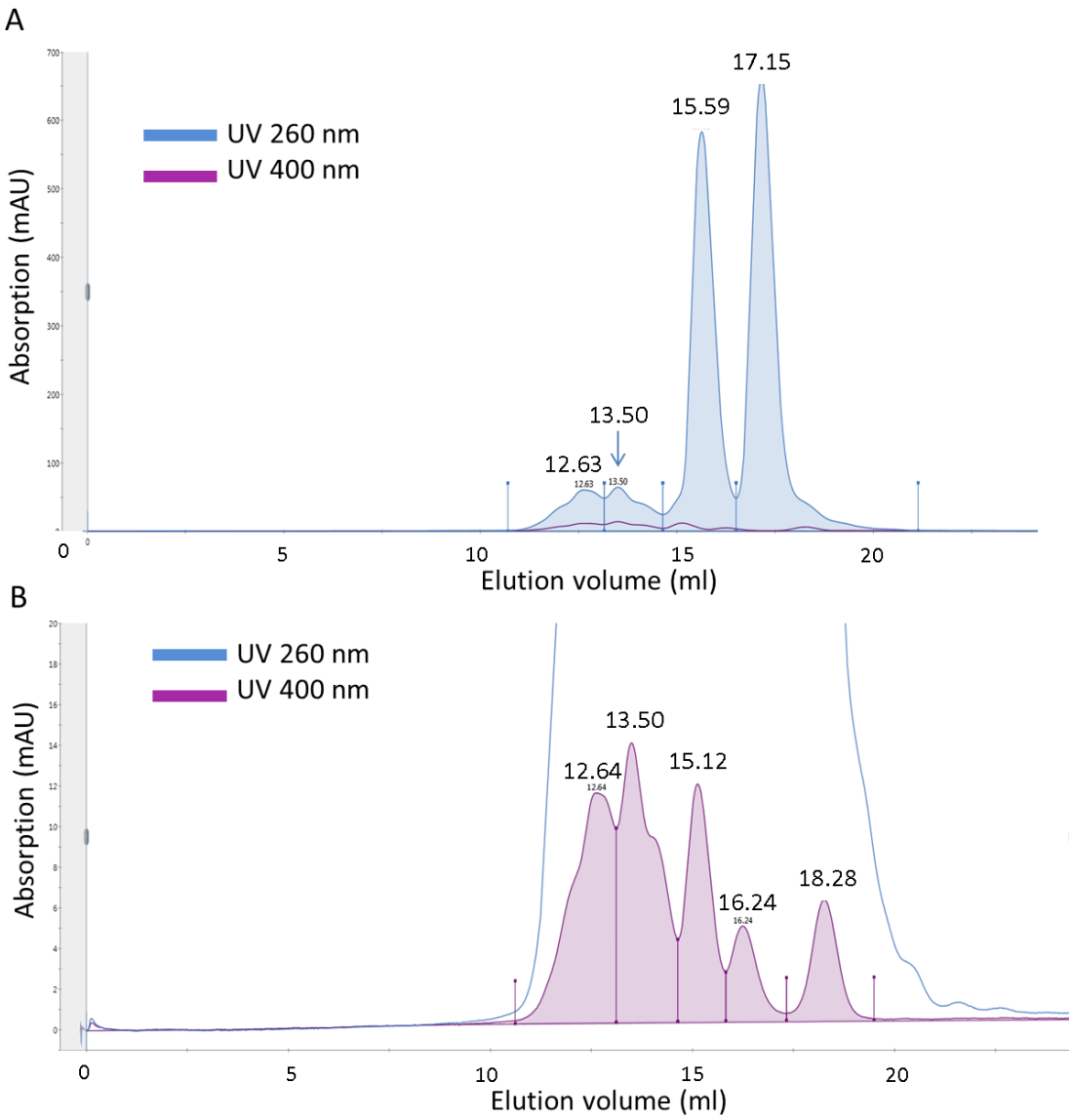

Figure 6.7. Formation of DNA-attached galactose-coated nanoparticles via ligand exchange reaction, after incubation for 3 days with excess of thiol- DNA. A. FPLC trace of DNA in the nanoparticle sample, B. FPLC trace of nanoparticles formed by this reaction. The experiment was performed once.

When monitoring the nanoparticle mixture after 3 days, there was a noticeable difference in proportions of peaks (compare Figure 6.6 with Figure 6.7). Firstly, the large thiol-DNA peak seen previously at 17.15 ml (Figure 6.4 and Figure 6.6A) decreased in its area in proportion to its second peak at 15.59 ml (Figure 6.7A). This may be interpreted as two thiol-DNA molecules reacted to form disulphide-bonded dimers. The peaks are nearly at similar area proportions in the mixture. Also, other peaks of 13.50 ml and 12.63 ml increased in area after 3

days of incubation at 37 °C. Secondly, the nanoparticle peak of unreacted galactose-coated nanoparticles (fraction at 18.28 ml) decreased in area proportion to other peaks of 16.24 ml, 15.12 ml, 13.50 ml and 12.64 ml. This may indicate the larger proportion of nanoparticles with attached DNA molecules. Therefore, this reaction led to a simple preparation of glyconanoparticles with attached DNA. Our next question was whether these nanoparticles can enter brain endothelial cells even though the mixture contained a large excess of free DNA.

The DNA loading of the nanoparticles in each fraction may also need to be determined in future studies. For this purpose, a perfectly clean solution of DNA-nanoparticles without any free DNA is a crucial step. Then, a fluorescent DNA oligonucleotide may be attached to the gold and then displaced either by DTT (Hurst et al. 2006; Conde et al. 2010) or by mercaptoethanol (Zhao et al. 2009). The fluorescence of the oligonucleotide can be measured to determine the concentration of DNA from which the concentration of the oligos per nanoparticle can be determined (Hurst et al. 2006).

6.2.3 Analysis of efficiency of uptake of dsDNA/galactose–coated nanoparticles in brain endothelial cells and astrocytes

In order to track and detect DNA cargo on DNA/galactose gold nanoparticles, the nanoparticle-bound DNA sequence was hybridized with a complementary strand that contained biotin. These biotin-attached DNA probes were used in a subsequent investigation of DNA localization within the cells by electron microscopy. Thus, dsDNA/galactose nanoparticles were created and used in cell uptake studies.

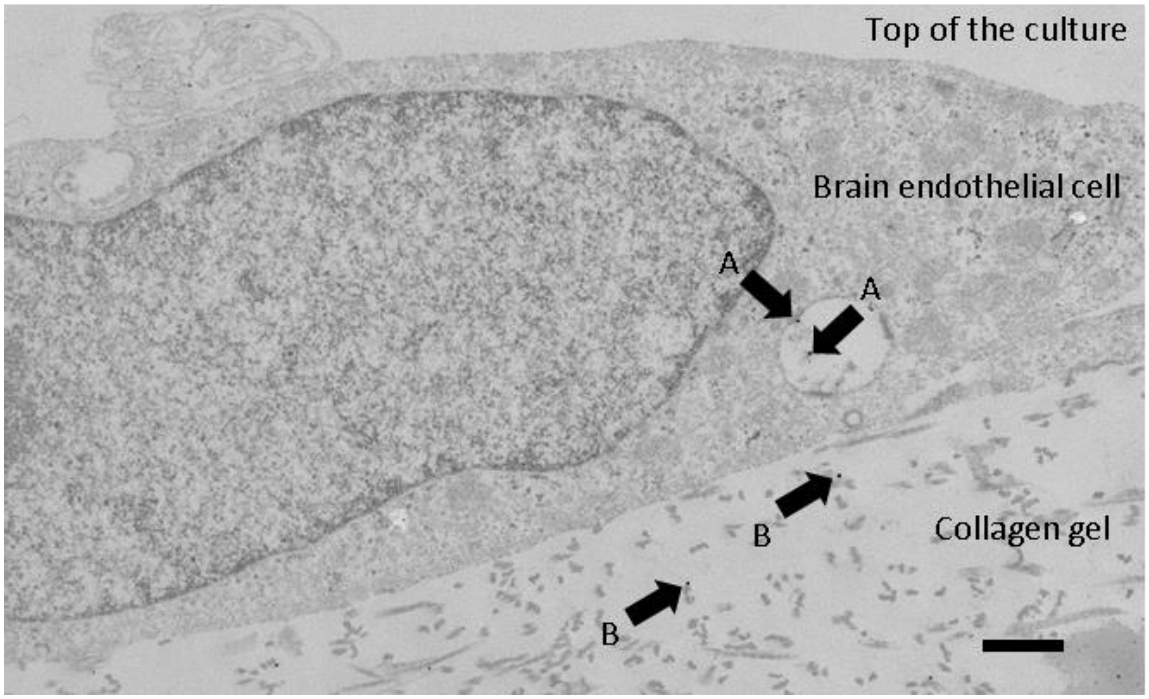

Figure 6.8. dsDNA/galactose gold nanoparticles in a brain endothelial cell cultured on top of a collagen hydrogel. Silver-enhanced gold nanoparticles (arrows) present in a vesicle of a brain endothelial cell hCMEC/D3 (A) and within a collagen gel (B). Representative image from three independent experiments is shown, scale bar 0.5 μm.

A co-culture model of the blood-brain barrier was used to assess the uptake of these nanoparticles into both brain endothelial cells and astrocytes. The uptake of dsDNA/galactose nanoparticles into brain endothelial cells (Figure 6.8) was similar to that of galactose -coated nanoparticles without attached DNA (Figure 6.9). Similarly, the nanoparticle uptake in astrocytes showed no difference in uptake efficiency between the two nanoparticle formulations. Thus, dsDNA neither decreased nor increased uptake efficiency of galactose-coated nanoparticles.

It may be also necessary to determine uptake efficiency of ssDNA/galactose nanoparticles into cells in follow-up studies. It has been observed that ssDNA-coated nanoparticles can have a higher uptake efficiency than dsDNA-coated nanoparticles (Massich et al. 2010).

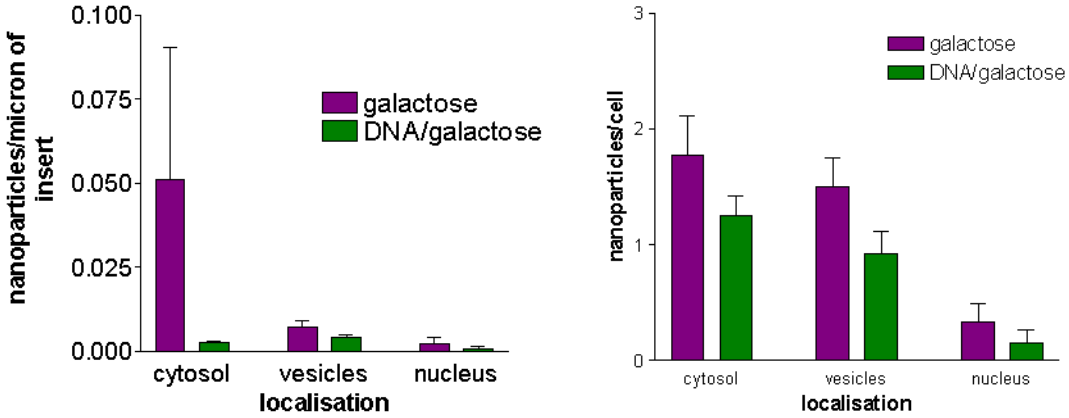

Figure 6.9. Uptake comparison of dsDNA/galactose and galactose -coated nanoparticles in co-cultures of brain endothelial cells and astrocytes after addition of 20 µg/ml nanoparticle concentration for 3 hr. A. the nanoparticle uptake into brain endothelial cells hCMEC/D3. B. nanoparticle uptake into co-cultured astrocytes. Note the different y-axis. The uptake of nanoparticles in astrocytes was assessed by counting nanoparticles per cell as the astrocytes were in a 3-dimensional gel. 3 independent experiments, data showing mean ± SEM, difference in each category was not significant (unpaired t-test).

6.2.4 Detection of DNA cargo in cell cultures

In order to track cargo intracellularly, a technique of localizing DNA in cells or cultures was required. It has been shown that ligands may be detected and localized in cells by release of fluorescence once they detach from the gold nanoparticles (Zhang et al. 2016). However, the determination of precise subcellular localisation of the cargo is limited. Electron microscopy is a sensitive and precise technique which may be able to detect a single molecule of DNA and also provide information on its subcellular localisation. Thus, a method to detect localisation of DNA was developed.

As the glyconanoparticles used had ~2 nm gold core, they were not observable within cells by the electron microscope unless they were silver-enhanced. Silver enhancement increased the size of nanoparticles to about 20 nm. We used this property and enhanced the

DNA attached to the nanoparticles by reacting it with biotin-DNA prior to addition to the cells. The complementary DNA strand carrying a biotin probe was then detected post-fixation of the cultures. We used a system of detection of the DNA cargo by adding streptavidin-peroxidase to the sample first and then adding commercial gold-biotin nanoparticles of 20 nm diameter as a secondary label, as shown in the scheme in Figure 6.10. Streptavidin alone could have been used as an alternative, however, the peroxidase function of this molecule was also briefly tested as a fast method to detect DNA in cells using immunohistochemistry.

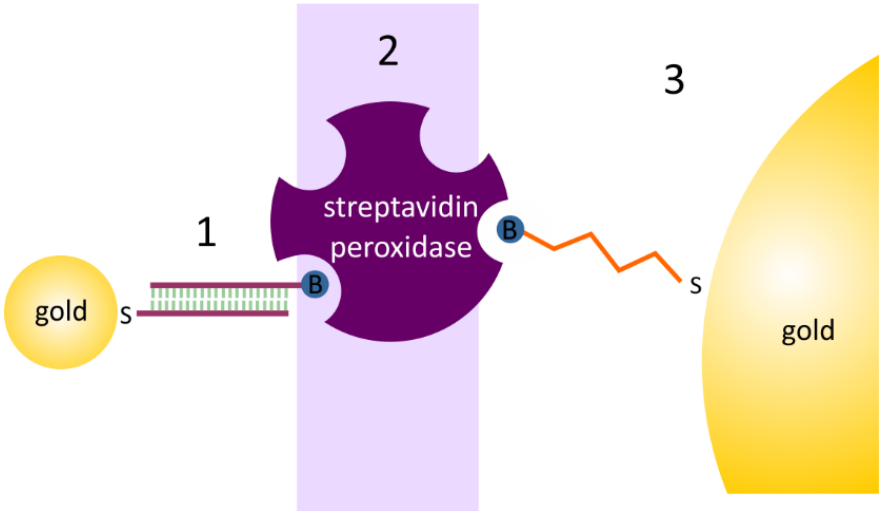

Figure 6.10. Scheme for detection of DNA cargo by electron microscopy. Step 1: DNA attached to ~2 nm nanoparticle is hybridized with complementary strand that has a biotin (B). This step was performed before addition to the cells. Once the cells have been incubated with the nanoparticles, the cultures were fixed. Step 2: Streptavidin peroxidase was added to the fixed cells; it bound onto biotin of the complementary DNA strand. Step 3: 20 nm diameter gold nanoparticles with covalently attached biotin (B) can react and bind to streptavidin peroxidase. This results in labelling of DNA-biotin with large 20 nm nanoparticles as ~2 nm nanoparticles are undetectable in cell cultures by the electron microscopy.

Using the same co-cultures of brain endothelial cells and astrocytes with the experimental setup of DNA/galactose uptake as shown in Figure 6.8 and Figure 6.9, we were able to detect DNA by electron microscopy. Gold nanoparticles of about 20 nm were observed (Figure 6.11). DNA was located on the plasma membrane of the brain endothelial cells and on plasma membrane of astrocytes. Moreover, a high number of DNA molecules was detected in

the collagen gel. Because this batch of nanoparticles contained large amounts of free DNA it was hard to distinguish whether the detected DNA was the free excess DNA or DNA attached to the nanoparticles.

From these observations it was apparent that there was a need to remove the unreacted free DNA from the nanoparticles after the preparation. Therefore, a preparation of a new batch of nanoparticles and separation from unbound DNA was the next step.

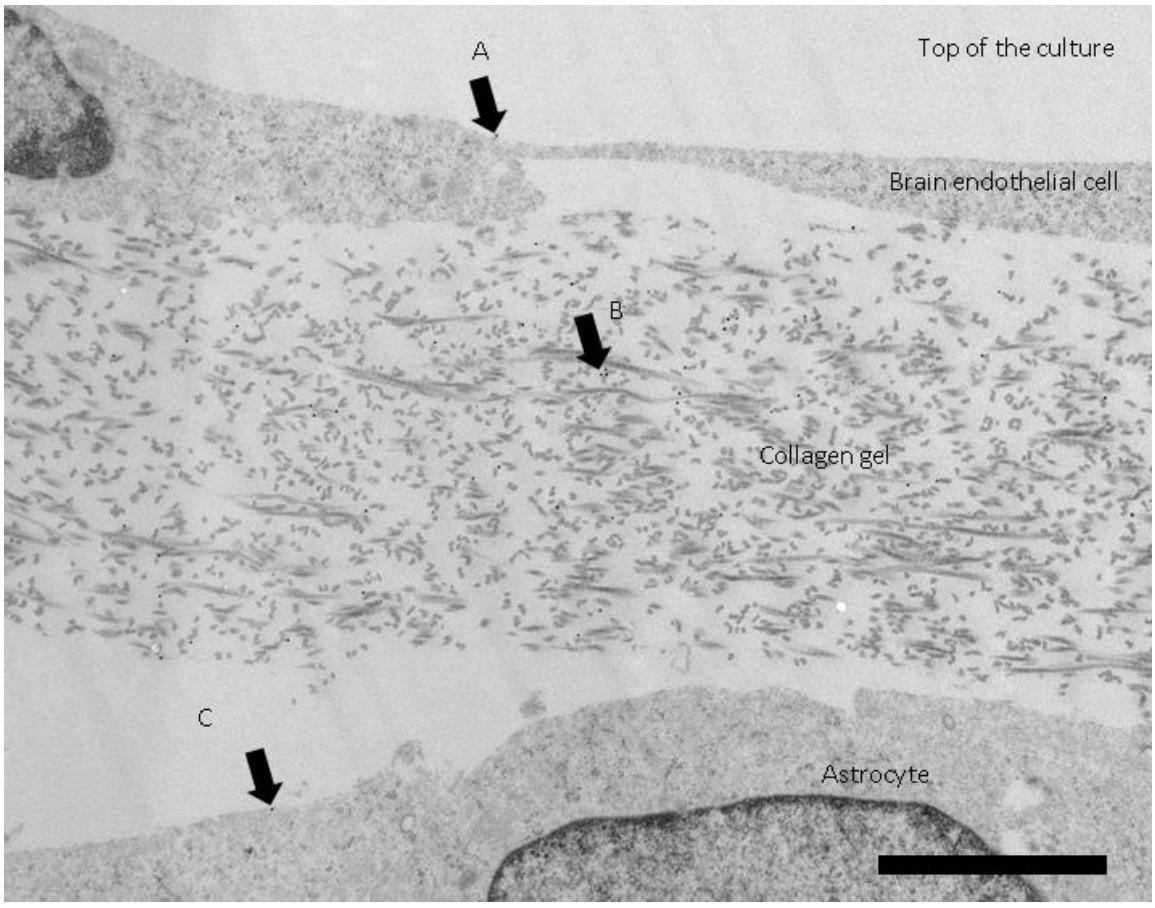

Figure 6.11. DNA detected by biotin-gold in 3D co-cultures of brain endothelial cells and astrocytes. 3D co-cultures consisted of human primary astrocytes that were grown within a collagen matrix and brain endothelial cells hCMEC/D3 grown on top of the collagen matrix. Biotin-DNA was detected with streptavidin peroxidase and 20 nm biotin-gold nanoparticles (arrows). Biotin DNA located at the surface of brain endothelial cells (A), within the collagen gel (B), at the surface of astrocytes (C). Scale bar 2 µm.

6.2.5 Fractionation of DNA/galactose nanoparticles by FPLC

20 nt DNA is similar in size to the nanoparticle but can be removed by a Superdex FPLC column while separating different fractions by the size of the elute. Therefore, a new batch of DNA/galactose nanoparticles was prepared by reacting galactose nanoparticles with freshly dissolved thiol-DNA. The reaction and FPLC separation was performed by Dr. Phil Williams at Midatech Pharma in Abingdon, UK.

Figure 6.12 shows the position of the elution peaks of thiol-DNA before the reaction. The largest peak area is at 17.19 ml, similar to the one shown previously (Figure 6.4). After 4 days (Figure 6.13), the DNA has 2 peaks, at ~17 ml and ~15 ml, indicating that the free thiol-DNA molecules may be oxidised, forming a dimer DNA-S-S-DNA.

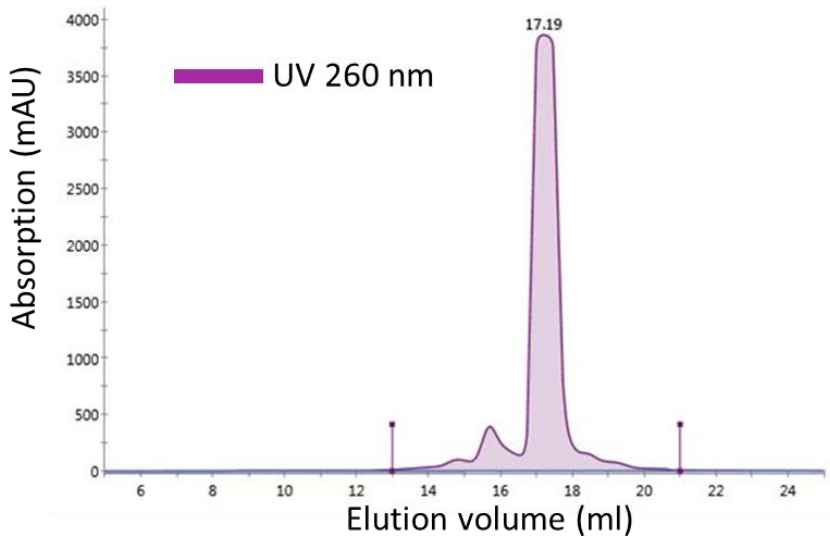

Figure 6.12. Characteristic of SEC profile of freshly prepared thiol-DNA. Fractionation performed by Phil Williams from Midatech Pharma.

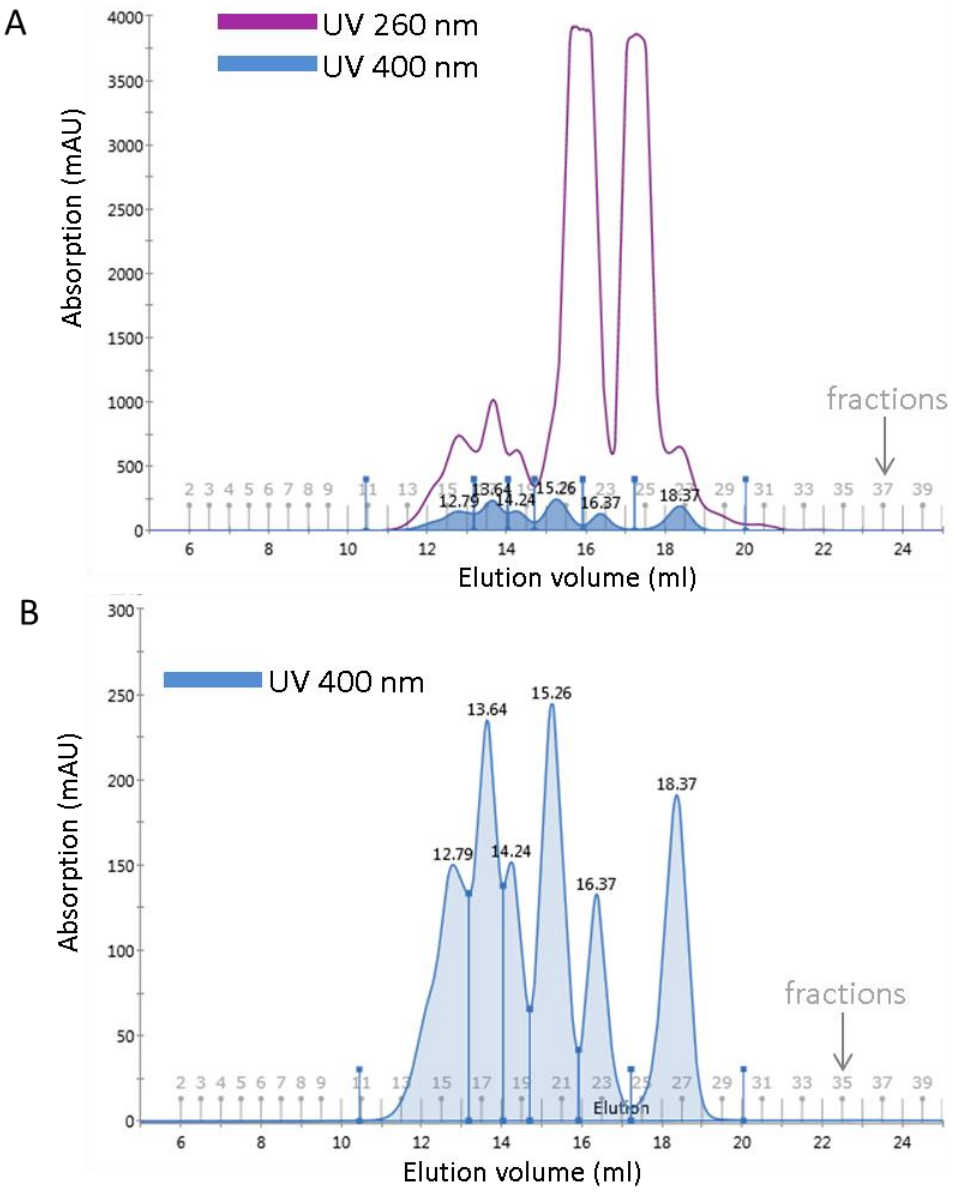

Figure 6.13. Formation of DNA-attached galactose-coated nanoparticles via ligand exchange reaction, after incubation for 4 days with excess of thiol-DNA as assessed by FPLC. A. SEC profiles of DNA in the nanoparticle sample, B. expansion of SEC profile of nanoparticles formed by this reaction. Fractionation performed by Phil Williams from Midatech Pharma.

There were several nanoparticle peaks as detected at 400 nm (Figure 6.13B). The peak at 18.37 corresponded to the peak of unreacted galactose nanoparticles (Figure 6.3), the following peaks of 16.37 ml, 15.26 ml, 14.24 ml, 13.64 ml and 12.79 ml corresponded to nanoparticles increasing in size. The area of the peaks was also taken into account in order to calculate the proportion of nanoparticles with DNA (82%) and nanoparticles without DNA (18%).

6.2.6 Detection of DNA attached to the fractionated DNA/galactose-coated nanoparticles by electrophoretic mobility shift assay (EMSA)

In order to establish whether the nanoparticle peaks detected by FPLC corresponded to nanoparticles with increasing number of DNA molecules attached, an electrophoretic mobility shift assay (EMSA) may be used. This technique is usually used to detect proteins (such as transcription factors) binding onto a certain sequence of DNA. The binding results in shifting the DNA band up the gel as it migrates at a slower rate after applying a current due to the protein attachment. Here we had nanoparticles carrying various amounts of DNA that we tested with EMSA. If a certain FPLC fraction contained more DNA molecules attached to the nanoparticle, the fraction would move slower through a polyacrylamide gel. The DNA attached on galactose-coated nanoparticles was detected by hybridizing it with a complementary probe containing biotin.

Certain FPLC fractions were selected for this purpose. Fractions 15, 17, 19, 21, 23, 27 corresponded to 6 FPLC peaks with decreasing size/charge (Figure 6.13). Some of these fractions (21 and 23) also contained unreacted DNA.

The selected fractions were reacted with the same amount of complementary biotinylated DNA probe and run on an 8% polyacrylamide gel (Figure 6.14). The fractions were not assessed for their gold concentration and thus the intensity of the bands that may correspond to gold nanoparticles with DNA may not be comparable between different fractions.

Fraction 27 did not contain any nanoparticles with DNA, confirming that the FPLC peak at 18.37 indeed corresponds to the nanoparticle fraction that has not reacted with the thiol-

DNA. Fraction 23 showed a very faint band higher up in about 2/3rd of the gel. This may correspond to either nanoparticles with single DNA or it may just be some of the free DNA that has dimerized, as shown in the FPLC peak of ~16 ml (Figure 6.13A). Fraction 21 showed a very strong band in a similar position to the previous experiment and again due to its high intensity it may correspond to the free dimerized DNA as this fraction contains most of the DNA FPLC peak of ~16 ml. The following fractions 19, 17 and 15 did not contain this strong band of DNA duplex and thus seemed to be free of unbound DNA. The high bands that slowed down in the gel in regular intervals may thus correspond to increasingly higher number of DNA molecules on the nanoparticles.

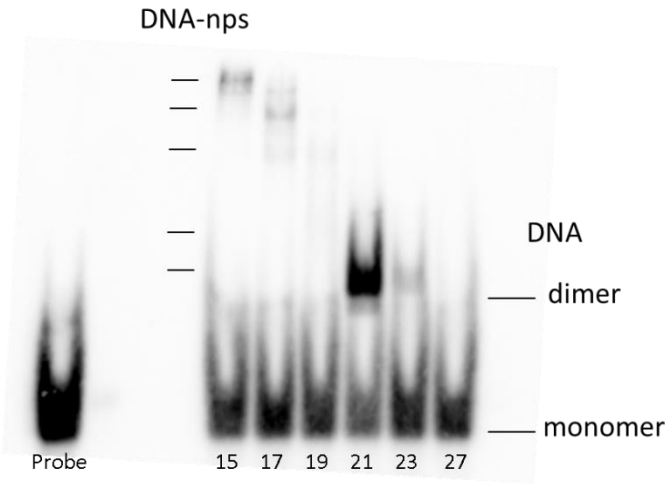

Figure 6.14. Electrophoretic mobility shift assay of selected fractions from FPLC separation of DNA/galactose-coated gold nanoparticles using biotinylated DNA probe. Probe = complementary sequence of DNA-biotin. 15, 17, 19, 21, 23, 27 = fraction numbers from FPLC separation. The bands are described as nanoparticles with DNA (DNA-nps) and free DNA, in a monomeric form (Thiol-DNA), or dimerized. A single EMSA experiment was carried out.

Using EMSA for separation of nanoparticles with different numbers of DNA molecules attached to them is novel. However, agarose gel electrophoresis has been used many times (Sandstrom et al. 2003; Pellegrino et al. 2007; Zanchet et al. 2001) and is believed to be one of the best techniques to resolve DNA-attached nanoparticles (Pellegrino et al. 2007). One study exploring gel electrophoresis of DNA-coated gold nanoparticles (Pellegrino et al. 2007) isolated

the nanoparticles from the gel which cleans them from the unbound DNA. Thus, agarose gel electrophoresis may be an alternative option for resolving the DNA-coated gold nanoparticles. Other options to determine DNA coverage of gold nanoparticles include fluorescence-based methods (Demers et al. 2000; Park et al. 2004).

To conclude, the FPLC peaks corresponded to the EMSA bands with the position of the EMSA bands dependent on the size/charge of the fraction.

The concentration of gold nanoparticles in selected fractions was analysed as well as the amount of DNA present in each fraction (Table 6.1). The gold concentration ranged between 250 and 350 μg/ml. The DNA concentration was analysed using Nanodrop. Here, the precision of pipetting 1 μl and the precision of detection of DNA oligonucleotides were not determined, therefore, the data in the table work are indicative only. As gold nanoparticles absorb light at 260 nm as well, it makes a determination of DNA loading of each fraction difficult. In particular, the FPLC data (Figure 6.13A) should correlate to this DNA concentration. However, fraction 21 also contained a large amount of unbound DNA (over 98%) that eluted into this fraction (by comparing the UV 260 nm peak to UV 400 nm peak). Therefore, DNA loading of fractions 20, 21 and 23 cannot be determined due to the presence of free DNA eluting at the same position. In order to determine DNA loading of fractions 19, 18, 17 and 15, we compared their 260 nm peak with the one of the background absorbance of gold nanoparticles without any DNA (fraction 27). This background of the 260 nm peak could be related to absorption of 720 mAU on the FPLC. As the UV 260 peak of fraction 19 and 18 does not rise above this background gold level, gel electrophoresis might be the more suitable method of detecting DNA loading efficiency.

The next step was to investigate the uptake of selected fractions of these nanoparticles into brain endothelial cells.

Table 6.1. Gold and DNA content in selected fractions.

Fraction number	Gold concentration (µg/ml) *	DNA concentration (µg/ml)*
15	330	190
17	320	370
18	350	280
19	270	190
20	330	350
21	310	3 880
23	280	1020
27	250	150

*Gold content determined by spectrophotometric gold assay, DNA content determined by NanoDrop. The data is a guide only as the precision of this technique was not determined.

6.2.7 Uptake of fractionated dsDNA/galactose -coated nanoparticles into brain endothelial cells

The selected FPLC fractions of DNA/galactose nanoparticles were investigated in their uptake efficiency in brain endothelial cells. Again, a complementary DNA was hybridized with the DNA/galactose nanoparticles in order to form dsDNA/galactose nanoparticles.

Figure 15 shows the nanoparticle uptake efficiency as examined in a pilot experiment. Fraction 15 showed increased cell uptake, both in cytosol and in vesicles. The rest of the fractions showed similar uptake to the control nanoparticles coated with galactose. However, it cannot be concluded whether this uptake efficiency of Fraction 15 differs from the control nanoparticles as more independent experiments need to be performed. Thus, the uptake of fractions 17 – 27 corresponds well with the previous finding of cell uptake of dsDNA/galactose nanoparticles before fractionation (Figure 6.9). However, nanoparticles with several dsDNA molecules (fraction 15) showed higher uptake than nanoparticles with fewer bound dsDNA molecules.

The phenomenon of negatively-charged nucleic acids increasing uptake efficiency into many different cell types has been reported previously (Giljohann et al. 2010). To date, one

study tried to elucidate the reason behind this increase in nanoparticle uptake into cells (Choi et al. 2013). The authors used ~10 nm gold nanoparticles coated with strongly anionic polyvalent nucleic acids. They found that polyvalent nucleic acids can bind to class A scavenger receptors, thus using caveolae-mediated endocytosis. However, in the present study only a pilot experiment has been performed and thus more investigations are necessary.

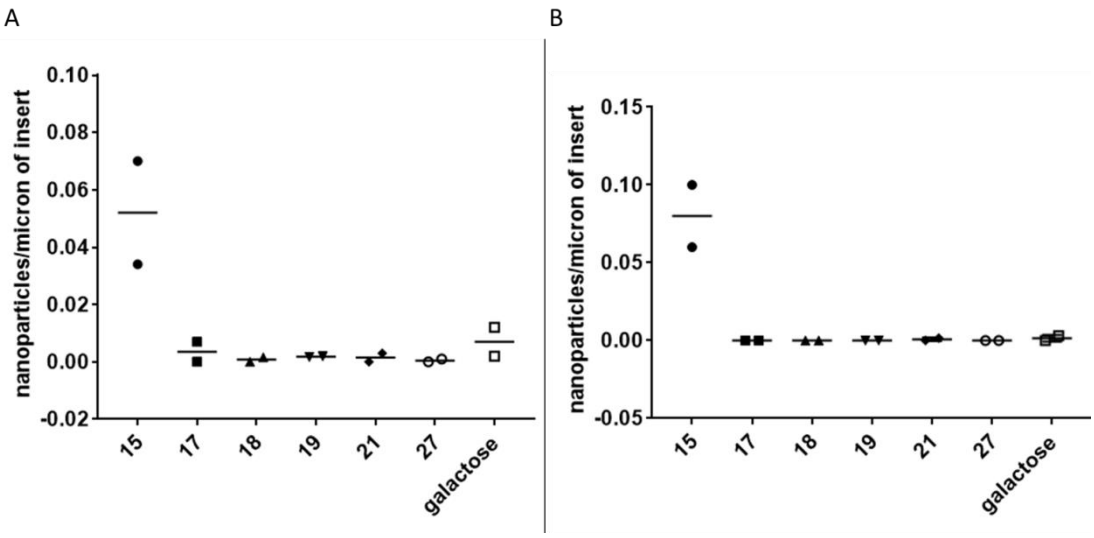

Figure 6.15. Pilot experiment of uptake of fractionated dsDNA/galactose nanoparticles into brain endothelial cells. Nanoparticles were quantified in cell cytosol (A) and in vesicles (B). Fractions 15 – 27 were investigated. In addition, galactose-coated gold nanoparticles (galactose) that were used for the reaction were an additional control. One experiment performed. Each point shows individual data from technical duplicates, horizontal line between the points represents mean.

6.2.8 Selection of therapeutic RNA oligonucleotide for gene knockdown in astrocytes

As we established the preparation of oligonucleotide nanoparticles, an oligonucleotide with a therapeutic potential for treating brain disorders was considered. One of these potential targets may be aquaporin-4. During a brain injury, aquaporin-4 has been found to increase water entry into the brain parenchyma, thus causing cerebral oedema. Down-regulation of aquaporin-4 may reduce oedema and thus increase recovery after brain injury (Fukuda & Badaut 2013).

Therefore, a viable siRNA that would knock-down aquaporin-4 in astrocyte cultures was investigated. The antibody and transfection procedure was based on previous work in our group (Peddagangannagari 2012; Lopez-Ramirez et al. 2014).

Firstly, the optimal culture conditions of astrocytes that would allow them to express the highest levels of aquaporin 4 were examined using flow cytometry. The conditions included cell density, time of transfection and transfection reagents. We modified the cell density in order to determine the best density that showed highest levels of aquaporin 4. This was found to be 60 – 70%. Next, the time of transfection of 4 and 6 hrs was tested where 6 hrs showed the most suitable levels of transfection. The best time post-transfection for highest knockdown of aquaporin levels was at day 6. These transfection conditions were also confirmed using a red fluorescent oligonucleotide (Alexa Fluoro). Moreover, 2 lipofection reagents were also compared; we found that Lipofectamine RNAiMAX was producing higher transfection rates than Lipofectamine 2000. The optimal amount of transfected RNA was found to be 20 pmoles – lowest level of RNA that produced knockdown.

To reduce aquaporin 4 expression, three different siRNA sequences were tested. However, there was no difference in their effect on AQP4 expression. The greatest reduction of AQP4 expression was about 20% (Figure 6.16). Knockdown of aquaporin-4 by siRNA has been shown in primary rat astrocytes (Nicchia et al. 2003). We adapted their sequence in our knockdown study. The silencing the authors of this study showed was greatest at 6 days post-transfection (Nicchia et al. 2003), similar to our findings. To our knowledge, transfection of human primary astrocytes for aquaporin-4 has not been performed before.

Since the level of astrocyte AQP4 knockdown in direct transfection was small, we did not consider that this was sufficient to achieve knockdown in the astrocytes after transport of nanoparticles across brain endothelium. The solution may lie in choosing a different target in astrocytes or testing a wider range of AQP4 siRNA sequences.

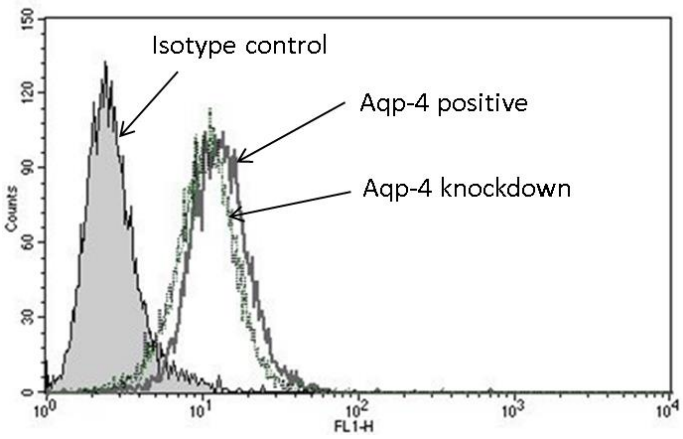

Figure 6.16. Knockdown of aquaporin-4 (aqp-4) in human astrocytes using a commercial siRNA. Representative FACS histogram (experiment performed twice) of knockdown of aquaporin-4 in human primary astrocytes. The isotype control is a population of unstained cells, population of cells expressing aqp-4 (Aqp-4 positive), population of cells treated with siRNA (Aqp-4 knockdown). Cells assessed 6 days post-transfection.

6.2.9 Summary

We established the rate of release of thiolated ligands from ~2 nm gold nanoparticles. Release of these ligands was dependent on the concentration of glutathione and time; whereas pH between 5 and 7.5 did not have an effect on ligand release. The release strategy for cargo molecules that are designed to move through one cell type to another requires transcytosis of the nanoparticles through the endothelium where cargo release is not required. Subsequently, the nanoparticle may need to enter the cytosol of the target cell in order to release its cargo via the glutathione place-exchange reaction.

Next, we examined ways to prepare small gold nanoparticles that would carry a DNA oligonucleotide and what was their cell uptake efficiency. The ligand-exchange reaction was the most successful synthetic method of the ones we tested. The uptake efficiency of dsDNA/galactose nanoparticles was found to be similar in comparison with its control, galactose nanoparticles. This was observed in both endothelial cells and astrocytes. However,

when the DNA/galactose nanoparticles were fractionated by FPLC, the largest one of the fractions pointed to the possibility that DNA-coated nanoparticles may be able to increase the uptake efficiency of galactose-coated nanoparticles in brain endothelial cells. As this was only a pilot experiment, more independent experiments are needed in order to establish the cell uptake.

An electron-microscopy based method of detection of DNA cargo in cells was established. This method may be used to localise DNA subcellularly. This method may also help optimisation of the oligonucleotide nano-carrier and may be also used for in vivo studies of cargo localisation.

A brain therapeutic oligonucleotide (siRNA) was not selected, as the silencing of aquaporin-4 in primary astrocytes was insufficient. Further optimisation of the siRNA and transfection efficiency may be required to progress this part of the work.

Chapter 7. Conclusions

7.1 Conclusions and contributions made by the thesis

Nanomedicine has shown promise in taking a nano-carrier and developing it into a possible treatment in the clinic (Libutti et al. 2010). Therefore, the rationale for this thesis was to investigate the potential of gold nanoparticles as a therapeutic delivery system for the brain. The work described in this thesis has contributed to the field of nanomedicine- (a) by increasing understanding of the interactions of small gold nanoparticles with endothelial cells, (b) by demonstrating the transport and delivery potential of small glyconanoparticles into the brain *in vitro* and *in vivo* and (c) by developing methods to attach oligonucleotides onto the glyconanoparticles, which might be used to deliver therapeutic polynucleotides into and across the brain endothelium.

In Chapter 3, we assessed the uptake of <5 nm gold glyconanoparticles into and across brain endothelium using three different coating formulations: glucose, galactose/OEG-amine and galactose/OEG-amine/insulin. The uptake efficiency of nanoparticles into brain endothelial cells depended on the ligand coating. Nanoparticles coated with OEG-amine/galactose and with OEG-amine/galactose/insulin had higher uptake efficiency than those coated with glucose. A similar uptake pattern was also observed using astrocytes, supportive glial cells that are also part of the blood-brain barrier. Next, astrocytes and endothelial cells were cultured together in a 3-dimensional co-culture model of the blood-brain barrier. Using this model, I demonstrated that gold nanoparticles were able to pass through the endothelial cells and enter astrocytes, and that their uptake efficiency was again dependent on nanoparticle coating; OEG-amine/galactose and OEG-amine/galactose/insulin showed higher uptake efficiency into vesicles than glucose-coated nanoparticles. Moreover, the data presented in Chapter 3 also support the hypothesis

that the toxicity of these gold nanoparticles to brain endothelial cells was low. The work in Chapter 3 extended our previous studies on glucose-coated nanoparticles (Gromnicova et al. 2013). Here we demonstrate the utility of a new type of nanoparticle coating – OEG-amine – which enhanced the uptake efficiency of gold glyconanoparticles into brain endothelial cells and astrocytes.

The work presented in Chapter 4 sought to determine the mechanism of transport of OEG-amine/galactose –coated gold nanoparticles in order to explain their high cell uptake efficiency. We found that the uptake of this nanoparticle formulation depended on both active and passive cell processes. Moreover, we compared the uptake of this nanoparticle formulation in several types of endothelial cells, i.e. kidney, lung and bone marrow, and noted a cell-selective transport. For example, the vesicular uptake of nanoparticles into kidney endothelium was higher than that of brain. This kind of cell-selective uptake has been observed previously (Freese et al. 2012; Freese et al. 2013; Albanese & Chan 2011), however, it was not explained. We compared the uptake-related characteristics of kidney and brain endothelium in order to understand the reason for this cell-selectivity. My data are consistent with a hypothesis in which the degree of endocytosis, as well as the glycocalyx composition, may determine this cell-selective uptake of OEG-amine/galactose nanoparticles. Thus, we were able to contribute to the nanotechnology field by increase in understanding of how specific cell types interact with gold nanoparticles.

The data presented in Chapter 5 extend the *in vitro* studies described in Chapter 3 and 4 show further insights into the cellular transport of the three gold glyconanoparticles formulations described above. This Chapter presents *in vivo* experiments that assess the initial uptake of gold glyconanoparticles into the brain, in addition to their overall body distribution. The animals were dosed with gold glyconanoparticles via injection into the carotid artery, and approach that has never been used in application of gold nanoparticles before. The

nanoparticles circulated in the body for only 10 minutes in order to capture the first encounter of gold nanoparticles with the brain. Using electron microscopy to assess nanoparticle location, a detailed ultrastructural analysis of this short encounter was described. I observed gold nanoparticles in the brain endothelial cells, neurons and glial cells of the cortex and striatum. This finding progressed understanding of interaction of gold glyconanoparticles with the brain parenchyma. As is typical for this size of nanoparticle (Skotland et al. 2010; Hillyer & Albrecht 2001), their major accumulation by kidney was also demonstrated by my studies.

The experiments described in Chapter 6 focused on creating gold glyconanoparticles that would be able to carry oligonucleotides across brain endothelial cells into astrocytes. The experimental approach was to use a thiolated DNA oligonucleotide that could cross the brain endothelial cells. Once transported across the brain endothelium, the particles could be taken up by glial cells and the DNA oligonucleotides released following a thiol exchange. It was considered that the release of thiolated DNA oligonucleotide would be time-dependent if the transport across the endothelium was to occur via the cytosol due to the high concentration of glutathione present there. Glutathione would exchange with thiol-bound DNA and thio-glycans, thus leading to their release. Notably however, the transit time of the nanoparticles is short in comparison with the time needed to release the cargo. Moreover, if the glyconanoparticles were to travel across the endothelium via transcytosis the lifetime of the thiol-attached DNA oligonucleotides would be even longer since the vesicles do not contain a high concentration of glutathione, and their low pH did not cause a release of fluorescent GSH. When examining the cell uptake efficiency of dsDNA-attached glyconanoparticles, the dsDNA cargo did not change their uptake profile in either endothelial cells or in astrocytes. Preliminary experiment was performed in order to determine whether fractionated dsDNA-attached nanoparticles reduced or increased the uptake efficiency. This investigation pointed out the possibility that certain types of DNA-coated nanoparticles may increase the uptake efficiency of glycan-coated nanoparticles. The work presented in this chapter generated many questions that

will need further investigations to determine the potential of these glyconanoparticles to be used for oligonucleotide delivery into the brain.

7.2 Using gold nanoparticles to deliver brain therapy

The blood-brain barrier prevents many types of molecule from entering the brain. Therefore, potential drugs and therapeutic molecules that are designed to target the brain have to be delivered in a way that overcomes the impervious blood-brain barrier (see Introduction 1.2). One of the approaches to overcome this problem is to use nanoparticle carriers. Nanoparticles have been employed to deliver many types of therapeutic agents across the blood brain barrier, such as:

a) Anti-tumour compounds, e.g. doxorubicin, methotrexate, ceramide, cisplatin, dalargin (Wong et al. 2012),
b) HIV antiretroviral drugs, e.g. ritonavir, atazanavir (Batrakova et al. 1999; Chattopadhyay et al. 2008),
c) Therapeutic agents for Alzheimer's and Parkinson's disease, e.g. that dissolve amyloid plaques or are agents of gene therapy (Cherny et al. 2001; Wong et al. 2012),
d) Drugs for acute ischemic stroke, e.g. superoxide dismutase (Reddy & Labhasetwar 2009),
e) Neuroprotective agents, e.g. brain-derived neurotrophic factor (Pilakka-Kanthikeel et al. 2013).

Gold nanoparticles could be used as carriers of these agents, if the design of the agent's attachment is considered (whether it is a covalent attachment via a thiol or other bond, or non-covalent one via electrostatic interactions of highly-charged ligands). Also a targeting molecule can be attached to the gold surface.

The large surface-to-volume ratio of nanoparticles may lead to improved therapeutic efficacies in terms of drug delivery across the blood-brain barrier, since one nanoparticle may

carry several molecules of a therapeutic agent. Gold nanoparticles in general have the advantage of being synthesized by a simple reaction, and having a small size. Small gold nanoparticles displayed enhanced penetration of brain endothelial cells in comparison to larger gold nanoparticles (Gromnicova et al. 2013). However, gold nanoparticles of larger sizes, i.e. >10 nm, have been shown to penetrate the blood-brain barrier *in vitro* (Clark & Davis 2015; Shilo et al. 2014) and *in vivo* (Schleh et al. 2012; Hirn et al. 2011; Sousa et al. 2010; Prades et al. 2012; Wiley et al. 2013). The use of larger sizes may be beneficial in some cases, especially when imaging or diagnostics are involved, since larger sized-nanoparticles have favourable optical properties (Webb & Bardhan 2014). On the other hand, the use of nanoparticle of size <5 nm, such as the ones used in this study, may be beneficial due to the route they use to enter the cells, employing passive uptake alongside active transport (Verma et al. 2008).

7.3 Administration of gold nanoparticles for brain delivery

The present study used intracarotid injection as a way to administer gold nanoparticles. Thus, the amount of gold that was able to enter the brain was substantial. However, the disadvantage of this approach is a poor control over the nanoparticle distribution into brain regions due to intravascular streaming (Saris et al. 1988). Intracarotid injections are used in clinic for treatment of ischemic stroke or intracranial malignancies (Joshi et al. 2007). Thus, this type of administration of nanoparticles could be potentially used in cases where occasional or planned drug application is needed. For a treatment involving regular drug application, an intravenous approach would be preferable due to ease of application. How well the gold nanoparticles enter the brain after intravenous administration would need to be investigated as brain targeting may need to be improved.

7.4 Targeting and selectivity of nanoparticles for brain tissue

There are several ways to improve brain targeting of gold nanoparticles. One way is to use targeting molecules that exploit receptor-mediated transcytosis and are selective to brain endothelium, such as transferrin (Wiley et al. 2013; Prades et al. 2012; Clark & Davis 2015), insulin (Shilo et al. 2014), or TAT peptide (Rao et al. 2008). The disadvantage of this approach is that receptors for receptor-mediated transcytosis (i.e. transferrin receptor or insulin receptor) are not strictly brain specific. For example, transferrin receptors are also present in liver, bone marrow (Simionescu et al. 2002) and on haemopoietic cells (Pelicci et al. 1982).

Another way to enhance brain selectivity is to use a peptide that will help to localise the nanoparticles specifically in brain tissue. For example, a phage display library has been used to identify tissue-specific peptides (Pasqualini & Ruoslahti 1996; Rajotte et al. 1998), sometimes called "homing" peptides (reviewed in Laakkonen & Vuorinen 2010) which may promote transport solely in the brain. These peptides were not localised in other organs, however, the specific receptor that may bind such homing peptides is not yet known. By using such peptides, the nanoparticles might localise preferentially in the brain. Furthermore, it remains to be seen whether this peptide would allow the nanoparticles to be transcytosed by brain endothelial cells.

Another point to consider is delivery of gold nanoparticles into the diseased areas of the brain. Alzheimer's disease affects the cortex and hippocampus, Parkinson's disease affects the substantia nigra and basal ganglia, and multiple sclerosis affects the brain and spinal cord. In an ideal situation, nanoparticles would only target diseased areas of the brain and not affect the other regions. The research into gold nanoparticle distribution and movement through the brain is in its infancy. More information would need to be gathered on how to enhance the specific

uptake of nanoparticles, e.g. which site of administration is advantageous, or which specific "diseased" molecules may be targeted.

7.5 Clinical use of gold nanoparticles

Gold nanoparticles have a potential to be used in clinic, and are already in clinical trials for treatment of cancer (Libutti et al. 2010). The nanoparticles used by Libutti et al. (2010) are 27 nm in diameter. The bodily clearance of the large nanoparticles may not be correlative to our small glyconanoparticles of <5 nm. Thus, investigations into clearance pattern must follow in order to establish their safety. For example, it may be necessary to perform a long-term study to detect accumulation within different organs of treated animals and keep them in a metabolic cage to measure excretion. Electron microscopy of kidney and liver may point to possible accumulation patterns within cells. Our industrial partner Midatech, has already had one of their formulations of gold nanoparticles coated with OEG-amine/galactose/insulin in a clinical trial. This formulation of nanoparticle was deemed safe by the FDA (Midatech Pharma, personal communication).

The issue of nanoparticle dose also needs to be considered. The advantage of using small diameter nanoparticles may help to reduce the dose necessary for delivery of a drug. For example, if 10 nanoparticles can cross into cells, and assuming that 20 nm nanoparticles have the same cell transport efficiency as 2 nm nanoparticles, then the required gold concentration would be lower in case of small-sized nanoparticles. This would lead to reduced cost of manufacturing, a factor that is crucial for realizing the potential of nanoparticle therapy (Webb & Bardhan 2014).

7.6 Consequences of therapy using gold nanoparticles

When considering using gold nanoparticles as a drug-delivery system for nucleic acids or other therapeutic agents, two aspects need to be considered:

a) Acute conditions, where immediate and fast treatment is needed;
b) Chronic conditions, where treatment is given over a long period of time.

In an acute condition, the action of nanoparticle therapy needs to be fast. One can consider traumatic brain injury as one of the possible condition that can be treated. In this case, the speed of complete clearance of gold nanoparticle carrier from the body may not be important. On the other hand, the speed of action is needed, i.e. the rapid penetration of brain and release of cargo. As we showed in Chapter 4, small glyconanoparticles used in this study may be very quick in accessing the brain parenchyma. Also, their movement through the brain may point to speed of movement in other organs, however, the time necessary for complete clearance from the body would need to be investigated.

Treatment of a chronic brain condition, for example Alzheimer's disease, Parkinson's disease or multiple sclerosis, requires regular and long-term application of medication. This may also be the case when using long-term downregulation of gene expression using siRNA or DNA carried by the gold nanoparticles to control the disease progress. Here, the time necessary for complete bodily clearance of gold nanoparticles must be addressed and needs to be monitored. Nanoparticle clearance has been studied in animals only. It was suggested that some gold nanoparticles, such as ones of 20 nm diameter, may accumulate in liver and kidney (Balasubramanian et al. 2010). In that case, the cumulative effect of long-term administration of <5 nm gold glyconanoparticles in organs over a long period of time would need to be investigated in animal and human studies. One of the options to overcome the issue of gold accumulation is to formulate a cross-linked shell of nanoparticle ligands, where the gold core can be digested as shown by Rotello's group (Cutler et al. 2011).

To conclude, gold glyconanoparticles, as shown in this thesis, may be a useful agent for treatment of acute brain disorders and may be administered intra-carotid to treat acute brain conditions. However, the use of gold glyconanoparticles for treatment of chronic diseases needs further investigation into the effect of long-term organ accumulation and clearance from the body.

Chapter 8. References

Abbott, N.J. et al., 2010. Structure and function of the blood-brain barrier. *Neurobiology of disease*, 37(1), pp.13–25.

Abdullah, K.M. et al., 1992. A neutral glycoprotease of Pasteurella haemolytica A1 specifically cleaves O-sialoglycoproteins. *Infection and Immunity*, 60(1), pp.56–62.

Ackerson, C.J., Jadzinsky, P.D. & Kornberg, R.D., 2005. Thiolate ligands for synthesis of water-soluble gold clusters. *Journal of the American Chemical Society*, 127(18), pp.6550–1..

Agasti, S.S. et al., 2009. Photoregulated release of caged anticancer drugs from gold nanoparticles. *Journal of the American Chemical Society*, 131(16), pp.5728–9..

Agrawal, N.J. & Radhakrishnan, R., 2007. The Role of Glycocalyx in Nanocarrier-Cell Adhesion Investigated Using a Thermodynamic Model and Monte Carlo Simulations. *The journal of physical chemistry. C, Nanomaterials and interfaces*, 111(43), pp.15848–15856..

Ahmed, M., Deng, Z. & Narain, R., 2009. Study of transfection efficiencies of cationic glyconanoparticles of different sizes in human cell line. *ACS Applied Materials and Interfaces*, 1(9), pp.1980–1987.

Aird, W.C., 2012. Endothelial cell heterogeneity. *Cold Spring Harbor perspectives in medicine*, 2(1), p.a006429.

Albanese, A. & Chan, W.C.W., 2011. Effect of Gold Nanoparticle Aggregation on Cell Uptake and Toxicity. *ACS nano*, 5(7), pp.5478–5489.

Alkilany, A.M. & Murphy, C.J., 2010. Toxicity and cellular uptake of gold nanoparticles: what we have learned so far? *Journal of nanoparticle research : an interdisciplinary forum for nanoscale science and technology*, 12(7), pp.2313–2333.

Alroy, J. et al., 1987. Lectin histochemistry of mammalian endothelium. *Histochemistry*, 86(6), pp.603–607.

Alyaudtin, R.N. et al., 2001. Interaction of poly(butylcyanoacrylate) nanoparticles with the blood-brain barrier in vivo and in vitro. *Journal of drug targeting*, 9(3), pp.209–21.

Alyautdin, R. et al., 2014. Nanoscale drug delivery systems and the blood-brain barrier. *International journal of nanomedicine*, 9, pp.795–811.

Alyautdin, R.N. et al., 1997. Delivery of loperamide across the blood-brain barrier with polysorbate 80-coated polybutylcyanoacrylate nanoparticles. *Pharmaceutical research*, 14(3), pp.325–8.

Alyautdin, R.N. et al., 1998. Significant entry of tubocurarine into the brain of rats by adsorption to polysorbate 80-coated polybutylcyanoacrylate nanoparticles: an in situ brain perfusion study. *Journal of microencapsulation*, 15(1), pp.67–74.

Ameres, S.L. et al., 2007. Molecular basis for target RNA recognition and cleavage by human RISC. *Cell*, 130(1), pp.101–12.

Anderson, M.E., 1998. Glutathione: an overview of biosynthesis and modulation. *Chemico-Biological Intreractions*, 111–112, pp.1–14.

Arvizo, R.A. et al., 2011. Effect of nanoparticle surface charge at the plasma membrane and beyond. *Nano letters*, 10(7), pp.2543–2548.

Arvizo, R.R. et al., 2012. Identifying new therapeutic targets via modulation of protein corona formation by engineered nanoparticles. *PloS one*, 7(3), p.e33650.

Atukorale, P.U. et al., 2015. Influence of the glycocalyx and plasma membrane composition on amphiphilic gold nanoparticle association with erythrocytes. *Nanoscale*, 7, pp.11420–11432.

Balasubramanian, S.K. et al., 2010. Biodistribution of gold nanoparticles and gene expression changes in the liver and spleen after intravenous administration in rats. *Biomaterials*, 31(8), pp.2034–2042.

Bana, L. et al., 2013. Liposomes bi-functionalized with phosphatidic acid and an ApoE-derived peptide affect Aβ aggregation features and cross the blood-brain-barrier: Implications for therapy of Alzheimer disease. *Nanomedicine : nanotechnology, biology, and medicine*.

Batrakova, E. V et al., 1999. Pluronic P85 increases permeability of a broad spectrum of drugs in polarized BBMEC and Caco-2 cell monolayers. *Pharmaceutical research*, 16(9), pp.1366–72.

Begley, D.J., 2004a. ABC transporters and the blood-brain barrier. *Current pharmaceutical design*, 10(12), pp.1295–312.

Begley, D.J., 2004b. Delivery of therapeutic agents to the central nervous system: the problems and the possibilities. *Pharmacology & therapeutics*, 104(1), pp.29–45.

van den Berg, B.M., Vink, H. & Spaan, J.A.E., 2003. The endothelial glycocalyx protects against myocardial edema. *Circulation research*, 92(6), pp.592–4.

Bernardi, A. et al., 2013. Multivalent glycoconjugates as anti-pathogenic agents. *Chemical Society reviews*, 42(11), pp.4709–27.

Bernstein, E. et al., 2001. Role for a bidentate ribonuclease in the initiation step of RNA interference. *Nature*, 409(6818), pp.363–6.

Bhumkar, D.R. et al., 2007. Chitosan Reduced Gold Nanoparticles as Novel Carriers for Transmucosal Delivery of Insulin. *Pharmaceutical Research*, 24(8), pp.1415–1426.

Bielinska, A.U. et al., 1999. DNA complexing with polyamidoamine dendrimers: Implications for transfection. *Bioconjugate Chemistry*, 10(5), pp.843–850.

Boudreau, R.L., Rodríguez-Lebrón, E. & Davidson, B.L., 2011. RNAi medicine for the brain: progresses and challenges. *Human molecular genetics*, 20(R1), pp.R21-7.

Boyer-Di Ponio, J. et al., 2014. Instruction of circulating endothelial progenitors in vitro towards specialized blood-brain barrier and arterial phenotypes M. A. Deli, ed. *PLoS ONE*, 9(1), p.e84179.

Bozzuto, G. & Molinari, A., 2015. Liposomes as nanomedical devices. *International journal of nanomedicine*, 10, pp.975–99.

Braun, G.B. et al., 2009. Laser-Activated Gene Silencing via Gold Nanoshell-siRNA Conjugates. *ACS Nano*, 3(7), pp.2007–2015.

Brust, M. et al., 1994. Synthesis of thiol-derivatised gold nanoparticles in a two-phase liquid-liquid system. *J. Chem. Soc., Chem. Commun.*,, (7), pp.801–802.

Burnett, J.C. & Rossi, J.J., 2012. RNA-based therapeutics: Current progress and future prospects. *Chemistry and Biology*, 19(1), pp.60–71.

Butt, A.M., Jones, H.C. & Abbott, N.J., 1990. Electrical resistance across the blood-brain barrier in anaesthetized rats: a developmental study. *The Journal of physiology*, 429, pp.47–62.

Casals, E. et al., 2010. Time evolution of the nanoparticle protein corona. *ACS nano*, 4(7), pp.3623–32.

Cecchelli, R. et al., 2014. A stable and reproducible human blood-brain barrier model derived from hematopoietic stem cells R. Klein, ed. *PLoS ONE*, 9(6), p.e99733.

Cecchelli, R. et al., 1999. In vitro model for evaluating drug transport across the blood-brain barrier. *Advanced drug delivery reviews*, 36(2–3), pp.165–178.

Cedervall, T. et al., 2007. Detailed identification of plasma proteins adsorbed on copolymer nanoparticles. *Angewandte Chemie (International ed. in English)*, 46(30), pp.5754–6.

Chattopadhyay, N. et al., 2008. Solid lipid nanoparticles enhance the delivery of the HIV protease inhibitor, atazanavir, by a human brain endothelial cell line. *Pharmaceutical research*, 25(10), pp.2262–71.

Chekhonin, V.P. et al., 2005. PEGylated immunoliposomes directed against brain astrocytes. *Drug delivery*, 12(1), pp.1–6.

Chekhonin, V.P. et al., 2012. Targeted delivery of liposomal nanocontainers to the peritumoral zone of glioma by means of monoclonal antibodies against GFAP and the extracellular loop of Cx43. *Nanomedicine : nanotechnology, biology, and medicine*, 8(1), pp.63–70.

Cheng, Y. et al., 2011. Addressing brain tumors with targeted gold nanoparticles: a new gold standard for hydrophobic drug delivery? *Small (Weinheim an der Bergstrasse, Germany)*, 7(16), pp.2301–6.

Cherny, R.A. et al., 2001. Treatment with a copper-zinc chelator markedly and rapidly inhibits beta-amyloid accumulation in Alzheimer's disease transgenic mice. *Neuron*, 30(3), pp.665–76.

Chiodo, F. et al., 2014. Glycosystems in nanotechnology: Gold glyconanoparticles as carrier for anti-HIV prodrugs. *Beilstein journal of organic chemistry*, 10, pp.1339–46.

Chithrani, B.D. & Chan, W.C.W., 2007. Elucidating the mechanism of cellular uptake and removal of protein-coated gold nanoparticles of different sizes and shapes. *Nano letters*, 7(6), pp.1542–50.

Chithrani, B.D., Ghazani, A. a & Chan, W.C.W., 2006. Determining the size and shape dependence of gold nanoparticle uptake into mammalian cells. *Nano letters*, 6(4), pp.662–8.

Cho, C.-W. et al., 2002. Ultrasound-induced mild hyperthermia as a novel approach to increase drug uptake in brain microvessel endothelial cells. *Pharmaceutical research*, 19(8), pp.1123–9.

Cho, E.C. et al., 2009. Understanding the role of surface charges in cellular adsorption versus internalization by selectively removing gold nanoparticles on the cell surface with a I 2/KI etchant. *Nano Letters*, 9(3), pp.1080–1084.

Cho, E.C., Liu, Y. & Xia, Y., 2010. A simple spectroscopic method for differentiating cellular uptakes of gold nanospheres and nanorods from their mixtures. *Angewandte Chemie (International ed. in English)*, 49(11), pp.1976–80.

Choi, C.H.J. et al., 2013. Mechanism for the endocytosis of spherical nucleic acid nanoparticle conjugates. *Proceedings of the National Academy of Sciences of the United States of America*, 110(19), pp.7625–30.

Choi, C.H.J. et al., 2010. Mechanism of active targeting in solid tumors with transferrin-containing gold nanoparticles. *Proceedings of the National Academy of Sciences*, 107(3), pp.1235–1240.

Choi, S.Y. et al., 2012. In vitro toxicity of serum protein-adsorbed citrate-reduced gold nanoparticles in human lung adenocarcinoma cells. *Toxicology in vitro : an international journal published in association with BIBRA*, 26(2), pp.229–37.

Clark, A.J. & Davis, M.E., 2015. Increased brain uptake of targeted nanoparticles by adding an acid-cleavable linkage between transferrin and the nanoparticle core. *Proceedings of the National Academy of Sciences of the United States of America*, 112(40), pp.12486–12491.

Comper, W.D., 2014. The limited role of the glomerular endothelial cell glycocalyx as a barrier to transglomerular albumin transport. *Connect Tissue Res*, 55(1), pp.2–7.

Conde, J., de la Fuente, J.M. & Baptista, P. V, 2010. In vitro transcription and translation inhibition via DNA functionalized gold nanoparticles. *Nanotechnology*, 21(50), p.505101.

Connor, E.E. et al., 2005. Gold nanoparticles are taken up by human cells but do not cause acute cytotoxicity. *Small (Weinheim an der Bergstrasse, Germany)*, 1(3), pp.325–7.

Coradeghini, R. et al., 2013. Size-dependent toxicity and cell interaction mechanisms of gold nanoparticles on mouse fibroblasts. *Toxicology letters*, 217(3), pp.205–16.

Costantino, L., 2010. Drug delivery to the CNS and polymeric nanoparticulate carriers. *Future medicinal chemistry*, 2(11), pp.1681–701.

Coulter, J.A. et al., 2012. Cell type-dependent uptake, localization, and cytotoxicity of 1.9 nm gold nanoparticles. *International Journal of Nanomedicine*, 7, pp.2673–2685.

Cutler, J.I. et al., 2011. Polyvalent nucleic acid nanostructures. *Journal of the American Chemical Society*, 133(24), pp.9254–7.

Dan, M. et al., 2013. Binding, transcytosis and biodistribution of anti-PECAM-1 iron oxide nanoparticles for brain-targeted delivery. *PloS one*, 8(11), p.e81051.

Dan, X., Liu, W. & Ng, T.B., 2016. Development and Applications of Lectins as Biological Tools in Biomedical Research. *Medicinal Research Reviews*, 36(2), pp.221–247.

Daniel, M.-C. & Astruc, D., 2004. Gold nanoparticles: assembly, supramolecular chemistry, quantum-size-related properties, and applications toward biology, catalysis, and nanotechnology. *Chemical reviews*, 104(1), pp.293–346.

Day, E.S. et al., 2011. Nanoshell-mediated photothermal therapy improves survival in a murine glioma model. *Journal of neuro-oncology*, 104(1), pp.55–63.

De, M., Ghosh, P.S. & Rotello, V.M., 2008. Applications of Nanoparticles in Biology. *Advanced*

Materials, 20(22), pp.4225–4241.

Demers, L.M. et al., 2000. A fluorescence-based method for determining the surface coverage and hybridization efficiency of thiol-capped oligonucleotides bound to gold thin films and nanoparticles. *Analytical chemistry*, 72(22), pp.5535–41.

Dhar, S. et al., 2009. Polyvalent oligonucleotide gold nanoparticle conjugates as delivery vehicles for platinum(IV) warheads. *Journal of the American Chemical Society*, 131(41), pp.14652–3.

Ding, Y. et al., 2014. Gold Nanoparticles for Nucleic Acid Delivery. *Molecular Therapy*, 22(6), pp.1075–1083.

Dixit, S. et al., 2015. Transferrin receptor-targeted theranostic gold nanoparticles for photosensitizer delivery in brain tumors. *Nanoscale*, 7(5), pp.1782–1790.

Drbohlavova, J. et al., 2009. Quantum dots - characterization, preparation and usage in biological systems. *International journal of molecular sciences*, 10(2), pp.656–73.

Dubertret, B., Calame, M. & Libchaber, a J., 2001. Single-mismatch detection using gold-quenched fluorescent oligonucleotides. *Nature biotechnology*, 19(4), pp.365–70.

Dudu, V., Rotari, V. & Vazquez, M., 2012. Sendai virus-based liposomes enable targeted cytosolic delivery of nanoparticles in brain tumor-derived cells. *Journal of nanobiotechnology*, 10(9), pp.1–9.

Dulkeith, E. et al., 2005. Gold nanoparticles quench fluorescence by phase induced radiative rate suppression. *Nano letters*, 5(4), pp.585–9.

Durieu-Trautmann, O. et al., 1991. Immortalization of brain capillary endothelial cells with maintenance of structural characteristics of the blood-brain barrier endothelium. *In vitro cellular & developmental biology : journal of the Tissue Culture Association*, 27A(10), pp.771–8.

Dykman, L. & Khlebtsov, N., 2012. Gold nanoparticles in biomedical applications: recent advances and perspectives. *Chemical Society reviews*, 41(6), pp.2256–82.

Ebong, E.E. et al., 2011. Imaging the endothelial glycocalyx in vitro by rapid freezing/freeze substitution transmission electron microscopy. *Arteriosclerosis, thrombosis, and vascular biology*, 31(8), pp.1908–15.

Eghtedari, M. et al., 2009. Engineering of hetero-functional gold nanorods for the in vivo molecular targeting of breast cancer cells. *Nano letters*, 9(1), pp.287–91.

El-Sayed, I.H., Huang, X. & El-Sayed, M.A., 2005. Surface plasmon resonance scattering and absorption of anti-EGFR antibody conjugated gold nanoparticles in cancer diagnostics: applications in oral cancer. *Nano letters*, 5(5), pp.829–34.

Elbakry, A. et al., 2009. Layer-by-layer assembled gold nanoparticles for siRNA delivery. *Nano letters*, 9(5), pp.2059–64.

Engelhardt, B., 2007. Development of the Blood-Brain Interface. In R. Dermietzel, D. C. Spray, & M. Nedergaard, eds. *Blood–Brain Barriers: From Ontogeny to Artificial Interfaces*. Weinheim, Germany: Wiley-VCH Verlag GmbH & Co. KGaA, pp. 9–39.

Etame, A.B. et al., 2011. Design and potential application of PEGylated gold nanoparticles with

size-dependent permeation through brain microvasculature. *Nanomedicine : nanotechnology, biology, and medicine*, 7(6), pp.992–1000.

Fire, A. et al., 1998. Potent and specific genetic interference by double-stranded RNA in Caenorhabditis elegans. *Nature*, 391(6669), pp.806–11.

Fischer, H., Gottschlich, R. & Seelig, A., 1998. Blood-brain barrier permeation: molecular parameters governing passive diffusion. *The Journal of membrane biology*, 165(3), pp.201–11.

Folbergrova, J., Rehncrona, S. & Siesjo, B.K., 1979. Oxidized and reduced glutathione in the rat brain under normoxic and hypoxic conditions. *Journal od Neurochemistry*, 32, pp.1621–1627.

Förster, C. et al., 2005. Occludin as direct target for glucocorticoid-induced improvement of blood-brain barrier properties in a murine in vitro system. *The Journal of physiology*, 565(Pt 2), pp.475–86.

Fraga, S. et al., 2013. Influence of the surface coating on the cytotoxicity, genotoxicity and uptake of gold nanoparticles in human HepG2 cells. *Journal of applied toxicology : JAT*, 33(10), pp.1111–9.

Freese, C. et al., 2012. Uptake and cytotoxicity of citrate-coated gold nanospheres: Comparative studies on human endothelial and epithelial cells. *Particle and fibre toxicology*, 9(1), p.23.

Freese, C. et al., 2013. Uptake of poly(2-hydroxypropylmethacrylamide)-coated gold nanoparticles in microvascular endothelial cells and transport across the blood-brain barrier. *Biomaterials Science*, 1, pp.824–833.

Frens, G., 1973. Controlled Nucleation for the Regulation of the Particle Size in Monodisperse Gold Suspensions. *Nature*, 241(105), pp.20–22.

Friden, P.M. et al., 1991. Anti-transferrin receptor antibody and antibody-drug conjugates cross the blood-brain barrier. *Proceedings of the National Academy of Sciences of the United States of America*, 88(11), pp.4771–5.

Friden, P.M. et al., 1996. Characterization, receptor mapping and blood-brain barrier transcytosis of antibodies to the human transferrin receptor. *The Journal of pharmacology and experimental therapeutics*, 278(3), pp.1491–8.

Fukuda, A.M. & Badaut, J., 2013. siRNA Treatment: "A Sword-in-the-Stone" for Acute Brain Injuries. *Genes*, 4(3), pp.435–56.

Gabizon, A. et al., 1994. Prolonged Circulation Time and Enhanced Accumulation in Malignant Exudates of Doxorubicin Encapsulated in Polyethylene-glycol Coated Liposomes. *Cancer Research*, 54, pp.987–992.

Gao, J.-Q. et al., 2013. Glioma targeting and blood-brain barrier penetration by dual-targeting doxorubincin liposomes. *Biomaterials*, 34(22), pp.5628–39.

García, I., Marradi, M. & Penadés, S., 2010. Glyconanoparticles: multifunctional nanomaterials for biomedical applications. *Nanomedicine (London, England)*, 5(5), pp.777–792.

Gessner, A. et al., 2000. Nanoparticles with decreasing surface hydrophobicities: influence on plasma protein adsorption. *International Journal of Pharmaceutics*, 196(2), pp.245–249.

Gibson, J.D., Khanal, B.P. & Zubarev, E.R., 2007. Paclitaxel-functionalized gold nanoparticles.

Journal of the American Chemical Society, 129(37), pp.11653–61.

Giljohann, D.A. et al., 2010. Gold nanoparticles for biology and medicine. *Angewandte Chemie - International Edition*, 49(19), pp.3280–3294.

Giljohann, D. a. et al., 2009. Gene regulation with polyvalent siRNA-nanoparticle conjugates. *Journal of the American Chemical Society*, 131(6), pp.2072–2073.

Ginzburg, V. V & Balijepalli, S., 2007. Modeling the thermodynamics of the interaction of nanoparticles with cell membranes. *Nano letters*, 7(12), pp.3716–22.

Gkeka, P. et al., 2014. Membrane partitioning of anionic, ligand-coated nanoparticles is accompanied by ligand snorkeling, local disordering, and cholesterol depletion. *PLoS computational biology*, 10(12), p.e1003917.

Goudas, L.C. et al., 1999. Acute decreases in cerebrospinal fluid glutathione levels after intracerebroventricular morphine for cancer pain. *Anesthesia and analgesia*, 89(5), pp.1209–15.

Griffiths, G. et al., 2010. Nanobead-based interventions for the treatment and prevention of tuberculosis. *Nature reviews. Microbiology*, 8(11), pp.827–34.

Gromnicova, R. et al., 2013. Glucose-coated gold nanoparticles transfer across human brain endothelium and enter astrocytes in vitro. *PloS one*, 8(12), p.e81043.

Gromnicova, R., Yilmaz, C.U., et al., 2016. Localisation and mobility of glucose-coated gold nanoparticles within the brain. *Nanomedicine (London, England)*, 11(6), pp.617–625.

Gromnicova, R., Kaya, M., et al., 2016. Transport of Gold Nanoparticles by Vascular Endothelium from Different Human Tissues. *Plos One*, 11(8), p.e0161610.

Grosse, S., Evje, L. & Syversen, T., 2013. Silver nanoparticle-induced cytotoxicity in rat brain endothelial cell culture. *Toxicology in vitro : an international journal published in association with BIBRA*, 27(1), pp.305–13.

Gu, Y.-J. et al., 2009. Nuclear penetration of surface functionalized gold nanoparticles. *Toxicology and applied pharmacology*, 237(2), pp.196–204.

Guarnieri, D. et al., 2013. Shuttle-mediated nanoparticle delivery to the blood-brain barrier. *Small (Weinheim an der Bergstrasse, Germany)*, 9(6), pp.853–62.

Guerrero, S. et al., 2010. Improving the brain delivery of gold nanoparticles by conjugation with an amphipathic peptide. *Nanomedicine (London, England)*, 6(5), pp.897–913.

Guo, S. et al., 2010. Enhanced Gene Delivery and siRNA Silencing by Gold Nanoparticles Coated with Charge-Reversal Polyelectrolyte. *ACS nano*, 4(9), pp.5505–5511.

van Haaren, P.M.A. et al., 2003. Localization of the permeability barrier to solutes in isolated arteries by confocal microscopy. *American journal of physiology. Heart and circulatory physiology*, 285(6), pp.H2848-56.

Hainfeld, J.F. et al., 2013. Gold nanoparticle imaging and radiotherapy of brain tumors in mice. *Nanomedicine (London, England)*, 8(10), pp.1601–9.

Hainfeld, J.F. et al., 2006. Gold nanoparticles: a new X-ray contrast agent. *The British Journal of Radiology*, 79(939), pp.248–253.

Hamilton, A.J. & Baulcombe, D.C., 1999. A Species of Small Antisense RNA in Posttranscriptional Gene Silencing in Plants. *Science*, 286(5441), pp.950–952.

Han, H.-K. & Amidon, G.L., 2000. Targeted prodrug design to optimize drug delivery. *AAPS pharmSci*, 2(1), pp.1–11.

Hao, X. et al., 2012. Caveolae-mediated endocytosis of biocompatible gold nanoparticles in living Hela cells. *Journal of physics. Condensed matter : an Institute of Physics journal*, 24(16), p.164207.

Havrankova, J., Brownstein, M. & Roth, J., 1981. Insulin and insulin receptors in rodent brain. *Diabetologia*, 20 Suppl, pp.268–73.

He, H. et al., 2013. Carbon nanotubes: applications in pharmacy and medicine. *BioMed research international*, 2013, p.578290.

Helms, H.C. et al., 2016. In vitro models of the blood-brain barrier: An overview of commonly used brain endothelial cell culture models and guidelines for their use. *Journal of cerebral blood flow and metabolism : official journal of the International Society of Cerebral Blood Flow and Metabolism*, 36(5), pp.862–890.

Hillyer, J.F. & Albrecht, R.M., 2001. Gastrointestinal persorption and tissue distribution of differently sized colloidal gold nanoparticles. *Journal of pharmaceutical sciences*, 90(12), pp.1927–36.

Hillyer, P., 2003. *Tissue-specific differences between endothelia: expression and presentation of chemokines and their receptors*. The Open University.

Hirn, S. et al., 2011. Particle size-dependent and surface charge-dependent biodistribution of gold nanoparticles after intravenous administration. *European journal of pharmaceutics and biopharmaceutics : official journal of Arbeitsgemeinschaft für Pharmazeutische Verfahrenstechnik e.V*, 77(3), pp.407–16.

Ho, K.-C. et al., 2004. Using biofunctionalized nanoparticles to probe pathogenic bacteria. *Analytical chemistry*, 76(24), pp.7162–8.

Hohnholt, M.C. et al., 2013. Handling of iron oxide and silver nanoparticles by astrocytes. *Neurochemical research*, 38(2), pp.227–39.

Holthöfer, H. et al., 1982. Ulex europaeus I lectin as a marker for vascular endothelium in human tissues. *Laboratory investigation; a journal of technical methods and pathology*, 47(1), pp.60–6.

Hong, R. et al., 2006. Glutathione-mediated delivery and release using monolayer protected nanoparticle carriers. *Journal of the American Chemical Society*, 128(4), pp.1078–1079.

Hostetler, M.J. et al., 1998. Alkanethiolate Gold Cluster Molecules with Core Diameters from 1.5 to 5.2 nm: Core and Monolayer Properties as a Function of Core Size. *Langmuir*, 14(1), pp.17–30.

Hostetler, M.J. et al., 1996. Monolayers in Three Dimensions : Synthesis and Electrochemistry of ω -Functionalized Alkanethiolate-Stabilized Gold Cluster Compounds. *J. Am. Chem. Soc.*, 118, pp.4212–4213.

Hu, M. et al., 2006. Gold nanostructures: engineering their plasmonic properties for biomedical

applications. *Chemical Society reviews*, 35(11), pp.1084–94.

Huang, F.-Y.J. et al., 2013. In vitro and in vivo evaluation of lactoferrin-conjugated liposomes as a novel carrier to improve the brain delivery. *International journal of molecular sciences*, 14(2), pp.2862–74.

Huang, R. et al., 2008. The use of lactoferrin as a ligand for targeting the polyamidoamine-based gene delivery system to the brain. *Biomaterials*, 29(2), pp.238–46.

Huang, X. et al., 2007. Gold nanoparticles: interesting optical properties and recent applications in cancer diagnostics and therapy. *Nanomedicine (London, England)*, 2(5), pp.681–93.

Huang, X. & El-Sayed, M. a., 2010. Gold nanoparticles: Optical properties and implementations in cancer diagnosis and photothermal therapy. *Journal of Advanced Research*, 1(1), pp.13–28.

Hurst, S.J., Lytton-Jean, A.K.R. & Mirkin, C.A., 2006. Maximizing DNA loading on a range of gold nanoparticle sizes. *Analytical chemistry*, 78(24), pp.8313–8.

Huwyler, J., Wu, D. & Pardridge, W.M., 1996. Brain drug delivery of small molecules using immunoliposomes. *Proceedings of the National Academy of Sciences of the United States of America*, 93(24), pp.14164–9.

Hvolbæk, B. et al., 2007. Catalytic activity of Au nanoparticles. *Nanotoday*, 2(4), pp.14–18.

Iversen, T.-G., Skotland, T. & Sandvig, K., 2011. Endocytosis and intracellular transport of nanoparticles: Present knowledge and need for future studies. *Nano Today*, 6(2), pp.176–185.

Jayagopal, A. et al., 2010. Hairpin DNA-functionalized gold colloids for the imaging of mRNA in live cells. *Journal of the American Chemical Society*, 132(28), pp.9789–96.

Jelveh, S. & Chithrani, D.B., 2011. Gold nanostructures as a platform for combinational therapy in future cancer therapeutics. *Cancers*, 3(1), pp.1081–110.

Jensen, S.A. et al., 2013. Spherical nucleic acid nanoparticle conjugates as an RNAi-based therapy for glioblastoma. *Science translational Medicine*, 5(209), p.209ra152.

Jiang, W. et al., 2008. Nanoparticle-mediated cellular response is size-dependent. *Nature nanotechnology*, 3(3), pp.145–50.

Jiang, Y. et al., 2015. The Interplay of Size and Surface Functionality on the Cellular Uptake of Sub-10 nm Gold Nanoparticles. *ACS Nano*, 10(9), pp.9986–9993.

Joh, D.Y. et al., 2013. Selective targeting of brain tumors with gold nanoparticle-induced radiosensitization. *PloS one*, 8(4), p.e62425.

De Jong, W.H. et al., 2008. Particle size-dependent organ distribution of gold nanoparticles after intravenous administration. *Biomaterials*, 29(12), pp.1912–9.

Joshi, H.M. et al., 2006. Gold nanoparticles as carriers for efficient transmucosal insulin delivery. *Langmuir*, 22(17), pp.300–305.

Joshi, S., Emala, C.W. & Pile-Spellman, J., 2007. Intra-arterial drug delivery: a concise review. *Journal of neurosurgical anesthesiology*, 19(2), pp.111–9.

Kang, K.A. et al., 2011. Fluorescence manipulation by gold nanoparticles: from complete

quenching to extensive enhancement. *Journal of nanobiotechnology*, 9, p.16.

Ke, W. et al., 2009. Gene delivery targeted to the brain using an Angiopep-conjugated polyethyleneglycol-modified polyamidoamine dendrimer. *Biomaterials*, 30(36), pp.6976–85.

Khlebtsov, N. & Dykman, L., 2011. Biodistribution and toxicity of engineered gold nanoparticles: a review of in vitro and in vivo studies. *Chemical Society reviews*, 40(3), pp.1647–71.

Kim, B. et al., 2010. Tuning payload delivery in tumour cylindroids using gold nanoparticles. *Nature nanotechnology*, 5(6), pp.465–472.

Klibanov, A.L. et al., 1991. Activity of amphipathic poly(ethylene glycol) 5000 to prolong the circulation time of liposomes depends on the liposome size and is unfavorable for immunoliposome binding to target. *Biochimica et biophysica acta*, 1062(2), pp.142–8.

Kreuter, J. et al., 1995. Passage of peptides through the blood-brain barrier with colloidal polymer particles (nanoparticles). *Brain Research*, 674(1), pp.171–174.

Kuntz, E. & Kuntz, H.-D., 2006. *Hepatology Principles and Practice: history, morphology, biochemistry, diagnostics, clinic, therapy* 2nd ed., Berlin/Heidelberg: Springer-Verlag.

Laakkonen, P. & Vuorinen, K., 2010. Homing peptides as targeted delivery vehicles. *Integrative biology : quantitative biosciences from nano to macro*, 2(7–8), pp.326–337.

Lacerda, S.H.D.P. et al., 2010. Interaction of gold nanoparticles with common human blood proteins. *ACS nano*, 4(1), pp.365–79.

Langley, G.R., 2014. Considering a new paradigm for Alzheimer's disease research. *Drug Discovery Today*, 19(8), pp.1114–1124.

Lasagna-Reeves, C. et al., 2010. Bioaccumulation and toxicity of gold nanoparticles after repeated administration in mice. *Biochemical and biophysical research communications*, 393(4), pp.649–55.

Lee, J.-S. et al., 2008. Thermodynamically controlled separation of polyvalent 2-nm gold nanoparticle-oligonucleotide conjugates. *Journal of the American Chemical Society*, 130(16), pp.5430–1. Available at: http://www.ncbi.nlm.nih.gov/pubmed/18370386.

Lee, J.K. et al., 2014. Organ-specific distribution of gold nanoparticles by their surface functionalization. *Journal of applied toxicology*, (August).

Lee, S.H. et al., 2008. Amine-functionalized gold nanoparticles as non-cytotoxic and efficient intracellular siRNA delivery carriers. *International Journal of Pharmaceutics*, 364, pp.94–101.

Van Lehn, R.C. et al., 2013. Effect of particle diameter and surface composition on the spontaneous fusion of monolayer-protected gold nanoparticles with lipid bilayers. *Nano letters*, 13(9), pp.4060–7.

Van Lehn, R.C. & Alexander-Katz, A., 2014. Fusion of Ligand-Coated Nanoparticles with Lipid Bilayers: Effect of Ligand Flexibility. *The journal of physical chemistry A*.

Leroueil, P.R. et al., 2008. Wide varieties of cationic nanoparticles induce defects in supported lipid bilayers. *Nano letters*, 8(2), pp.420–4.

Letsinger, R.L. et al., 2000. Use of a steroid cyclic disulfide anchor in constructing gold

nanoparticle-oligonucleotide conjugates. *Bioconjugate Chemistry*, 11(2), pp.289–291.

Levin, V.A., 1980. Relationship of octanol/water partition coefficient and molecular weight to rat brain capillary permeability. *Journal of medicinal chemistry*, 23(6), pp.682–4.

Li, W. et al., 2012. Glutathione in cerebral microvascular endothelial biology and pathobiology: Implications for brain homeostasis. *International Journal of Cell Biology*, 2012, pp.1–14.

Li, X.-Y. et al., 2014. Multifunctional liposomes loaded with paclitaxel and artemether for treatment of invasive brain glioma. *Biomaterials*.

Libutti, S.K. et al., 2010. Phase I and pharmacokinetic studies of CYT-6091, a novel PEGylated colloidal gold-rhTNF nanomedicine. *Clinical cancer research : an official journal of the American Association for Cancer Research*, 16(24), pp.6139–49.

Lin, I.C. et al., 2012. Cellular transport pathways of polymer coated gold nanoparticles. *Nanomedicine: Nanotechnology, Biology, and Medicine*, 8(1), pp.8–11.

Lin, J. et al., 2010. Penetration of Lipid Membranes by Gold Nanoparticles: Insights into Cellular Uptake, Cytotoxicity, and Their Relationship. *ACS nano*, 4(9), pp.5421–5429.

Lin, J. & Alexander-Katz, A., 2013. Cell Membranes Open "Doors" for Cationic Nanoparticles/Biomolecules: Insights into Uptake Kinetics. *ACS nano*, 7(12), pp.10799–10808.

Link, S. et al., 1999. Laser Photothermal Melting and Fragmentation of Gold Nanorods: Energy and Laser Pulse-Width Dependence. *The Journal of Physical Chemistry A*, 103(9), pp.1165–1170.

Lippmann, E.S. et al., 2012. Derivation of blood-brain barrier endothelial cells from human pluripotent stem cells. *Nature biotechnology*, 30(8), pp.783–91.

Liu, D. & Balasubramanian, S., 2003. A Proton-Fuelled DNA Nanomachine. *Angewandte Chemie International Edition*, 42(46), pp.5734–5736.

Liu, J. et al., 2010. Computational model for nanocarrier binding to endothelium validated using in vivo, in vitro, and atomic force microscopy experiments. *Proceedings of the National Academy of Sciences of the United States of America*, 107(38), pp.16530–5.

Liu, J. et al., 2011. Multivalent binding of nanocarrier to endothelial cells under shear flow. *Biophysical journal*, 101(2), pp.319–26.

Liu, X. et al., 2013. Surface and size effects on cell interaction of gold nanoparticles with both phagocytic and nonphagocytic cells. *Langmuir : the ACS journal of surfaces and colloids*, 29(29), pp.9138–48.

Liu, Y. et al., 2009. Brain-targeting gene delivery and cellular internalization mechanisms for modified rabies virus glycoprotein RVG29 nanoparticles. *Biomaterials*, 30(25), pp.4195–202.

Lochhead, J.J. & Thorne, R.G., 2012. Intranasal delivery of biologics to the central nervous system. *Advanced drug delivery reviews*, 64(7), pp.614–28.

Longmire, M., Choyke, P.L. & Kobayashi, H., 2008. Clearance properties of nano-sized particles and molecules as imaging agents: considerations and caveats. *Nanomedicine (London, England)*, 3(5), pp.703–17.

Lopez-Ramirez, M.A. et al., 2014. MicroRNA-155 negatively affects blood-brain barrier function during neuroinflammation. *FASEB journal*, 28(6), pp.2551–65.

Lund, T. et al., 2011. The influence of ligand organization on the rate of uptake of gold nanoparticles by colorectal cancer cells. *Biomaterials*, 32(36), pp.9776–84.

Lundqvist, M. et al., 2011. The evolution of the protein corona around nanoparticles: a test study. *ACS nano*, 5(9), pp.7503–9.

Ma, Y.-P. et al., 2007. Intranasally delivered TGF-β1 enters brain and regulates gene expressions of its receptors in rats. *Brain Research Bulletin*, 74(4), pp.271–277.

Maeda, T. et al., 2013. Establishment and characterization of spinal cord microvascular endothelial cell lines. *Clinical and Experimental Neuroimmunology*, 4(3), pp.326–338.

Mahringer, A. et al., 2011. The ABC of the Blood-Brain Barrier - Regulation of Drug Efflux Pumps. *Current Pharmaceutical Design*, 17(26), pp.2762–2770.

Male, D.K., Gromnicova, R. & McQuaid, C., 2016. Gold Nanoparticles for Imaging and Drug Transport to the CNS. In *International Review of Neurobiology*.

Markoutsa, E. et al., 2011. Uptake and permeability studies of BBB-targeting immunoliposomes using the hCMEC/D3 cell line. *European journal of pharmaceutics and biopharmaceutics : official journal of Arbeitsgemeinschaft für Pharmazeutische Verfahrenstechnik e.V*, 77(2), pp.265–74.

Massich, M.D. et al., 2010. Cellular Response of Polyvalent Oligonucleotide-Gold Nanoparticle Conjugates. *ACS nano*, 4(10), p.5641.

Mateo, D. et al., 2013. Oxidative stress contributes to gold nanoparticle-induced cytotoxicity in human tumor cells. *Toxicology mechanisms and methods*, 6516(3), pp.161–172.

Matranga, C. et al., 2005. Passenger-strand cleavage facilitates assembly of siRNA into Ago2-containing RNAi enzyme complexes. *Cell*, 123(4), pp.607–20.

McIntosh, C.M. et al., 2001. Inhibition of DNA transcription using cationic mixed monolayer protected gold clusters. *Journal of the American Chemical Society*, 123(31), pp.7626–7629.

McIntosh, D.P. et al., 2002. Targeting endothelium and its dynamic caveolae for tissue-specific transcytosis in vivo: a pathway to overcome cell barriers to drug and gene delivery. *Proceedings of the National Academy of Sciences of the United States of America*, 99(4), pp.1996–2001.

Menei, P. et al., 2004. Stereotaxic implantation of 5-fluorouracil-releasing microspheres in malignant glioma. *Cancer*, 100(2), pp.405–10.

Michaelis, K. et al., 2006. Covalent linkage of apolipoprotein e to albumin nanoparticles strongly enhances drug transport into the brain. *The Journal of pharmacology and experimental therapeutics*, 317(3), pp.1246–53.

Milani, S. et al., 2012. Reversible versus irreversible binding of transferrin to polystyrene nanoparticles: soft and hard corona. *ACS nano*, 6(3), pp.2532–41.

Minn, A. et al., 1991. Drug metabolizing enzymes in the brain and cerebral microvessels. *Brain Research Reviews*, 16(1), pp.65–82.

Morshed, R.A. et al., 2016. Cell-Penetrating Peptide-Modified Gold Nanoparticles for the Delivery of Doxorubicin to Brain Metastatic Breast Cancer. *Molecular Pharmaceutics*, 13(6), pp.1843–1854.

Mosmann, T., 1983. Rapid colorimetric assay for cellular growth and survival: Application to proliferation and cytotoxicity assays. *Journal of Immunological Methods*, 65(1–2), pp.55–63.

Muhamad, I.I. et al., 2014. Designing Polymeric Nanoparticles for Targeted Drug Delivery System. In A. Seifalian, A. de Mel, & M. D. Kalaskar, eds. *Nanomedicine*. pp. 287–313.

Nealon, G.L. et al., 2012. Magnetism in gold nanoparticles. *Nanoscale*, 4(17), p.5244.

Neuwelt, E.A. et al., 1991. Primary CNS lymphoma treated with osmotic blood-brain barrier disruption: prolonged survival and preservation of cognitive function. *Journal of clinical oncology : official journal of the American Society of Clinical Oncology*, 9(9), pp.1580–90.

Nicchia, G.P. et al., 2003. Inhibition of aquaporin-4 expression in astrocytes by RNAi determines alteration in cell morphology, growth, and water transport and induces changes in ischemia-related genes. *The FASEB journal : official publication of the Federation of American Societies for Experimental Biology*, 17, pp.1508–1510.

Nicholson, C., 2001. Diffusion and related transport mechanisms in brain tissue. *Reports on Progress in Physics*, 64, pp.815–884.

Niidome, T. et al., 2006. PEG-modified gold nanorods with a stealth character for in vivo applications. *Journal of Controlled Release*, 114(3), pp.343–347.

Niikura, K. et al., 2014. Amphiphilic Gold Nanoparticles Displaying Flexible Bifurcated Ligands as a Carrier for siRNA Delivery into the Cell Cytosol. *ACS Applied materials and interfaces*, 6, pp.22146–22154.

Nishikawa, K. et al., 2012. Development of anti-HB-EGF immunoliposomes for the treatment of breast cancer. *Journal of controlled release : official journal of the Controlled Release Society*, 160(2), pp.274–80.

Nitta, T. et al., 2003. Size-selective loosening of the blood-brain barrier in claudin-5-deficient mice. *The Journal of cell biology*, 161(3), pp.653–60.

Nolting, B. et al., 2003. Synthesis of Gold Glyconanoparticles and Biological Evaluation of Recombinant Gp120 Interactions. *Langmuir*, 19(16), pp.6465–6473.

Oh, N. & Park, J.-H., 2014. Surface chemistry of gold nanoparticles mediates their exocytosis in macrophages. *ACS nano*, 8(6), pp.6232–41.

Oishi, M. et al., 2006. Smart PEGylated Gold Nanoparticles for the Cytoplasmic Delivery of siRNA to Induce Enhanced Gene Silencing. *Chemistry Letters*, 35(9), pp.1046–1047.

Olesen, J. & Leonardi, M., 2003. The burden of brain diseases in Europe. *European Journal of Neurology*, 10(5), pp.471–477.

Omidi, Y. et al., 2003. Evaluation of the immortalised mouse brain capillary endothelial cell line, b.End3, as an in vitro blood-brain barrier model for drug uptake and transport studies. *Brain research*, 990(1–2), pp.95–112.

Ommaya, A.K., 1963. Subcutaneous reservoir and pump for sterile access to ventricular

cerebrospinal fluid. *Lancet*, 2(7315), pp.983–4.

Osaki, F. et al., 2004. A quantum dot conjugated sugar ball and its cellular uptake. On the size effects of endocytosis in the subviral region. *Journal of the American Chemical Society*, 126(21), pp.6520–1.

Paino, I.M.M. et al., 2012. Cyto and genotoxicity of gold nanoparticles in human hepatocellular carcinoma and peripheral blood mononuclear cells. *Toxicology letters*, 215(2), pp.119–25.

Pan, Y. et al., 2009. Gold nanoparticles of diameter 1.4 nm trigger necrosis by oxidative stress and mitochondrial damage. *Small (Weinheim an der Bergstrasse, Germany)*, 5(18), pp.2067–76.

Pardridge, W.M., 2010. Biopharmaceutical drug targeting to the brain. *Journal of drug targeting*, 18(3), pp.157–167.

Pardridge, W.M. et al., 1995. Human insulin receptor monoclonal antibody undergoes high affinity binding to human brain capillaries in vitro and rapid transcytosis through the blood-brain barrier in vivo in the primate. *Pharmaceutical research*, 12(6), pp.807–16.

Pardridge, W.M., 2005. The blood-brain barrier: bottleneck in brain drug development. *NeuroRx : the journal of the American Society for Experimental NeuroTherapeutics*, 2(1), pp.3–14.

Pardridge, W.M., Buciak, J.L. & Friden, P.M., 1991. Selective transport of an anti-transferrin receptor antibody through the blood-brain barrier in vivo. *The Journal of pharmacology and experimental therapeutics*, 259(1), pp.66–70.

Park, S., Brown, K.A. & Hamad-schifferli, K., 2004. Changes in Oligonucleotide Conformation on Nanoparticle Surfaces by Modification with Mercaptohexanol. *Nano letters*, 4(10), pp.1925–1929.

Parton, R.G. & Simons, K., 2007. The multiple faces of caveolae. *Nature Reviews Molecular Cell Biology*, 8(3), pp.185–194.

Pasqualini, R. & Ruoslahti, E., 1996. Organ targeting in vivo using phage display peptide libraries. *Nature*, 380(6572), pp.364–366.

Patel, M.M. et al., 2009. Getting into the brain: approaches to enhance brain drug delivery. *CNS Drugs*, 23(1), pp.35–59.

Peckys, D.B. & de Jonge, N., 2014. Gold Nanoparticle Uptake in Whole Cells in Liquid Examined by Environmental Scanning Electron Microscopy. *Microscopy and Microanalysis*, 20(1), pp.189–197.

Peddagangannagari, S.R., 2012. *An in vitro human 3D co-culture model to study endothelial-astrocyte interactions*. Open University.

Pelicci, P.G. et al., 1982. Hemin regulates the expression of transferrin receptors in human hematopoietic cell lines. *FEBS Letters*, 145(2), pp.350–354.

Pellegrino, T. et al., 2007. Gel Electrophoresis of Gold-DNA Nanoconjugates. *Journal of Biomedicine and Biotechnology*, 2007.

Pilakka-Kanthikeel, S. et al., 2013. Targeted brain derived neurotropic factors (BDNF) delivery across the blood-brain barrier for neuro-protection using magnetic nano carriers: an in-

vitro study. *PloS one*, 8(4), p.e62241.

Pinto Reis, C. et al., 2006. Nanoencapsulation I. Methods for preparation of drug-loaded polymeric nanoparticles. *Nanomedicine: Nanotechnology, Biology, and Medicine*, 2(1), pp.8–21.

Pinzón-Daza, M. et al., 2012. The association of statins plus LDL receptor-targeted liposome-encapsulated doxorubicin increases in vitro drug delivery across blood-brain barrier cells. *British journal of pharmacology*, 167(7), pp.1431–47.

Pitsillides, C.M. et al., 2003. Selective cell targeting with light-absorbing microparticles and nanoparticles. *Biophysical journal*, 84(6), pp.4023–32.

Potter, D.R. & Damiano, E.R., 2008. The hydrodynamically relevant endothelial cell glycocalyx observed in vivo is absent in vitro. *Circulation research*, 102(7), pp.770–6.

Prades, R. et al., 2012. Delivery of gold nanoparticles to the brain by conjugation with a peptide that recognizes the transferrin receptor. *Biomaterials*, 33(29), pp.7194–205.

Qin, Y. et al., 2012. Comparison of four different peptides to enhance accumulation of liposomes into the brain. *Journal of drug targeting*, 20(3), pp.235–45.

Rajotte, D. et al., 1998. Molecular Heterogeneity of the Vascular Endothelium Revealed by In Vivo Phage Display. *Journal of Clinical Investigations*, 102(2), pp.430–437.

Rao, K.S. et al., 2008. TAT-conjugated nanoparticles for the CNS delivery of anti-HIV drugs. *Biomaterials*, 29(33), pp.4429–38.

Reddy, M.K. & Labhasetwar, V., 2009. Nanoparticle-mediated delivery of superoxide dismutase to the brain: an effective strategy to reduce ischemia-reperfusion injury. *FASEB journal : official publication of the Federation of American Societies for Experimental Biology*, 23(5), pp.1384–95.

Reichardt, N.C., Martín-Lomas, M. & Penadés, S., 2013. Glyconanotechnology. *Chemical Society Reviews*, 42(10), p.4358.

Reiss, Y. et al., 1998. T cell interaction with ICAM-1-deficient endothelium in vitro: essential role for ICAM-1 and ICAM-2 in transendothelial migration of T cells. *European journal of immunology*, 28(10), pp.3086–99.

Reitsma, S. et al., 2007. The endothelial glycocalyx: composition, functions, and visualization. *Pflügers Archiv : European journal of physiology*, 454(3), pp.345–59.

Remant Bahadur, K.C., Thapa, B. & Bhattarai, N., 2014. Gold nanoparticle-based gene delivery: Promises and challenges. *Nanotechnology Reviews*, 3(3), pp.269–280.

Ribatti, D. et al., 2006. Development of the blood-brain barrier: A historical point of view. *Anatomical Record - Part B New Anatomist*, 289(1), pp.3–8.

Roggers, R. et al., 2014. The practicality of mesoporous silica nanoparticles as drug delivery devices and progress toward this goal. *AAPS PharmSciTech*, 15(5), pp.1163–71.

Rojo, J. et al., 2004. Gold glyconanoparticles as new tools in antiadhesive therapy. *Chembiochem : a European journal of chemical biology*, 5(3), pp.291–7.

Rosi, N.L. et al., 2006. Oligonucleotide-Modified Gold Nanoparticles for Intracellular Gene Regulation. *Science*, 312(5776), pp.1027–1030.

Roux, F. et al., 1994. Regulation of gamma-glutamyl transpeptidase and alkaline phosphatase activities in immortalized rat brain microvessel endothelial cells. *Journal of cellular physiology*, 159(1), pp.101–13.

Rüdiger, H. & Gabius, H.J., 2002. Plant lectins: Occurrence, biochemistry, functions and applications. *Glycoconjugate Journal*, 18(8), pp.589–613.

Sadauskas, E. et al., 2007. Kupffer cells are central in the removal of nanoparticles from the organism. *Particle and fibre toxicology*, 4, p.10.

Saha, K. et al., 2012. Gold nanoparticles in chemical and biological sensing. *Chemical reviews*, 112(5), pp.2739–79.

Sakane, T. et al., 1991. The transport of a drug to the cerebrospinal fluid directly from the nasal cavity: the relation to the lipophilicity of the drug. *Chemical & pharmaceutical bulletin*, 39(9), pp.2456–8.

Salvati, A. et al., 2013. Transferrin-functionalized nanoparticles lose their targeting capabilities when a biomolecule corona adsorbs on the surface. *Nature nanotechnology*, 8(2), pp.137–43.

Salvati, E. et al., 2013. Liposomes functionalized to overcome the blood-brain barrier and to target amyloid-β peptide: the chemical design affects the permeability across an in vitro model. *International journal of nanomedicine*, 8, pp.1749–58.

Sandhu, K.K. et al., 2002. Gold nanoparticle-mediated transfection of mammalian cells. *Bioconjugate Chemistry*, 13(1), pp.3–6.

Sandstrom, P., Boncheva, M. & Åkerman, B. rn, 2003. Nonspecific and Thiol-Specific Binding of DNA to Gold. *Langmuir*, 19, pp.7537–7543.

dos Santos, T. et al., 2011. Effects of transport inhibitors on the cellular uptake of carboxylated polystyrene nanoparticles in different cell lines. *PloS one*, 6(9), p.e24438.

Saris, S.C. et al., 1988. Intravascular streaming and variable delivery to brain following carotid artery infusions in the Sprague-Dawley rat. *Journal of cerebral blood flow and metabolism*, 8, pp.116–120.

Satchell, S.C. et al., 2006. Conditionally immortalized human glomerular endothelial cells expressing fenestrations in response to VEGF. *Kidney international*, 69(9), pp.1633–40.

Schaeublin, N.M. et al., 2011. Surface charge of gold nanoparticles mediates mechanism of toxicity. *Nanoscale*, 3(2), pp.410–20.

Schirmacher, A. et al., 2000. Electromagnetic fields (1.8 GHz) increase the permeability to sucrose of the blood-brain barrier in vitro. *Bioelectromagnetics*, 21(5), pp.338–45.

Schlageter, K.E. et al., 1999. Microvessel Organization and Structure in Experimental Brain Tumors: Microvessel Populations with Distinctive Structural and Functional Properties. *Microvascular Research*, 58(3), pp.312–328.

Schleh, C. et al., 2012. Size and surface charge of gold nanoparticles determine absorption across intestinal barriers and accumulation in secondary target organs after oral administration. *Nanotoxicology*, 6(1), pp.36–46.

Schmidt, J. et al., 2003. Drug targeting by long-circulating liposomal glucocorticosteroids

increases therapeutic efficacy in a model of multiple sclerosis. *Brain : a journal of neurology*, 126(Pt 8), pp.1895–904.

Schnyder, A. & Huwyler, J., 2005. Drug transport to brain with targeted liposomes. *NeuroRx : the journal of the American Society for Experimental NeuroTherapeutics*, 2(1), pp.99–107.

Schürer, L. et al., 1989. Blood-brain barrier permeability and vascular reactivity to bradykinin after pretreatment with dexamethasone. *Acta neuropathologica*, 77(6), pp.576–81.

Seferos, D.S. et al., 2007. Locked nucleic acid-nanoparticle conjugates. *Chembiochem: a European journal of chemical biology*, 8(11), pp.1230–2.

Sharma, G. et al., 2013. Cell penetrating peptide tethered bi-ligand liposomes for delivery to brain in vivo: Biodistribution and transfection. *Journal of controlled release : official journal of the Controlled Release Society*, 167(1), pp.1–10.

Sharma, G. et al., 2012. Grafting of cell-penetrating peptide to receptor-targeted liposomes improves their transfection efficiency and transport across blood-brain barrier model. *Journal of pharmaceutical sciences*, 101(7), pp.2468–78.

Shilo, M. et al., 2014. Transport of nanoparticles through the blood-brain barrier for imaging and therapeutic applications. *Nanoscale*, 6(4), pp.2146–52.

Shukla, R. et al., 2005. Biocompatibility of gold nanoparticles and their endocytotic fate inside the cellular compartment: a microscopic overview. *Langmuir : the ACS journal of surfaces and colloids*, 21(23), pp.10644–54.

Silwedel, C. & Förster, C., 2006. Differential susceptibility of cerebral and cerebellar murine brain microvascular endothelial cells to loss of barrier properties in response to inflammatory stimuli. *Journal of Neuroimmunology*, 179(1–2), pp.37–45.

Simionescu, M., Gafencu, A. & Antohe, F., 2002. Transcytosis of plasma macromolecules in endothelial cells: A cell biological survey. *Microscopy Research and Technique*, 57(5), pp.269–288.

Simionescu, M., Simionescu, N. & Palade, G.E., 1982. Differentiated microdomains on the luminal surface of capillary endothelium: distribution of lectin receptors. *The Journal of cell biology*, 94(2), pp.406–13.

Simionescu, M., Simionescu, N. & Palade, G.E., 1974. Morphometric data on the endothelium of blood capillaries. *Journal of Cell Biology*, 60(1), pp.128–152.

Simpson, C. a et al., 2013. In vivo toxicity, biodistribution, and clearance of glutathione-coated gold nanoparticles. *Nanomedicine : nanotechnology, biology, and medicine*, 9(2), pp.257–63.

Singh, A. et al., 2007. Glomerular endothelial glycocalyx constitutes a barrier to protein permeability. *Journal of the American Society of Nephrology : JASN*, 18(11), pp.2885–93.

Singh, S.K. et al., 1998. LNA (locked nucleic acids): synthesis and high-affinity nucleic acid recognition. *Chemical Communications*, 90(4), pp.455–456.

Skotland, T., Iversen, T.-G. & Sandvig, K., 2010. New metal-based nanoparticles for intravenous use: requirements for clinical success with focus on medical imaging. *Nanomedicine : nanotechnology, biology, and medicine*, 6(6), pp.730–7.

Sonavane, G., Tomoda, K. & Makino, K., 2008. Biodistribution of colloidal gold nanoparticles after intravenous administration: effect of particle size. *Colloids and surfaces. B, Biointerfaces*, 66(2), pp.274–80.

Song, L. et al., 2013. Efficient, pH-Triggered Drug Delivery Using a pH-Responsive DNA-Conjugated Gold Nanoparticle. *Advanced Healthcare Materials*, 2(2), pp.275–280.

Soni, V., Kohli, D. V & Jain, S.K., 2008. Transferrin-conjugated liposomal system for improved delivery of 5-fluorouracil to brain. *Journal of drug targeting*, 16(1), pp.73–8.

Sorkin, A. & von Zastrow, M., 2002. Signal transduction and endocytosis: close encounters of many kinds. *Nature Reviews Molecular Cell Biology*, 3(8), pp.600–614.

Sousa, F. et al., 2010. Functionalized gold nanoparticles: a detailed in vivo multimodal microscopic brain distribution study. *Nanoscale*, 2(12), pp.2826–34.

Squire, J.M. et al., 2001. Quasi-Periodic Substructure in the Microvessel Endothelial Glycocalyx: A Possible Explanation for Molecular Filtering? *Journal of Structural Biology*, 136, pp.239–255.

Sreekanthreddy, P. et al., 2015. A three-dimensional model of the human blood-brain barrier to analyse the transport of nanoparticles and astrocyte/endothelial interactions. *F1000Research*, 4.

Stanness, K.A. et al., 1999. A new model of the blood--brain barrier: co-culture of neuronal, endothelial and glial cells under dynamic conditions. *Neuroreport*, 10(18), pp.3725–31.

Stewart, P.A., 2000. Endothelial vesicles in the blood-brain barrier: Are they related to permeability? *Cellular and Molecular Neurobiology*, 20(2), pp.149–163.

Stins, M.F. et al., 1997. Selective expression of adhesion molecules on human brain microvascular endothelial cells. *Journal of neuroimmunology*, 76(1–2), pp.81–90.

Stins, M.F., Badger, J. & Sik Kim, K., 2001. Bacterial invasion and transcytosis in transfected human brain microvascular endothelial cells. *Microbial pathogenesis*, 30(1), pp.19–28.

Swierczewska, M., Lee, S. & Chen, X., 2011. The design and application of fluorophore-gold nanoparticle activatable probes. *Physical chemistry chemical physics : PCCP*, 13(21), pp.9929–41.

Sykova, E. & Nicholson, C., 2008. Diffusion in Brain Extracellular Space. *Physiological reviews*, 88(4), pp.1277–1340.

Tang, J. et al., 2010. Silver nanoparticles crossing through and distribution in the blood-brain barrier in vitro. *Journal of nanoscience and nanotechnology*, 10(10), pp.6313–7.

Tateno, H. et al., 2011. Glycome diagnosis of human induced pluripotent stem cells using lectin microarray. *Journal of Biological Chemistry*, 286(23), pp.20345–20353.

Teifel, M. & Friedl, P., 1996. Establishment of the permanent microvascular endothelial cell line PBMEC/C1-2 from porcine brains. *Experimental cell research*, 228(1), pp.50–7.

Templeton, A.C. et al., 1998. Reactivity of Monolayer-Protected Gold Cluster Molecules: Steric Effects. *Journal of the American Chemical Society*, 120(8), pp.1906–1911.

Templeton, A.C., Wuelfing, W.P. & Murray, R.W., 2000. Monolayer-protected cluster molecules.

Accounts of Chemical Research, 33(1), pp.27–36.

Thomas, M. & Klibanov, A.M., 2003. Conjugation to gold nanoparticles enhances polyethylenimine's transfer of plasmid DNA into mammalian cells. *Proceedings of the National Academy of Sciences of the United States of America*, 100(16), pp.9138–9143.

Thorne, R.G. et al., 2004. Delivery of insulin-like growth factor-I to the rat brain and spinal cord along olfactory and trigeminal pathways following intranasal administration. *Neuroscience*, 127(2), pp.481–496.

Thorne, R.G. et al., 2008. Delivery of interferon-β to the monkey nervous system following intranasal administration. *Neuroscience*, 152(3), pp.785–797.

Thorne, R.G. et al., 1995. *Quantitative analysis of the olfactory pathway for drug delivery to the brain*,

Tkachenko, A.G. et al., 2004. Cellular trajectories of peptide-modified gold particle complexes: comparison of nuclear localization signals and peptide transduction domains. *Bioconjugate chemistry*, 15(3), pp.482–90.

Tomalia, D.A. et al., 1985. A New Class of Polymers: Starburst-Dendritic Macromolecules. *Polymer Journal*, 17, pp.117–132.

Tröster, S.D., Müller, U. & Kreuter, J., 1990. Modification of the body distribution of poly(methyl methacrylate) nanoparticles in rats by coating with surfactants. *International Journal of Pharmaceutics*, 61(1–2), pp.85–100.

Tsoli, M. et al., 2005. Cellular uptake and toxicity of Au55 clusters. *Small (Weinheim an der Bergstrasse, Germany)*, 1(8–9), pp.841–4.

Turkevich, J., Stevenson, P.C. & Hillier, J., 1951. A study of the nucleation and growth process in the synthesis of colloidal gold. *Discuss. Faraday. Soc*, 11, pp.55–75.

Uster, P.S. et al., 1996. Insertion of poly(ethylene glycol) derivatized phospholipid into pre-formed liposomes results in prolonged in vivo circulation time. *FEBS letters*, 386(2–3), pp.243–6.

VanTeeffelen, J.W. et al., 2007. Endothelial Glycocalyx: Sweet Shield of Blood Vessels. *Trends in Cardiovascular Medicine*, 17(3), pp.101–105.

Veiseh, O., Gunn, J.W. & Zhang, M., 2010. Design and fabrication of magnetic nanoparticles for targeted drug delivery and imaging. *Advanced drug delivery reviews*, 62(3), pp.284–304.

Verma, A. et al., 2008. Surface-structure-regulated cell-membrane penetration by monolayer-protected nanoparticles. *Nature materials*, 7(7), pp.588–95.

Verma, A. et al., 2004. Tunable reactivation of nanoparticle-inhibited beta-galactosidase by glutathione at intracellular concentrations. *Journal of the American Chemical Society*, 126(43), pp.13987–91.

Villiers, C. et al., 2010. Analysis of the toxicity of gold nano particles on the immune system: effect on dendritic cell functions. *Journal of nanoparticle research : an interdisciplinary forum for nanoscale science and technology*, 12(1), pp.55–60.

Visaria, R.K. et al., 2006. Enhancement of tumor thermal therapy using gold nanoparticle-assisted tumor necrosis factor-alpha delivery. *Molecular cancer therapeutics*, 5(4), pp.1014–

1020.

Walkey, C.D. & Chan, W.C.W., 2012. Understanding and controlling the interaction of nanomaterials with proteins in a physiological environment. *Chemical Society reviews*, 41(7), pp.2780–99.

Wang, R. et al., 2013. Enhancement effect of cytotoxicity response of silver nanoparticles combined with thermotherapy on C6 rat glioma cells. *Journal of nanoscience and nanotechnology*, 13(6), pp.3851–4.

Webb, J. a & Bardhan, R., 2014. Emerging advances in nanomedicine with engineered gold nanostructures. *Nanoscale*, 6(5), pp.2502–30.

Weksler, B., Romero, I.A. & Couraud, P.-O., 2013. The hCMEC/D3 cell line as a model of the human blood brain barrier. *Fluids and barriers of the CNS*, 10(1), p.16.

Weksler, B.B. et al., 2005. Blood-brain barrier-specific properties of a human adult brain endothelial cell line. *FASEB journal : official publication of the Federation of American Societies for Experimental Biology*, 19(13), pp.1872–4.

Whitehead, K. a, Langer, R. & Anderson, D.G., 2009. Knocking down barriers: advances in siRNA delivery. *Nature reviews. Drug discovery*, 8(2), pp.129–138.

Wiley, D.T. et al., 2013. Transcytosis and brain uptake of transferrin-containing nanoparticles by tuning avidity to transferrin receptor. *Proceedings of the National Academy of Sciences of the United States of America*, 110(21), pp.8662–7.

Williams, M.J. et al., 2005. Cadherin-10 is a novel blood–brain barrier adhesion molecule in human and mouse. *Brain Research*, 1058(1), pp.62–72.

Wolburg, H. et al., 2003. Localization of claudin-3 in tight junctions of the blood-brain barrier is selectively lost during experimental autoimmune encephalomyelitis and human glioblastoma multiforme. *Acta neuropathologica*, 105(6), pp.586–92.

Wong, H.L., Wu, X.Y. & Bendayan, R., 2012. Nanotechnological advances for the delivery of CNS therapeutics. *Advanced drug delivery reviews*, 64(7), pp.686–700.

Wu, J. et al., 2011. Neurotoxicity of silica nanoparticles: brain localization and dopaminergic neurons damage pathways. *ACS nano*, 5(6), pp.4476–89.

Wu, S.Y.S. et al., 2014. RNAi Therapies: Drugging the Undruggable. *Science translational medicine*, 6(240).

Wurster, E.-C. et al., 2013. Layer-by-Layer Assembled Gold Nanoparticles for the Delivery of Nucleic Acids. In M. Ogris & D. Oupicky, eds. *Nanotechnology for Nucleic Acid Delivery: Methods and Protocols*. Totowa, NJ: Humana Press, pp. 171–182.

Xia, Y. et al., 2011. Gold Nanocages: From Synthesis to Theranostic Applications. *Accounts of chemical research*, 44(10), pp.914–924.

Yan, Q. et al., 1994. Distribution of Intracerebral Ventricularly Administered Neurotrophins in Rat Brain and Its Correlation with Trk Receptor Expression. *Experimental Neurology*, 127(1), pp.23–36.

Yang, H., 2010. Nanoparticle-mediated brain-specific drug delivery, imaging, and diagnosis.

Pharmaceutical research, 27(9), pp.1759–71.

Yang, J.-P. et al., 2009. *The dose-effectiveness of intranasal VEGF in treatment of experimental stroke*,

Yang, P.-H. et al., 2005. Transferrin-Mediated Gold Nanoparticle Cellular Uptake. *Bioconjugate Chemistry*, 16(3), pp.494–496.

Ye, D. et al., 2013. Nanoparticle accumulation and transcytosis in brain endothelial cell layers. *Nanoscale*, 5(22), pp.11153–65.

Ye, D., Dawson, K.A. & Lynch, I., 2015. A TEM protocol for quality assurance of in vitro cellular barrier models and its application to the assessment of nanoparticle transport mechanisms across barriers. *The Analyst*, 140, pp.83–97.

Ying, X. et al., 2010. Dual-targeting daunorubicin liposomes improve the therapeutic efficacy of brain glioma in animals. *Journal of controlled release : official journal of the Controlled Release Society*, 141(2), pp.183–92.

Zanchet, D. et al., 2001. Electrophoretic Isolation of Discrete Au Nanocrystal / DNA Conjugates. *Nano letters*, 1(1), pp.32–35.

van der Zande, M. et al., 2012. Distribution, elimination, and toxicity of silver nanoparticles and silver ions in rats after 28-day oral exposure. *ACS nano*, 6(8), pp.7427–42.

Zhang, R. et al., 2012. The potential health risk of titania nanoparticles. *Journal of hazardous materials*, 211–212, pp.404–13.

Zhang, S. et al., 2009. Size-Dependent Endocytosis of Nanoparticles. *Advanced materials (Deerfield Beach, Fla.)*, 21, pp.419–424.

Zhang, W. et al., 2016. PH and near-infrared light dual-stimuli responsive drug delivery using DNA-conjugated gold nanorods for effective treatment of multidrug resistant cancer cells. *Journal of Controlled Release*, 232, pp.9–19.

Zhang, Y. et al., 2002. Receptor-mediated delivery of an antisense gene to human brain cancer cells. *The journal of gene medicine*, 4(2), pp.183–94.

Zhao, E. et al., 2012. Surface engineering of gold nanoparticles for in vitro siRNA delivery. *Nanoscale*, 4, p.5102.

Zhao, M. & Weissleder, R., 2004. Intracellular Cargo Delivery Using Tat Peptide and Derivatives. *Medicinal Research Reviews*, 24(1), pp.1–12.

Zhao, W., Lin, L. & Hsing, I.M., 2009. Rapid synthesis of DNA-functionalized gold nanoparticles in salt solution using mononucleotide-mediated conjugation. *Bioconjugate Chemistry*, 20(6), pp.1218–1222.

Zlokovic, B. V, 2005. Neurovascular mechanisms of Alzheimer's neurodegeneration. *Trends in neurosciences*, 28(4), pp.202–8.

Zozulya, A., Weidenfeller, C. & Galla, H.-J., 2008. Pericyte-endothelial cell interaction increases MMP-9 secretion at the blood-brain barrier in vitro. *Brain research*, 1189, pp.1–11.

Chapter 9. Appendix

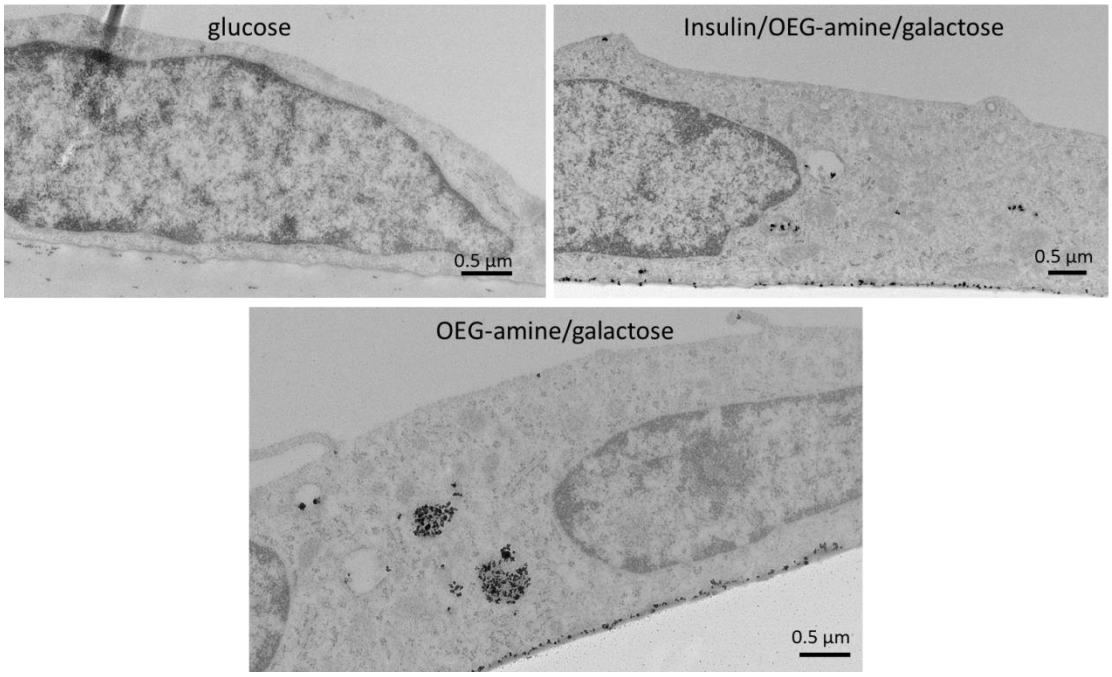

Appendix Figure 1: Representative electron images of analysed samples of hCMEC/D3 cells treated with different types of nanoparticle formulation (i.e. coated with glucose, insulin or OEG-amine).

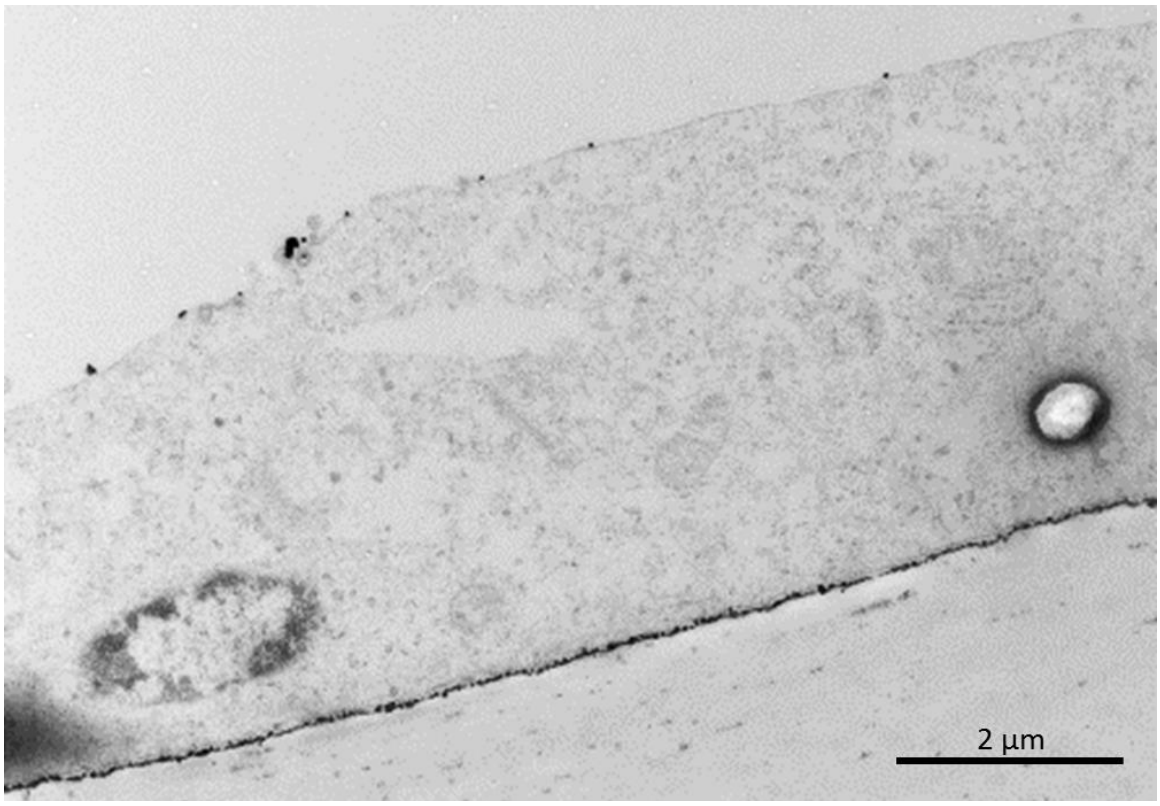

Appendix Figure 2: A representative micrograph of a hCMEC/D3 cell treated with OEG-amine/galactose nanoparticles at 4 °C.

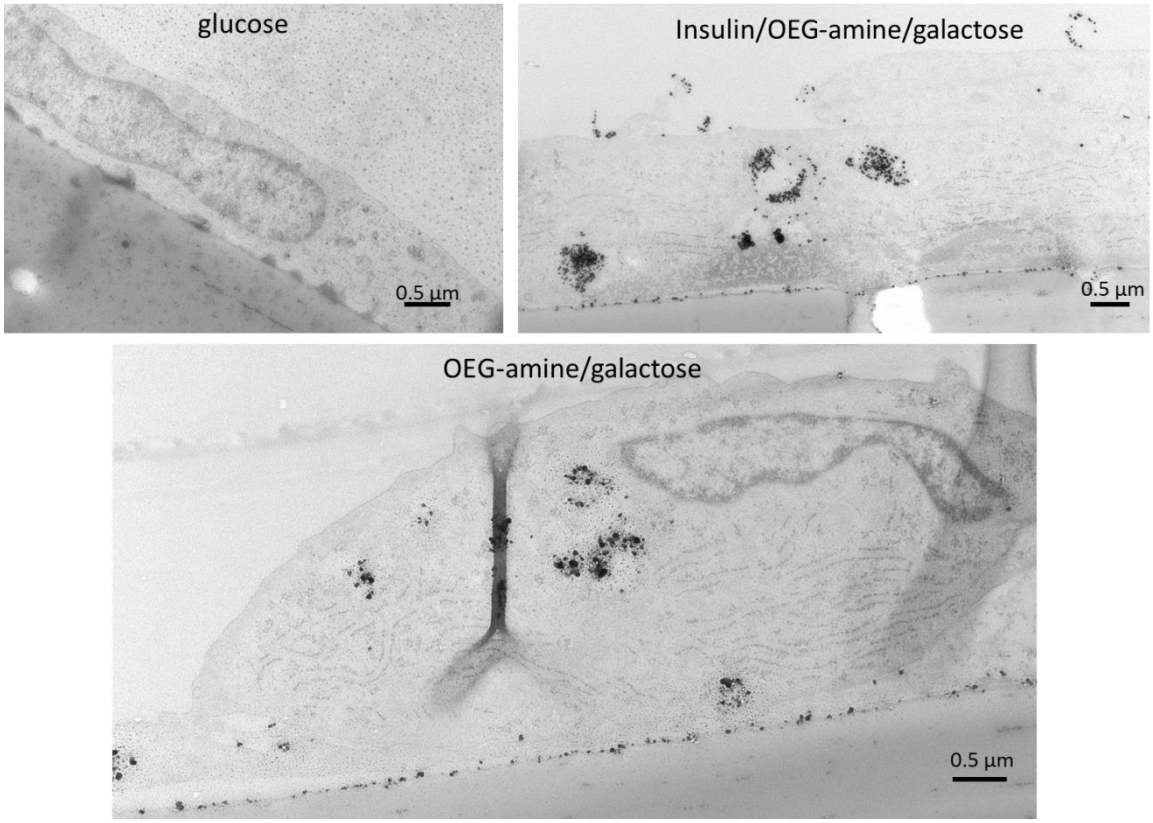

Appendix Figure 3: Representative electron images of analysed samples of ciGENC cells treated with different types of nanoparticle formulation (i.e. coated with glucose, insulin or OEG-amine).

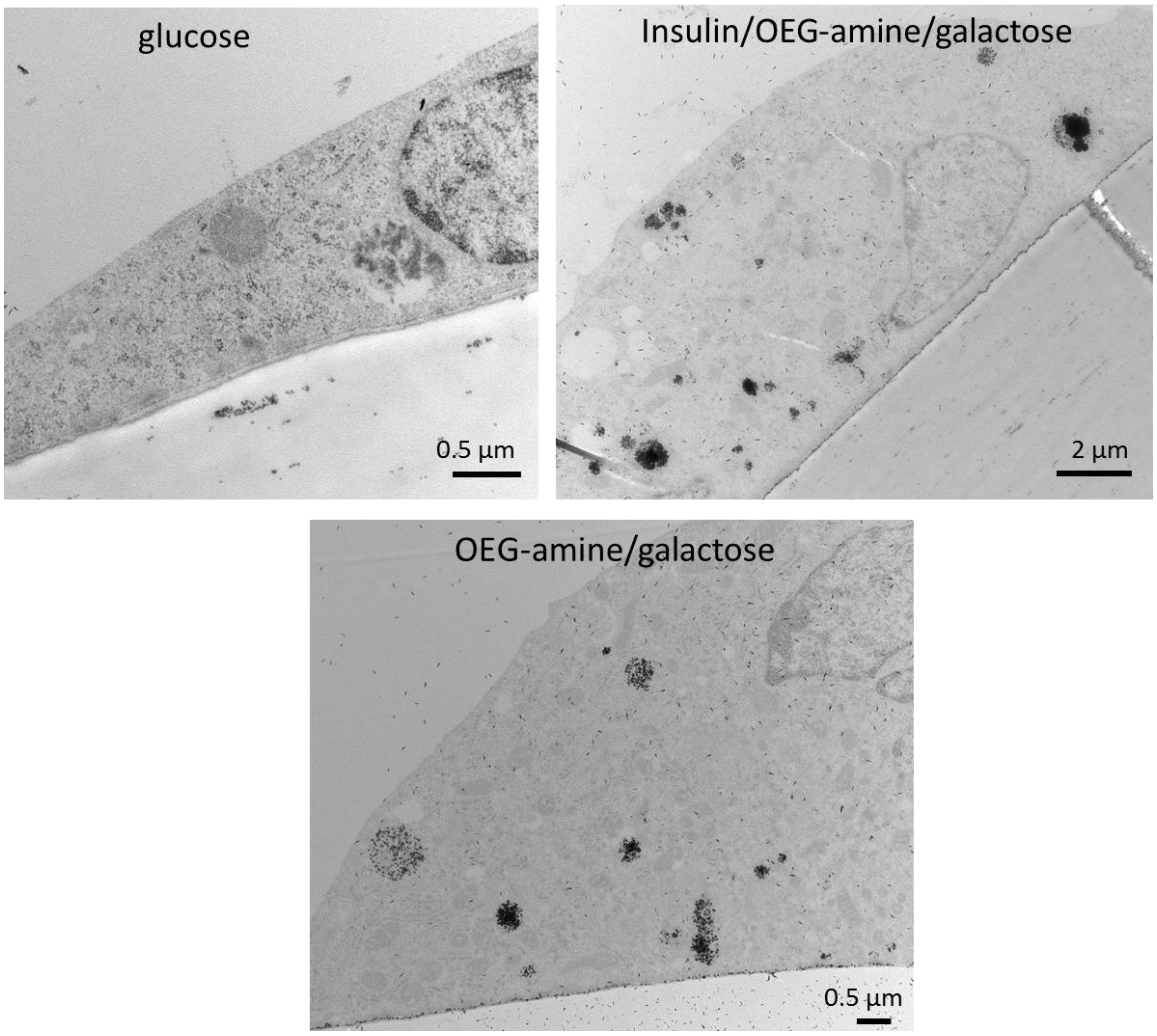

Appendix Figure 4: Representative electron images of analysed samples of BMEC cells treated with different types of nanoparticle formulation (i.e. coated with glucose, insulin or OEG-amine).

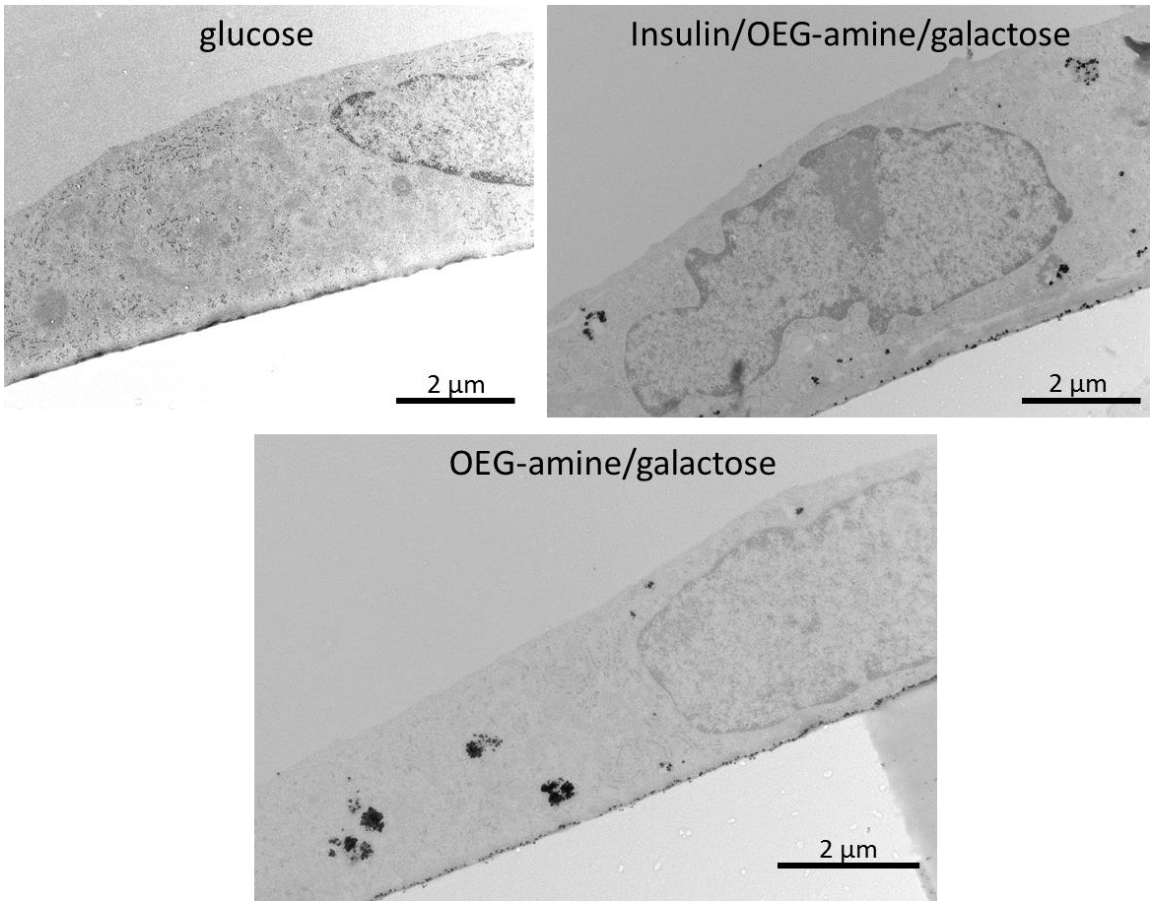

Appendix Figure 5: Representative electron images of analysed samples of HMVEC-L cells treated with different types of nanoparticle formulation (i.e. coated with glucose, insulin or OEG-amine).

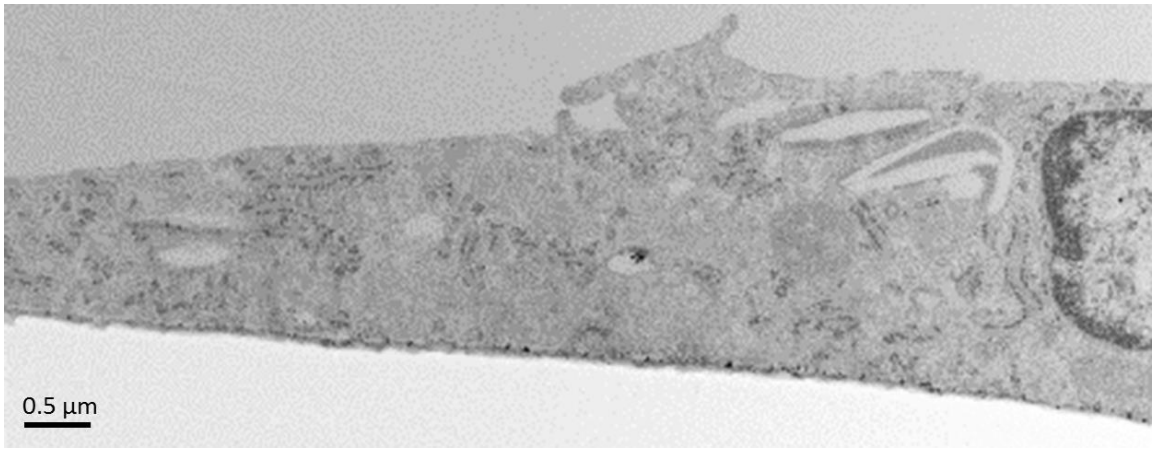

Appendix Figure 6: A representative micrograph of a hCMEC/D3 cell treated with OEG-amine/galactose nanoparticles during exposure to 50 µg/ml of nystatin.